8-1991

Inverse Dynamics and Control for Nuclear Power Plants

Riza C. Berkan
University of Tennessee - Knoxville

To the Graduate Council:

I am submitting herewith a dissertation written by Riza C. Berkan entitled "Inverse Dynamics and Control for Nuclear Power Plants." I have examined the final electronic copy of this dissertation for form and content and recommend that it be accepted in partial fulfillment of the requirements for the degree of Doctor of Philosophy, with a major in Nuclear Engineering.

Belle Upadhyaya, Major Professor

We have read this dissertation and recommend its acceptance:

John M. Bailey, Robert E. Uhrig, Lefteri Tsoukalas

Accepted for the Council:

Carolyn R. Hodges

Vice Provost and Dean of the Graduate School

(Original signatures are on file with official student records.)

To the Graduate Council:

I am submitting herewith a dissertation written by Riza C. Berkan entitled "Inverse Dynamics and Control for Nuclear Power Plants." I have examined the final copy of this dissertation for form and content and recommend that it be accepted in partial fulfillment of the requirements for the degree of Doctor of Philosophy, with a major in Nuclear Engineering.

Belle R Upadhyaya

B. R. Upadhyaya, Major Professor

We have read this dissertation
and recommend its acceptance:

Accepted for the Council:

Vice Provost
and Dean of The Graduate School

Inverse Dynamics and Control for Nuclear Power Plants

A Dissertation
Presented for the Doctor of Philosophy
Degree
The University of Tennessee, Knoxville

Riza C. Berkan

August 1991

Aklın kanatlarıyla uçsamda üzerinden
bilmem bu çınardan başka daha kaç çınar vardır?

to Gönül and Atilla

Acknowledgments

The author expresses his gratitude to his academic advisor Dr. Belle Upadhyaya for his invaluable support, encouragement and technical advice throughout the entire period of this research.

The author is most grateful to the former department head, emeritus Pietro Pasqua and the department head Dr. Thomas W. Kerlin for providing the necessary financial foundation and academic advice which have made the completion of this work possible.

The members of the doctoral committee, Professors Robert E. Uhrig, Lefteri Tsoukalas and Professor of Electrical Engineering John M. Bailey are sincerely acknowledged for their constructive criticism and technical advice.

The ideas developed within this dissertation would undoubtedly not exist if the author had not taken Dr. Rafael Perez's 600 level "Advanced Topics" class. His motivative approach and ingenious comments are very much appreciated.

The author is very thankful to Dr. Ben Fitzpatrick, Professor of Mathematics, for his technical assistance and useful comments which led to an appropriate mathematical representation of the ideas.

This work was sponsored by the Instrumentation and Controls Division, Oak Ridge National Laboratory, under the Advanced Controls Program. The author is very thankful to the program director J. D. White and group leader Roger A. Kisner for their advice and continued support throughout the completion of this work. The EBR-II data were acquired from Argonne National Laboratory-West.

Finally, the author would like to express his appreciation to the members of the first radioactive coffee club of the world for their consistent efforts in understanding humor and rumor that made life bearable during tough times.

Abstract

A new nonlinear control technique was developed by reformulating one of the "inverse problems" techniques in mathematics, namely the reconstruction problem. The theory identifies an important concept called inverse dynamics which is always a known property for systems already developed or designed. Accordingly, the paradigm is called "reconstructive inverse dynamics" (RID) control. The standard state-space representation of dynamic systems constitutes a sufficient foundation to derive an algebraic RID control law that provides solutions in one step computation. The existence of an inverse solution is guaranteed for a limited dynamic space. Outside the guaranteed range, existence depends on the nature of the system under consideration. Derivations include adaptive features to minimize the effects of modeling errors and measurement degradation on control performance.

A comparative study is included to illustrate the relationship between the RID control and optimal control strategies. A set of performance factors were used to investigate the robustness against various uncertainties and the suitability for digital implementation in large-scale systems. All of the illustrations are based on computer simulations using nonlinear models. The simulation results indicate a significant improvement in robust control strategies. The control strategy can be implemented on-line by exploiting its algebraic design property.

Three applications to nuclear reactor systems are presented. The objective is to investigate the merit of the RID control technique to improve nuclear reactor operations and increase plant availability. The first two applications include xenon induced power oscillations and feedwater control in conventional light water reactors. The third application consists of an automatic control system design for the startup of the Experimental Breeder Reactor-II (EBR-II). The nonlinear dynamic models used in this analysis were previously validated against available plant data. The simulation results show that the RID technique has the potential to improve reactor control strategies significantly. Some of the observations include accurate xenon control, and rapid feedwater maneuvers in pressurized water reactors, and successful automated startup of the EBR-II.

The scope of the inverse dynamics approach is extended to incorporate artificial intelligence methods within a systematic strategy design procedure. Since the RID control law includes the dynamics of the system, its implementation may influence plant component and measurement design. The inverse dynamics concept is further studied in conjunction with artificial neural networks and expert systems to develop practical control tools.

Contents

1 Introduction **1**

1.1 General Motivation 1

1.2 Specific Objectives 4

1.3 Background 5

1.4 Original Contributions 7

1.5 Terminology 8

1.6 Organization of the Dissertation 10

2 Theory of Inverse Dynamics **11**

2.1 Inverse Problems 11

2.2 Dynamic Equilibrium of Control 13

2.3 State Reconstructing Inverse Control Law 14

2.3.1 Demand Law 15

2.3.2 Existence 17

2.4 Feasibility of Control 18

2.4.1 Measurement Problems 18

2.4.2 Inexact Inverse Dynamics 19

2.5 Adaptive Control 22

2.6 Auxiliary States 26

2.7 Comparison with Optimal Control 27

2.7.1 Inverse Dynamics Component of the LQR 28

2.7.2 Optimality and Asymptotic Behavior 30

2.7.3 Implementing LQR versus RID control 32

2.8 RID Control Design Steps 33

3 Performance Characteristics **36**
3.1 Framework for Evaluation 36
3.2 A Benchmark Problem 38
3.2.1 Modeling the Benchmark Problem 39
3.2.2 Discrepancies Between the Plant and Model 40
3.2.3 Control Problem Definition 41
3.2.4 Performance Factors 42
3.3 Design 43
3.3.1 RID Control (DS1) 43
3.3.2 Adaptive RID Control Design (DS2) 46
3.3.3 Lagrangian Derivation of Optimal Control (DS3) 49
3.4 Simulation Results 51
3.4.1 Test-1 (T1): Plant and Model Perfectly Match 51
3.4.2 Test-2 (T2): Partially Unknown Plant Dynamics 56
3.4.3 Test-3 (T3): Measurement Time-Delay Problem 72
3.4.4 Test-4 (T4): Actuator Limitations 76
3.4.5 Overall Performance Evaluation 97

4 Application to Nuclear Systems **102**
4.1 Introduction 102
4.2 Xenon Oscillation Control in PWRs 103
4.2.1 Previous Accomplishments in Spatial Control 105
4.2.2 Axial Xenon Oscillation Model 106
4.2.3 RID Control Design 111
4.2.4 Closed-loop Simulation Results 113
4.2.5 Conclusions 120
4.3 Feedwater-Train Control in PWRs 127
4.3.1 Nonlinear Modeling of PWR Feedwater-Train 129
4.3.2 RID Controller Design 132
4.3.3 Implementation 137
4.3.4 Simulation Results 137
4.3.5 Conclusions 150
4.4 EBR-II Startup Control 150

4.4.1 Plant Description 151
4.4.2 Existing Control Capabilities 151
4.4.3 EBR-II Operations 154
4.4.4 Startup Control Strategy 156
4.4.5 RID Control Design 157
4.4.6 Simulation Results 160

5 Integration of Artificial Intelligence Tools 170
5.1 Significance of the "Inverse" Approach 170
5.2 Strategy Design 172
5.2.1 Representation of the Control Problem 173
5.2.2 Potential Advantage of the SIM Analysis 175
5.2.3 SIM Analysis for Previous Applications 176
5.3 Fuzzy Control and Inverse Dynamics 179
5.4 Artificial Motor-Learning 182

6 Concluding Remarks 185
6.1 Accomplishments 185
6.2 Comparison with Similar Methods 187
6.3 Advantages 188
6.4 Limitations 190
6.5 Recommendations for Future Research 191

Bibliography 193

Appendixes 199

A. ACSL Code of the Benchmark Problem. 200

B. ACSL Code of the Xenon Oscillation Problem. 225

Vita 230

List of Tables

3.1 Labels for Control Algorithm Testing 45
3.2 Tests Performed 46

4.1 One group diffusion parameters of the axial xenon oscillation model. 109

List of Figures

2.1 Feedback arrangement of inverse dynamics control. 23
2.2 Use of on-line model in RID control. 24

3.1 Measures of Utilities 37
3.2 Desired trajectories for the reactor power (top) and core-coolant temperature (bottom). 44
3.3 Reactor power H_1 response using the RID controller. Reactor follows the demand D_1 with a negligible error. In Test-1, plant and model exactly match. 52
3.4 Reactor power P_1 response using the LDOC paradigm. Reactor follows the demand D_1 with a negligible error. In Test-1, plant and model exactly match. 53
3.5 Reactor coolant temperature responses using the LDOC and RID controllers (P_4, H_4). Reactor follows the demand D_4 with a negligible error. In Test-1, plant and model exactly match. 54
3.6 Control inputs of reactivity and flow using the LDOC and RID controllers. (Y_1 and Y_4 with LDOC, V_1 and V_4 with RID). In Test-1, plant and model exactly match. 55
3.7 Time-variant parametric changes in the plant. Maximum deviation is about 30 % of the initial value. Parametric changes are initiated at the 10th second and generated by arbitrary constants. The 8 parameters of the on-line model are constant and equal to the initial values of plant parameters. 57

3.8 Unmodeled nonlinear dynamics incorporated into the plant. The nonlinearity relates the fuel temperature to the reactor power. It is unobservable through direct measurements which complicates the diagnostic task of the adaptive control. 58
3.9 Reactor power response H_1 using the RID control paradigm. Reactor follows the demand D_1 with a negligible error. Test-2 introduces 30% discrepeancy between the plant and its model. 59
3.10 Reactor power response P_1 using the LDOC paradigm. Reactor follows the demand D_1 with a negligible error. Test-2 introduces 30% discrepeancy between the plant and its model. 60
3.11 Reactor coolant temperature response H_4 using the RID control paradigm. Reactor follows the demand D_4 with a negligible error. Test-2 introduces 30% discrepeancy between the plant and its model. 62
3.12 Reactor coolant temperature response P_4 using the LDOC paradigm. Reactor follows the demand D_4 with a significant error. Test-2 introduces 30% discrepeancy between the plant and its model. 63
3.13 Control inputs generated by the LDOC and RID control paradigms. Reactivity inputs (Y_1 with LDOC, V_1 with RID) and flow inputs (Y_4 with LDOC, V_4 with RID) are consistent between the two paradigms. Test-2 introduces 30% discrepancy between the plant and its model. 64
3.14 Adaptive control inputs using the LDOC and RID control paradigms. LDOC inputs are G_1 and G_4, RID inputs are R_{G1}, R_{G3} and N_3^*. The adaptive control captures the discrepeancies caused by time-variant parametric changes and unknown nonlinear plant dynamics. Test-2 introduces 30% discrepancy between the plant and its model. 65
3.15 Reactor power response H_1 using the RID control paradigm. Reactor departures from the demand D_1 as time elapses. The discrepancies between the plant and model are magnified to reach 300 % at the 200th second. This is practically not possible in any nuclear reactor. 66

3.16 Reactor power response P_1 using the LDOC paradigm. Reactor departures from the demand D_1 as time elapses and shows unstable behavior. The discrepancies between the plant and model are magnified to reach 300 % at the 200th second. This is practically not possible in any nuclear reactor. 67
3.17 Reactor coolant temperature response H_4 using the RID control paradigm. Reactor follows the demand D_4 with a significant error. The discrepancies between the plant and model are magnified to reach 300 % at the 200th second. This is practically not possible in any nuclear reactor. 68
3.18 Reactor coolant temperature response P_4 using the LDOC paradigm. Reactor follows the demand D_4 with a significant error. The discrepancies between the plant and model are magnified to reach 300 % at the 200th second. This is practically not possible in any nuclear reactor. 69
3.19 Control inputs using the LDOC and RID control paradigms. Reactivity inputs (Y_1 with LDOC and V_1 with RID) and flow inputs (Y_4 with LDOC and V_4 with RID) are consistent between each other. The discrepancies between the plant and model are magnified to reach 300 % at the 200th second. This is practically not possible in any nuclear reactor. 70
3.20 Adaptive Control inputs using the LDOC and RID control paradigms. LDOC inputs (G_1 and G_4) and RID inputs (R_{G1}, R_{G3}, N_3^*) are diverging as time elapses. The discrepancies between the plant and model are magnified to reach 300 % at the 200th second. This is practically not possible in any nuclear reactor. 71
3.21 Reactor Power responses P_1,H_1 using the LDOC and RID control paradigms. Reactor follows the demand D_1 with a negligible error. In Test-3, measurements from the plant are delayed (0.1 second delay in reactor power, 2 seconds delay in coolant temperature signals). 73

3.22 Coolant temperature responses P_4,H_4 using the LDOC and RID control paradigms. Reactor follows the demand D_4 with a significant error. At the beginning of the transient, the accumulation of the error can not be detected. Few seconds later, the magnified error causes a steep early response in coolant temperature. In Test-3, measurements from the plant are delayed (0.1 second delay in reactor power, 2 seconds delay in coolant temperature signals). . . . 74
3.23 Control inputs generated by the LDOC and RID control paradigms. (reactivity Y_1,V_1, and coolant flow Y_4,V_4) In Test-3, measurements from the plant are delayed (0.1 second delay in reactor power, 2 seconds delay in coolant temperature signals). Delayed sensor signals cause an excessive response in flow control signals at the beginning of the transient. 75
3.24 Coolant temperature responses P_4,H_4 using the LDOC and RID control paradigms. Reactor follows the demand D_4 with a significant error. The prompt jump at the begining of the transient is more severe as the delay-time prolongs. In Test-3, measurements from the plant are delayed (0.1 second delay in reactor power, 5 seconds delay in coolant temperature signals). 77
3.25 Control inputs generated by the LDOC and RID control paradigms. (coolant flow Y_4,V_4) In Test-3, measurements from the plant are delayed (0.1 second delay in reactor power, 5 seconds delay in coolant temperature signals). Delayed sensor signals cause an excessive response in flow control signals at the beginning of the transient. Increased delay-time causes more severe prompt response. 78
3.26 Reactor power responses P_1, H_1 using the LDOC and RID control paradigm. Reactor follows the demand D_1 with a negligible error. In Test-4, reactivity insertion rate and coolant flow rate are constrained. 80
3.27 Reactor coolant temperature responses P_4,H_4 using the LDOC and RID control paradigms. Reactor follows the demand D_4 with a negligible error. In Test-4, reactivity insertion rate and coolant flow rate are constrained. 81

3.28 Reactivity inputs using the LDOC and RID control paradigms. Figure compares the unconstrained control signals (Y_1,V_1) with the constrained ones (YY_1,VV_1). In test-4, reactivity insertion rate and coolant flow rate are constrained. 82
3.29 Constrained and unconstrained coolant flow inputs generated by the RID control paradigm. Speed rate is violated by the unconstrained control signal. However, constrained input is capable of efficient demand following control. 83
3.30 Constrained and unconstrained coolant flow inputs generated by the LDOC paradigm. Speed rate is violated by the unconstrained control signal. However, constrained input is capable of efficient demand following control. 85
3.31 External disturbance applied to the reactor power during the demand following control. The step disturbance is equal to 0.2 $positive reactivity. 86
3.32 Reactor power response H_1 using the RID control paradigm. The reactor is subject to a +20 cents step disturbance where the controls are constrained. Reactor follows the demand D_1 before and after the disturbance. 87
3.33 Reactor power response P_1 using the LDOC paradigm. The reactor is subject to a +20 cents step disturbance where the controls are constrained. Reactor follows the demand D_1 before and after the disturbance. 88
3.34 Reactor coolant temperature response H_4 using the RID control paradigm. The reactor is subject to a +20 cents step disturbance where the controls are constrained. Reactor follows the demand D_4 before and after the disturbance. 89
3.35 Reactor coolant temperature response H_4 using the LDOC paradigm. The reactor is subject to a +20 cents step disturbance where the controls are constrained. Reactor follows the demand D_4 before and after the disturbance. 90

3.36 Constrained VV_1 and unconstrained V_1 reactivity inputs generated by the RID control paradigm. The closed-loop plant uses the constrained control signal. The reactor is subject to a +20 cents step disturbance. 91
3.37 Constrained YY_1 and unconstrained Y_1 reactivity inputs generated by the LDOC paradigm. The closed-loop plant uses the constrained control signal. The reactor is subject to a +20 cents step disturbance. 92
3.38 Constrained VV_4 and unconstrained V_4 flow inputs generated by the RID control paradigm. The closed-loop plant uses the constrained control signal. The reactor is subject to a +20 cents step disturbance. 93
3.39 Constrained YY_4 and unconstrained Y_4 reactivity inputs generated by the LDOC paradigm. The closed-loop plant uses the constrained control signal. The reactor is subject to a +20 cents step disturbance. 94
3.40 Rod speed with the LDOC and RID control paradigms during the demand following reactor. Reactor is subject to a +20 cents step disturbance. Rod speed is constrained ±0.1$ per second. 95
3.41 Coolant flow rate with the LDOC and RID control paradigms during the demand following reactor. Reactor is subject to a +20 cents step disturbance. Flow rate is constrained ±0.05 fraction per second. . . 96
3.42 Tuning parameters used in the RID and LDOC designs. 99

4.1 Limit cycle behavior due to xenon buildup in Oconee Unit #2 plant. The xenon oscillation estimated by the model is in agreement with the plant data. 110
4.2 Block diagram of the RID controller in application to the xenon-oscillation control problem of PWRs. 114
4.3 Normalized flux, xenon, and iodine oscillations in the lower half of the core. Oscillations are initiated by a step reactivity shift at t=0. 115
4.4 Normalized flux, xenon, and iodine oscillations in the lower half of the core. RID controller is activated at the 23rd hour. 117
4.5 Control trajectory of the absorber shift towards the top of the core. RID controller is activated at the 23rd hour. 118
4.6 First 20 minutes of the control rod trajectory. 119

4.7 Normalized flux, xenon and iodine oscillations in the lower half of the core. RID controller is activated at the 8th hour. 121
4.8 Control trajectory of the absorber shift. RID controller is activated at the 8th hour. 122
4.9 First 20 minutes of the control trajectory started at the 8th hour. . 123
4.10 Normalized xenon-iodine phase plane plot. RID controller is activated at the 8th hour. 124
4.11 Normalized xenon-iodine phase plane plot. RID controller is activated at the 23rd hour. 125
4.12 Axial xenon oscillation damping example: Half-Cycle Damping Strategy. 126
4.13 The schematic of the feedwater-train system and associated system variables. 128
4.14 RID controller and its interaction with the plant (feedwater-train system) and on-line model. Model estimates one of the four state variables where the rest are obtained from the plant as direct measurements. 138
4.15 Feedwater flow response in comparison with the demand. The demand is followed with a negligible error that is not visible in the figure. As an external disturbance, the steam generator pressure (boundary condition) is lowered 25 % with oscillation. 140
4.16 External disturbance during the demand following control. Steam generator pressure (boundary condition) is lowered 25 % with oscillation. 141
4.17 Turbine (YPVLV) and feedwater valve (YACT) positions (control inputs) during the demand following control. As an external disturbance, the steam generator pressure (boundary condition) is lowered 25 % with oscillation. 142
4.18 Pressure drop across the feedwater valve. As an external disturbance, the steam generator pressure (boundary condition) is lowered 25 % with oscillation. 143

4.19 External disturbance during the demand following control. Steam generator pressure (boundary condition) is lowered 25 % with high frequency oscillation. 144
4.20 Feedwater flow response in comparison with the demand. The demand is followed with a negligible error that is not visible in the figure. As an external disturbance, the steam generator pressure (boundary condition) is lowered 25 % with high frequency oscillation. 145
4.21 Turbine (YPVLV) and feedwater valve (YACT) positions (control inputs) during the demand following control. As an external disturbance, the steam generator pressure (boundary condition) is lowered 25 % with high frequency oscillation. 146
4.22 Pressure drop across the feedwater valve. As an external disturbance, the steam generator pressure (boundary condition) is lowered 25 % with high frequency oscillation. 147
4.23 Feedwater flow response in comparison with the demand. A 10 % error is introduced to the model based state estimation. Responses verify the robustness against estimation errors. 148
4.24 Feedwater flow response in comparison with the demand. A 25 % error is introduced to the model based state estimation. Responses verify the robustness against estimation errors. 149
4.25 EBR-II Plant Schematic 153
4.26 EBR-II Startup Procedure. 155
4.27 RID controller in application to the EBR-II startup task. 161
4.28 Reactor power responses during startup at EBR-II. Reactor controlled by RID, Fuzzy, and NNET controllers. Simulation results compared with plant data. 162
4.29 Core exit temperature responses during startup at EBR-II. Reactor controlled by RID, Fuzzy, and NNET controllers. Simulation results compared with plant data. 163
4.30 Bulk tank temperature responses during startup at EBR-II. Reactor controlled by RID, Fuzzy, and NNET controllers. During the startup mode, sodium bulk temperature is desired to remain constant. Simulation results compared with plant data. 164

4.31 IHX secondary-outlet temperature responses during startup at EBR-II. Reactor controlled by RID, Fuzzy, and NNET controllers. Simulation results compared with plant data. 165
4.32 In-core sodium temperature responses during startup at EBR-II. Reactor controlled by RID, Fuzzy, and NNET controllers. Simulation results compared with plant data. 166
4.33 Control rod position (control input-1) during startup at EBR-II. Reactor controlled by RID, Fuzzy, and NNET controllers. Simulation results compared with plant data. 167
4.34 Secondary sodium flow (control input-2) response during startup at EBR-II. Reactor controlled by RID, Fuzzy, and NNET controllers. Simulation results compared with plant data. 168

5.1 A hypothetical mirror placed perpendicular to the plane of motion yields inverse dynamics of the mass-spring system. If unknown control u employs the inverse dynamics, system remains at equilibrium. 171
5.2 Topological representation of SISO, MISO, and MIMO control strategies (high level problems). These solutions may be obtained using symbolic computations for systems with large degrees of freedom. . 177
5.3 Functionally symmetric neural networks for modeling motor-control phenomena of biological systems. Model is based on the inverse dynamics approach. Network (A) learns the dynamics of the body through routine movements whereas network (B) learns the inverse dynamics for the purpose of control 184

Symbols

ACRDS	Automatic Control Rod Drive System
AGR	Advanced Gas-cooled Reactor
AI	Artificial Intelligence
ANS	Artificial Neural Networks
ASI	Axial-Shape Index
ACSL	Advanced Computer Simulation Language (Software)
BWR	Boiling Water Reactor
DET	Dynamic Equilibrium Testing
EM	Electromagnetic
FOTL	First-Order Transport Lag
EBR-II	Experimental Breeder Reactor-II
ID	Inverse Dynamics
IHX	Intermediate Heat Exchanger
LDOC	Lagrangian Derivation of Optimal Control
LQG	Linear Quadratic Gaussian compensator
LQR	Linear Quadratic Regulator
MIMO	Multiple-Input Multiple-Output
MRAC	Model-Reference Adaptive Control
MISO	Multiple-Input Single-Output
NNET	Neural Network
PHWR	Pressurized Heavy Water Reactor
PID	Proportional-Integral-Derivative
PWR	Pressurized Water Reactor
RID	Reconstructive Inverse Dynamics
SIM	Stable-Inverse-Map
SISO	Single-Input Single-Output
TAO	Target Axial Offset
VOR	Vestibuloocular Reflex
XIPO	Xenon Induced Power Oscillations

Chapter 1

Introduction

The inverse dynamics concept for the control and identification of complex nonlinear processes was developed in this dissertation. This concept is described as follows: *The dynamics of a moving object in a fixed reference frame is defined by the evolution of its coordinates in time. The "inverse" dynamics of the same object is defined by the evolution of its coordinates in time observed from a hypothetical mirror that is placed perpendicular to the plane of motion.* An immediate corollary is that the inverse dynamics is a property of every dynamic system. This concept leads to a control paradigm based on a dynamic cancellation by the inverse property and reconstruction of the desired system behavior. Accordingly, the paradigm is called the reconstructive inverse dynamics (RID). The RID paradigm, in turn, leads to a procedural design method where the problem solution can be extended towards suggesting different control strategies to improve system operations. The present research uses an interdisciplinary approach to incorporate mathematics, artificial intelligence, and principles from several engineering disciplines. This research includes the description of the concept, development of the theory, and applications to nuclear power plants.

1.1 General Motivation

The main objective of this research was based on a collection of reasons most of which are related to the operational problems encountered in conventional large-scale systems, especially in nuclear power plants. In this section, these reasons are

presented in general terms. The discussion focuses on the weaknesses of conventional control methods in application to complex engineering systems.

The definition of complex systems within the domain of this analysis may include one or more of the following conditions to exist:

(1) The state of the process at different operational levels/modes is loosely correlated in the linear domain,
(2) System measurements are not complete or accurate to represent its dynamic behavior properly,
(3) System is subjected to frequent disturbances due to its environment,
(4) System's degree of freedom is too large to allow an exhaustive evaluation of every possible control action within a reasonable time frame.

Especially large-scale systems such as power plants, production facilities, and chemical processes are likely to inherit at least one of the conditions stated above.

The conditions (1), (3), and (4) are related to nonlinear behavior of complex systems. When linear control methods fail to represent nonlinear behavior, these conditions may lead to operational problems. This fact has been the motivation for the development of nonlinear methods such as fuzzy control and neural networks. Although there is a sizable body of literature in the area of nonlinear analysis, the number of useful applications is limited due to the gap between the theory and practice. Thus, it is of primary importance to develop a nonlinear paradigm based on a well-defined theory as well as to provide a significant margin of feasibility in application to conventional systems.

Condition (2), which implies the lack of enough information from the process, often causes problems because of some undetected shift in the state of operation. Adaptive control theory is primarily developed to deal with such problems [1]. The time variant parametric changes or uncertainties can be tracked using a set of available information. The tracking of unknown dynamics, which is also called system identification, is used to update the parameters of the on-line control algorithm.

The performance using the standard adaptive control methods depends on the accuracy of the identification capability at various levels. Optimality, stability and robustness characteristics may deteriorate due to poor identification. Thus, one of the important objectives is to develop a control paradigm that does not strongly rely on identification without a significant comprimise in its adaptive performance.

In general, there are two control approaches. The first approach considers the open-loop system as a black-box, and utilizes measurements to estimate, adapt, and control the process. Most of the control theory and the conventional control systems fall into this category. The second approach takes an extra step to incorporate the principles of the process within the control law. This may be the right direction to overcome problems arising from the conditions (1), (3) and (4), because the control law explicitly carries the properties of the process and its environment. The chemical process industry has been the most affected sector from the lack of such control strategies. As one author puts it "understanding of the distillation operation is the theme that differentiates distillation control from their more generalized counterparts" [2]. The rule-based approach such as fuzzy control falls into the second category. However, there is no general and systematic way of creating fuzzy rules besides the pure heuristic approach. Therefore, it is very beneficial to develop a control paradigm that allows process-related information to be part of the control law in a systematic manner.

The standard philosophy in conventional systems has been to design a process using the novel techniques and consider the design of automatic control system after the system layout and process design is fixed. In many cases, there is even not much room left for the proper instrumention strategy. This tradition has been encouraged mistakenly by the comfort of using the black-box control methods which yield piece-meal installed control strategies. Considering the recent upsurge of interest to renew the traditional philosophy, it is necessary to develop a control paradigm that can provide useful guidelines and be part of the overall system design.

1.2 Specific Objectives

An inadequate control strategy constitutes one of the important reasons for poor plant availability. Comparing the power plant availability records in Western Europe, Japan, and the U.S., there is a significant difference in favor of foreign reactors. One obvious reason is that advanced control technologies have significantly entered into the design of foreign reactors. Recent automatic control applications in Japan [3] and Canada [4] and automatic xenon monitoring system in France [5] are a few examples of this trend.

The specific objective of this work is to investigate the effectiveness of the RID control paradigm in application to nuclear power plant operations. The investigation is focused on the improvement in control strategies which increase plant availability. Three different cases are considered. These cases refer to control problems in which the plant operations are most likely to be improved by advanced control strategies.

In pressurized water reactors (PWRs), one common problem is the build up of xenon and iodine isotopes in the fuel as a result of fission reactions. These fission products affect the reactor dynamics and result in axial and radial flux oscillations in the core. Depending upon the conditions of the plant such as burnup and boration, the reactor dynamics may show a limit-cycle behavior. In practice, emergency systems intervene and a reactor trip occurs when the oscillations get out of control and exceed a target band [6]. The control of xenon induced power oscillations (XIPO) in conventional reactors is mainly accomplished by plant operators. The most commonly used method is called the half-cycle damping strategy where the operator inserts/withdraws control rods in the middle of half-observed half-anticipated cycle [7]. Operator's decisions are based on experience and heuristic reasoning which do not guarantee to prevent unscheduled shutdowns. Therefore, the improvement in plant availability depends on an appropriate xenon control system which can provide trip avoidance solutions in a consistent manner.

Another common problem in PWRs is caused by the U-tube steam generator

dynamics. At low power levels, the steam generator level may swing due to the nonminimum phase behavior. The emergence of such behavior in steam generator dynamics is believed to be related to inaccurate feedwater flow measurement, especially during startup [8]. The steam generator related problems also include the well-known shrink and swell phenomena [9]. One of the effective ways of trip avoidance in the event of such problems is to have a fast maneuvering capability in feedwater flow. A typical feedwater flowrate change of 5 % per minute must be provided without causing an excessive pressure drop across the feedwater valve. In this dissertation, a detailed nonlinear analysis is considered using a model of the standard feedwater-train system. The objective is to investigate the possibility of improving feedwater flow maneuvers using a multivariable RID control technique.

The advantage of using an appropriate nonlinear control law is best shown by a control task that covers the full envelope operation. A particular emphasis is given to the startup control of nuclear reactors in an automatic mode. Startup of nuclear reactors include full-scale power levels with varying plant conditions [10]. The nonlinearities and uncertainties become significant as the reactor power level progressively changes. The automatic startup control of the Experimental Breeder Reactor-II (EBR-II) requires a multivariable nonlinear strategy. One of the objectives is to design a RID controller for this task. Simulation results were compared with the EBR-II startup data to determine the effectiveness of the new control strategy.

1.3 Background

The theory presented in this dissertation is based on some of the concepts of control theory, inverse problems in mathematics, and artificial intelligence. However, there are very few studies in the literature which are directly related to the inverse dynamics concept introduced in this research.

Inverse problems have been used in many applications over the past fifteen years. Recent investigations have been in the following areas: Reconstruction

of unknown sources and signals, image reconstruction, computer tomography in medicine, geophysics, optics, compartment analysis, identification of static and dynamic processes, seismic exploration, electrocardiography and magnetocardiography, inverse scattering, radiography, evolution backwards in time, inverse heat conduction, inverse melting problems. An extensive bibliography on inverse and ill-posed problems is contained in [11].

One of the earliest attempts to combine the principles of inverse problems used in different areas under one discipline was made by Baumeister [12]. Because any backward mathematical or algorithmic solution can be called an inverse approach, most of these studies contain the same terminology which often causes confusion. Thus, the systematic definition of forward and inverse problems given by Baumeister has an essential academic importance.

The definition of inverse problems in the literature consists of solving x from a standard matrix equation $y = \mathbf{A}x$ which may pose numerical problems depending upon the condition of matrix $\mathbf{A}$. A typical application in the control area is the manipulator-arm control in robotics [13]. The kinematics of the robot-arm can be represented by the matrix equation $y = \mathbf{A}x$. The definition of inverse kinematics in the robotics field refers to a backward solution that determines the coordinates of the end-effector x given the final (desired) coordinates y. Compared to the forward solution, the inverse kinematics yields several advantages depending on the degrees of freedom of the robotic arm. The inverse problems in kinematics is investigated extensively in the Russian literature. Krutko [14] has analyzed the dynamic behavior of inverse kinematics approach. He has also shown the relation between the optimum control and inverse problems in dynamics.

The inverse dynamics concept introduced in this dissertation is entirely developed in a nonlinear dynamic form, that is $\dot{x} = f(x, u)$, where x and u are state and control variables, respectively. This approach is not directly related to the standard inverse problems or inverse kinematics methods described in the literature.

There are two different areas in control theory which are more directly related

to the inverse dynamics concept. The pole-zero cancellation method is one of them [15]. However, this method is developed purely in the frequency domain and is restricted to linear analysis. In addition, this technique does not specify how to rebuild the cancelled dynamics. The pole-placement method is a more direct approach for building the desired dynamics [16]. Because a desired pole location for a nonlinear process is undefined, the method is not applicable outside the linear regime. The second closely related method employs adaptive control using inverse modeling. Widrow [17] has suggested this approach to be implemented in the linear domain. This method uses an on-line inverse model in an open-loop arrangement which causes stability problems for non-minimum systems. Although the inverse modeling accomplishes a similar goal as in the RID paradigm, the conceptual difference between the model-reference adaptive control (MRAC) and the RID paradigm remains vivid. In MRAC approach, the control law is a function of the error between the plant output and its estimate based on an on-line model (or inverse model) [1]. The main idea of the RID control is to create inverses within the control law rather than employing a model-based strategy. Thus, the RID control law is not an on-line model. This difference in the design philosophies can also be seen between conventional control and knowledge-based control methods. The knowledge-based control has been studied for a long period of time and has shown its first successful application in the form of fuzzy-logic control [18]. In fuzzy control, the control law embodies the characteristics of the process in the form of fuzzy rules.

1.4 Original Contributions

The inverse dynamics concept and the development of the theory presented in this dissertation are not based on any previous work in the literature. When the inverse dynamics concept is considered from a mathematical point of view, it may not seem to be an original contribution because the inverse solutions have been implemented in several fields. This concept, however, is original from the system science and control perspective. It defines a unique property for dynamic systems which yields useful analytical solutions for control and diagnostics problems. The summary of contributions is given below.

Definition of the inverse dynamics concept was established.

The reconstruction problem defined in mathematics was adopted for trajectory following control. A closed-form solution of the reconstructive inverse dynamics (RID) control law was derived. The derivations were extended to include adaptive and multivariable control design.

An inverse dynamics component was shown to exist within the LQR control law for first order systems.

Closed-loop performance of the RID control in application to a nonlinear problem was studied. Robustness characteristics were analyzed in comparison with the Lagrangian Derivation of Optimal Control.

The RID control was applied to three different problems. These included the xenon oscillations in PWRs, feedwater control in PWRs, and the starup control at the EBR-II. The control performance was verified through simulations.

A topological method was developed to integrate artificial intelligence methods for strategy design. A model for the self-learning control strategy was presented using neural networks and inverse dynamics.

1.5 Terminology

The control of dynamic systems has two basic objectives: (1) to achieve a desired change in system behavior, and (2) to regulate the existing state of a system. The first objective is often referred to as the *set-point change* or less frequently as the *demand following* control whereas the second objective is called the *regulation* problem. Most of the conventional control systems incorporate the regulation and set-point change tasks. In reality, none of the control systems can exactly satisfy a required set-point change (discontinuity) in system variables. This is due to

some inertia inherited by every physical system. Despite this conflict, a set-point change requirement is very suitable for the development of control policies using performance factors such as overshoot and settling time. A set-point change can be represented by a ramp trajectory within some finite (practical) time interval. The regulation problem can be represented by a stationary reference trajectory. Therefore, the terminology *trajectory following* used in this dissertation represents a general requirement rather than a specific control problem. The terms "reference trajectory" and "demand" are used interchangably throughout the dissertation.

The term *reconstruction*, close to its syntactic meaning in daily language, means rebuilding some process information after it was removed, used out, or deteriorated. In the inverse problems literature, the reconstruction problem has been clearly defined as a special type of inverse problems [12]. The usage of this term has no further emphasis in this work beyond the reconstruction of the desired system dynamics by control actions.

Achievability is not a common descriptor in control language. In optimum control theory, it is used to identify an achievable performance region [19]. The achievability defines a condition for the reference trajectories in the RID paradigm. This condition determines if the demand is acceptable with respect to the physical restrictions and safety regulations of the system.

The term *heuristics*, which defines an object oriented search in artificial intelligence, is used in a more flexible manner in this work. In this work, heuristics primarily implies the use of process-related knowledge in a non rule-based form. The development of the inverse dynamics is partially heuristic which depends on the experience of the designer. Its formulation can include definition of unknown terms that are best characterized by the knowledge of the system under consideration.

Strategy is the combination and organization of tasks to achieve a given objective. It automatically defines the existence of other possible solutions. In the control area, a strategy includes selecting important measurements, determining

the roles of the actuators, choosing set points, and establishing a set of procedures for design and operation.

1.6 Organization of the Dissertation

The introduction of the inverse dynamics concept, the development of the theory, its relationship to optimum control, and the design procedures are given in Chapter 2. This section provides closed-form solutions for a general problem.

In Chapter 3, a benchmark problem is considered that includes a typical reactor core model with multivariable control possibilities. The primary objective here is to test the RID control paradigm extensively to determine its performance characteristics. The simulation results are compared with a nonlinear optimum control method developed recently [20].

Three applications to nuclear reactor systems are considered in Chapter 4. These applications include the RID control designs for xenon oscillations in PWRs, feedwater train system of PWRs, and automated startup of the EBR-II. The simulation results are evaluated to determine if the RID control strategy improves the system operations.

Chapter 5 describes the inverse dynamics concept from a different perspective that leads to providing guidelines for strategy evaluation. The relationship with artificial intelligence is also considered. The discussion focuses on the possibility of incorporating expert systems and neural networks with the inverse dynamics approach to develop useful tools.

A summary of the dissertation is presented in Chapter 6, including theoretical and practical conclusions and suggestions for future research.

Chapter 2

Theory of Inverse Dynamics

2.1 Inverse Problems

Inverse problems appearing in various fields of applied sciences exhibit differences in mathematical formulation. Despite the variations, the similarities are significant enough to treat them as the same class of problems. The following describes basic definitions given in the literature [12].

Consider a mathematical model representing a physical process. Typical architecture consists of principal quantities such as input, system parameters, and output. The description of the process is often charaterized by a set of equations (ordinary and/or partial differential/integral equations) with bounded parameters.

The analysis of the given process via the mathematical model may be separated into three distinct types of problems.

(A) The *direct* problem. Given the input and the system parameters, determine the output of the model. Also known as the *forward* problem.

(B) The *reconstruction* problem. Given the system parameters and the output, determine which input has led to this output.

(C) The *identification* problem. Given the input and output, determine the system parameters which are in agreement with the relationship between input and output.

The problem of type (B) and (C) are called inverse problems because known consequences are used to determine unknown causes. The mathematical representation of the forward and inverse problems can be carried out by defining:

X = space of input quantities;

Y = space of output quantities;

$\mathfrak{R}$ = space of system parameters;

$A(p)$ = system operator from X into Y associated to $p \in \mathfrak{R}$.

Using the terminology above we can formulate the three types of problems.

(A) Given $x \in X$ and $p \in \mathfrak{R}$, find $y := A(p)x$.

(B) Given $y \in Y$ and $p \in \mathfrak{R}$, solve the equation

$$Ax = y \qquad (x \in X)$$

where $A := A(p)$

(C) Given $y \in Y$ and $x \in X$, find $p \in \mathfrak{R}$ such that

$$A(p)x = y.$$

The reconstruction problem for linear case, that is if A is a linear map, has been studied extensively and its theory is well-developed. The situation in the nonlinear case is somewhat less satisfactory. Linearization is very successful to find an acceptable solution to a nonlinear problem but in general this principle provides only a partial answer.

A typical example of the type **(B)** inverse problems consists of dynamic forces acting on a mechanical system. The problem statement is as follows.

> **Determine the unknown dynamic force having a measured vibration response of a system, whose parameters are considered to be known.**

Considering a one-degree-of freedom mechanical system, the dynamics may be described by the following ordinary differential equation

$$m\ddot{x}(t) + kx(t) = f(t) \tag{2.1}$$

where m and k are the mass and stiffness constant, respectively. The driving force $f(t)$, which is also considered as a control variable, can be solved provided the displacement measurement $x(t)$ exists and is twice differentiable.

$$f(t) = m\ddot{x}(t) + kx(t) \tag{2.2}$$

The solution would not work in practice if the measurement $x(t)$ is contaminated by noise ϑ for which the derivatives do not exist. Even if ϑ is regular enough $m\ddot{\vartheta}$ may be a highly oscillating function.

It is obvious that the existence and uniqueness are required for the solution of inverse problems. In parameter identification and signal reconstruction problems, stability is of major concern since unstable problems are ill-posed [11].

2.2 Dynamic Equilibrium of Control

Consider a process dynamics described by

$$\dot{x}(t) = \mathcal{F}[x(t), u(t)] \ , \ t > 0 \tag{2.3}$$

where x and u are state and control variables, respectively. Provided a solution exists, control is solved from the above to yield

$$u(t) = \mathcal{G}[x(t), \dot{x}(t)] \tag{2.4}$$

where $\mathcal{G}$ indicates the inverse dynamics with respect to the solution u. The existence of such a solution strictly depends on the explicit nature of $\mathcal{F}$. Note that Eq.(2.4) is the closed form of the inverse dynamics example of Eq.(2.2). The equilibrium of control for a given time t_0 is given by

$$u(t_0) = \mathcal{G}[x(t_0), \dot{x}(t_0) = 0] \tag{2.5}$$

The condition $\dot{x}(t_0) = 0$ represents a stable solution. In a similar fashion, a dynamic equilibrium of control is given by

$$u_{eq}(t) = \mathcal{G}[x(t), \dot{x}(t) = 0] \ , \ t > 0 \tag{2.6}$$

where u_{eq} denotes the dynamic equilibrium If $\mathcal{F}$ is a linear function of state and control variables, u_{eq} corresponds to the standard pole-zero cancellation method [15]. The dynamic equilibrium of control is used during various stages of control design.

2.3 State Reconstructing Inverse Control Law

The reconstruction principle defined by Baumeister [12] states that u_{eq} in Eq.(2.6) can be computed provided measurement $x(t)$ is available and $\mathcal{G}$ is known. It is known from the classical control theory that exact pole-zero cancellation is not possible in practice due to imperfect measurements and limited knowledge of $\mathcal{G}$. Thus, the primary goal in nonlinear control is to **find an appropriate reconstruction of u for the trajectory following case where the effect of imperfect measurements and partially unknown $\mathcal{G}$ are guaranteed to be insignificant for all practical purposes.**

Referring to Eq.(2.3), we define a new dynamics for the process which allows a trajectory following in a first-order-transport-lag (FOTL) fashion. The definition is given by

$$\dot{x}(t) = k[x_r(t) - x(t)] = E(t) \tag{2.7}$$

where k is an adjustable constant, x_r is the reference trajectory and $E(t)$ is the dynamic error in trajectory following. Then, the reconstruction problem may be

stated as follows:

$$\begin{gathered} \textit{Find } u(t) \textit{ such that } k[x_r(t) - x(t)] = \mathcal{F}[x(t), u(t)] \\ \textit{where } x(t) \textit{ is the solution of } \dot{x}(t) = k[x_r(t) - x(t)], \\ \textit{for } k > 0 \textit{ and } t > 0. \end{gathered}$$

Solution to the problem requires combining Eq.(2.3) with Eq.(2.7). Eliminating $\dot{x}(t)$ between these two equations gives

$$E(t) = \mathcal{F}[x(t), u(t)] \tag{2.8}$$

The reconstruction of $u(t)$ from the above requires "inverse" $\mathcal{G}$ such that

$$u(t) = \mathcal{G}[E(t), x(t)]. \tag{2.9}$$

Thus, Eq.(2.9) is the control design for a system described by Eq.(2.3) that requires the knowledge of $\mathcal{G}$ and measurement $x(t)$. The closed-loop dynamics can be found by substituting $u(t)$ in Eq.(2.3)

$$\dot{x}(t) = \mathcal{F}\{x(t), \mathcal{G}[E(t), x(t)]\} \tag{2.10}$$

which further reduces to

$$\dot{x}(t) = E(t) = k[x_r(t) - x(t)]$$

as defined in Eq.(2.7), because $\mathcal{G}$ is the inverse dynamics of the forward plant dynamics $\mathcal{F}$. Comparing controls given by Eq.(2.6) and Eq.(2.9), it can be interpreted that the latter is a dynamic equilibrium of control along the bounded trajectory $\dot{x}(t) = E(t)$ instead of $\dot{x}(t) = 0$.

2.3.1 Demand Law

The new plant behavior given by Eq.(2.7) does not accomplish an exact trajectory following due to the FOTL behavior. The plant lags k^{-1} seconds (or other time unit) behind the desired trajectory. There may be cases where the selection of k can not be made arbitrarily large. For small values of k, the delay may be undesirable according to procedures or other system specifications. Regardless of

the factors stated above, the RID design includes an exact compensation for the time delay.

The reference trajectory x_r used in Eq.(2.7) can be treated as the delayed version of the actual demand x_a. Similar to the definition of Eq.(2.7), a FOTL dynamics is defined between the actual demand and reference trajectory.

$$\dot{x}_a(t) = k[x_r(t) - x_a(t)] \tag{2.11}$$

Solving for the reference trajectory above yields

$$x_r(t) = \frac{1}{k}\dot{x}_a(t) + x_a(t) \tag{2.12}$$

Thus, a desired trajectory $x_a(t)$ is sent to the RID controller as $x_r(t)$ calculated from Eq.(2.12) which is k^{-1} seconds (or other time unit) ahead of the actual demand. Note that the factor k is the same as the one used in the RID design. As one can easily infer from the above, the effect of time-delay caused by the tuning parameter k can be fully compensated using Eq.(2.12) which is called the *demand-law*.

Another important issue is the achievability of the reference trajectories. They cannot be chosen arbitrarily because of the actuator constraints and safety limitations. The following illustrates a trajectory design for a given actuator constraint.

Consider a first-order system given by

$$\dot{x} = ax + u \tag{2.13}$$

The RID control law is given by

$$u = -ax + k(x_r - x) \tag{2.14}$$

where x_r is the reference trajectory. Assume that the trajectory is a ramp change

$$x_r(t) = mt \tag{2.15}$$

with a slope m. Suppose the control is constrained such that the rate of change in u per unit time must not exceed K_c. Then

$$|\dot{u}| \leq K_c \tag{2.16}$$

$$|-a\dot{x} + k\dot{x}_r - k\dot{x}| \leq K_c \tag{2.17}$$

$$|-(a+k)\dot{x} + k\dot{x}_r| \leq K_c \tag{2.18}$$

Since the relationships

$$\dot{x} \simeq \dot{x}_r \tag{2.19}$$

$$\dot{x}_r = m \tag{2.20}$$

are true, the slope can be determined by

$$|\,(-(a+k)+k)\,m\,| \leq K_c \tag{2.21}$$

$$m \leq \frac{K_c}{a} \tag{2.22}$$

Allthough the derivation above does not hold for higher-order systems, the properties of desired trajectories may be related to the constraints of a given problem. The construction of demands is completed by incorporating the demand law.

2.3.2 Existence

As one can infer easily, the existence of the closed form solution of control given by Eq.(2.9) depends strictly on $\mathcal{G}$, or equivelantly $\mathcal{F}$, which is a property of the system under consideration. However, under certain assumptions the existence can be guaranteed. The *implicit function theorem* [21] can be used for this purpose.

Implicit Function Theorem

Let $\Phi^1, \cdots, \Phi^m$ be of class $C^{(q)}$ on an open set D containing x_0, where $q \geq 1$ and $1 \leq m < n$. Assume that $\Phi(x_0) = 0$ and that the following holds:

$$\frac{\partial(\Phi^1, \cdots, \Phi^m)}{\partial(x^{r+1}, \cdots, x^n)} \neq 0 \quad at \;\; x_0. \tag{2.23}$$

Then there exists a neighborhood U of x_0, an open set $R \subset E^r$ containing $\hat{x}_0$, and functions $\phi^1, \cdots, \phi^m$ of class $C^{(q)}$ on R such that

$$\frac{\partial(\Phi^1, \cdots, \Phi^m)}{\partial(x^{r+1}, \cdots, x^n)} \neq 0 \quad \forall \; x \in U; \tag{2.24}$$

and

$$\{x \in U : \Phi(x) = 0\} = \{x \in U : \hat{x} \in R, x^{r+1} = \phi^l(\hat{x}) \quad \forall \ l = 1, \cdots, m\}. \tag{2.25}$$

Proof of this theorem is given in the literature [21]. The implicit function theorem simply states that within some neighborhood of a fixed value of the control u and state variable x, the existence can be guaranteed. Rewritting Eq.(2.8) (omit time dependence for simplicity)

$$E = \mathcal{F}(x, u)$$

we can define a new function

$$\Psi(x, u, E) = \mathcal{F}(x, u) - E = 0 \tag{2.26}$$

Then the implicit function theorem can be applied to $\Psi(x, u, E)$.

If there exist some neighborhood of x_0 *and* u_0 *such that*
$\Psi(x_0, u_0, E_0) = 0$ and $\partial\Psi/\partial u$ exists
then there is an open set $\mathcal{E}$, *with* $x_0 \in \mathcal{E}$ *and a function:*
$\tilde{u} : \mathcal{E} \rightarrow U$ with
$\Psi[x, \tilde{u}(x)] = 0$ for all $x \in \mathcal{E}$

2.4 Feasibility of Control

It is of primary importance to state the conditions under which the control given by Eq. (2.9) is valid. There are two conditions associated with this approach. First, reconstruction of $u(t)$ requires the measurement $x(t)$ to be available and regular. Second, the inverse dynamics design $\mathcal{G}$ must be an exact-inverse of the forward dynamics of the process $\mathcal{F}$. However, as it will be explained later, these conditions are flexible enough to be satisfied by some adaptive techniques (some conditions are inherently flexible that may not require adaptation) yielding robust performance.

2.4.1 Measurement Problems

Even though there is no differentiation of $x(t)$ required in Eq. (2.9), noise contamination may still deteriorate the closed-loop performance. There are several

methods to handle noise problems, one of which simply suggests using a model-based estimation $\hat{x}(t)$. Availability of measurements from a process may be another limitation. It is clear that the inverse control law strictly depends on a unique set of measurements for single-input single-output (SISO) systems. Thus, the flexibility of selecting process signals encountered in many standard control methods does not apply here. Although there may be multiple solutions of the inverse control law for multi-input multi-output (MIMO) systems, state variables not available as measurements might be unavoidable. The problems stated above suggest that the RID control law be implemented as a model-reference technique when it includes several unmeasurable system parameters.

2.4.2 Inexact Inverse Dynamics

The closed-loop system dynamics given by Eq.(2.10) does not reduce to the definition given by Eq.(2.7) if the design knowledge of $\mathcal{G}$ is not the exact inverse of the forward dynamics $\mathcal{F}$. In such cases, the closed-loop system is not expected to follow the desired trajectory $x_r(t)$ in a first-order transport-lag (FOTL) fashion and the resultant dynamic behavior is unknown. The FOTL is a linear dynamics with a left-plane pole determined by k. Thus, it is asymptotically stable for any positive k. Departure from the FOTL behavior may result in stability problems.

The uncertainties in the inverse function $\mathcal{G}$ can be compensated by an adaptive solution. However, it is important to investigate the effect of such uncertainties on the closed-loop system behavior before incorporating any adaptive features. For simplicity, consider a linear system given by

$$\dot{\underline{x}} = \mathbf{A}_p\underline{x} + \mathbf{B}_p\underline{u} \tag{2.27}$$

$$\underline{y} = \mathbf{C}\underline{x} \tag{2.28}$$

where $\mathbf{A}_p$ and $\mathbf{B}_p$ are the plant parameters.

Assume $\mathbf{B}_p^{-1}$ exists and all measurements available (i.e. $\mathbf{C} = I$), then the trajectory following control $u(t)$ is solved from Eq.(2.27),

$$\underline{u} = \mathbf{B}_p^{-1}\dot{\underline{x}} - \mathbf{B}_p^{-1}\mathbf{A}_p\underline{x}$$

Using the definition of Eq.(2.7),

$$\dot{\underline{x}} = \mathbf{K}(\underline{x}_r - \underline{x})$$

the control $\underline{u}$ is rewritten as

$$\underline{u} = \mathbf{B}_p^{-1}\mathbf{K}(\underline{x}_r - \underline{x}) - \mathbf{B}_p^{-1}\mathbf{A}_p\underline{x} \tag{2.29}$$

where $\mathbf{K}$ is a diagonal, positive-definite gain matrix and $\underline{x}_r$ is the trajectory vector. Note that the reconstruction of $\underline{u}$ above uses available plant measurement vector $\underline{x}$. The system matrices $\mathbf{A}_p$ and $\mathbf{B}_p$ may not be exactly known. Thus, the control vector $\underline{u}$ above is reconstructed using the best design parameters.

$$\underline{u} = \mathbf{B}_m^{-1}\mathbf{K}(\underline{x}_r - \underline{x}) - \mathbf{B}_m^{-1}\mathbf{A}_m\underline{x} \tag{2.30}$$

The matrices $\mathbf{A}_m$ and $\mathbf{B}_m$ are the estimates of the system matrices $\mathbf{A}_p$ and $\mathbf{B}_p$. Substituting Eq.(2.30) into Eq.(2.27) gives the closed-loop dynamics.

$$\dot{\underline{x}} = \mathbf{A}_p\underline{x} - \mathbf{B}_p\mathbf{B}_m^{-1}\mathbf{A}_m\underline{x} - \mathbf{B}_p\mathbf{B}_m^{-1}\mathbf{K}\underline{x} + \mathbf{B}_p\mathbf{B}_m^{-1}\mathbf{K}\underline{x}_r$$

$$\dot{\underline{x}} = (\mathbf{A}_p - \mathbf{B}_p\mathbf{B}_m^{-1}\mathbf{A}_m - \mathbf{B}_p\mathbf{B}_m^{-1}\mathbf{K})\underline{x} + \mathbf{B}_p\mathbf{B}_m^{-1}\mathbf{K}\underline{x}_r \tag{2.31}$$

Define the following

$$\Delta\mathbf{A} = \mathbf{A}_p - \mathbf{B}_p\mathbf{B}_m^{-1}\mathbf{A}_m \tag{2.32}$$

$$\mathbf{K}^* = \mathbf{B}_p\mathbf{B}_m^{-1}\mathbf{K} \tag{2.33}$$

$$\underline{f} = \mathbf{B}_p\mathbf{B}_m^{-1}\mathbf{K}\underline{x}_r \tag{2.34}$$

Then the closed-loop dynamics is rewritten as

$$\dot{\underline{x}} = (\Delta\mathbf{A} - \mathbf{K}^*)\underline{x} + \underline{f}. \tag{2.35}$$

It is clear from the last equation that the uncertainty $\Delta\mathbf{A}$ induces instability for positive eigenvalues. However, all of the closed-loop poles can be pushed into the left-plane by increasing $\mathbf{K}^*$. In practical applications, the choice of $\mathbf{K}$ matrix largely compensates for the effect of such uncertainties.

Definition:

An $n \times n$ matrix $A = (a_{i,j})$ is diagonally dominant if

$$| a_{i,i} | \geq \sum_{\substack{j=1 \\ j \neq i}}^{n} | a_{i,j} | = \Lambda_i \tag{2.36}$$

for all $1 \leq i \leq n$. An $n \times n$ matrix A is strictly diagonally dominant (SDD) if strict inequality in Eq.(2.36) is valid for all $1 \leq i \leq n$ [22].

Theorem: [22]

Let $A = (a_{i,j})$ be an $n \times n$ strictly diagonally dominant complex matrix. Then the matrix A is nonsingular. If all the diagonal entries of A are in addition negative real numbers, then the eigenvalues λ_i of A satisfy

$$Re\, \lambda_i < 0, \qquad 1 \leq i \leq n \tag{2.37}$$

Since a Hermitian matrix has real eigenvalues, we have an immediate consequence of this theorem.

Corollary: [22]

If $A = (a_{i,j})$ is a Hermitian $n \times n$ strictly diagonally dominant matrix with negative real diagonal entries, then A is negative definite.

Using the matrix properties stated above, the stability condition of the closed-loop matrix $\Delta\mathbf{A} - \mathbf{K}^*$ can be investigated. First consider the input uncertainty matrix $\mathbf{B}_p\mathbf{B}_m^{-1}$. For all practical purposes, the input uncertainty matrix will be close to an identity matrix with small off-diagonal elements. Thus, we assume that modeling error in $\mathbf{B}_p$ is within some tolerable range such that the matrix norm

$$\| \mathbf{I} - \mathbf{B}_p\mathbf{B}_m^{-1} \| \leq \epsilon \tag{2.38}$$

is satisfied for small ϵ and $\mathbf{B}_p\mathbf{B}_m^{-1}$ is positive definite. Then $\mathbf{B}_p\mathbf{B}_m^{-1}\mathbf{K} = \mathbf{K}^*$ is strictly diagonally dominant. The same argument is valid for the plant uncertainty matrix $\Delta\mathbf{A}$. Note that the modeling error between $\mathbf{A}_p$ and $\mathbf{A}_m$ is magnified by the input uncertainty matrix. Because $\Delta\mathbf{A}$ reflects this magnification, the tolerable

error condition can be restated in a conservative way as

$$\| \Delta \mathbf{A} \| \leq \| \mathbf{A}_m \| \tag{2.39}$$

which roughly implies an error range of almost 100 %. Then the stability robustness condition can be given by

$$\| \mathbf{K} \| \gg \| \mathbf{A}_m \| \tag{2.40}$$

which, for all practical purposes, can be restated as

$$k_{i,i} \gg \sum_{j=1}^{n} | a_{i,j} | \tag{2.41}$$

where $a_{i,j}$ are the elements of the $(n \times n)$ design matrix $\mathbf{A}_m$.

The discussion above shows the robustness property of the "inverse" method against possible uncertainties in modeling. Recall that the above illustration is valid for the special case where (1) the measurement vector $\underline{x}$ is available, (2) system dynamics is linear, (3) system matrices are time-invariant, and (4) no adaptive design is incorporated. A similar illustration of the stability-robustness property for nonlinear systems strictly depends on the explicit nature of the forward dynamics $\mathcal{F}$ of Eq.(2.3) and cannot be easily developed using analytical methods.

2.5 Adaptive Control

The RID control law given by Eq.(2.9) operates on the measurement vector $\underline{x}$ in a unique form defined by the inverse dynamics operator $\mathcal{G}$ which yields a feedback-control structure shown in Fig. 2.1. As described in the previous section, the two possible problems (1) corrupted or lack of measurements, and (2) inexact operator $\mathcal{G}$ may deteriorate the closed-loop performance. Therefore, a model-reference adaptive method is employed. Both the problems stated above can be handled by incorporating an on-line model where the state variables are estimated. Only the estimation of unmeasurable state variables is required. Figure 2.2 illustrates the use of an on-line model for this purpose.

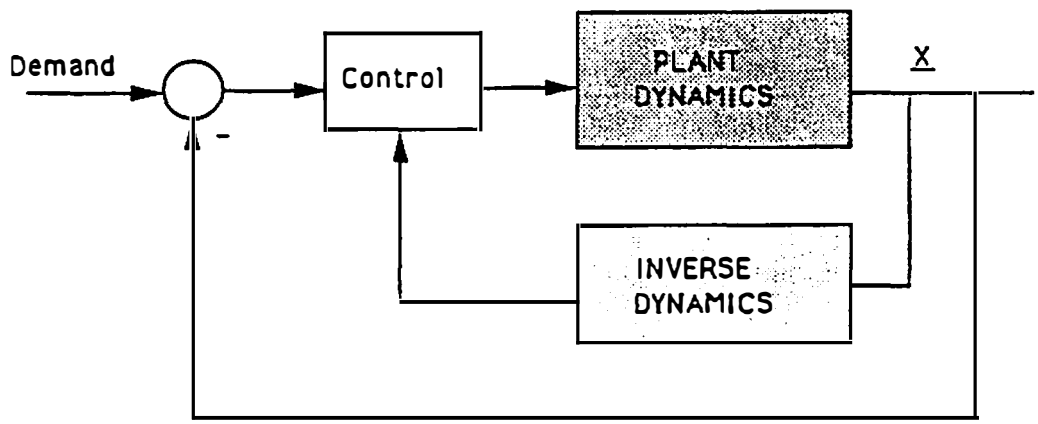

Figure 2.1: Feedback arrangement of inverse dynamics control.

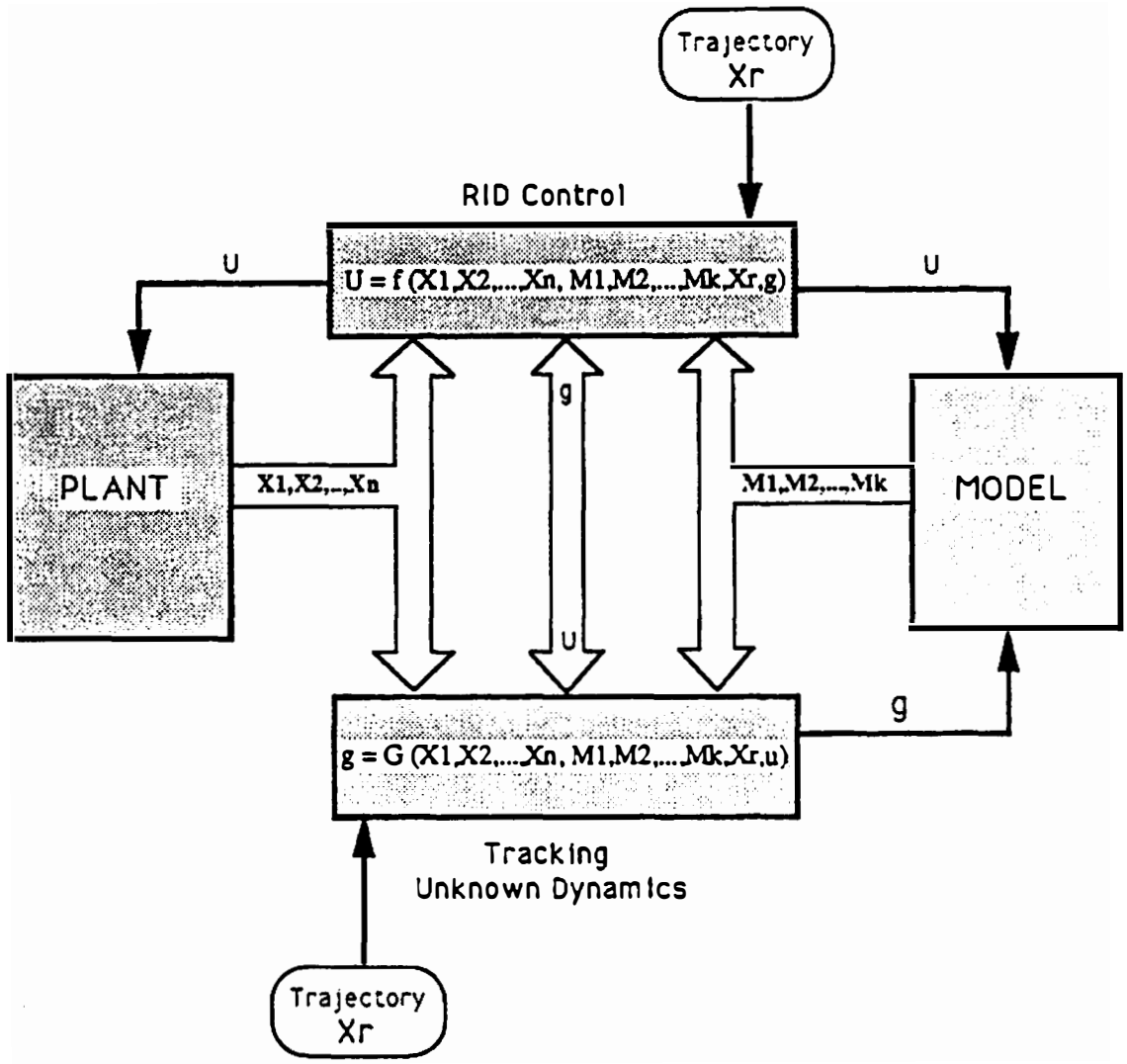

Figure 2.2: Use of on-line model in RID control.

Uncertainties such as modeling errors, time-variant plant parameters, and unanticipated disturbances can be represented by a variable g, called "unknown dynamics". Therefore, solution of the uncertainty problem reduces to tracking of g by some adaptive mechanism. Reconsider the nonlinear process given by Eq.(2.3)

$$\dot{x} = \mathcal{F}_x(x, u) \tag{2.42}$$

where $\mathcal{F}_x$ is partially unknown. Tracking of the unknown dynamics requires an on-line model given by

$$\dot{m} = \mathcal{F}_m(m, u, g) \tag{2.43}$$

where g is the unknown dynamics. The process dynamics in Eq.(2.42) which is measured through x can be considered as a reference trajectory to be followed by the model. If a particular state variable x is not available as a measurement, a substitute (auxiliary state) can be used. This is illustrated in the next section. Thus, the statement of the tracking problem is identical to that of the trajectory following control problem. First define a FOTL dynamics

$$\dot{m}(t) = k[x(t) - m(t)] = E(t) \tag{2.44}$$

where k is an adjustable quantity, and $x(t)$ is the measurement. The reconstruction of g may be stated as follows:

$$\begin{gathered} \textit{Find } g(t) \textit{ such that } k[x(t) - m(t)] = \mathcal{F}_m[m(t), u(t), g(t)] \\ \textit{where } m(t) \textit{ is the solution of } \dot{m}(t) = k[x(t) - m(t)] \\ \textit{for } k > 0 \textit{ and } t > 0. \end{gathered}$$

Note that the treatment of g is identical to any control variable u. Solution to the problem requires combining Eq.(2.43) with Eq.(2.44). Eliminating $\dot{m}(t)$ between these two equations yields

$$E(t) = \mathcal{F}_m[m(t), u(t), g(t)]. \tag{2.45}$$

The reconstruction of $g(t)$ from above requires "inverse" $\mathcal{G}_m$ such that

$$g(t) = \mathcal{G}_m[E(t), m(t), u(t)] \tag{2.46}$$

The model is corrected by $g(t)$ such that it follows the plant dynamics with k^{-1} seconds (or other time units) time delay. The demand law can be applied to compensate the delay. In this case, the actual measurement $x_a(t)$ is used to calculate the "reference" measurement $x(t)$.

$$x(t) = \frac{1}{k}\dot{x}_a(t) + x_a(t) \tag{2.47}$$

The actual measurement must be noise free.

2.6 Auxiliary States

The design of the RID control law depends on the distribution of control variables versus trajectory assignments. In some cases, a reference trajectory may be assigned to a state equation where there is no direct entry of control.

$$\dot{x}_1(t) = \mathcal{F}_1[x_1(t), x_2(t)] \quad , \quad x_1(t) \overset{follow}{\Rightarrow} x_r(t) \tag{2.48}$$

Assume there exists a coupled system with a direct entry of control.

$$\dot{x}_2(t) = \mathcal{F}_2[x_1(t), x_2(t), u(t)] \tag{2.49}$$

such that the coupled system is controllable. Solution to the trajectory following control problem requires an additional reconstruction through an auxiliary state. The statement of the problem can be made as follows.

Find an auxiliary state $x_2^*(t)$ *such that* $k_1[x_r(t) - x_1(t)] = \mathcal{F}_1[x_1(t), x_2^*(t)]$
where $x_1(t)$ *is the solution of* $\dot{x}_1 = k_1[x_r(t) - x_1(t)]$
then, find $u(t)$ *such that* $k_2[x_2^*(t) - x_2(t)] = \mathcal{F}_2[x_1(t), x_2(t), u(t)]$
where $x_2(t)$ *is the solution of* $\dot{x}_2 = k_2[x_2^*(t) - x_2(t)]$
for $k_1 > 0$, $k_2 > 0$ *and* $t > 0$.

Solution to this problem can be found using the implicit function theorem within some fixed neighborhood of u_0, x_{10}, x_{20}, and x_{20}^*. If an explicit solution exists outside this neighborhood, it requires two "inverse" operators $\mathcal{G}_1$ and $\mathcal{G}_2$. The auxiliary state x_2^* is solved from Eq.(2.48).

$$x_2^*(t) = \mathcal{G}_1[x_1(t), \dot{x}_1(t)]. \tag{2.50}$$

Similarly the control $u(t)$ is solved from Eq.(2.49).

$$u(t) = \mathcal{G}_2[x_1(t), x_2(t), \dot{x}_2(t)]. \tag{2.51}$$

The derivatives are replaced by the dynamic errors given by

$$\dot{x}_1(t) = k_1[x_r(t) - x_1(t)] \tag{2.52}$$

$$\dot{x}_2(t) = k_2[x_2^*(t) - x_2(t)] \tag{2.53}$$

The set of equations (2.50-2.53) complete the RID control law.

The use of auxiliary states may be extended to include more coupled systems and more "inverse" operators. In the MIMO case, there may be more than one "inverse" operator to satisfy the same trajectory following task. Unlike in many other control techniques, the abundance of control alternatives is a very useful information and can be used to determine the best strategy (see Chap. 5). In general, the choice of the best strategy depends on the specifics of the system. The auxiliary states can also be used for the adaptive part of the design. As a rule of thumb, the number of trajectory assignments must not exceed the number of control variables. This is not a specific requirement of the RID design since it applies to every control design technique.

2.7 Comparison with Optimal Control

The optimal control theory is well developed for linear systems such as the linear quadratic regulator (LQR), linear quadratic Gaussian compensator (LQG) [16] with Kalman filtering, and the loop-transfer recovery method LQR/LTR for robust control [23]. On the other hand the nonlinear optimal control theory encounters several problems due to the complex nature of nonlinear system dynamics. Recent studies have dealt with the classical dilemma of two-point boundary value problem [24]. However, the assumptions made often conflict with the optimality criteria. Although the RID control is very powerful in the nonlinear domain, there are no strong theoretical foundations to compare the two approaches using analytical methods. In the nonlinear domain, Lagrangian Derivation of Optimal Control (LDOC) method [20] is compared with the RID control using numerical methods. The details are included in Chapter-III.

2.7.1 Inverse Dynamics Component of the LQR

Consider the Linear Quadratic Regulator (LQR) problem for a first order system

$$\dot{x} = ax + bu \quad , \quad x(0) = x_0 \tag{2.54}$$

with

$$J = \int_t^{\infty} (x^2 + \rho^2 u^2) d\tau \tag{2.55}$$

where J is the cost function ρ is the control weight, respectively. The scalar gain g is given by

$$g = \frac{b\,m}{\rho^2} \tag{2.56}$$

where m is the positive root of the algebraic Ricatti equation

$$2am - \frac{b^2 m^2}{\rho^2} + 1 = 0 \tag{2.57}$$

The two roots of the quadratic equation are

$$m = \frac{\rho^2}{b^2}\left(a \pm \sqrt{a^2 + \frac{b^2}{\rho^2}}\right) \tag{2.58}$$

Since the radical is always greater than the absolute value of a, it is obvious that the positive sign is the only possible choice for $m > 0$ (condition for positive definite Ricatti matrix). The optimal gain is

$$g = \frac{1}{b}\left(a + \sqrt{a^2 + \frac{b^2}{\rho^2}}\right) \tag{2.59}$$

Then the optimal feedback control u_{op} is given by

$$u_{op} = -gx \tag{2.60}$$

$$u_{op} = -\left[\frac{1}{b}\left(a + \sqrt{a^2 + \frac{b^2}{\rho^2}}\right)\right] x \tag{2.61}$$

$$\tag{2.62}$$

The closed-loop system dynamics using the optimal feedback control reduces to

$$\dot{x} = ax - b\,gx \tag{2.63}$$

$$\dot{x} = ax - ax - \left(\sqrt{a^2 + \frac{b^2}{\rho^2}}\right) x \tag{2.64}$$

$$\dot{x} = -\left(\sqrt{a^2 + \frac{b^2}{\rho^2}}\right) x \tag{2.65}$$

The regulation problem with the RID design assumes the trajectory x_r to represent the steady-state value of x. Using the state-space representation with x being a deviation from the steady-state, the regulation problem requires $x_r = 0$. The control u_{rid} is given by

$$u_{rid} = -\frac{1}{b}(ax + kx) \tag{2.66}$$

where k is an adjustable quantity. The closed-loop system can be stated as

$$\dot{x} = ax - b\left[\frac{1}{b}(ax + kx)\right]$$

which reduces to

$$\dot{x} = ax - ax - kx = -kx \tag{2.67}$$

The second term $-ax$ of the last equation, which is the *inverse dynamics* component of the RID control, cancels the forward dynamics ax yielding a simple dynamics $-kx$. It is interesting that the closed-loop system using the optimum control given in Eq.(2.64) has an identical cancellation $ax - ax$. Thus, it is concluded that **the LQR control contains an inverse component $\mathcal{G}(x)$ for the regulation problem of first-order systems.** The control laws using both techniques can be restated in the following manner.

$$u_{LQR} = \underbrace{-(a/b)\,x}_{\mathcal{G}(x)} - \underbrace{(1/b)\sqrt{a^2 + b^2/\rho^2}}_{K_{op}}\,x \tag{2.68}$$

$$u_{RID} = \underbrace{-(a/b)\,x}_{\mathcal{G}(x)} - \underbrace{(1/b)k}_{K_{rid}}\,x \tag{2.69}$$

Obviously, the optimal control is the combination of the two components of u_{LQR}. Note that the inverse operator $\mathcal{G}$ as one of the components of u_{LQR} does not depend on the weight ρ. This illustrates the importance of the inverse operator for the optimality condition.

The linear quadratic regulator problem can be converted into a trajectory following control problem by applying the gain K_{op} to the reference input. This creates a FOTL dynamics identical to that of the RID control. Thus the reference trajectory must be filtered through the demand law. The LQR control law is given by

$$u_{LQR} = -(a/b)x - K_{op}x + K_{op}x_r \tag{2.70}$$

$$K_{op} = \sqrt{a + b^2/\rho^2} \tag{2.71}$$

$$x_r = \left(\frac{1}{K_{op}}\right)\dot{x}_a + x_a \tag{2.72}$$

where x_a and x_r are the actual and reference trajectories, respectively.

2.7.2 Optimality and Asymptotic Behavior

An optimum k for the RID design can be found by the condition $u_{LQR} = u_{RID}$ in Eqs. (2.68-2.69)

$$K_{rid} = K_{op} \tag{2.73}$$

$$k = \sqrt{a + b^2/\rho^2} \tag{2.74}$$

Since ρ and k both are adjustable quantities, the solutions are equally optimal only for the arbitrary choices of these parameters. However, the weight ρ is not entirely an arbitrary choice because it represents the "cost" of control. Similarly, we can conclude that k also respresents the "cost" of control but in the reverse direction. That is, k is small for a high cost of control.

The asymptotic properties of the optimal control law can be examined in comparison to the RID control law.

> *"As the control weighting ρ^2 tends to zero (i.e. the control becomes increasingly " cheap") the closed-loop pole moves out to infinity along the negative real axis as b/ρ. The feedback gain becomes infinite as does the bandwith of the system. This is entirely reasonable."* [16].

It is seen from Eq.(2.74) that as ρ^2 tends to zero, the RID solution with large values of k approaches that of the LQR.

$$\lim_{\rho \to 0} k = \infty \tag{2.75}$$

$$u_{RID} \cong u_{LQR} \tag{2.76}$$

Thus, if k is chosen to be large (cheap control), its performance approaches that of the LQR with a small weight. Note that large k corresponds to a small delay between the trajectory and plant responses for the trajectory following case.

"As the weight ρ^2 tends to ∞ (i.e. the control becomes increasingly "expensive") the closed-loop pole tends to $-\mid a \mid$. If $a < 0$ (i.e., the open-loop system is asymptotically stable) then $a_c \rightarrow a$ as the control gain $g \rightarrow 0$. This again is reasonable. If control costs a great deal, its usage must be minimized. This strategy is obviously unsatisfactory when $a > 0$ (i.e., open-loop system is unstable). In this case $a_c \rightarrow -a$ and the gain $g \rightarrow 2a$ which results in high cost of control." [16].

Considering a first order system, it is easier to show the stability robustness characteristics of the RID control. Theoretically, $ax - ax$ cancellation solves the instability problem. A problem would arise when the parameter a of the controller is mistakenly different from the plant parameter a. In such a case, Δa may be positive resulting in instability. Then, the closed-loop system is given by

$$\dot{x} = (\Delta a - k)x \tag{2.77}$$

If there is no restriction on k, large values will yield a negative eigenvalue and restore stability. When Δa is positive and k is strongly restricted (i.e. expensive control, actuator limitations) the stability becomes more dependent on modeling errors. However, the auxiliary states method allows different strategies with cheaper cost of control (larger k).

The question of "to what extent do the results for a first-order system carry over to a general k*th* order system" was studied by Kalman [25] and Kwakernaak [26]. The discussions above also hold for a k*th* order system except for the effect of zeros which complicates the analysis. This is mainly due to the dependence between the regulator gain vector and the system matrices. It is obvious that the asymptotic behavior of the RID control is not significantly affected by the open-loop zeros since the inverse operator cancels the forward dynamics.

2.7.3 Implementing LQR versus RID control

The solution of the linear quadratic regulator problem for a kth order system requires a cost function given by

$$J_\infty = \int_t^\infty (x'Qx + u'Ru)d\tau \tag{2.78}$$

where Q and R are state and input weight matrices, respectively. For an infinite terminal time

$$J_\infty = x'\bar{M}x \tag{2.79}$$

where $\bar{M}$ satisfies the algebraic Riccati equation (ARE)

$$0 = \bar{M}A + A'\bar{M} - \bar{M}BR^{-1}B'\bar{M} + Q \tag{2.80}$$

and the optimum gain at steady state is given by

$$\bar{G} = R^{-1}B'\bar{M} \tag{2.81}$$

The matrix equation (2.80) represents a set of $k(k+1)/2$ coupled scalar quadratic equations. Because each quadratic equation in the set has two solutions, the total number of solutions is $k(k+1)$.

The algebraic Riccati equation has a unique, positive definite solution $\bar{M}$ which minimizes J_∞ when the control law $u = -BR^{-1}\bar{M}x$ is used. This solution depends on (1) the stability of the open-loop system, and (2) the controllability and observability of the system defined by A, B, C. Thus, if the above conditions are satisfied, one of the $k(k+1)$ solutions (not more than one) is positive-definite.

Establishing which of the solutions of the Riccati equation, if any, is the correct one imposes great difficulty because in most practical cases, the equation must be solved numerically and the numerical problem is not an easy one. A computer algorithm may not iterate to the correct solution. So it is important to determine whether the sought-after solution exists before trying iterative techniques.

The effort for finding an optimum solution may be unreasonable, especially for large-scale systems. In practice, the plant parameters are time-variant which

would require the computation to be performed in an on-line computer. This may cause problems in real-time solutions. It is obvious that the RID control does not include any iterative algorithm. If an on-line model is required, large values of k may result in a stiff model. Although there are efficient stiff-system solvers, real-time problems may arise. This problem can be resolved by a proper tuning of k at the design stage.

2.8 RID Control Design Steps

The RID design requires reasonably adequate knowledge of the dynamics of the system under consideration. Although the RID method yields very robust control strategies against modeling errors, accurate modeling facilitates the task of the adaptive part and improves the robustness against other types of anomalies. The second reason for an accurate model is related to testing. These tests would not yield reliable results unless a set of previously recorded plant data is available. The design includes the following steps.

1. Modeling: A nonlinear model must be developed using the state space representation. The model should include all of the known nonlinearities as well as the uncertainties. For example, the thermal-hydraulic modeling often suffers from the complicated nature of heat-transfer coefficients. In such cases, the nonlinearities can be formulated using the best available knowledge, then an uncertainty term may be incorporated. These uncertainty terms play an important role later during the adaptive design.

2. Control Law Derivation: Using the nonlinear model, the control law is derived (provided a solution exists) as shown in Eqs.(2.7), (2.9), (2.50-2.53). These solutions do not include adaptive control, but they may include the uncertain terms. The analytical derivations should be carried out even if there are more than one solution to satisfy a given demand. The abundance of solutions can be a great benefit in select-

ing the best strategy. The derivation step is completed by assessing which state variables are not available as measurements. If any, then an on-line model is appended to the control law in order to provide the estimations of those missing state variables.

3. Dynamic Equilibrium Testing(DET): The RID control law contains two components. (1) inverse dynamics, and (2) state reconstruction using dynamic error of Eq.(2.7). The DET requires the second component to be zero. Thus, the RID control law without the state reconstruction must yield the dynamic equilibrium of control. The uncertainty terms should be set to 1 or zero (whichever ignores the uncertainty). The test is implemented using a previously recorded transient data from the process. An independent model of the process is driven by the RID control law (without the 2nd component) both of which utilize previous plant signals. The missing states, if any, are provided from the model. The DET must result in a steady-state behavior, otherwise the inverse dynamics $\mathcal{G}$ is not appropriately designed. Engineering judgement may be used to determine the tolerable amount of unsteady-state DET output which can be compensated by the adaptive design. For MIMO control, the DET outputs clearly indicate which uncertainty terms must have a significant contribution to the unsteady-state DET output.

4. Best Strategy Selection: This step is taken if there are multiple solutions for a given demand. For example; consider three pipes in parallel that drain liquid from the same tank. If there are three valves incorporated within these pipes, the tank level controller can use any one of the valves or all of them. The DET outputs from the multiple control laws can be evaluated to determine which inverse dynamics is more accurately known. Other factors can include the availability of measurements and the actuator constraints. As one can infer from this discussion, the cost of control is partially (if not completely) determined by the DET. Thus the solution with a minimum cost must be

selected.

5. Adaptive Design: Once the DET outputs are evaluated to identify the most significant uncertainties, the adaptive control is derived using Eq.(2.47). The uncertain terms of the on-line model are updated by the adaptive control law.

6. Demand Construction: Control tasks are often specified in terms of trajectories. Set-point requirements can also be represented using steady-state trajectories. If there is no specific reason for the step change requirement, a set-point change is converted into a ramp change such that the steepness of its slope can be adjusted. The desired trajectories must be evaluated to determine if they are "achievable".

7. Tuning: This step includes simulation studies where the complete RID control design is appended to the model. Tuning is a straight forward task because the Ks are one directional (only positive values). As a rule of thumb, large values of K yield better performance. There are two restrictions: (1) the cost of control, and (2) the stiffness condition of the on-line model, if used. The tuning takes place mainly to resolve these issues.

8. Final Testing: The final step uses the model in a modified manner. The model parameters (previously assumed constant) are made time variant to test the robustness of the RID controller. Accordingly, the tuning is updated. This test may also include verifying the disturbance rejection capability and robustness against unknown dynamics.

Chapter 3

Performance Characteristics

3.1 Framework for Evaluation

A systematic approach needs to be taken to evaluate a control technique and to study the feasibility of implementing it in a plant. The classical time/frequency domain performance characteristics convey meaningful information, however further evaluation may be necessary to determine the feasibility in a broader sense. Particularly in nonlinear control, the classical measures may not be applicable or adequate for a complete performance evaluation. A previous study [27] has introduced the concept of *measures of utility*, which defines various performance factors. These factors include classical time-domain and frequency-domain characteristics as well as more specific "process-related" requirements. A new control strategy may be considered as feasible if all the measures of utilities are examined and found to be satisfactory. As expected, a new control method may be feasible for one process, but not for another. This fact justifies the necessity of the process-related performance factors. The measures of performance (or utilities) are shown in Fig. 3.1.

a)- *TIME-DOMAIN PERFORMANCE*

b)- *FREQUENCY-DOMAIN PERFORMANCE*

c)- *ROBUSTNESS*

- *Additive Noise*
- *Process Parameter Variation*
- *Sensor and Actuator Failure*

d)- *DOWNSTREAM EFFECTS*

e)- *ABILITY TO TUNE IN THE FIELD*

f)- *ABILITY TO CONVEY MEANINGFUL INFORMATION*

- *Explanation of Controller Actions*
- *Observation of Unmeasurable States*
- *Tracking of Plant Parameters*

g)- *USER UNDERSTANDABILITY*

- *Complexity*

h)- *RESOURCE REQUIREMENTS*

- *Real-time Computational Requirements*
- *Sensor Count and Accuracy Requirements*

Figure 3.1: Measures of Utilities

Control system performance can be evaluated by measuring rise time, overshoot, settling time, and integral square error. Generally, closed-loop systems should exhibit less than 30 % overshoot to a step change in set point. Graphical techniques are mainstay of frequency-domain analysis. Examples include Bode plot, Nyquist plot, root-locus and Nichols chart. From the Bode plot, stability measures such as gain and phase margins are calculated. For SISO systems, a 45 degree phase margin and 6-12 db gain margins are desired. The classic definition of a robust system is one which is insensitive to bounded plant parameter variations, disturbances, noise, sensor failures, and design (modeling) errors. Dowstream effects include actuator integrity and wear-out. Control strategy must minimize the actuator usage and eliminate stress factors (mechanical, electrical, thermal, chemical, and radiation). Ability to tune in the field is another requirement that must be satisfied. The control of large-scale systems requires more information from a controller than what the conventional controllers offer. Explanation of controller actions, observation of unmeasurable states, and tracking uncertain parameters are important information for operators. The availability of such information can improve the reliability of control systems. Other requirements may be associated with the complexity of control systems. New strategies should invoke an interface capability which provides communication with operators on a continuous basis. Such an interface must facilitate operator's understanding of the control system. Resource requirements determine the feasibility from the hardware point of view. This includes computations faster than real-time, and suitability between the control and measurement systems.

3.2 A Benchmark Problem

The performance evaluation using the criteria stated above cannot be easily assessed unless the system is defined. This is due to some performance factors that would have different importance from one process to another. In addition, the theory behind the RID yields a unique control law for every different system, and its evaluation is limited using a generalized analytical method. Thus, a benchmark problem is considered that represents some basic nuclear phenomena with a variety of control problems. The problem is formulated to cover a maximum number of

performance issues using a simple nonlinear model.

3.2.1 Modeling the Benchmark Problem

A nonlinear, state-space model has been previously developed to represent a compact, high power density nuclear reactor [28]. The plant is modeled by a point kinetics model with a single group of delayed neutrons and fuel and coolant temperature feedback terms. Enthalpy balances in the core and coolant lumps determine the core and coolant temperatures as a function of the inlet coolant temperature and the coolant flow rate. Power P_1 and delayed neutron concentration P_2 are normalized to their respective equilibrium values, whereas fuel temperature P_3 and average coolant temperature P_4 are normalized at the steady-state value of the inlet temperature. The plant dynamics is described by the following set of equations:

$$\dot{P}_1 = \frac{1}{\lambda_g^p}[(U_1 - 1)P_1 + P_2] - [\alpha_c^p(P_4 - P_{40}) + \alpha_f^p(P_3 - P_{30})]P_1 \quad (3.1)$$

$$\dot{P}_2 = \lambda_d^p(P_1 - P_2) \quad (3.2)$$

$$\dot{P}_3 = \lambda_p^p P_1 - \lambda_f^p(P_3 - P_4) \quad (3.3)$$

$$\dot{P}_4 = \lambda_c^p(P_3 - P_4) - U_4\lambda_r^p(P_4 - 1) \quad (3.4)$$

where

$U_1 \equiv$ Reactivity control,
$U_4 \equiv$ Flow control,
$\alpha_{c,f}^p, \lambda_{s,c,p,f,d,r}^p \equiv$ Parameters of the plant.

It is necessary to use a duplicate model to study the robustness properties. The parameters of the original model (plant) can be disturbed externally whereas the duplicate model is isolated from such effects. The control system utilizes state estimation from the duplicate model. With this approach, it is possible to evaluate the robustness properties of control systems against unknown dynamics. The duplicate model is rewritten below using a new notation to indicate that it is the on-line state-estimator (model).

$$\dot{N}_1 = \frac{1}{\lambda_g^m}[(U_1 - 1)N_1 + N_2] - [\alpha_c^m(N_4 - N_{40}) + \alpha_f^m(N_3 - N_{30})]N_1 \quad (3.5)$$

$$\dot{N}_2 = \lambda_d^m(N_1 - N_2) \tag{3.6}$$

$$\dot{N}_3 = \lambda_p^m N_1 - \lambda_f^m(N_3 - N_4) \tag{3.7}$$

$$\dot{N}_4 = \lambda_c^m(N_3 - N_4) - U_4\lambda_r^m(N_4 - 1) \tag{3.8}$$

where

$N_1 \equiv$ Reactor power,
$N_2 \equiv$ Precursor concentration,
$N_3 \equiv$ Fuel temperature,
$N_4 \equiv$ Coolant temperature,
$\alpha_{c,f}^m, \lambda_{s,c,p,f,d,r}^m \equiv$ Parameters of the model.

Note that the model and plant, both are driven by controls U_1 and U_4.

It is assumed that the plant state variables, reactor power P_1 and coolant temperature P_4, are measured. The two remaining plant states, precursor concentration P_2 and fuel temperature P_3, are estimated using N_2 and N_3 of the on-line model.

3.2.2 Discrepancies Between the Plant and Model

The plant dynamics is deliberately made different from that of the model to simulate a realistic case. The control design is not modified accordingly, which would be the case in actual practice. However, the design incorporates adaptive features in which the primary task is to estimate changes in the plant and update the model and control. Using such a methodology, different robustness tests are performed by introducing different uncertainties in the plant. Referring to Eqs.(3.2-3.4), the plant equations are modified in the following manner:

$$\dot{P}_1 = \frac{1}{\lambda_s^p(t)}[(U_1 - 1)P_1 + P_2] - [\alpha_c^p(t)(P_4 - P_{40}) + \alpha_f^p(t)(P_3 - P_{30})]P_1 \tag{3.9}$$

$$\dot{P}_2 = \lambda_d^p(t)(P_1 - P_2) \tag{3.10}$$

$$\dot{P}_3 = \lambda_p^p(t)P_1 - \lambda_f^p(t)(P_3 - P_4) + \overbrace{A\cos(P_3 - P_1)f(t)}^{Unknown-dynamics} \tag{3.11}$$

$$\dot{P}_4 = \lambda_c^p(t)(P_3 - P_4) - U_4\lambda_r^p(t)(P_4 - 1) \tag{3.12}$$

The plant parameters $\lambda_i^p(t)$ and $\alpha_j^p(t)$,($i = 1, \cdots, 8$ and $j = 1, 2$) are made time variant whereas the model parameters λ_i^m and α_j^m are constant. The perturbations are given by

$$\lambda_i^p(t) = C_i t + Z_i cos(w_i t - \pi_i) \tag{3.13}$$

$$\alpha_j^p(t) = C_j t + Z_j cos(w_j t - \pi_j) \tag{3.14}$$

where $C_i, C_j, Z_i, Z_j, w_i, w_j, \pi_i$ and π_j are arbitrarily selected constants. Note that the arbitrary choices are within a normalized range so that the amount of perturbation can be assessed. In Eq.(3.11) an additional term is incorporated to represent unknown dynamics. The parameter A is a normalized arbitrary constant whereas $f(t)$ is a normalized arbitrary oscillation. The model does not include this information either. The unknown dynamics is incorporated in the third equation (fuel temperature) deliberately because it is not measurable. This is a very challenging task for the control and diagnostic systems. The simulation studies use the perturbed plant equations and unpertubed model equations.

The final form of the plant dynamics described by Eqs. (3.9-3.14) corresponds to a hypothetical case where the possibility of such discrepancies is almost impossible. Any plant behavior matching the one above would probably correspond to an accident situation. Consequently, if the control system can yield a reasonable performance under such circumstances, it can be considered "robust" for all practical purposes.

3.2.3 Control Problem Definition

A control task is described for the given system. It is assumed that the control task includes two trajectories (demands) to be followed, one for the reactor power and the other for the coolant temperature. The overall target is a power level increase of about 25 %. The trajectories designed for this scenario have two distinct parts.

The first part, which takes place during the first 100 seconds, includes a smooth power and coolant temperature increase. Obviously, it is expected that the power increase will require a positive reactivity input (control input-1). This input will

cause the fuel and coolant temperatures to increase, accordingly. However, this increase may not match the demand on the coolant temperature. The reactor coolant flow (control input-2) is expected to decrease such that the coolant resides longer in the active core region resulting in a higher coolant temperature to match the demand. Note that the model also includes the reactivity feedback phenomena.

The second part, which takes place between the 100 and 200 seconds, is employed to test the extended maneuvering capability of the controllers under investigation. The reactor power is lowered smoothly to a level higher than the initial value. This will require a negative reactivity input (control input-1). The coolant temperature, on the other hand, is required to maintain its level that is reached after the first 100 seconds. The effect of lowering reactor power will cause less heat production. Thus the coolant flow (control input-2) is expected to decrease again to prolong the residence time of the coolant in the core region.

The scenario described above requires reasonable reactivity and coolant flow adjustments, thus it can be considered practical for a power change operation from 75 % to 100 %. However, the time frame may be prolonged to avoid reaching actuator limits.

3.2.4 Performance Factors

The benchmark problem defined above is subjected to various performance tests to evaluate some of the feasibility characteristics of the RID control. Referring to the performance factors given in Fig 3.1, the scope of the framework is modified according to the specifics of the benchmark problem.

a) Time-domain analysis for a nonlinear, demand following
problem reduces to evaluating the error and time delay between the demand and plant transients. Since the demand is not a set-point, factors such as overshoot, rise-time and settling-time do not apply.

b) Frequency-domain analysis is not applicable because
the problem is nonlinear.

c) Robustness against parametric variations, sensory failure and additive noise.

d) Downstream effects.

e) Tuning characteristics.

f) Ability to convey meaningful information.

The performance tests evaluate the effectiveness of the parameter identification capability incorporated within the RID design.

g) User understandability.

h) Resource requirements.

The optimal control method [20] is incorporated for the purpose of comparison. This method uses Lagrangian density and freedom functions to derive a nonlinear control law. For the purpose of simplicity, we call this method the "Lagrangian Derivation of Optimal Control" (LDOC). Each performance test is also applied to LDOC so that the differences between the optimal control and RID control can be assessed. The performance tests are labeled for convenience. The prescribed trajectories for the reactor power and coolant temperature are shown in Fig. 3.2. Table 3.1 shows two-digit labels, whereas the proceeding table shows the combination of the tests performed.

3.3 Design

3.3.1 RID Control (DS1)

Consider the nonlinear model given by Eqs.(3.5-3.8). The "bare" design, which assumes that the model exactly represents the plant, is derived from Eqs. (3.5) and (3.8). The control law for the pair of reactivity control-power demand is solved from Eq.(3.5)

$$V_1 = 1 + \frac{\lambda_s^m}{N_1}\dot{N}_1 - \frac{N_2}{N_1} + \lambda_s^m[\alpha_c^m(N_4 - N_{40}) + \alpha_f^m(N_3 - N_{30})] \qquad (3.15)$$

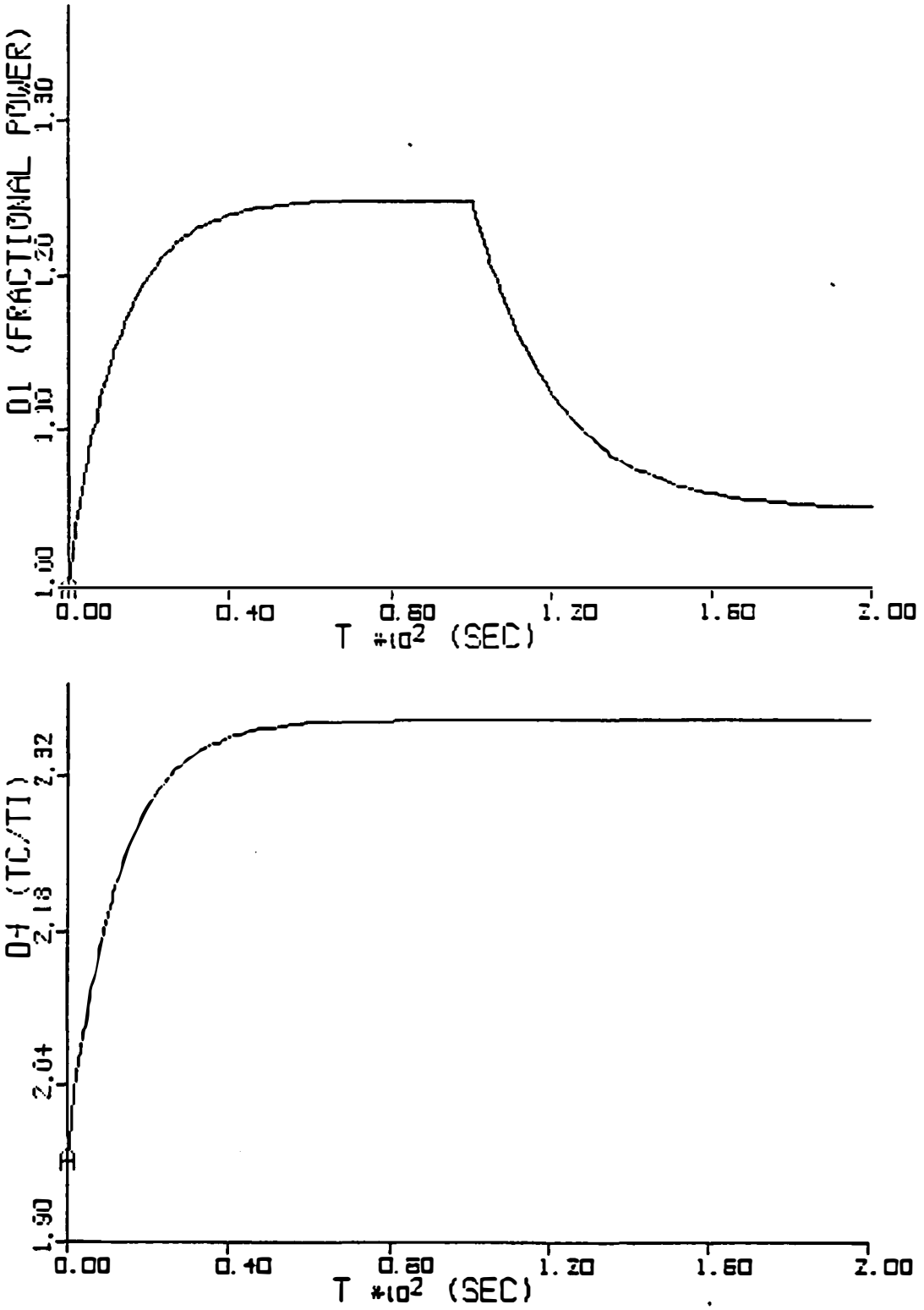

Figure 3.2: Desired trajectories for the reactor power (top) and core-coolant temperature (bottom).

Table 3.1: Labels for Control Algorithm Testing

ITEM	LABEL	DESCRIPTION
Test1	T1	Model and plant perfectly match
Test2	T2	Robustness to unknown dynamics
Test3	T3	Measurement time-delay
Test4	T4	Actuator constraints
Design1	DS1	RID design (bare)
Design2	DS2	RID design with adaptive features
Design3	DS3	Optimal Control (LDOC)

Definition of dynamic error between the reactor power and demand D_1 given by

$$\dot{N}_1 = K_1(D_1 - N_1) = E_1 \tag{3.16}$$

is substituted in Eq.(3.15) to yield

$$V_1 = 1 + \frac{\lambda_s^m}{N_1} K_1(D_1 - N_1) - \frac{N_2}{N_1} + \lambda_s^m[\alpha_c^m(N_4 - N_{40}) + \alpha_f^m(N_3 - N_{30})] \tag{3.17}$$

where K_1 is an adjustable quantity. Note that the state variables N_1 and N_4 are available as measurements P_1 and P_4 from the plant. Thus the reactivity control law is updated accordingly to give

$$V_1 = 1 + \frac{\lambda_s^m}{P_1} K_1(D_1 - P_1) - \frac{N_2}{P_1} + \lambda_s^m[\alpha_c^m(P_4 - P_{40}) + \alpha_f^m(N_3 - N_{30})] \tag{3.18}$$

The reactor coolant flow control is treated in a similar way. The control law for the pair of flow control-coolant temperature demand is obtained from Eq.(3.8).

$$V_4 = \frac{\lambda_c^m(N_3 - N_4)}{\lambda_r^m(N_4 - 1)} - \frac{\dot{N}_4}{\lambda_r^m(N_4 - 1)} \tag{3.19}$$

Dynamic error between the coolant temperature and demand is given by

$$\dot{N}_4 = K_4(D_4 - N_4) \tag{3.20}$$

The substitution of Eq.(3.20) into Eq.(3.19) yields

$$V_4 = \frac{\lambda_c^m(N_3 - N_4)}{\lambda_r^m(N_4 - 1)} - \frac{K_4(D_4 - N_4)}{\lambda_r^m(N_4 - 1)} \tag{3.21}$$

Table 3.2: Tests Performed

⋆	T1	T2	T3	T4
DS1	×			
DS2		×	×	×
DS3	×	×	×	×

where D_4 and K_4 are the coolant temperature demand and an adjustable parameter, respectively. The control law is updated using the available measurements from the plant, in this case P_4.

$$V_4 = \frac{\lambda_c^m(N_3 - P_4)}{\lambda_r^m(P_4 - 1)} - \frac{K_4(D_4 - P_4)}{\lambda_r^m(P_4 - 1)} \tag{3.22}$$

3.3.2 Adaptive RID Control Design (DS2)

The need for an adaptive design emerges from the fact that the RID control law given by Eqs.(3.18) and (3.22) use state estimations N_2 and N_3 generated by the model. Modeling errors and inexact inverse dynamics formulation may deteriorate the performance. When the RID design is performed on a real system, a set of transient data must be available. Thus, the RID control law is modified to yield the dynamic equilibrium of control for the dynamic equilibrium testing.

The dynamic equilibrium of control (inverse dynamics) is obtained by setting the reconstruction terms (K) equal to zero. Using Eq. (3.18) the equilibrium reactivity control is given by

$$(V_1)_{eq} = 1 - \frac{N_2}{P_1} + \lambda_s^m[\alpha_c^m(P_4 - P_{40}) + \alpha_f^m(N_3 - N_{30})] \tag{3.23}$$

Similarly the dynamic equilibrium of control for the coolant flow is obtained from Eq.(3.22)

$$(V_4)_{eq} = \frac{\lambda_c^m(N_3 - P_4)}{\lambda_r^m(P_4 - 1)} \tag{3.24}$$

The model for DET is similar to that of Eqs.(3.4-3.8) except the available measurements (P_1,P_4) and the equilibrium controls are substituted as forcing functions. The DET model is given by

$$\dot{N}_1 = \frac{1}{\lambda_s^m}[((V_1)_{eq} - 1)\overbrace{P_1}^{\downarrow} + N_2] - [\alpha_c^m(\overbrace{P_4}^{\downarrow} - N_{40}) + \alpha_f^m(N_3 - N_{30})]\overbrace{P_1}^{\downarrow} \quad (3.25)$$

$$\dot{N}_2 = \lambda_d^m(\overbrace{P_1}^{\downarrow} - N_2) \quad (3.26)$$

$$\dot{N}_3 = \lambda_p^m\overbrace{P_1}^{\downarrow} - \lambda_f^m(N_3 - \overbrace{P_4}^{\downarrow}) \quad (3.27)$$

$$\dot{N}_4 = \lambda_c^m(N_3 - \overbrace{P_4}^{\downarrow}) - (V_4)_{eq}\lambda_r^m(\overbrace{P_4}^{\downarrow} - 1) \quad (3.28)$$

where the arrows indicate data entries.

Obviously, the dynamic equilibrium of controls are expected to cancel the forward dynamics in Eqs.(3.25) and (3.28) and yield $\dot{N}_1 = \dot{N}_4 = 0$. Note that these derivatives are not equal to zero in practice because the controls used during the plant transient are different from $(V_1)_{eq}$ and $(V_4)_{eq}$. Otherwise, the data would represent the steady-state system behavior which is not useful for the DET. The DET outputs are evaluated based on these two derivatives for this specific example. Examining the deviations from zero and the analytical structure of controls, we can easily diagnose the approximate locations of uncertainties in the model.

Adaptive design starts with identifying the uncertain terms in the model either by DET or using heuristic approach. The model (on-line estimator) is then expressed as follows.

$$\dot{N}_1 = \frac{1}{\lambda_s^m}[(V_1 - 1)N_1 + N_2] - [\alpha_c^m(N_4 - N_{40}) + \alpha_f^m(N_3 - N_{30})]N_1 + R_{G1} \quad (3.29)$$

$$\dot{N}_2 = \lambda_d^m(N_1 - N_2) \quad (3.30)$$

$$\dot{N}_3 = \lambda_p^m N_1 - \lambda_f^m(N_3 - N_4) + R_{G3} \quad (3.31)$$

$$\dot{N}_4 = \lambda_c^m(N_3 - N_4) - V_4\lambda_r^m(N_4 - 1) \quad (3.32)$$

where R_{G1} and R_{G3} represent the uncertainties. The placement of R_{G3} is necessary and an additional R_{G4} is avoidable using the auxiliary-states technique.

The two uncertain terms associated with the model are treated as new control variables that must provide appropriate compensation for the discrepancy between the plant and model. Uncertainty terms respresent all unknown effects including time varying parameters and unknown disturbances. The uncertainty in reactor power R_{G1} is derived from Eq.(3.29).

$$R_{G1} = -\mathcal{F}_4(\bar{N}, V_1) + \dot{N}_1 \tag{3.33}$$

$$\dot{N}_1 = K_{G1}(P_1 - N_1) \tag{3.34}$$

where

$$\mathcal{F}_4(\bar{N}, V_1) = \frac{1}{\lambda_s^m}[(V_1 - 1)N_1 + N_2] - [\alpha_c^m(N_4 - N_{40}) + \alpha_f^m(N_3 - N_{30})]N_1 \tag{3.35}$$

Similarly, the uncertainty in the fuel and coolant temperatures are solved using Eqs. (3.31) and (3.32). Using the auxiliary-states technique we define an auxiliary state variable N_3^* in Eq.(3.32) such that it will force the coolant temperature of the model N_4 to follow its measured value P_4. Thus, from Eq.(3.32)

$$N_3^* = \frac{\dot{N}_4}{\lambda_c^m} + N_4 + \frac{V_4\lambda_r^m(N_4 - 1)}{\lambda_c^m} \tag{3.36}$$

$$\dot{N}_4 = K_{G4}(P_4 - N_4) \tag{3.37}$$

The control term R_{G3} is then designed to force the fuel temperature of the model N_3 to follow the auxiliary state N_3^*. From Eq.(3.31)

$$R_{G3} = -\mathcal{F}_3(N_1, N_3, N_4) + \dot{N}_3 \tag{3.38}$$

$$\dot{N}_3 = K_{G3}(N_3^* - N_3) \tag{3.39}$$

where

$$\mathcal{F}_3(N_1, N_3, N_4) = \lambda_p^m N_1 - \lambda_f^m(N_3 - N_4) \tag{3.40}$$

The final form of the RID control design includes controls V_1 and V_4 of Eqs. (3.18) and (3.22), adaptive controls R_{G1}, R_{G3}, and auixiliary state N_3^* of Eqs. (3.33), (3.36) and (3.38). The adaptive control utilizes state estimations from the on-line model given by Eqs.(3.28-3.32). Two measurements P_1 and P_4 are obtained from the plant whereas the two demands D_1 and D_4 are prescribed and supplied by the operator.

3.3.3 Lagrangian Derivation of Optimal Control (DS3)

An analytical comparison between the RID and optimal control methods given in Chapter 2 was performed in the linear domain. Most of the nonlinear methods such as Pontryagin's maximum principle suffer from theoretical limitations as well as from numerical problems. A recent accomplishment in nonlinear control [20] uses Lagrangian density-freedom function approach to yield a rather simple and powerful control technique. The performance evaluation of the RID method includes comparisons with the Lagrangian derivation of optimal control (LDOC) through simulations.

The LDOC can be considered as a model-reference adaptive control (MRAC) method. Its model dependence is somewhat less complicated compared to that of the RID. For the benchmark problem, the LDOC method uses a model given by

$$\dot{M}_1 = (Y_1 - 1)\frac{M_1}{\lambda_s^m} + G_1 \tag{3.41}$$

$$\dot{M}_4 = -Y_4\lambda_r^m(M_4 - 1) + G_4 \tag{3.42}$$

where M_1 and M_4 are reactor power and coolant temperature, Y_1 and Y_4 are reactivity and flow controls, and G_1 and G_4 are unknown dynamics, respectively. Comparing Eqs. (3.41,3.42) with Eqs. (3.9-3.12), it can be seen that the adaptive control in the LDOC design has a more challenging objective than that of the RID design. However, it is inherently less model dependent. The model given above is redefined in terms of control and state functions.

$$C_1 = Y_1 - 1 \tag{3.43}$$

$$F_1 = \frac{M_1}{\lambda_s^m} \tag{3.44}$$

$$C_4 = -Y_4 \tag{3.45}$$

$$F_4 = \lambda_r^m(M_4 - 1) \tag{3.46}$$

The controls Y_1 and Y_4 are given by

$$Y_1 = R_{1a}Y_{10} + R_{1b} - R_{1c}C_{1T} \tag{3.47}$$

$$Y_4 = R_{4a}Y_{40} + R_{4c}C_{4T} \tag{3.48}$$

$$\tag{3.49}$$

where

$$R_{1a} = \frac{1 + ln(F_{10})}{1 + ln(F_1)} \tag{3.50}$$

$$R_{1b} = \frac{ln\frac{F_1}{F_{10}}}{1 + ln(F_1)} \tag{3.51}$$

$$R_{1c} = \frac{F_1}{1 + ln(F_1)} \tag{3.52}$$

$$R_{4a} = \frac{1 + ln(F_{40})}{1 + ln(F_4)} \tag{3.53}$$

$$R_{4c} = \frac{F_4}{1 + ln(F_4)} \tag{3.54}$$

$$C_{1T} = P_{c10} - P_{1I}Z_{1B} + R_{1p}(P_1 - D_1) \tag{3.55}$$

$$C_{4T} = P_{c40} - P_{4I}Z_{4B} + R_{4p}(P_4 - D_4) \tag{3.56}$$

Controls given above include tuning parameters $P_{c10}, P_{1I}, R_{1p}, P_{c40}, P_{4I}$ and R_{4p}. The terms Z_{1B} and Z_{4B} represent integral errors given by

$$Z_{1B} = \int_0^t d\tau(P_1 - D_1) \tag{3.57}$$

$$Z_{4B} = \int_0^t d\tau(P_4 - D_4) \tag{3.58}$$

Adaptive control is designed in a similar fashion and given by

$$G_1 = G_{10} + F_{10} - F_1 - B_{1T} \tag{3.59}$$

$$G_2 = G_{40} + F_{40} - F_4 - B_{4T} \tag{3.60}$$

where

$$B_{1T} = -K_{1I}Z_{1A} + K_{1p}(M_1 - P_1) \tag{3.61}$$

$$B_{4T} = -K_{4I}Z_{4A} + K_{4p}(M_4 - P_4) \tag{3.62}$$

The adaptive control includes tuning parameters $K_{1I}, K_{1p}, K_{4I}, K_{4p}$ and initial values G_{10}, G_{40}. The terms Z_{1A}, Z_{4A} represent the integral errors given by

$$Z_{1A} = \int_0^t d\tau(M_1 - P_1) \tag{3.63}$$

$$Z_{4A} = \int_0^t d\tau(M_4 - P_4) \tag{3.64}$$

3.4 Simulation Results

The benchmark problem is applied to three different designs for four different tests (see Tables 3.1 and 3.2). The computer codes (in ACSL) are given in Appendix A. The simulations are performed on a VAX-2000 Work Station using the ACSL software.

3.4.1 Test-1 (T1): Plant and Model Perfectly Match

The performance evaluation of the RID control technique with comparison to the LDOC, first includes the case where the plant and its model exactly match. Although this assumption is never true for real systems, these simulations help understand if the basic theory is valid. The RID and LDOC controllers are tuned through trial and error. The RID control requires tuning 5 parameters whereas the LDOC requires 12 parameters. These parameters are given in Sect. 3.4.5 and kept the same in each test.

The reactor power response using the RID controller is shown in Fig. 3.3 and is compared with the demand. A similar comparison is shown in Fig. 3.4 using the LDOC controller. As it is seen from these figures, the reactor power follows the demand very closely such that the difference cannot easily be visualized on the graphs. The core coolant temperature responses using the RID and LDOC controllers are shown in Fig. 3.5 in comparison with the demand. The responses in this figure are also not distinguishable because the controllers perform very efficiently.

Figure 3.6 compares the RID control inputs with that of the LDOC. The differences are consistently negligible. The reactivity input, as expected, increases during the first 100 seconds to match the power with the increasing demand. During the second 100 seconds, a negative reactivity is introduced to follow the decreasing power demand. The core coolant flow is decreased to prolong the residence time to match the increasing temperature demand. Although the temperature demand is constant during the second 100 seconds, decreasing reactor power causes less heat production thus the coolant residence time needs to be prolonged further.

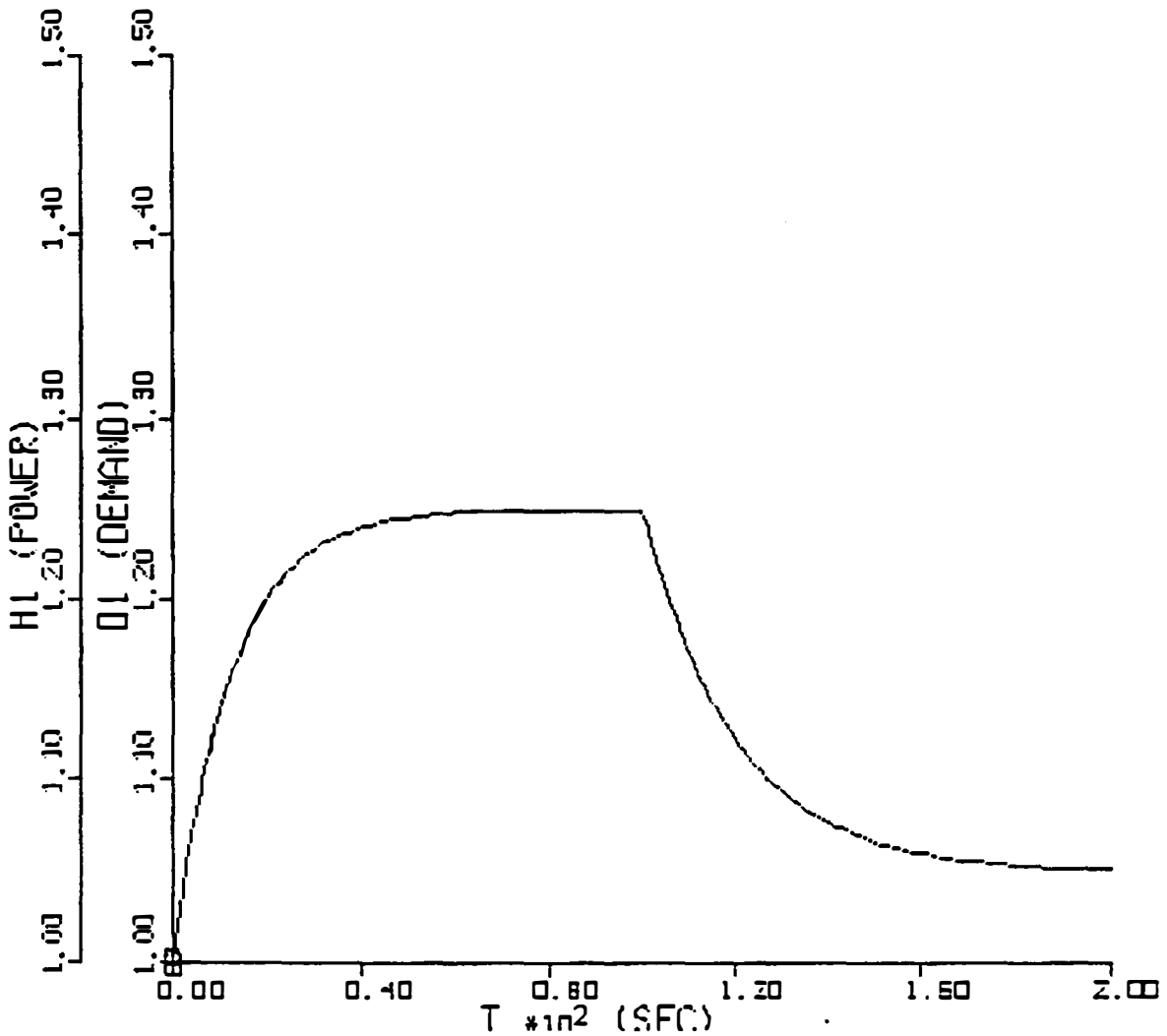

Figure 3.3: Reactor power H_1 response using the RID controller. Reactor follows the demand D_1 with a negligible error. In Test-1, plant and model exactly match.

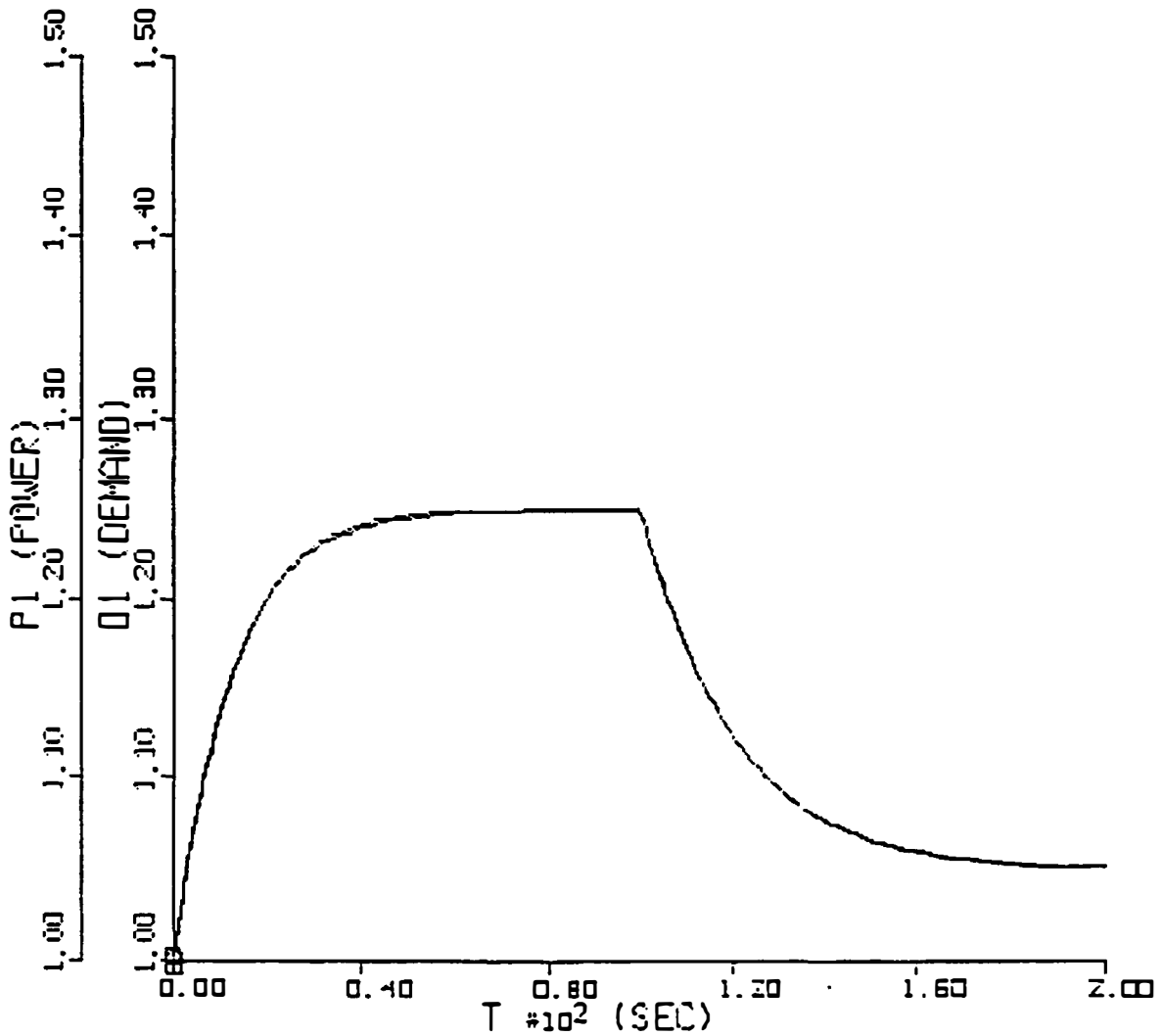

Figure 3.4: Reactor power P_1 response using the LDOC paradigm. Reactor follows the demand D_1 with a negligible error. In Test-1, plant and model exactly match.

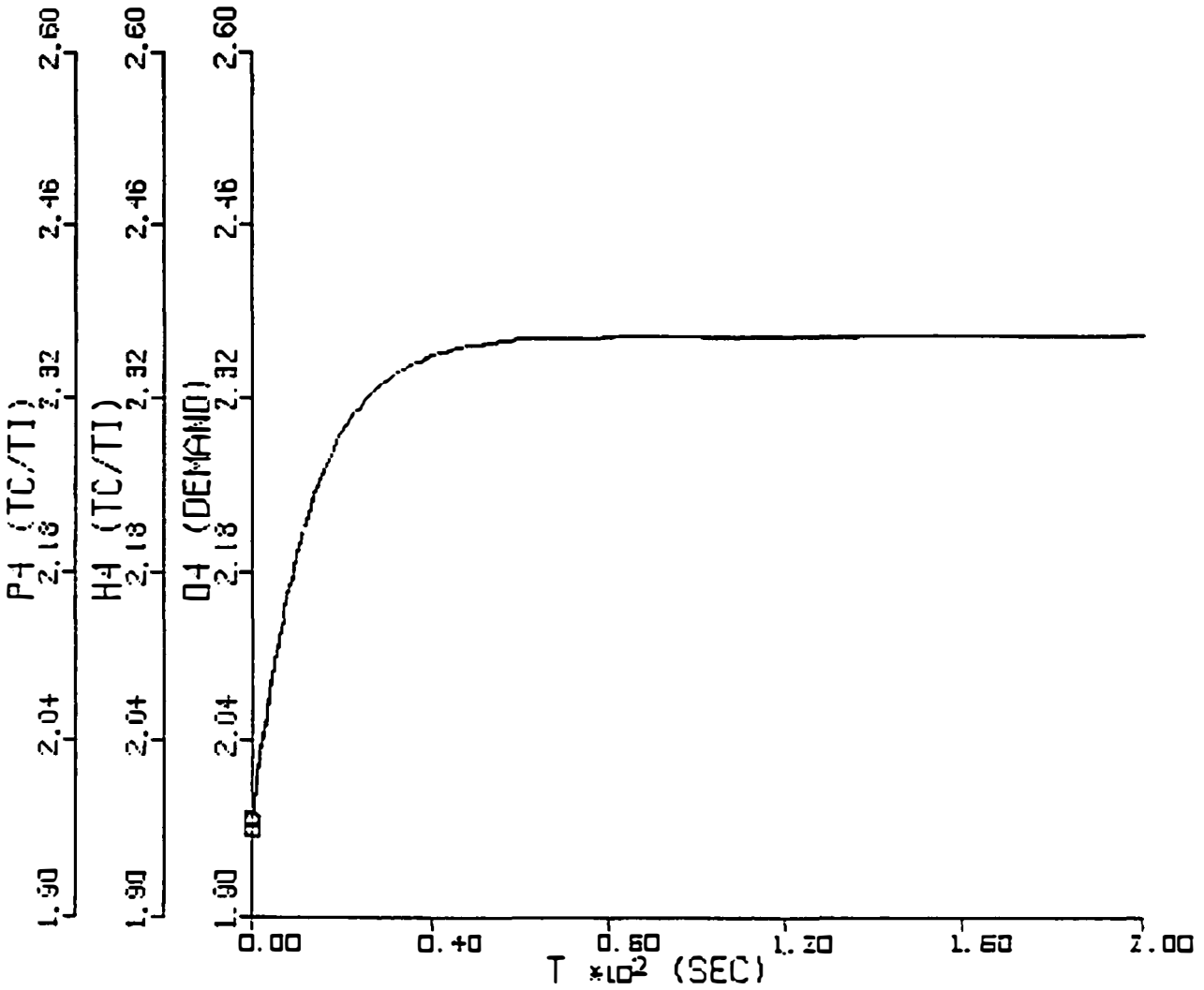

Figure 3.5: Reactor coolant temperature responses using the LDOC and RID controllers (P_4, H_4). Reactor follows the demand D_4 with a negligible error. In Test-1, plant and model exactly match.

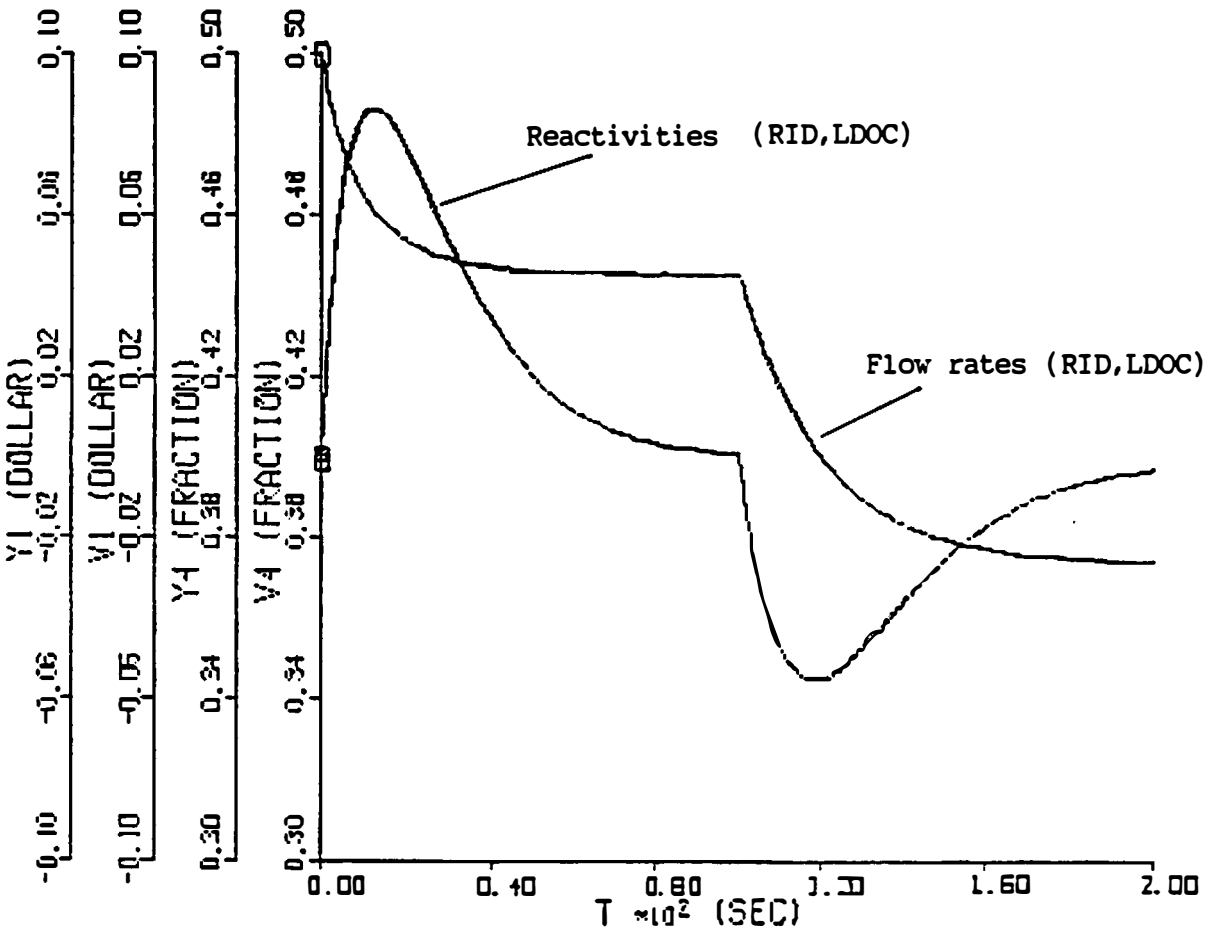

Figure 3.6: Control inputs of reactivity and flow using the LDOC and RID controllers. (Y_1 and Y_4 with LDOC, V_1 and V_4 with RID). In Test-1, plant and model exactly match.

The simulation results of Test-1 indicate that the RID control law yields efficient trajectory following capability when the on-line model matches the plant perfectly. For this specific example, the RID controller performance is almost identical to that of the Lagrangian derivation of optimal control. The simulation results can be reproduced using the ACSL code given in Appendix A.

3.4.2 Test-2 (T2): Partially Unknown Plant Dynamics

The performance evaluation of the RID method includes robustness testing against unknown plant dynamics. The unknown plant dynamics includes all possible deteriorating effects such as time-varying parametric changes, unmodeled nonlinearities and measurement problems. In Test-2, the RID and LDOC controllers are expected to accomplish the trajectory following task under two effects: (1) time-varying parametric changes in the plant, and (2) unknown nonlinear dynamics of the plant. The on-line model used in the RID and LDOC designs do not include these effects. Thus, this test also evaluates the robustness property against modeling errors.

The time-varying parametric changes of the plant are shown in Fig. 3.7. The parameters increase or decrease constantly with different oscillations which are generated by arbitrarily chosen constants. At the end of the 200 second period, these parameters are about 30 % different from their initial values. Figure 3.8 shows the additional nonlinearity introduced to the plant dynamics which is an unknown in the on-line model. The constant change in plant parameters and the unknown nonlinear dynamics causes instability which is assessed by linearizing the "plant" model at the 200th second. The linearized open-loop plant has 2 eigenvalues with positive real parts.

The reactor power and core coolant temperature responses using the RID and LDOC controllers show that these methods yield very robust and stable performance. Figure 3.9 compares the RID controller performance with respect to power demand. Figure 3.10 shows the power response using the LDOC controller. The error in trajectory following is visible in this graph.

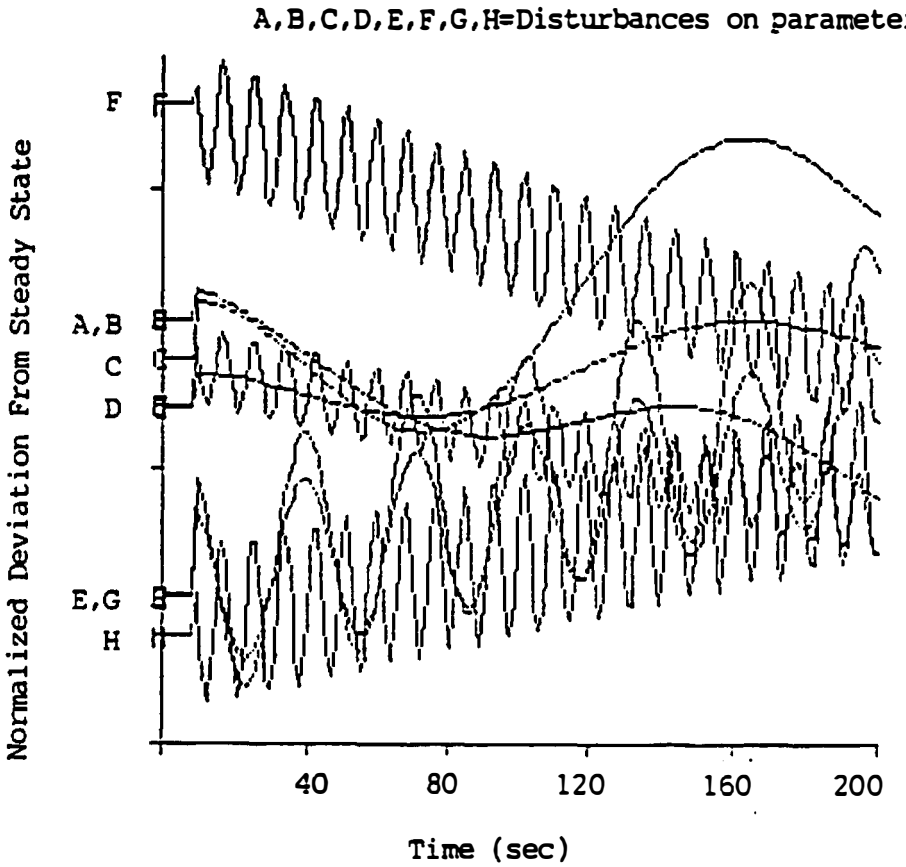

Figure 3.7: Time-variant parametric changes in the plant. Maximum deviation is about 30 % of the initial value. Parametric changes are initiated at the 10th second and generated by arbitrary constants. The 8 parameters of the on-line model are constant and equal to the initial values of plant parameters.

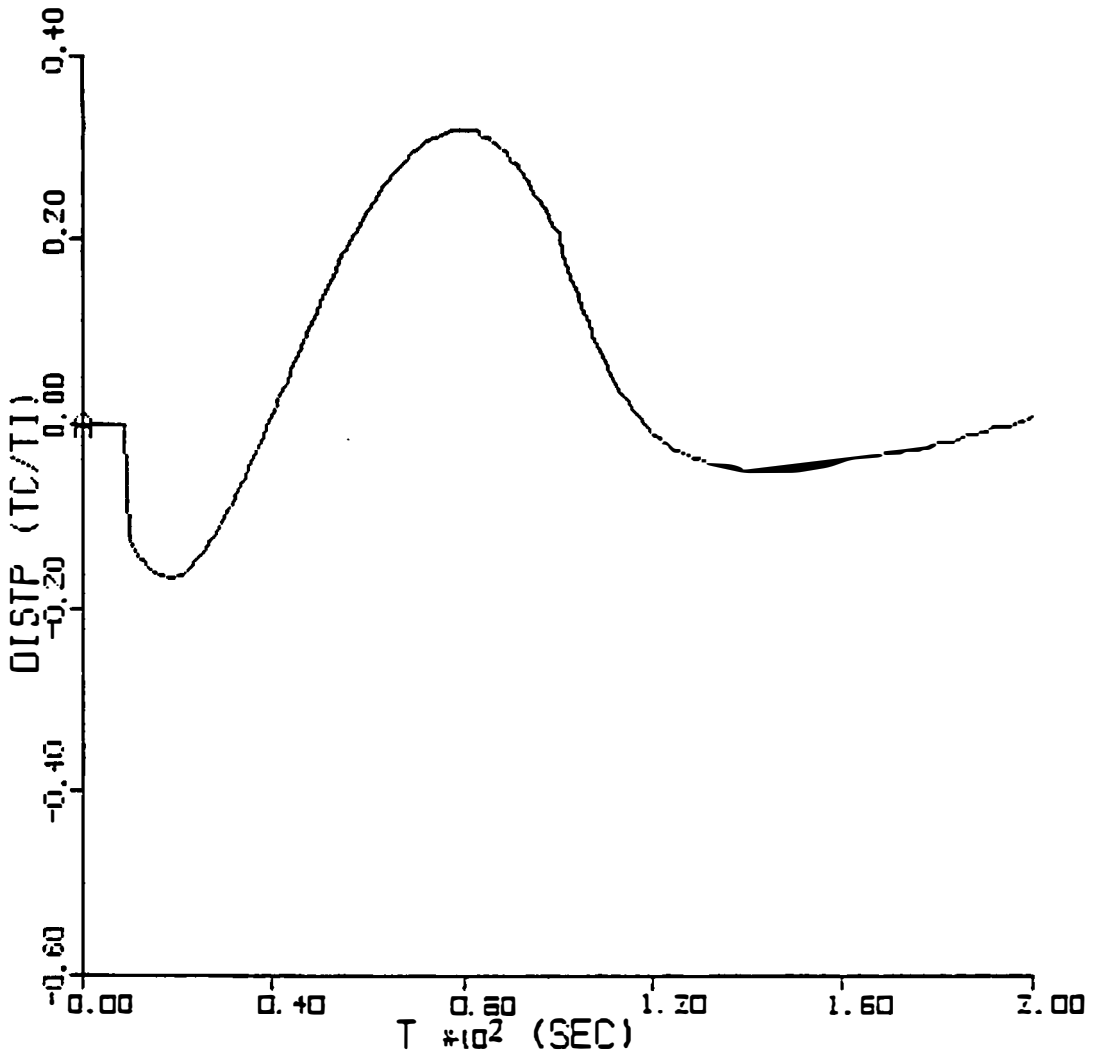

Figure 3.8: Unmodeled nonlinear dynamics incorporated into the plant. The nonlinearity relates the fuel temperature to the reactor power. It is unobservable through direct measurements which complicates the diagnostic task of the adaptive control.

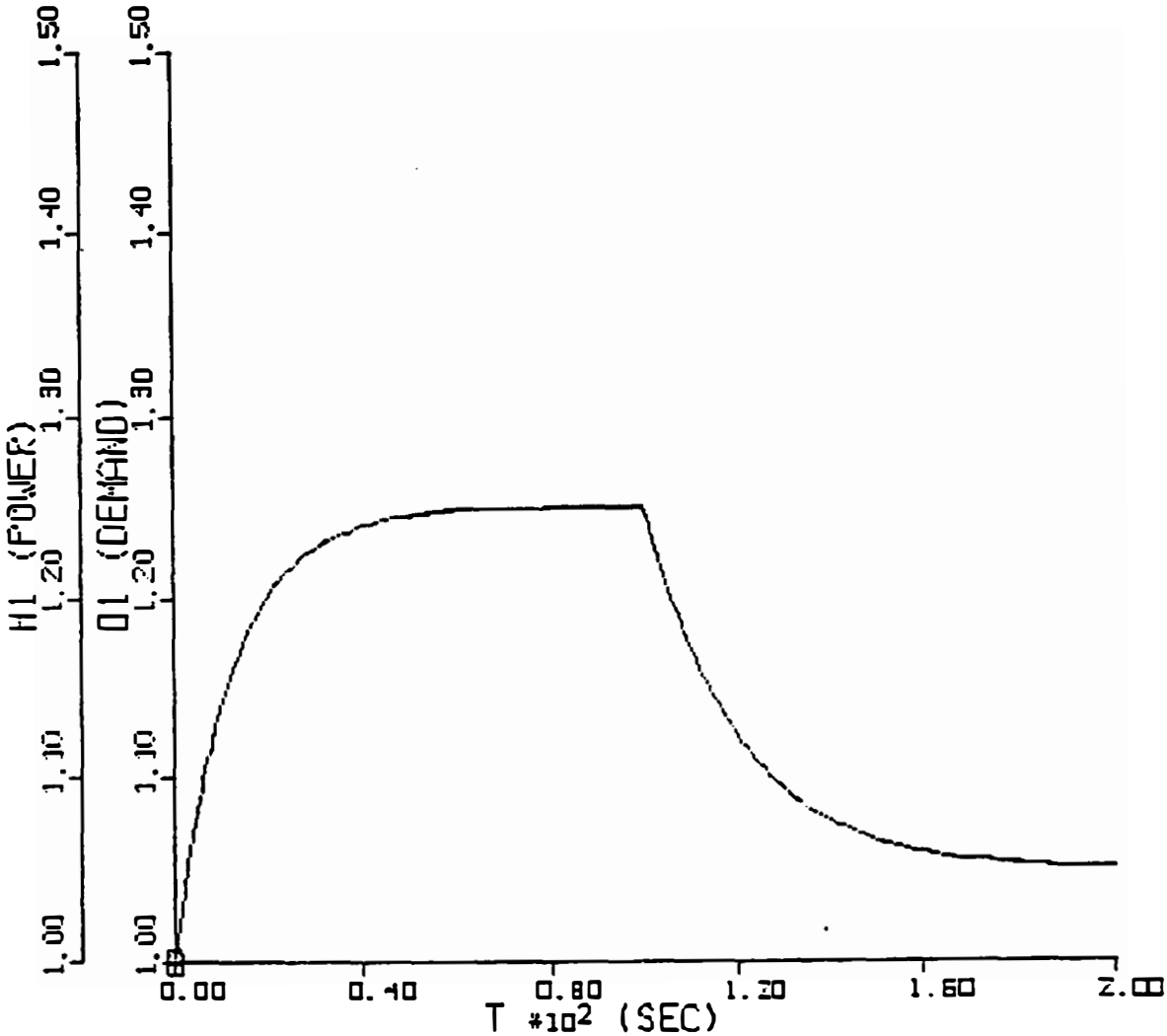

Figure 3.9: Reactor power response H_1 using the RID control paradigm. Reactor follows the demand D_1 with a negligible error. Test-2 introduces 30% discrepeancy between the plant and its model.

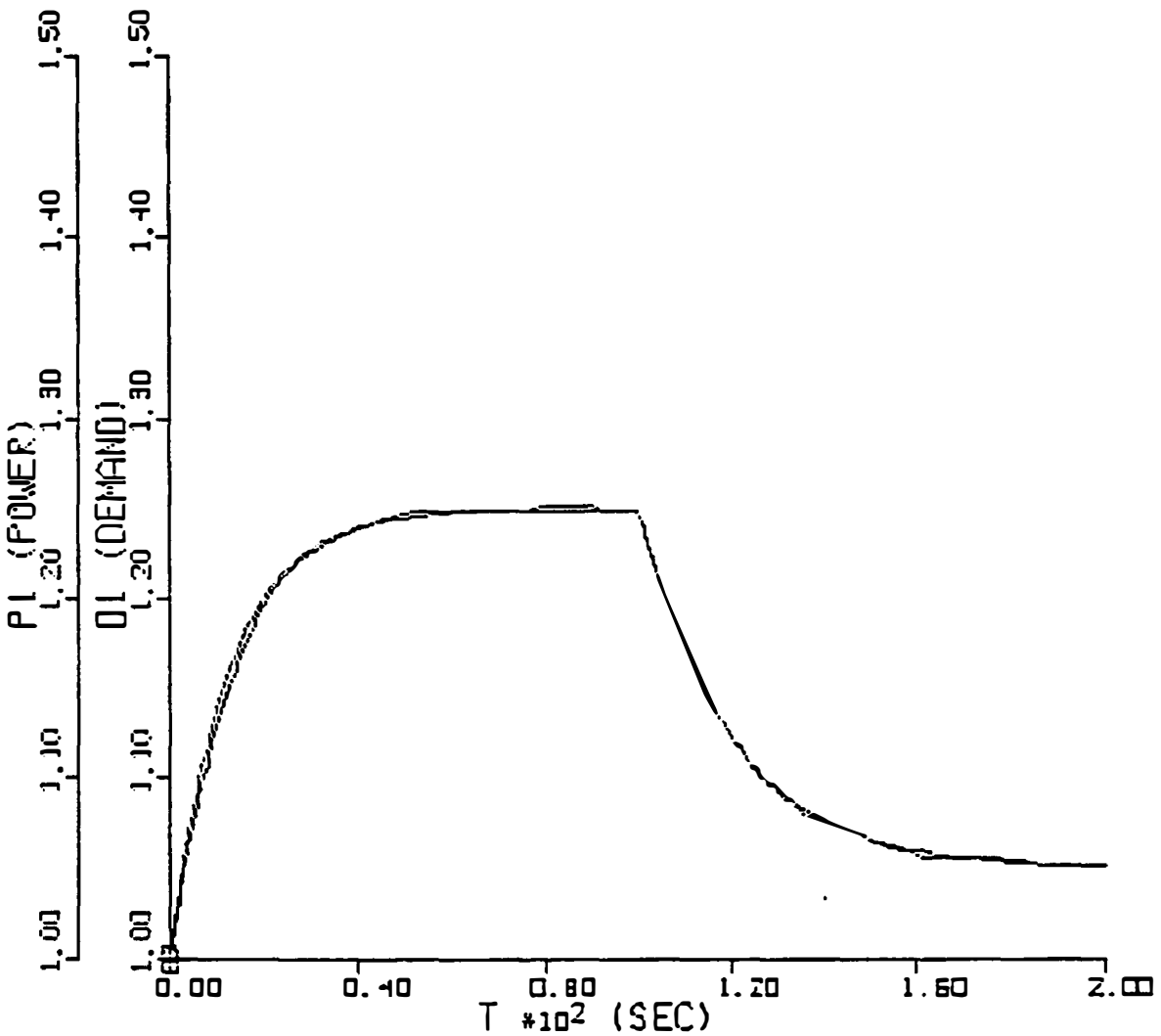

Figure 3.10: Reactor power response P_1 using the LDOC paradigm. Reactor follows the demand D_1 with a negligible error. Test-2 introduces 30% discrepeancy between the plant and its model.

The LDOC performance may be improved by a better tuning. Figures 3.11 and 3.12 show the reactor coolant temperature responses using the RID and LDOC controllers, respectively. Considering the amount of discrepancy introduced between the plant and model, the closed-loop performances using the RID and LDOC are outstanding. Linearization at the 200th second shows that none of the closed-loop poles have a positive real part, thus the stability-robustness property is verified.

Figure 3.13 shows the control inputs generated by the RID and LDOC paradigms. It is clear that the irregular appearence of control inputs is due to the compensation of the disturbance effects externally introduced to the plant. The adaptive control inputs are shown in Fig. 3.14. These graphs illustrate the discrepancy captured by the adaptive control paradigm. In case of the model exactly matching the plant, the adaptive control inputs would have a steady-state behavior.

The discrepancy introduced between the plant and its model is increasingly magnified to reach a point where the stability no longer holds. These simulations were performed to observe how much discrepancy these control systems could handle without loosing stability. Figure 3.15 shows the power response using the RID controller where the plant parameters deviate almost 300 % from their initial values at the 200th second. Figure 3.16 shows the LDOC performance. The closed-loop poles have small positive real parts and the stability is lost. The core coolant temperature responses using the RID and LDOC paradigms are shown in Figs. 3.17 and 3.18. Figure 3.19 shows the control inputs. The unstable behavior can be seen in Fig. 3.20 where the adaptive terms oscillate with a higher amplitude every period.

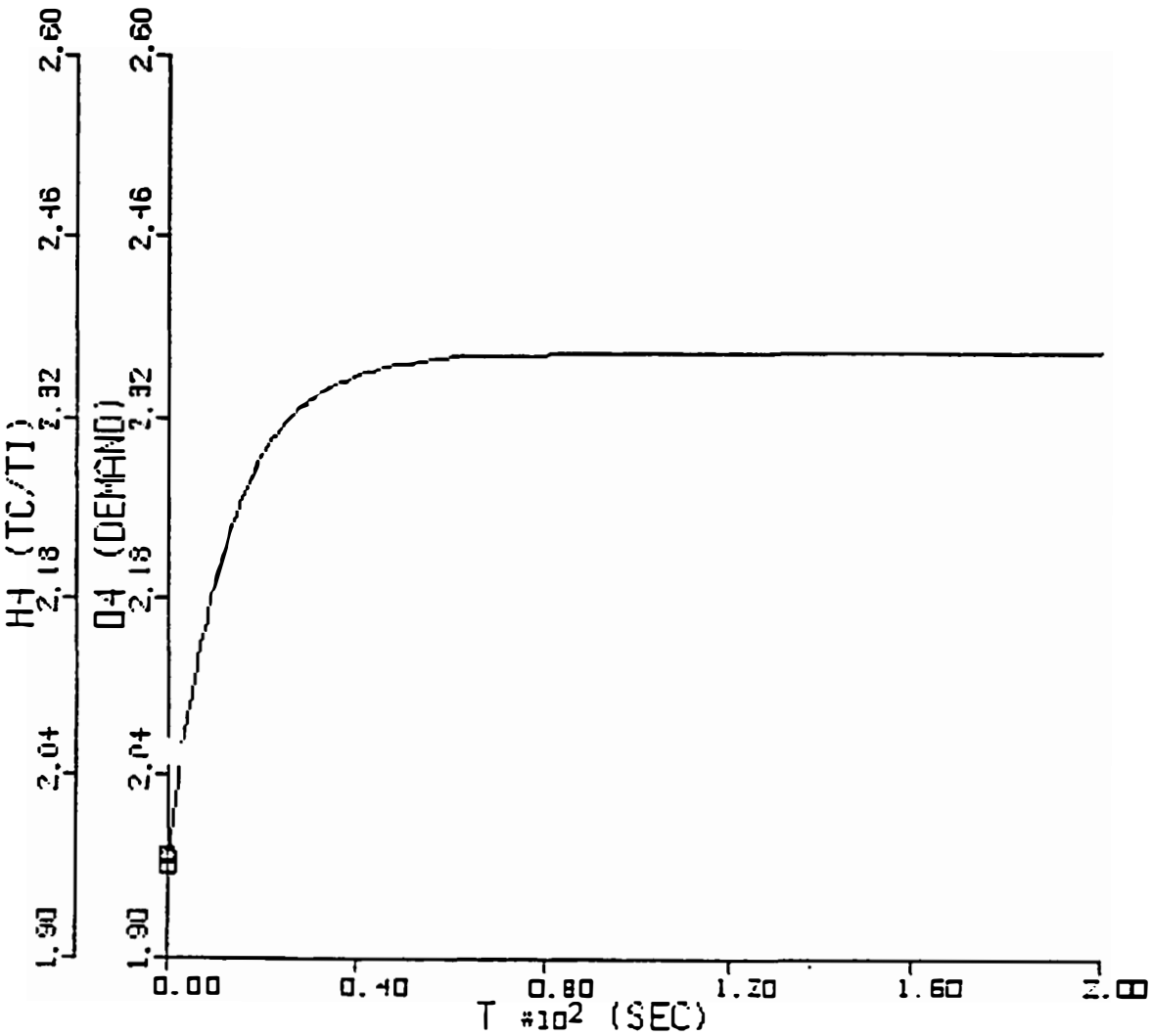

Figure 3.11: Reactor coolant temperature response H_4 using the RID control paradigm. Reactor follows the demand D_4 with a negligible error. Test-2 introduces 30% discrepeancy between the plant and its model.

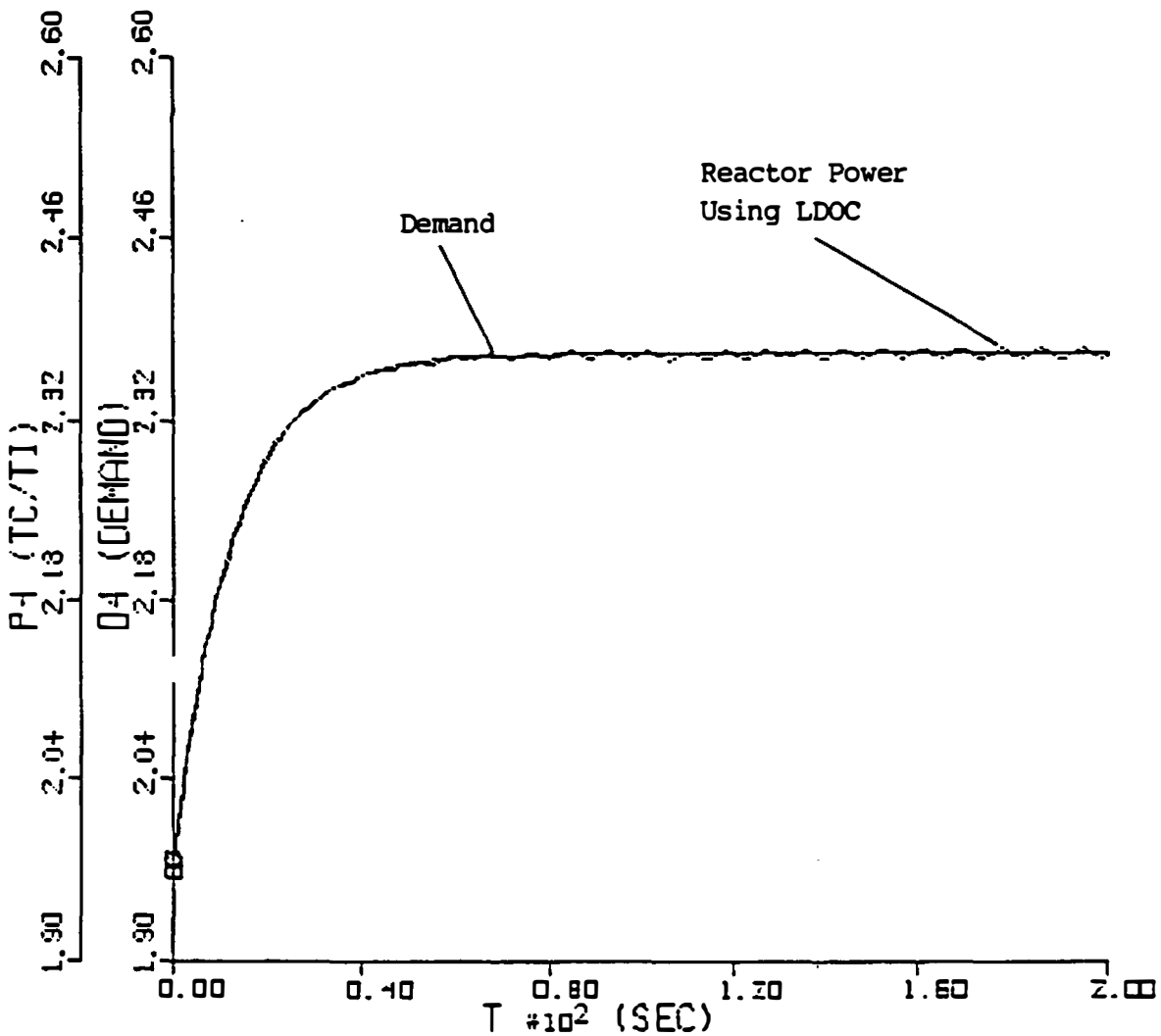

Figure 3.12: Reactor coolant temperature response P_4 using the LDOC paradigm. Reactor follows the demand D_4 with a significant error. Test-2 introduces 30% discrepeancy between the plant and its model.

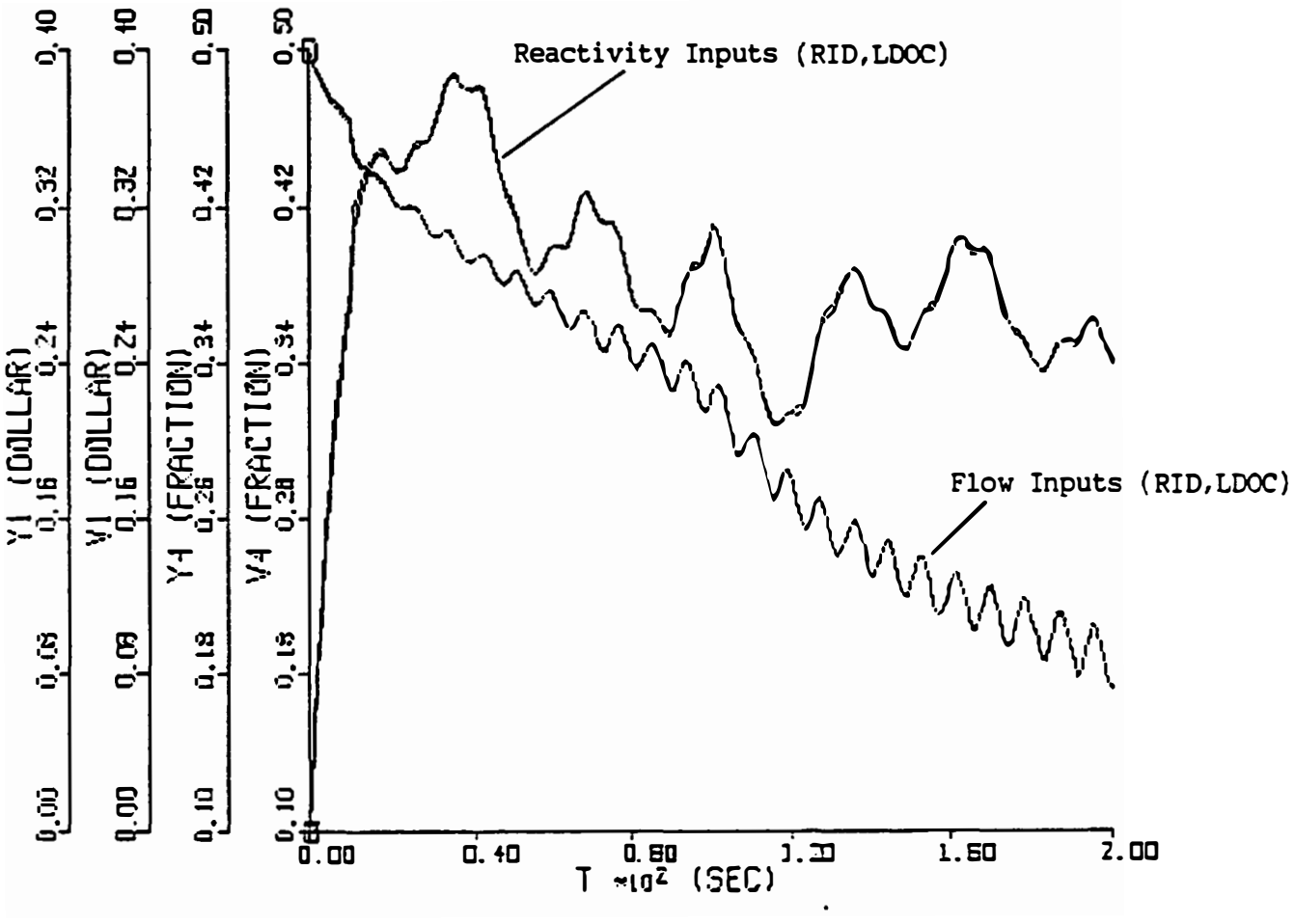

Figure 3.13: Control inputs generated by the LDOC and RID control paradigms. Reactivity inputs (Y_1 with LDOC, V_1 with RID) and flow inputs (Y_4 with LDOC, V_4 with RID) are consistent between the two paradigms. Test-2 introduces 30% discrepeancy between the plant and its model.

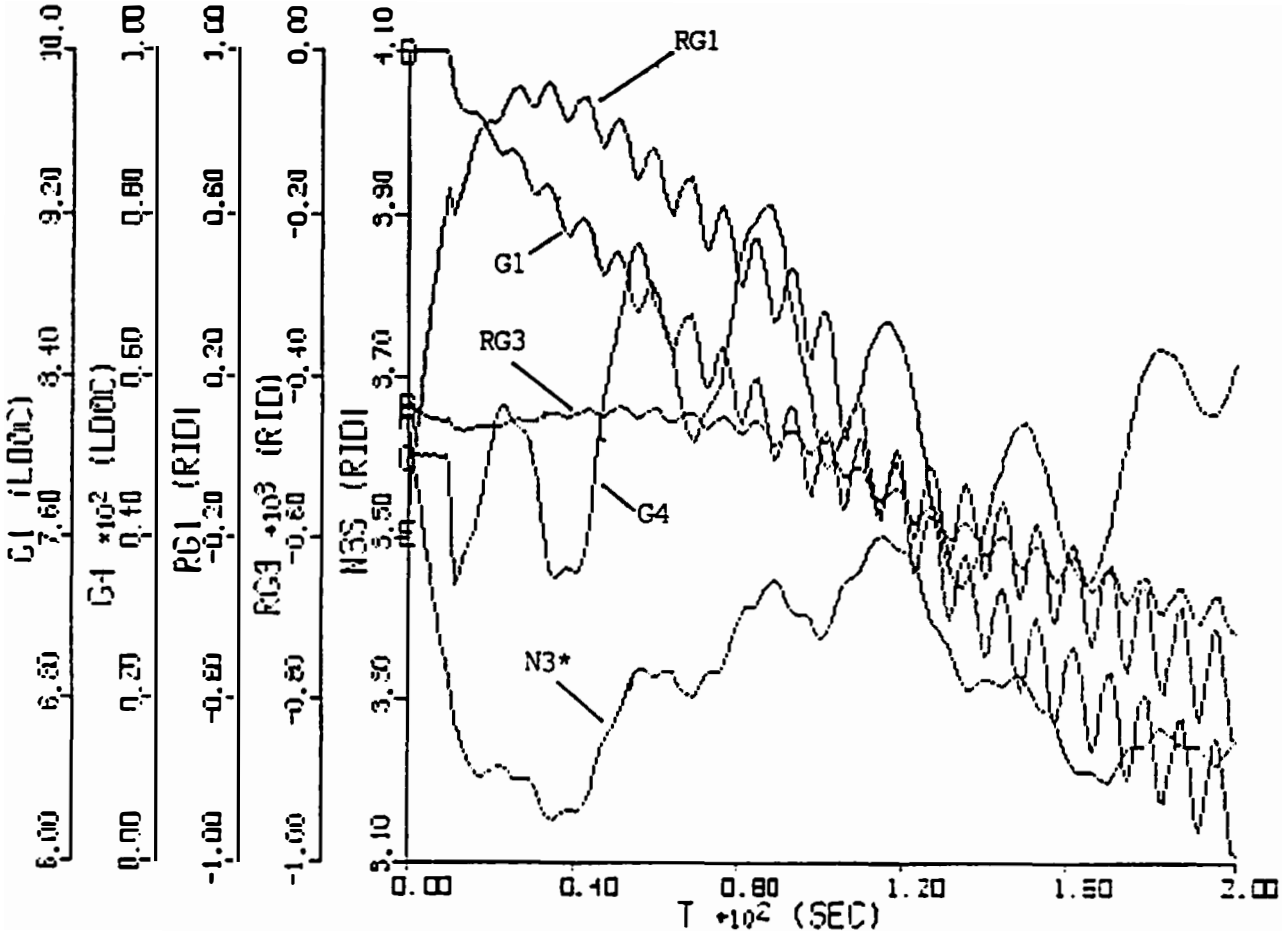

Figure 3.14: Adaptive control inputs using the LDOC and RID control paradigms. LDOC inputs are G_1 and G_4, RID inputs are R_{G1}, R_{G3} and N_3^*. The adaptive control captures the discrepeancies caused by time-variant parametric changes and unknown nonlinear plant dynamics. Test-2 introduces 30% discrepeancy between the plant and its model.

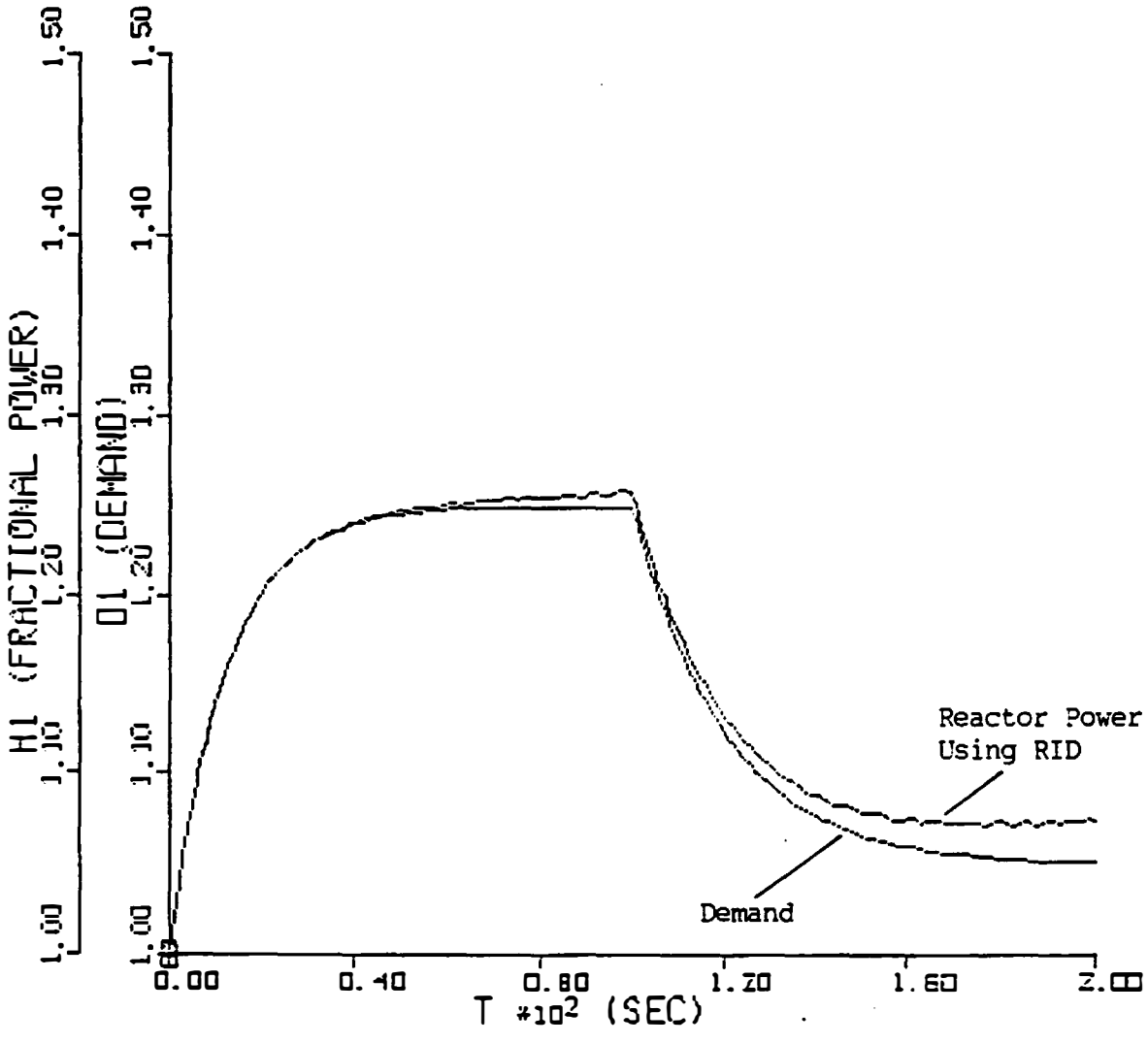

Figure 3.15: Reactor power response H_1 using the RID control paradigm. Reactor departures from the demand D_1 as time elapses. The discreapencies between the plant and model are magnified to reach 300 % at the 200th second. This is practically not possible in any nuclear reactor.

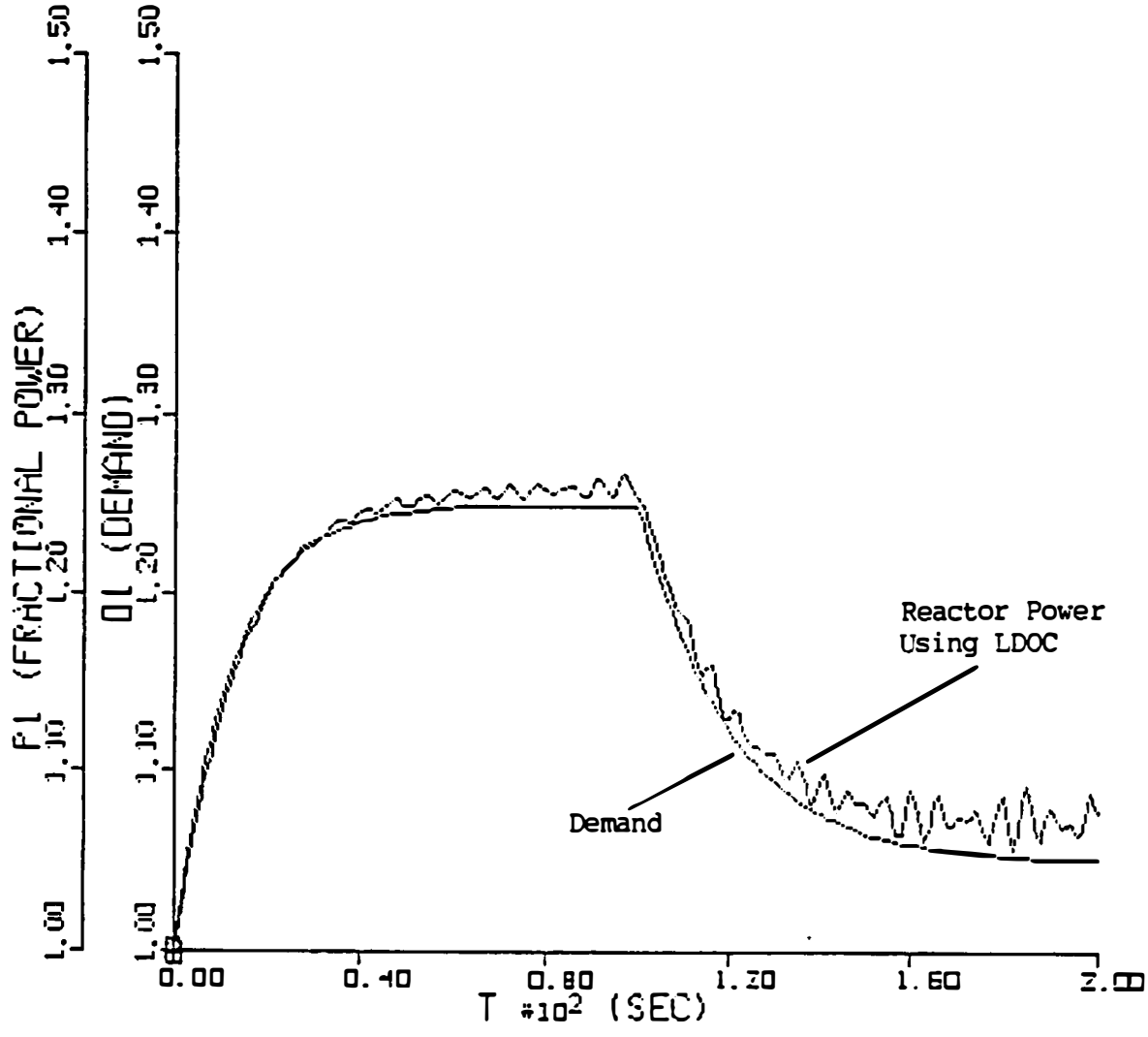

Figure 3.16: Reactor power response P_1 using the LDOC paradigm. Reactor departures from the demand D_1 as time elapses and shows unstable behavior. The discreapencies between the plant and model are magnified to reach 300 % at the 200th second. This is practically not possible in any nuclear reactor.

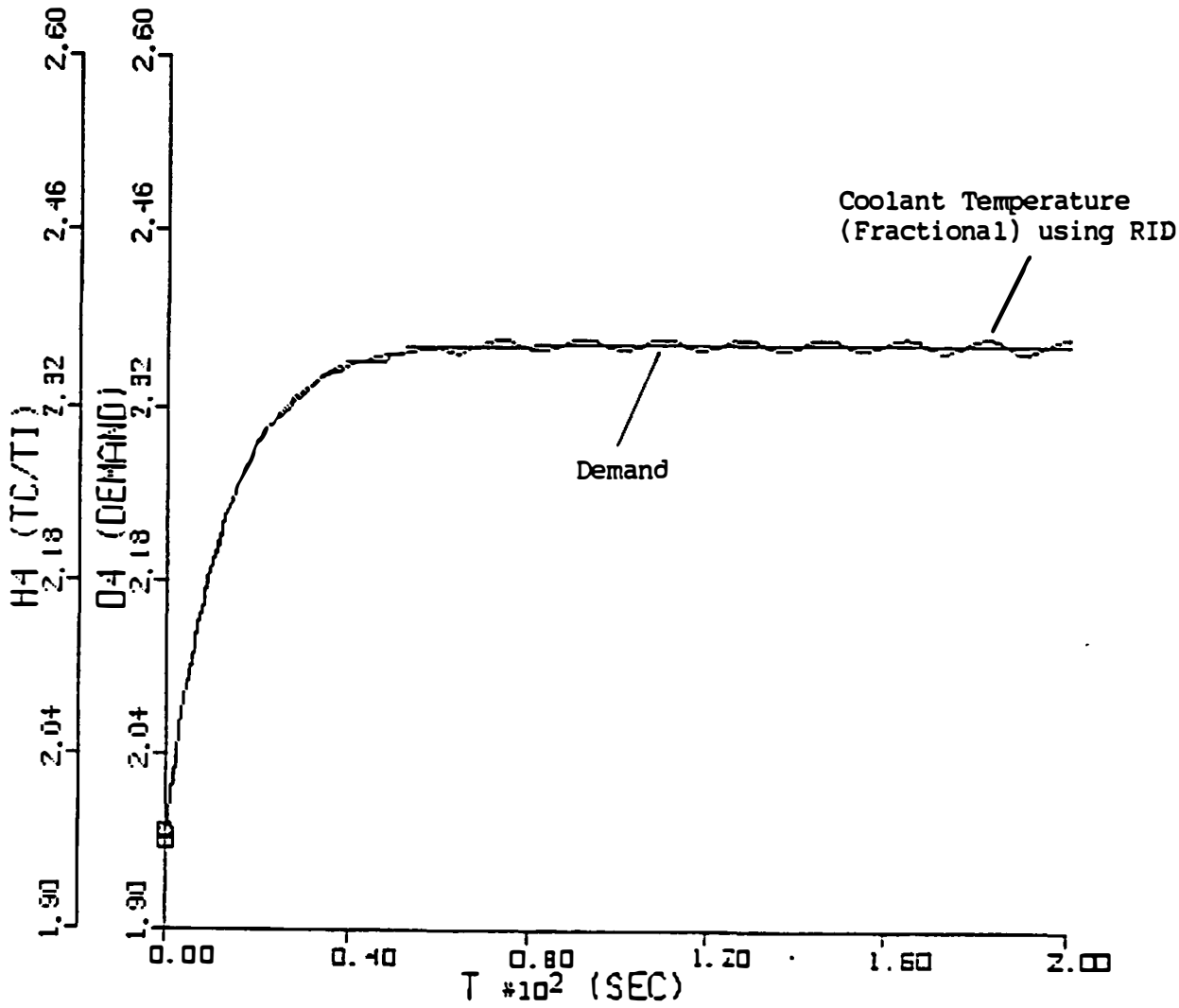

Figure 3.17: Reactor coolant temperature response H_4 using the RID control paradigm. Reactor follows the demand D_4 with a significant error. The discreapencies between the plant and model are magnified to reach 300 % at the 200th second. This is practically not possible in any nuclear reactor.

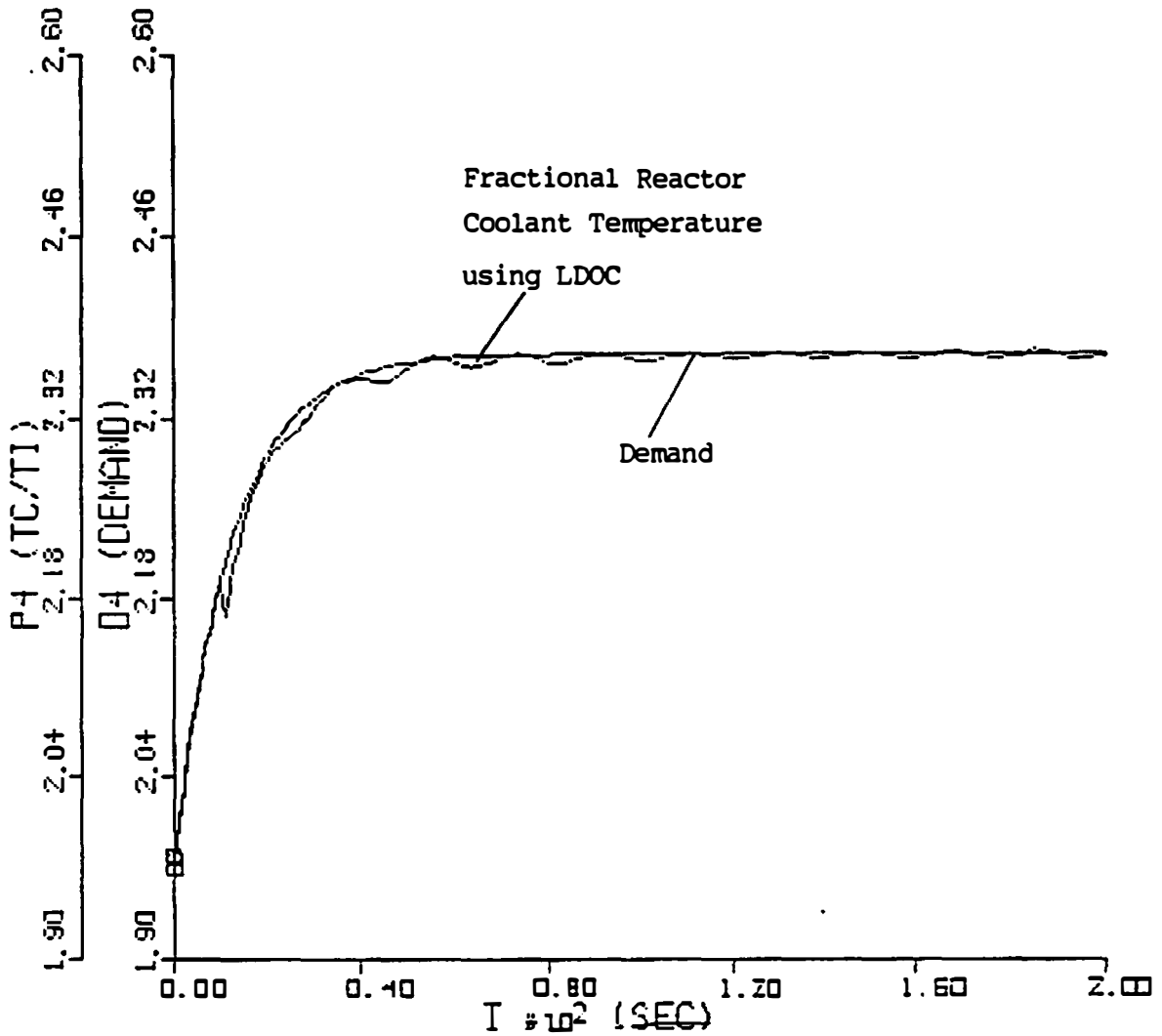

Figure 3.18: Reactor coolant temperature response P_4 using the LDOC paradigm. Reactor follows the demand D_4 with a significant error. The discreapencies between the plant and model are magnified to reach 300 % at the 200th second. This is practically not possible in any nuclear reactor.

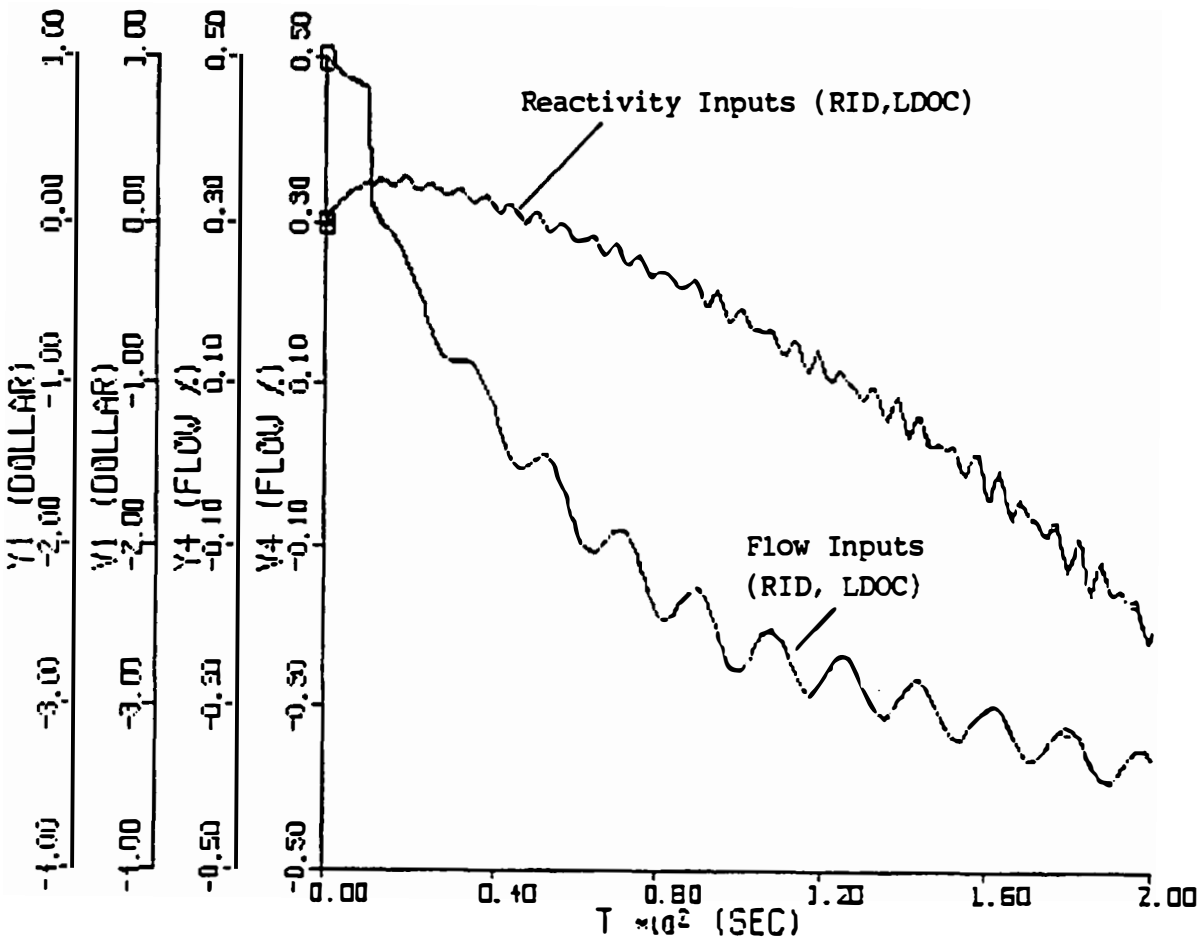

Figure 3.19: Control inputs using the LDOC and RID control paradigms. Reactivity inputs (Y_1 with LDOC and V_1 with RID) and flow inputs (Y_4 with LDOC and V_4 with RID) are consistent between each other. The discreapencies between the plant and model are magnified to reach 300 % at the 200th second. This is practically not possible in any nuclear reactor.

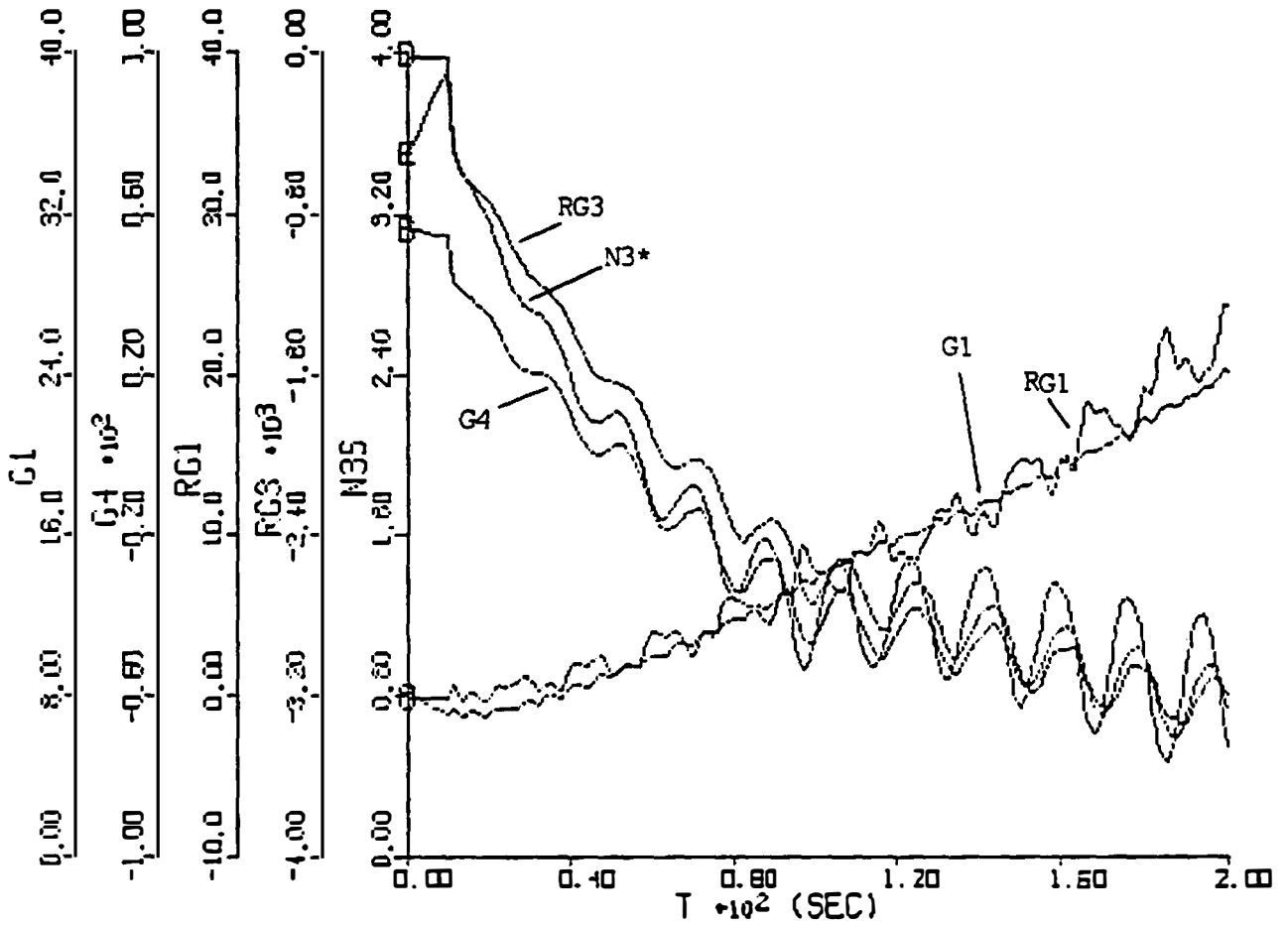

Figure 3.20: Adaptive Control inputs using the LDOC and RID control paradigms. LDOC inputs (G_1 and G_4) and RID inputs (R_{G1}, R_{G3}, N_3^*) are diverging as time elapses. The discreapencies between the plant and model are magnified to reach 300 % at the 200th second. This is practically not possible in any nuclear reactor.

3.4.3 Test-3 (T3): Measurement Time-Delay Problem

One of the problems associated with control systems is their robustness against abnormalities in measured signals. Sensors often undergo a gradual degradation before they are completely non-operational. Especially, temperature sensing devices such as thermocouples respond increasingly slower as their response characteristics degrade. Before a sensor anomaly is detected by any signal validation technique, it is important that control systems respond properly during this period. In Test-3, the simulations include time-delays in reactor power measurement P_1 and core coolant temperature P_4. The power measurement is a fast process and a 100 milliseconds time delay is quite undesirable. The temperature measurement on the other hand becomes significantly bad with a delay in the order of seconds. The measurement time delay is modeled using a first-order transport lag dynamics and is given by

$$\dot{P}_s = \frac{1}{\tau}(P - P_s) \tag{3.65}$$

where P_s, P and τ are the measured signal, plant state variable, and sensor time-constant, respectively.

The first simulation introduces a 100 millisecond time delay in the power measurement and a 2 seconds time delay in the temperature measurement. These delays are considered to be in addition to the normal time-constants of the sensors. Figure 3.21 shows the reactor power responses using the LDOC and RID controllers. The power responses slightly fall behind the demand, however it is insignificant for all practical purposes. On the other hand, the coolant temperature responses shown in Fig. 3.22 indicate a steep rise as the demand starts increasing. This is a contrary effect since the delayed signals cause early responses. The steep rise is due to the accumulation of errors which cannot be detected in time. The delayed version of errors are accumulated and magnified, thus the controllers respond excessively strong. Figure 3.23 shows the control signals generated by the LDOC and RID paradigms. As it can be seen from this figure, the coolant flow has dropped considerably during the first few seconds.

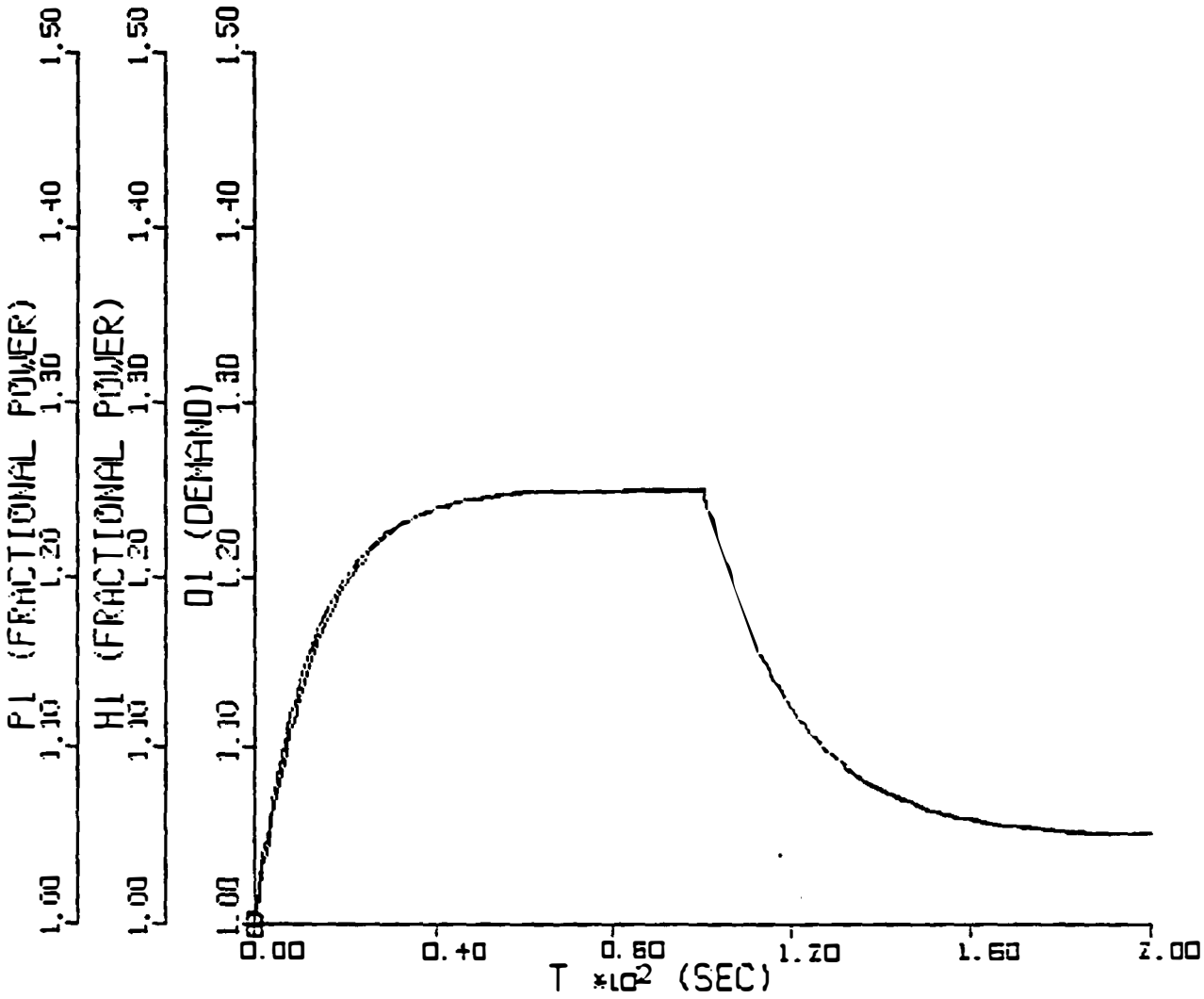

Figure 3.21: Reactor Power responses P_1,H_1 using the LDOC and RID control paradigms. Reactor follows the demand D_1 with a negligible error. In Test-3, measurements from the plant are delayed (0.1 second delay in reactor power, 2 seconds delay in coolant temperature signals).

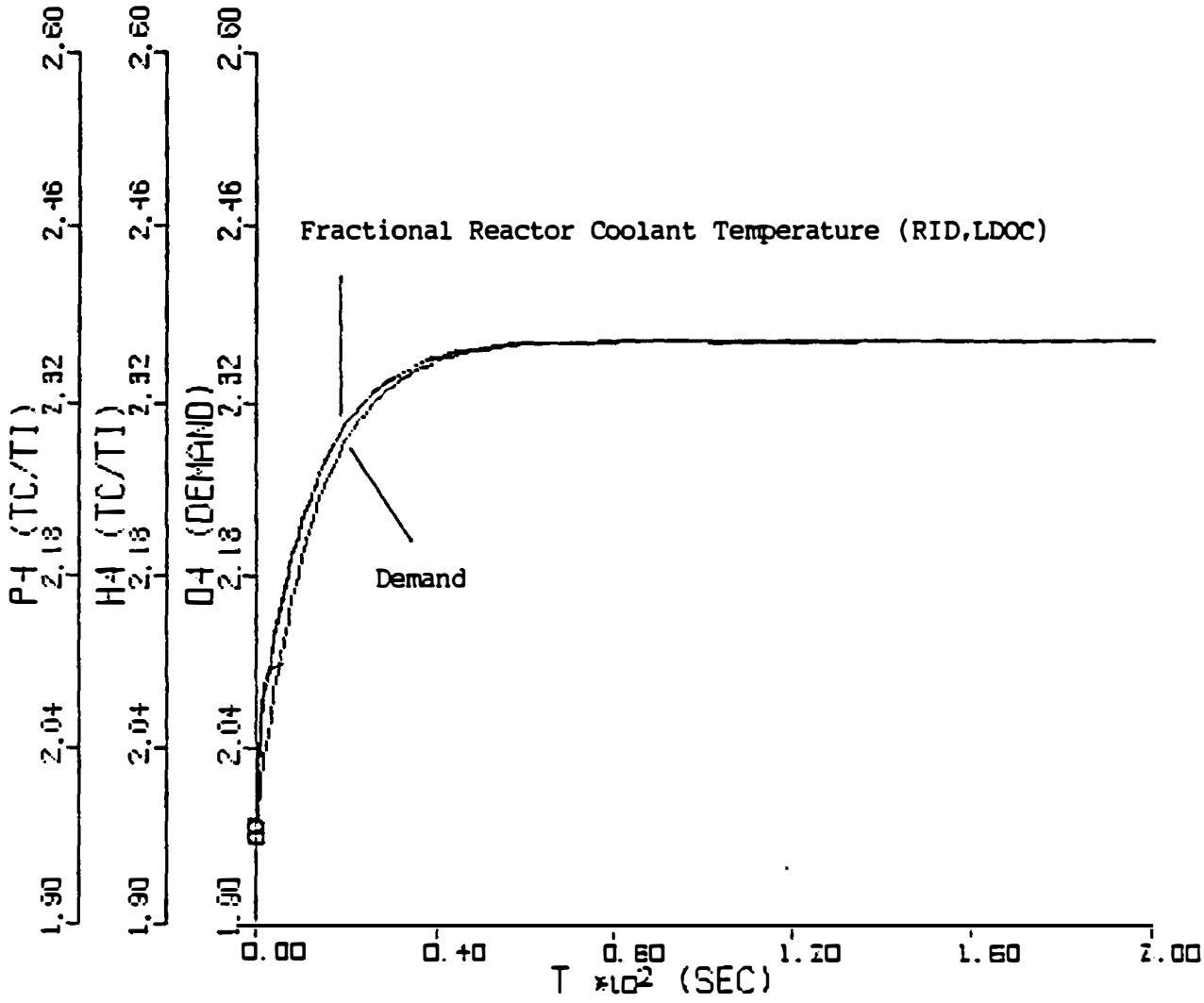

Figure 3.22: Coolant temperature responses P_4,H_4 using the LDOC and RID control paradigms. Reactor follows the demand D_4 with a significant error. At the beginning of the transient, the accumulation of the error can not be detected. Few seconds later, the magnified error causes a steep early response in coolant temperature. In Test-3, measurements from the plant are delayed (0.1 second delay in reactor power, 2 seconds delay in coolant temperature signals).

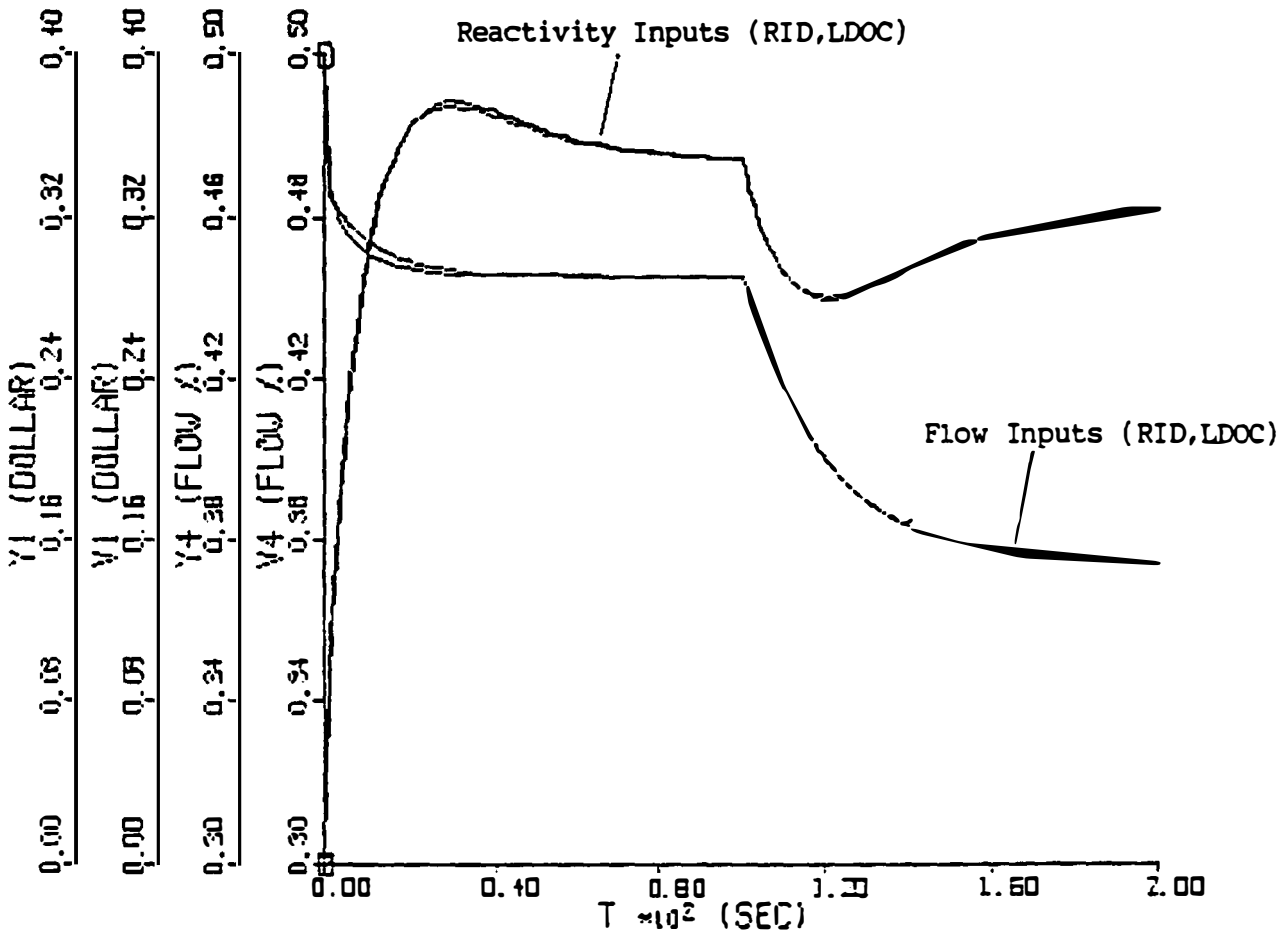

Figure 3.23: Control inputs generated by the LDOC and RID control paradigms. (reactivity Y_1,V_1, and coolant flow Y_4,V_4) In Test-3, measurements from the plant are delayed (0.1 second delay in reactor power, 2 seconds delay in coolant temperature signals). Delayed sensor signals cause an excessive response in flow control signals at the beginning of the transient.

The second simulation includes a 5 seconds time delay in the measurement of coolant temperature. Figure 3.24 shows the coolant temperature responses using the LDOC and RID paradigms. In comparison with the demand, the temperature responses are faster. The effect of longer time delays in the measurement causes faster response that may be undesirable for different reasons. Figure 3.25 shows the overshooting behavior of the flow response due to the time delay in measurements.

It is apparent that the low performance observed due to measurement time-delay is not design dependent since both of the techniques result in the same closed-loop behavior. The accumulation of errors is a common problem for every control paradigm. These tests verify that the RID control technique does not produce extra problems such as instability due to time delays in measurements. However, this statement may not be true when the actuator constraints do not allow such a fast response. Thus, further testing is performed for a constrained problem.

3.4.4 Test-4 (T4): Actuator Limitations

Actuator constraints limit the capability of control systems because of electro-mechanical or safety related limitations. Obviously, the error between the desired trajectory and system response should be minimized by modifying the trajectory such that the actuator limitations are not exceeded. There is a maximum rate for the control-rod motion, coolant pumps, and valve positioning in nuclear reactors where the safety limitations may even impose more restrictive rates. Thus, the trajectories must be designed conservatively to avoid violating such limitations.

Problems arise not during a normal operation with smooth trajectories but in case of high-frequency disturbances on the system. The inverse dynamics component of the RID control law creates a "mirror image" of the disturbance to completely cancel it. This fast component of the control signal may overdrive the actuator. Protecting the actuators from an excessive control signal can be accomplished by using limited integrators.

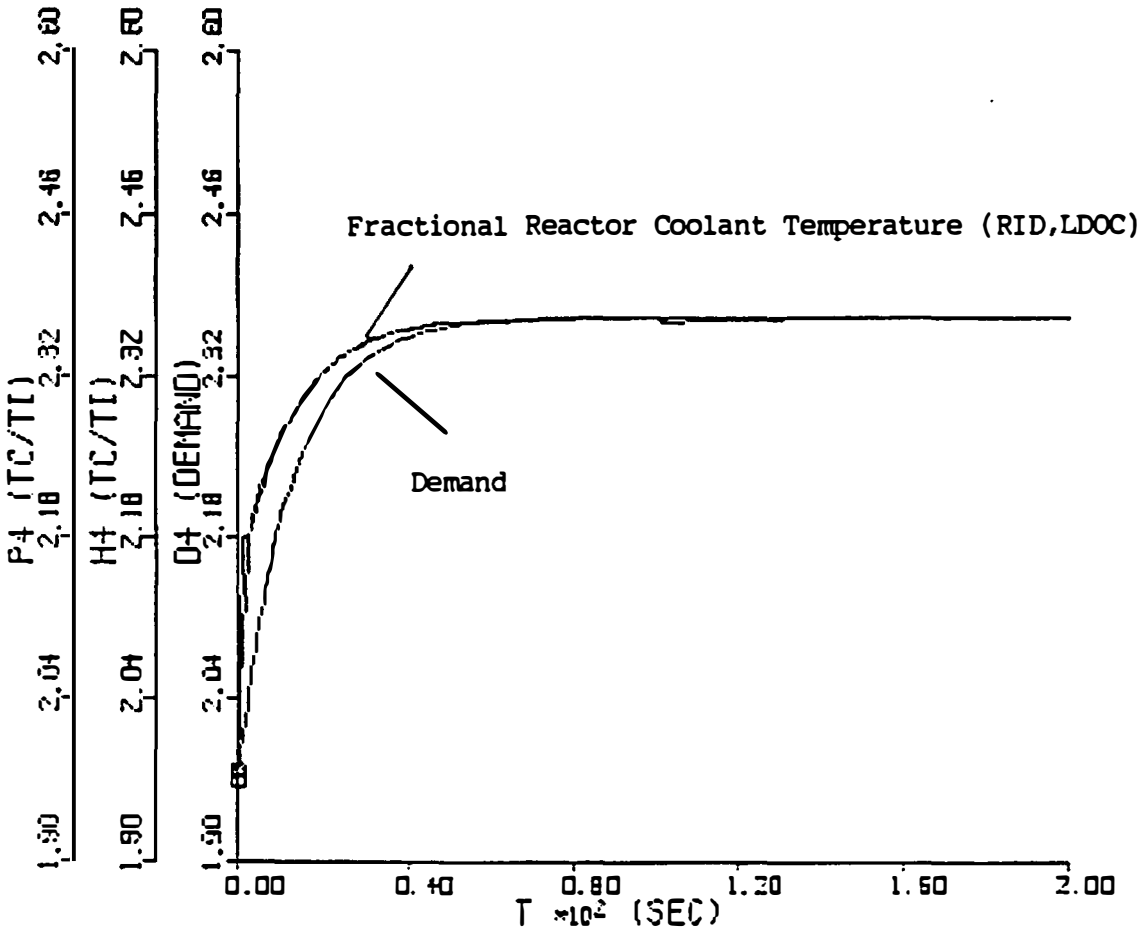

Figure 3.24: Coolant temperature responses P_4,H_4 using the LDOC and RID control paradigms. Reactor follows the demand D_4 with a significant error. The prompt jump at the begining of the transient is more severe as the delay-time prolongs. In Test-3, measurements from the plant are delayed (0.1 second delay in reactor power, 5 seconds delay in coolant temperature signals).

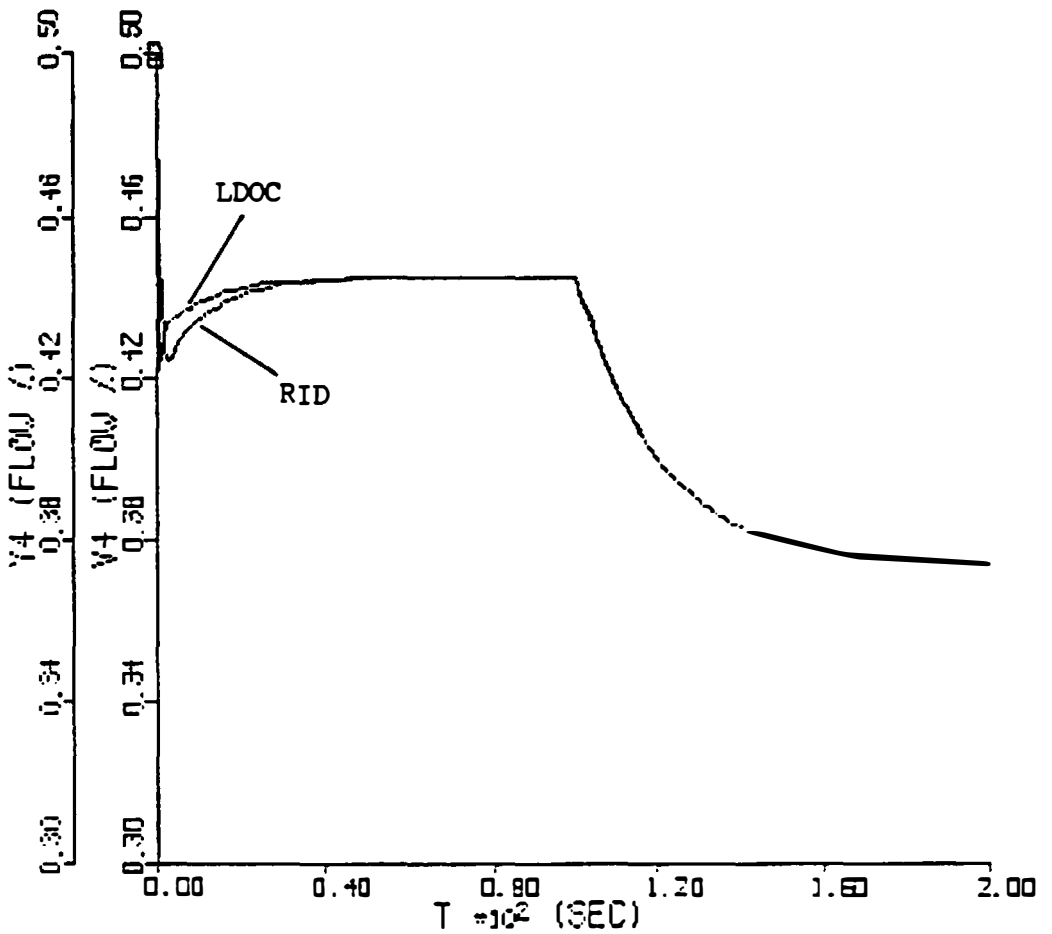

Figure 3.25: Control inputs generated by the LDOC and RID control paradigms. (coolant flow Y_4, V_4) In Test-3, measurements from the plant are delayed (0.1 second delay in reactor power, 5 seconds delay in coolant temperature signals). Delayed sensor signals cause an excessive response in flow control signals at the beginning of the transient. Incresed delay-time causes more severe prompt response.

Then the question is "how will the closed-loop system behave with a limited inverse-dynamics compensator?". The stability characteristics of the RID control with limited actuators are investigated in Test-4.

The simulations include previously stated demand following requirement and limited integrators that bound the control signal rates within some prescribed range. For this specific example, the reactivity insertion/withdrawal and coolant flow rates are chosen ± 0.1 and ± 0.005 per second. The actuator dynamics can be expressed as

$$\frac{dz}{dt} = \begin{cases} R_{max}, & k_v(u-z) \geq R_{max} \quad (3.66) \\ k_v(u-z), & R_{max} > k_v(u-z) > R_{min} \quad (3.67) \\ R_{min}, & k_v(u-z) \leq R_{min} \quad (3.68) \end{cases}$$

where R_{max} and R_{min} represent the upper and lower boundaries of the actuator signal rate $\frac{dz}{dt}$, and k_v is the time-constant of the actuator.

The constained problem when applied to the demand following reactor results in plant responses similar to that of the unconstrained problem. Figure 3.26 shows the reactor power responses using the LDOC and RID control paradigms. Compared with the demand, the error in trajectory following is negligible. The reactor coolant temperature responses in comparison with the demand are shown in Fig. 3.27. The LDOC and RID controllers perform efficient demand following task with a negligible error. The reactivity control inputs (Y_1 with LDOC, V_1 with RID) shown in Fig. 3.28 are compared with the constrained inputs (YY_1 of LDOC, VV_1 of RID) which are not allowed to change faster than ± 0.1\$ per second. This requirement is more restricted in power plants such as ± 0.01\$ per second. This figure shows that the original control signals were within the prescribed speed limit. On the other hand, the flow inputs generated by these controllers (Y_4 with LDOC, V_4 with RID) violate the rate limit of ± 0.005 fraction per second. Figure 3.29 shows the constrained flow VV_4 versus unconstrained flow V_4 generated by the RID control paradigm.

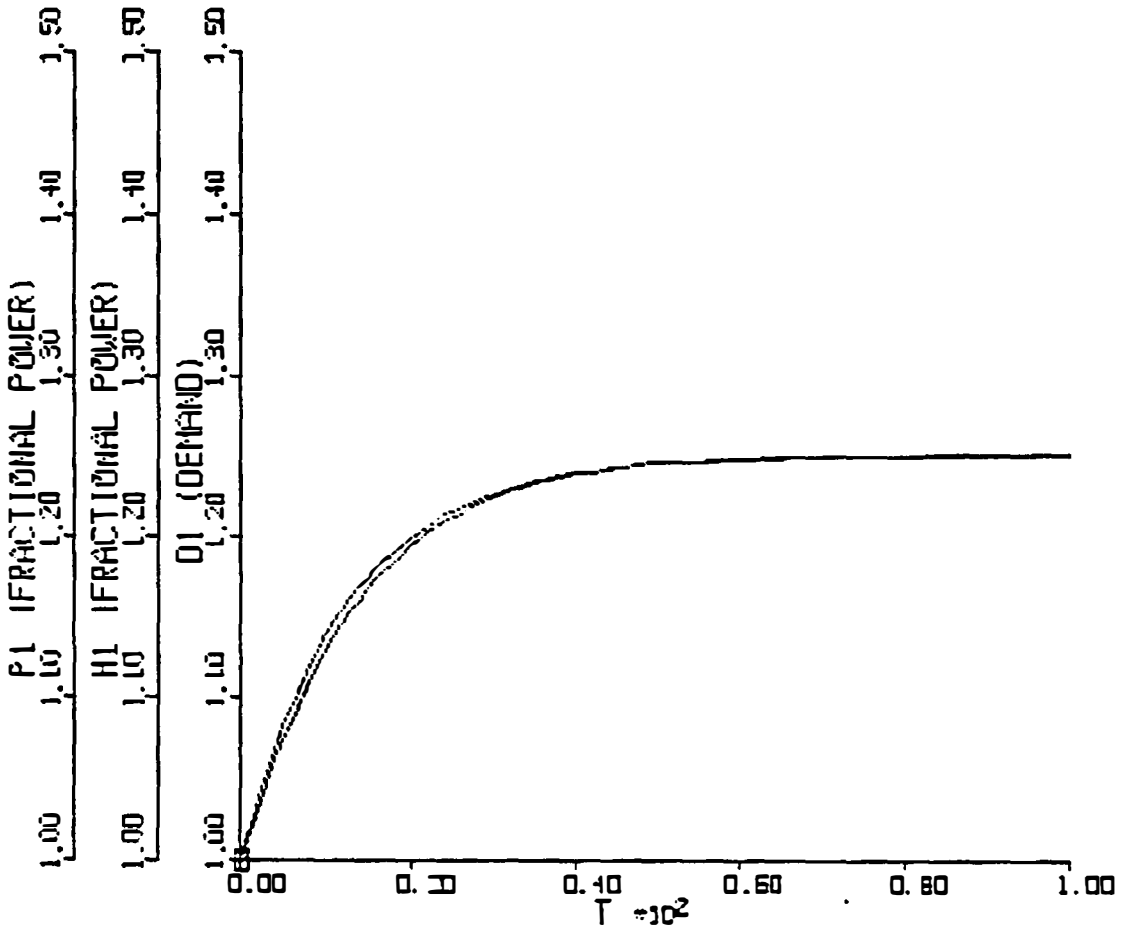

Figure 3.26: Reactor power responses P_1, H_1 using the LDOC and RID control paradigm. Reactor follows the demand D_1 with a negligible error. In Test-4, reactivity insertion rate and coolant flow rate are constrained.

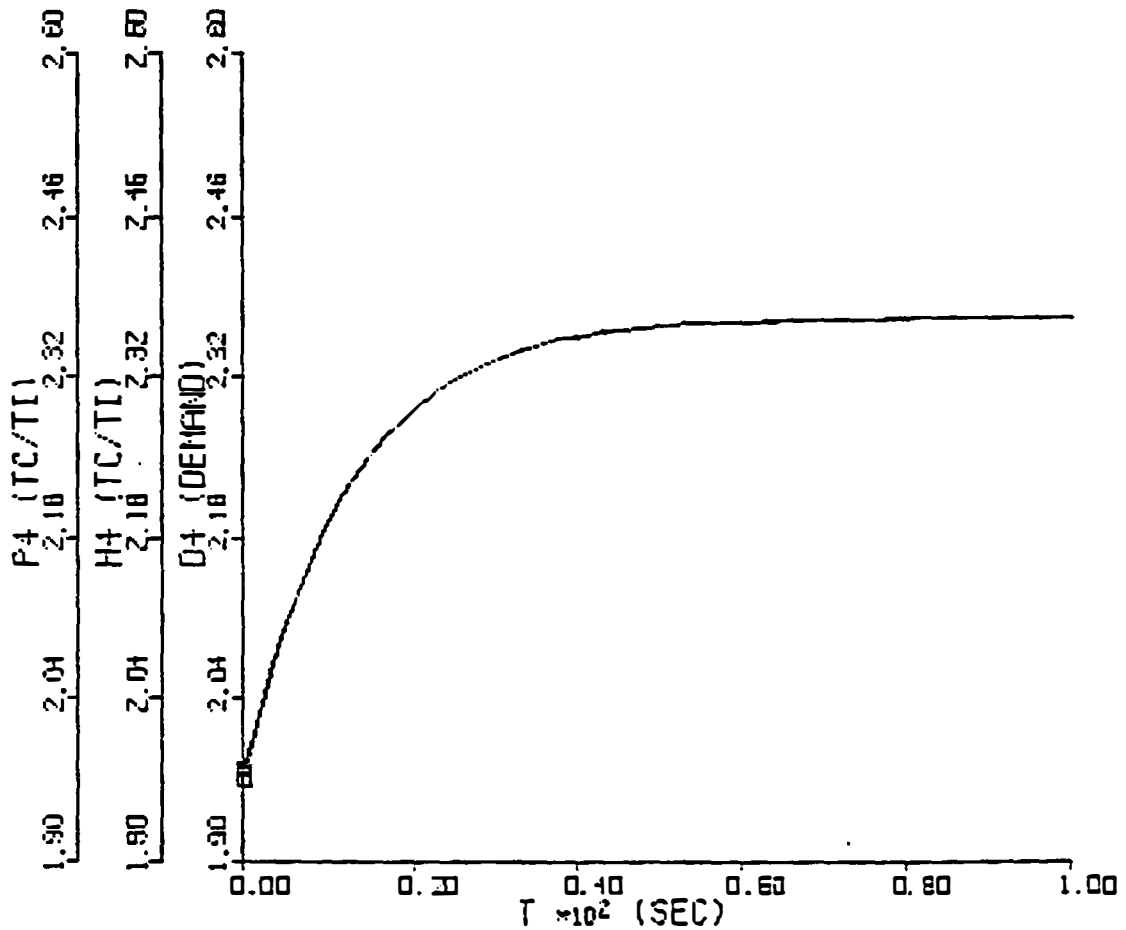

Figure 3.27: Reactor coolant temperature responses P_4,H_4 using the LDOC and RID control paradigms. Reactor follows the demand D_4 with a negligible error. In Test-4, reactivity insertion rate and coolant flow rate are constrained.

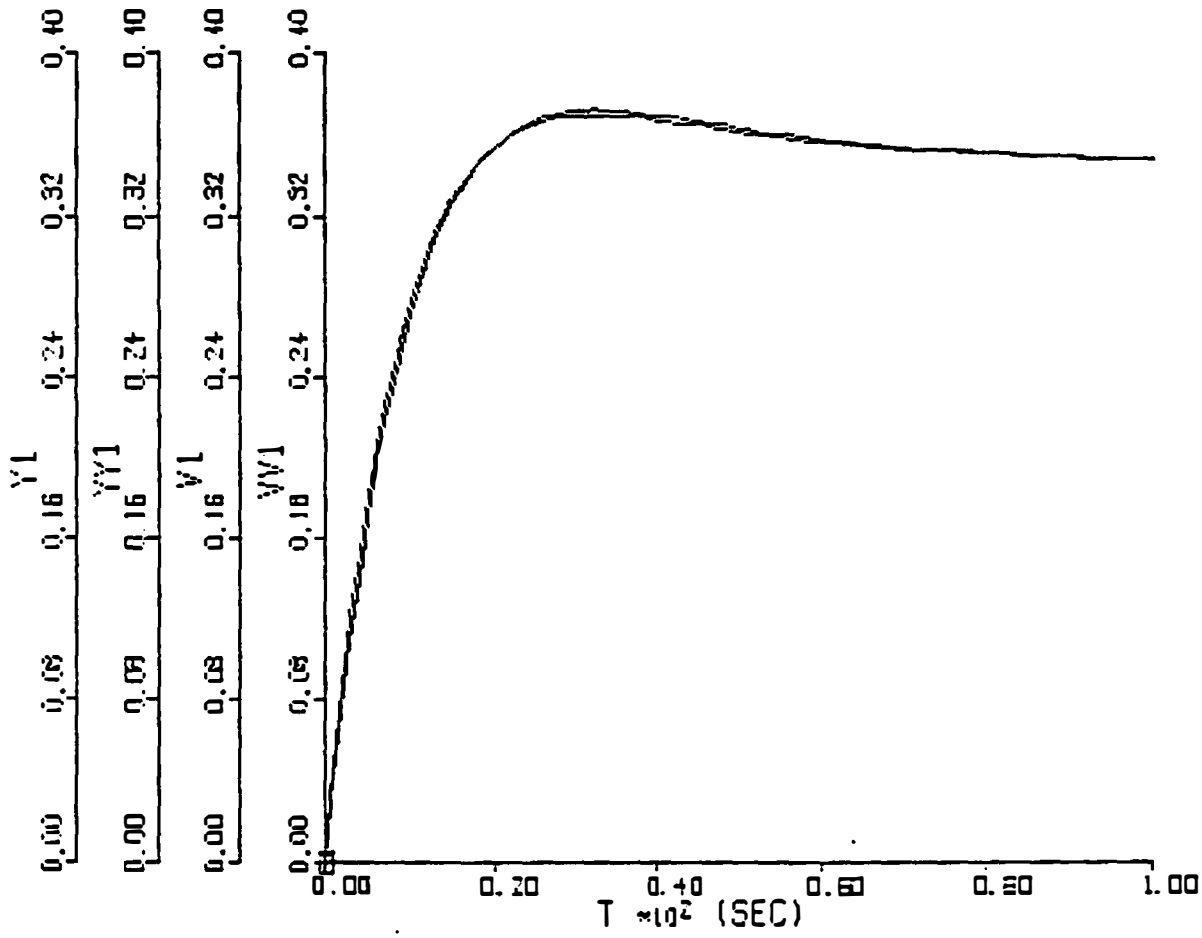

Figure 3.28: Reactivity inputs using the LDOC and RID control paradigms. Figure compares the unconstrained control signals (Y_1,V_1) with the constrained ones (YY_1,VV_1). In test-4, reactivity insertion rate and coolant flow rate are constrained.

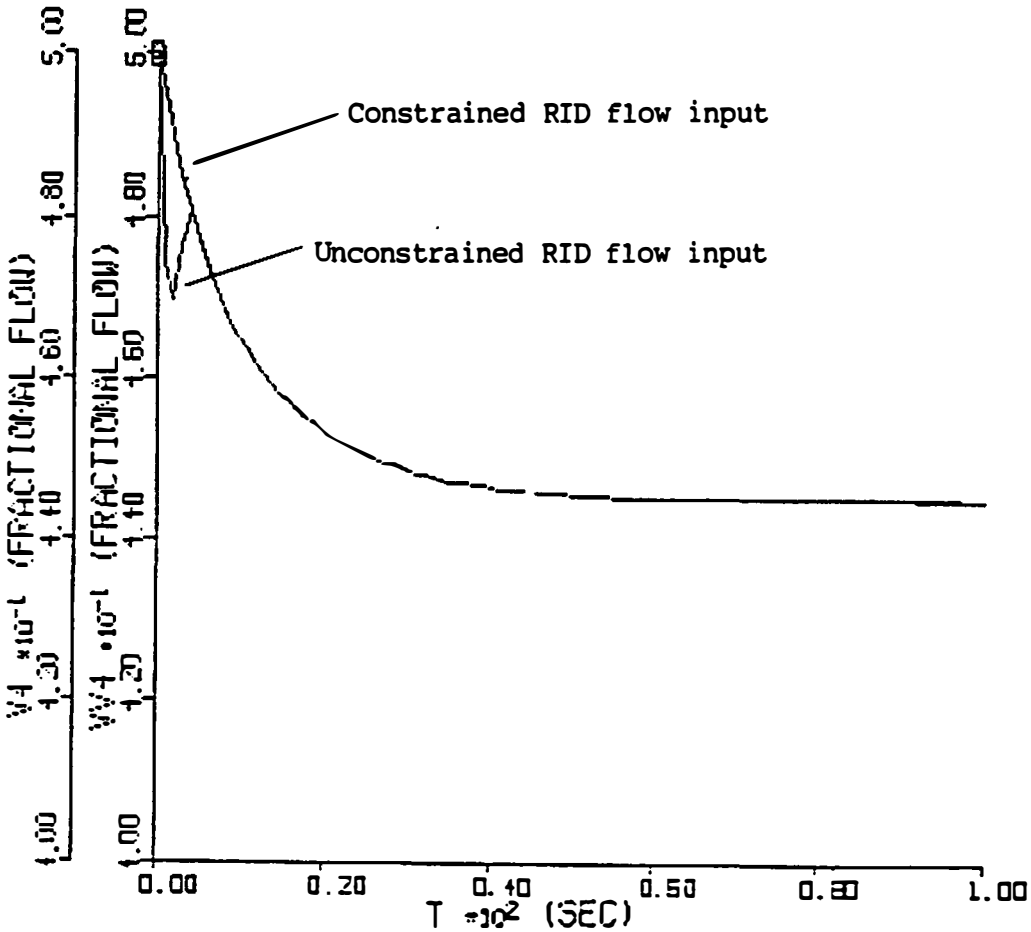

Figure 3.29: Constrained and unconstrained coolant flow inputs generated by the RID control paradigm. Speed rate is violated by the unconstrained control signal. However, constrained input is capable of efficient demand following control.

Similar comparison is shown in Fig. 3.30 illustrating the constrained flow $Y'Y_4$ and unconstrained flow Y_4 generated by the LDOC paradigm. Referring back to Fig. 3.27, it is seen that the effects of constrained inputs are negligible.

The second part of Test-4 includes a step disturbance on the reactor power which is similar to dropping a fuel rod inside the core that is worth 20 cents positive reactivity. The step reactivity of 20 cents causes a "mirror image" dynamics of -20 cents step reactivity with the RID control law. Obviously, this violates the actuator limitations. Thus, Test-4 investigates the control performance when the actuation capability is limited. Figure 3.31 shows the disturbance applied to the plant.

The reactor power response in comparison with the demand is shown in Fig. 3.32 where the RID controller is constrained. The demand is followed efficiently before and after the disturbance. Note that the peak in this figure cannot be compensated due to the limited rod speed. Figure 3.33 shows the reactor power response using the LDOC paradigm for the same scenario. Figures 3.34 and 3.35 show the coolant temperature responses using the RID and LDOC paradigms, respectively. From these figures it is clear that the reactor follows the demand before and after the perturbation in an efficient way. Again, the peak cannot be compensated due to the limitation on the coolant flow rate.

The reactivity control inputs generated by the RID control paradigm are shown in Fig. 3.36. The closed-loop plant uses the constrained input. The reactivity control inputs with the LDOC paradigm is shown in Fig. 3.37. Constrained and unconstrained flow inputs generated by the RID control and LDOC paradigms are shown in Figs. 3.38 and 3.39, respectively. Figures 3.40 and 3.41 show the speed of control signals which are bounded during operation ($\pm 0.1\$$per sec for the reactivity, $\pm 0.05 fraction$ per sec for the flow rate).

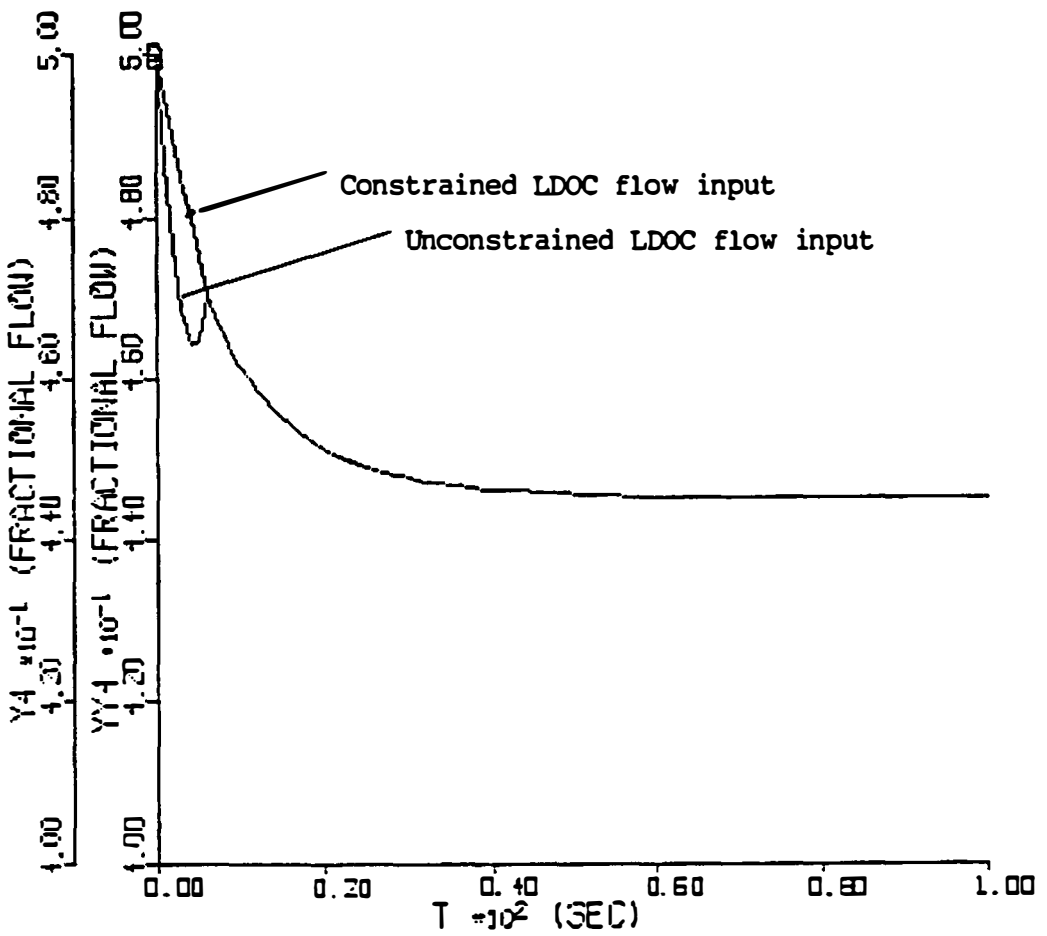

Figure 3.30: Constrained and unconstrained coolant flow inputs generated by the LDOC paradigm. Speed rate is violated by the unconstrained control signal. However, constrained input is capable of efficient demand following control.

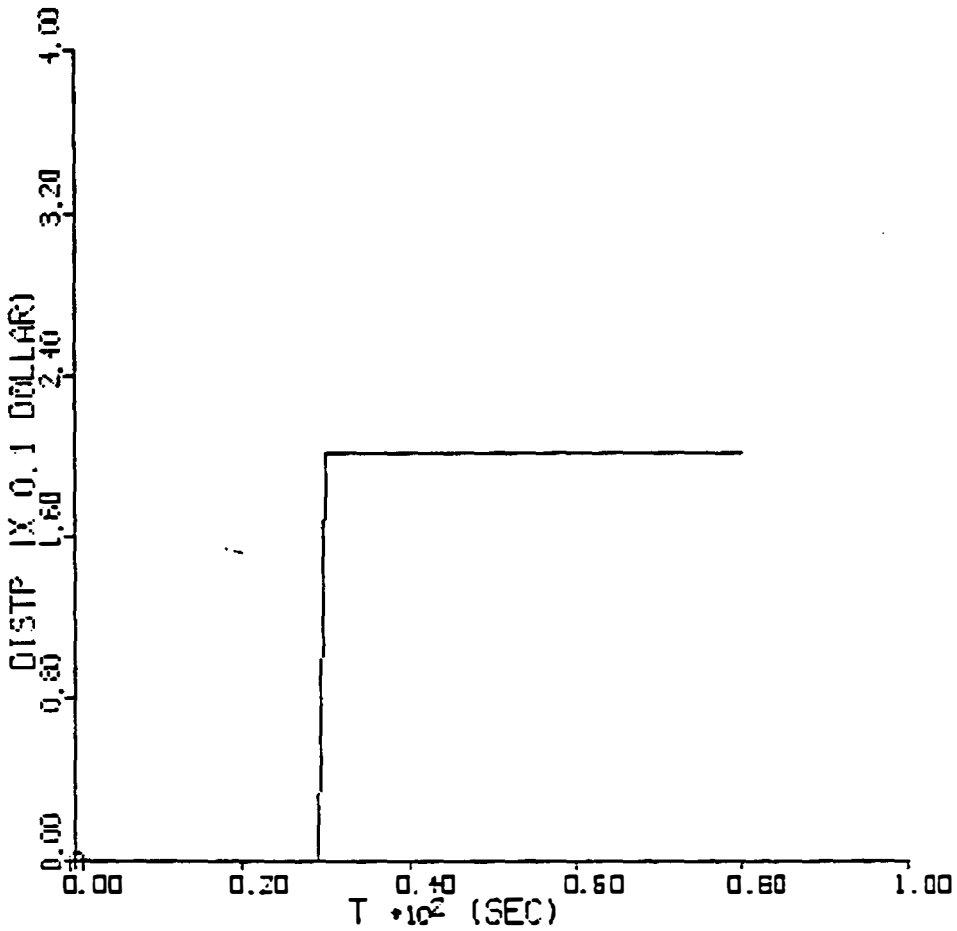

Figure 3.31: External disturbance applied to the reactor power during the demand following control. The step disturbance is equal to 0.2 $ positive reactivity.

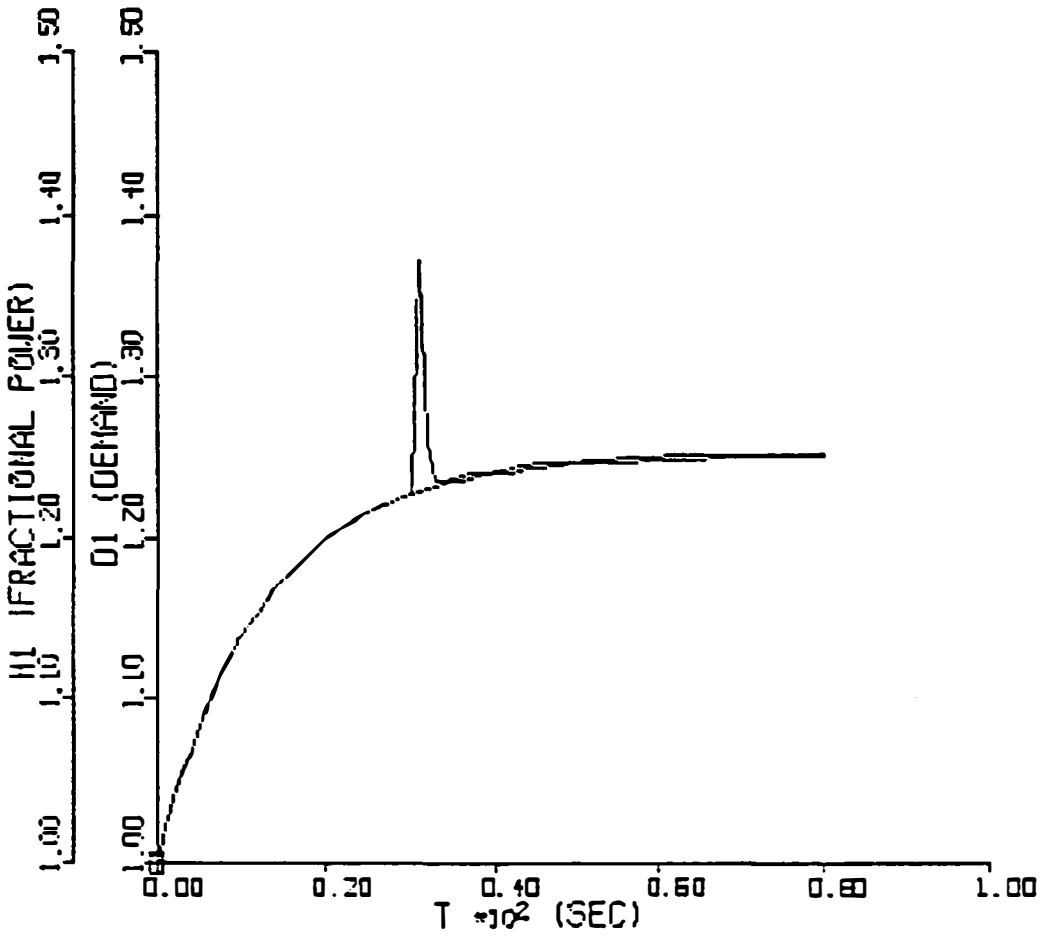

Figure 3.32: Reactor power response H_1 using the RID control paradigm. The reactor is subject to a +20 cents step disturbance where the controls are constrained. Reactor follows the demand D_1 before and after the disturbance.

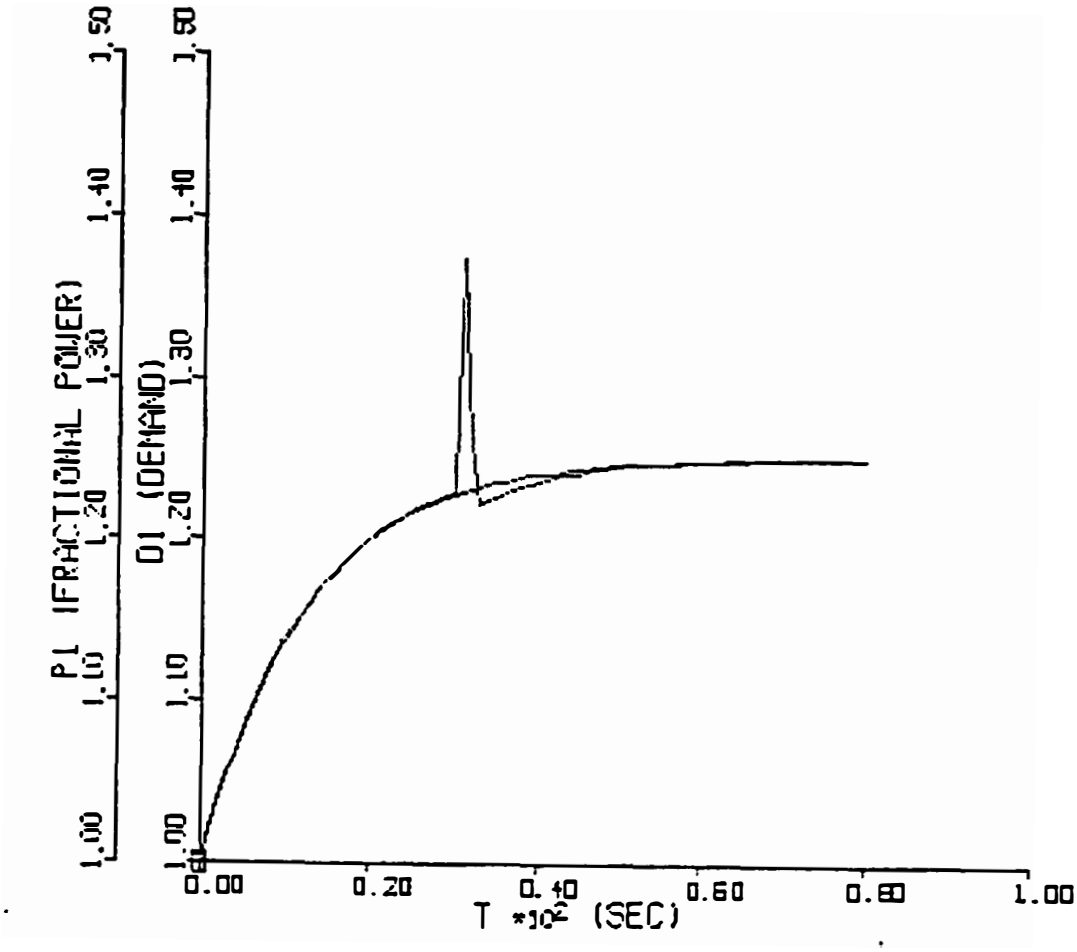

Figure 3.33: Reactor power response P_1 using the LDOC paradigm. The reactor is subject to a +20 cents step disturbance where the controls are constrained. Reactor follows the demand D_1 before and after the disturbance.

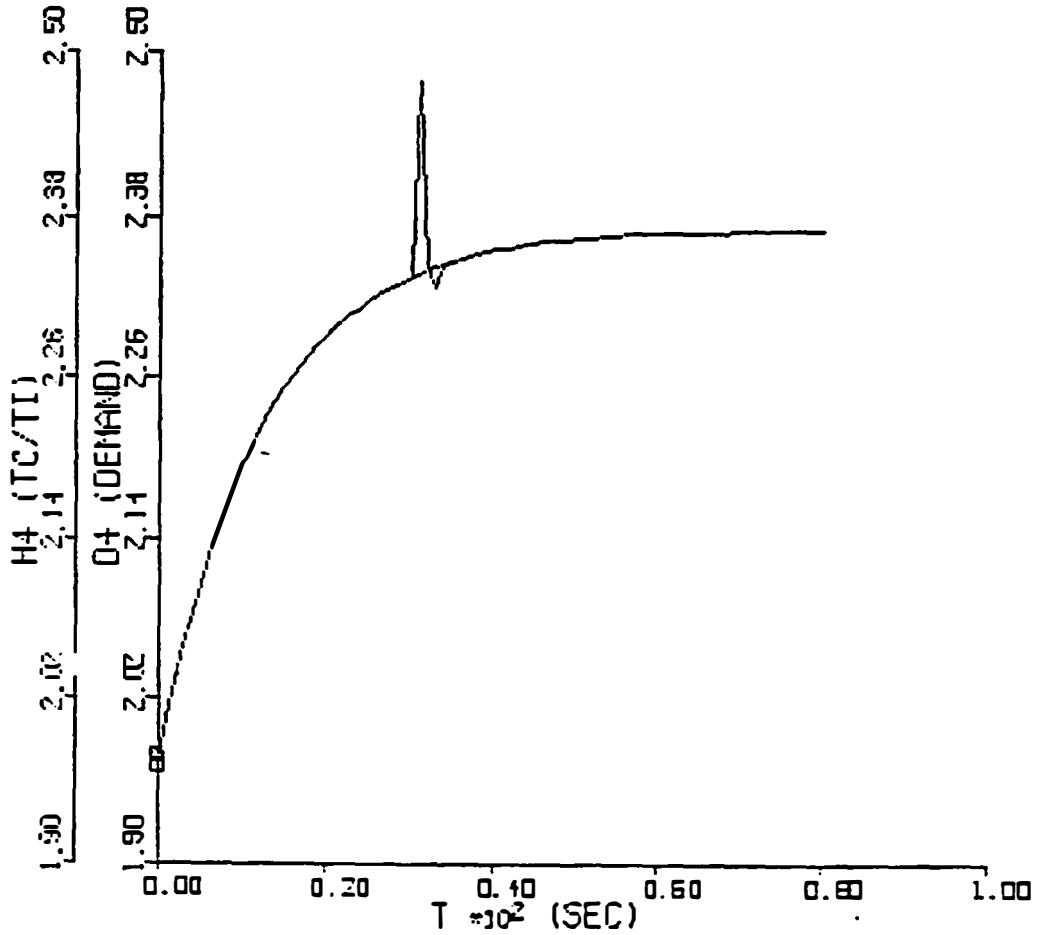

Figure 3.34: Reactor coolant temperature response H_4 using the RID control paradigm. The reactor is subject to a +20 cents step disturbance where the controls are constrained. Reactor follows the demand D_4 before and after the disturbance.

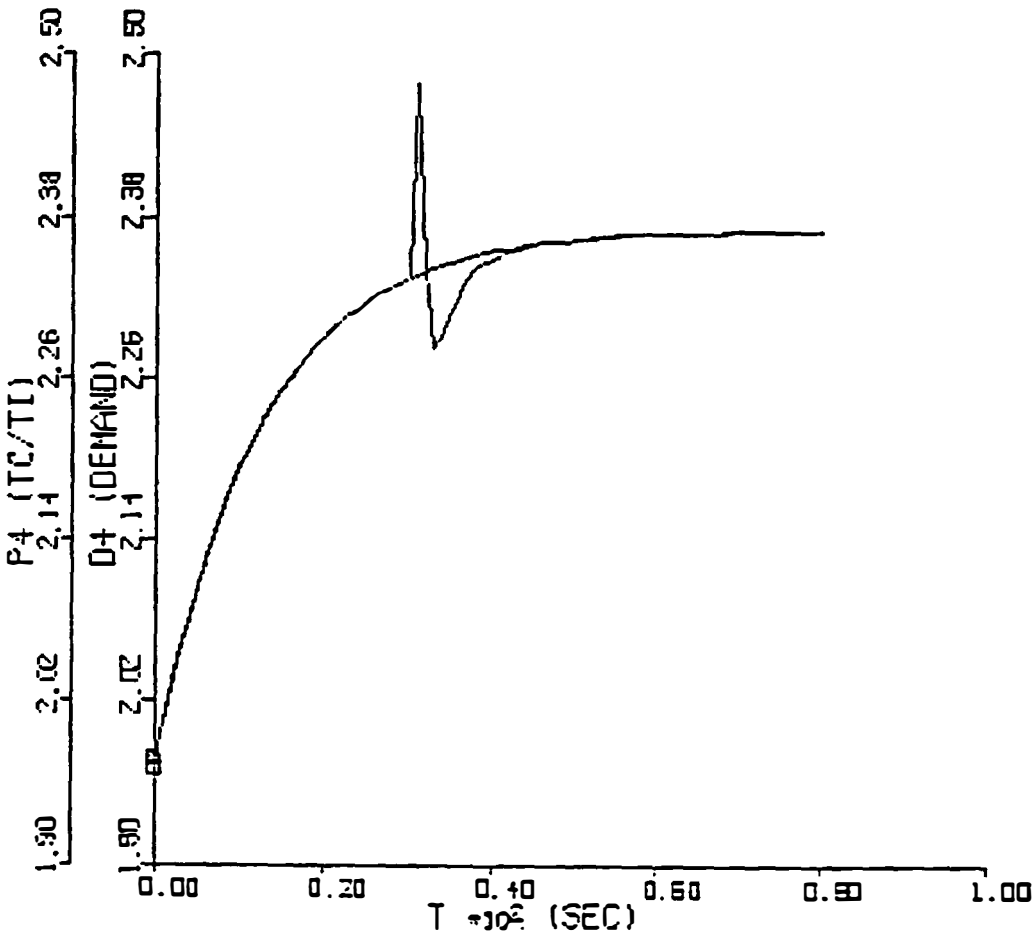

Figure 3.35: Reactor coolant temperature response using the LDOC paradigm. The reactor is subject to a +20 cents step disturbance where the controls are constrained. Reactor follows the demand D_4 before and after the disturbance.

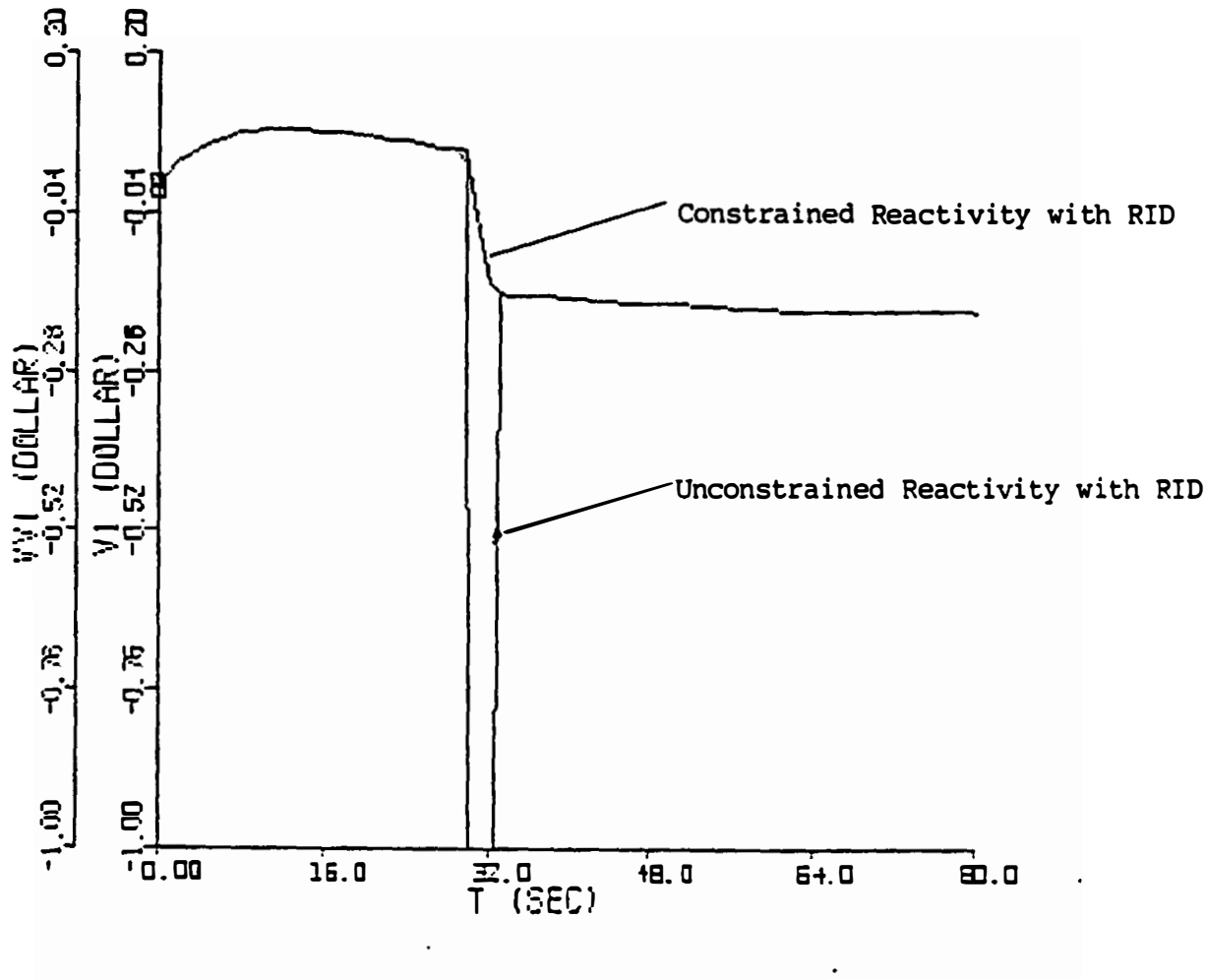

Figure 3.36: Constrained VV_1 and unconstrained V_1 reactivity inputs generated by the RID control paradigm. The closed-loop plant uses the constrained control signal. The reactor is subject to a +20 cents step disturbance.

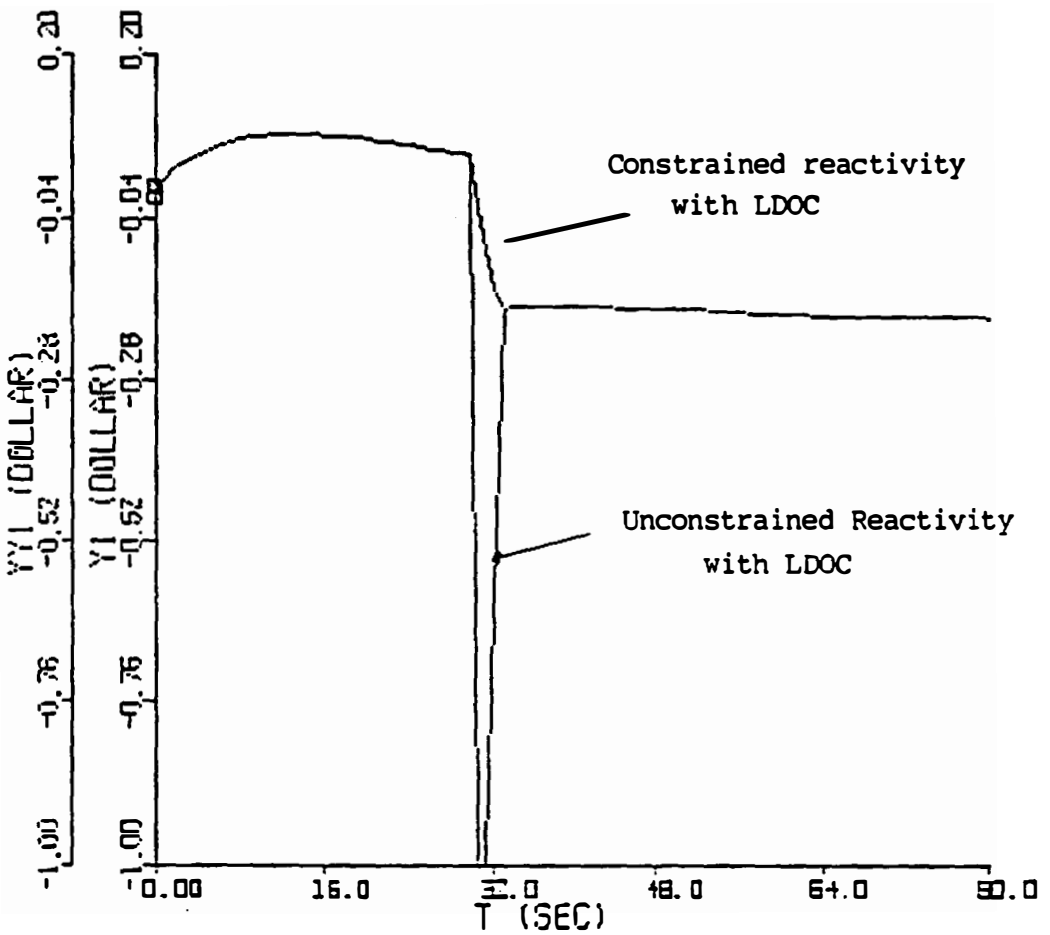

Figure 3.37: Constrained YY_1 and unconstrained Y_1 reactivity inputs generated by the LDOC paradigm. The closed-loop plant uses the constrained control signal. The reactor is subject to a +20 cents step disturbance.

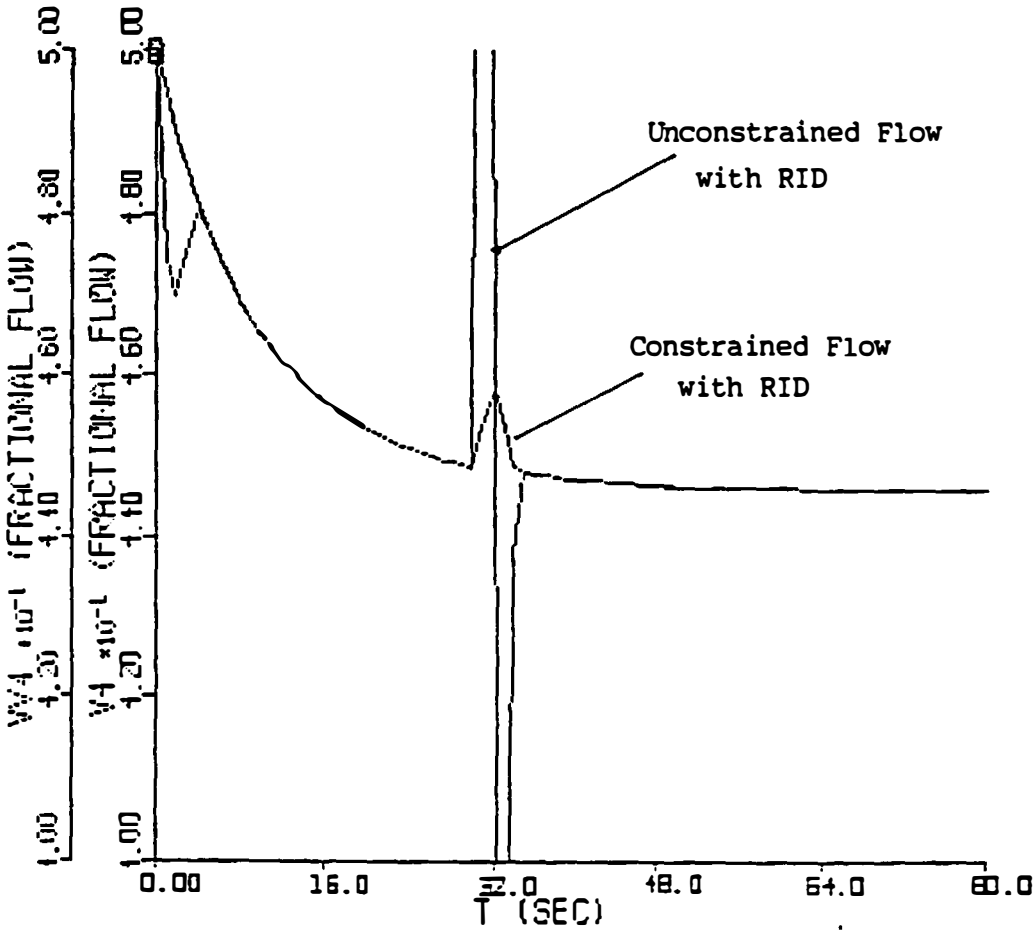

Figure 3.38: Constrained VV_4 and unconstrained V_4 flow inputs generated by the RID control paradigm. The closed-loop plant uses the constrained control signal. The reactor is subject to a +20 cents step disturbance.

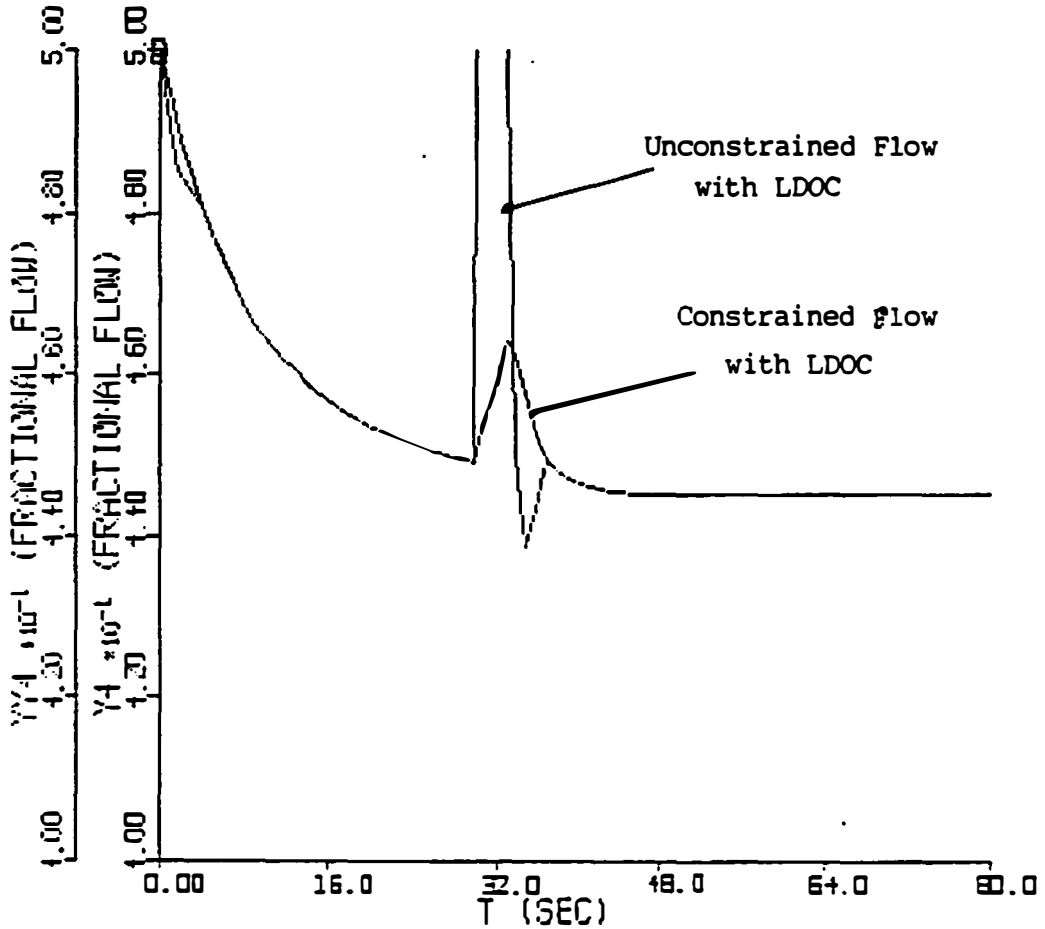

Figure 3.39: Constrained YY_4 and unconstrained Y_4 reactivity inputs generated by the LDOC paradigm. The closed-loop plant uses the constrained control signal. The reactor is subject to a +20 cents step disturbance.

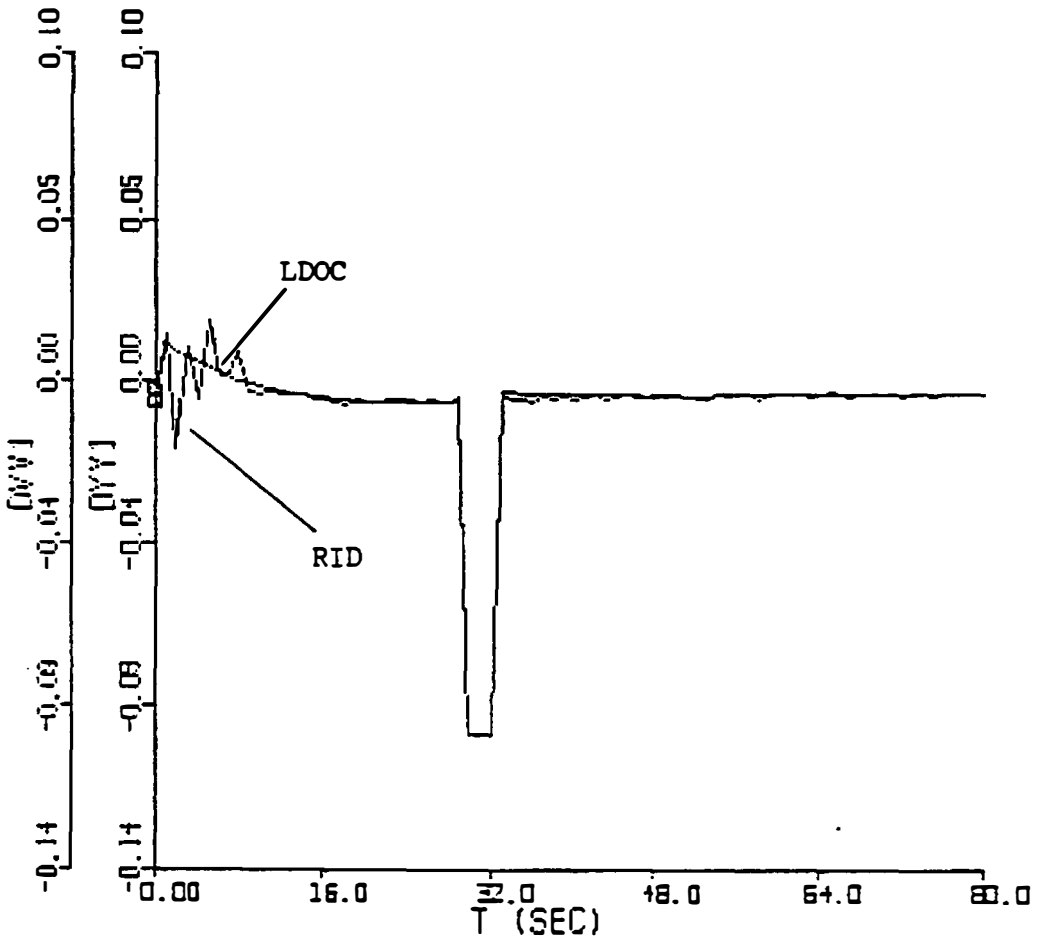

Figure 3.40: Rod speed with the LDOC and RID control paradigms during the demand following reactor. Reactor is subject to a +20 cents step disturbance. Rod speed is constrained ±0.1$ per second.

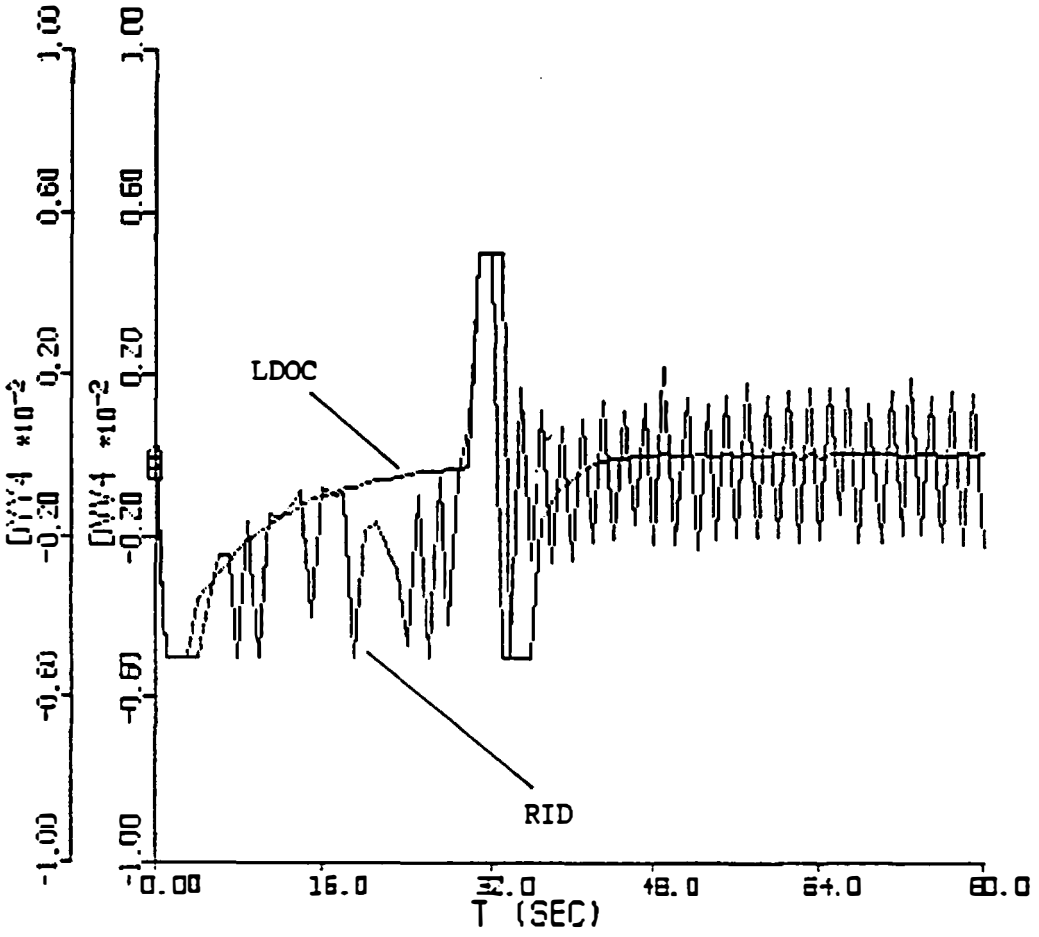

Figure 3.41: Coolant flow rate with the LDOC and RID control paradigms during the demand following reactor. Reactor is subject to a +20 cents step disturbance. Flow rate is constrained ±0.05 fraction per second.

3.4.5 Overall Performance Evaluation

Refering to the performance factors listed in Fig.3.1 and their interpretation given in Sect. 2.4, the simulation results are evaluated and the characteristics of the RID control paradigm are summarized below.

Time-Domain Characteristics: The RID control paradigm in MIMO application is observed to yield practically insignificant errors between the prescribed trajectories and plant responses. The errors during the transients and steady-state are both negligible and cannot be seen in the time plots. The same performance is observed in different tests (T1,T2,T3,T4) for cases where the deteriorating effects are tolerable or physically possible.

Frequency-Domain Characteristics: Because the problem is a non-linear one, the frequency-domain tools are not applicable in general. However, the models are linearized at the 200th second to check the eigenvalues and to determine the stability. In Test-2, the open-loop plant shows two eigenvalues with a positive real part, thus indicating unstable plant regime. Upon appending the RID controller, the closed-loop eigenvalues are all in the left side of the complex plane. This shows the restoration of stability by the RID control paradigm. Further analysis using the eigenvalue method is not useful because the nonlinearities may change the pole-zero locations.

Robustness: Although the real plants are not made of parameters or state variables, we refer to these terms to identify a reference point with respect to our modeling knowledge. Thus, a time-varying parametric change or an unknown nonlinearity both represent the same class of discrepancy between the plant and its model. Similarly, unexpected time-delays in sensor signals also fall into this class. Tests T2 and T3 show that the RID control paradigm is extremely robust against unknown

events of the plant. In Test-2, despite the unusually large discrepancy introduced, the RID controller is capable of providing stable and efficient plant behavior. This scenario can be converted such that the plant behaves reasonably whereas its model is extremely "bad". Obviously, the RID performance would be the same, may be even better since the controller mostly uses plant measurements. It can be concluded that the RID control paradigm allows modeling errors and almost guarantees robust performance when such errors are tolerable. It is observed that the measurement time-delays may cause an accumulated reaction and magnify the control signal superficially. However, the constrained control inputs, as explained below, are observed to maintain the high performance characteristics of the unconstrained control.

Downstream Effects: Because the ongoing discussion focuses on the evaluation of a control law, the downstream effects are only considered in this domain. One of the most important issues is to avoid the excessive and harsh usage of actuators that may shorten their average life-time. Preventing actuators from such deteriorating effects requires the assignment of constraints on control inputs. Constraints may also be assigned to provide safe operations. The simulations in Test 4 include constraints on control inputs. It is observed that the RID control paradigm retains high performance characteristics even with a limited actuation capability.

Tuning Characteristics: One of the most useful properties of the RID control paradigm is related to its tuning. Figure 3.42 shows the RID tuning compared with the LDOC paradigm. Obviously, the RID tuning task can be reduced to tuning of only two parameters ($K = 1000, K_G = 10$) for the benchmark problem. The range of tuning parameters often lies between positive numbers 1 and 1000.

RID Tuning	LDOC Tuning
$K_1 = 1000$	$P_{C10} = 0.$
$K_4 = 1000$	$P_{C40} = 0.$
$K_{G1} = 10$	$K_{1I} = -0.5$
$K_{G3} = 10$	$K_{4I} = -4.2$
$K_{G4} = 10$	$K_{1P} = 0.5$
	$K_{4P} = 0.1$
	$R_{1P} = 4.0$
	$R_{4P} = 0.1$
	$P_{1I} = -0.5$
	$P_{4I} = -0.04$

Figure 3.42: Tuning parameters used in the RID and LDOC designs.

The control gains (K) when selected larger than 1000 may cause the on-line model, if any used, to become stiff which may impose computational problems. It is observed that the sensitivity to the tuning parameter K is low whereas the adaptive term K_G is slightly higher. On the other hand, the LDOC paradigm requires careful tuning of parameters that can have negative and positive values. The simplicity of the RID tuning suggests that it will impose no problems for the in-situ tuning task.

Ability to Convey Meaningful Information: The RID control paradigm uses adaptive features that are verified to be efficient through tests T2 and T3. The adaptive control signals constitute a useful tool to monitor the unanticipated plant behavior. Depending on the design, different adaptive control signals represent anomalies of different nature. In the benchmark problem for example, the adaptive term R_{G1} represents the anomalies with respect to reactivity feedback (or disturbance), whereas the terms R_{G3} and N_3^* are related to the heat transfer mechanism between the fuel and core coolant. In MIMO applications where a cross-talk between the control inputs exist, the identification of the anomaly may require further analysis for tightly coupled mechanisms.

User Understandability: Compared to other control methods, the RID control paradigm clearly states how its control law is derived. A user who is familiar with the design characteristics of the system can understand the control law, thus would be able to interpret control actions if they are monitored on-line in the plant. This facilitates the on-line tuning task. In the RID design, it is clear that higher gains provide stronger control actions similar to that of a simple proportional controller tuning. The concept of inverse dynamics (mirror image dynamics) may be much easier for a plant operator to understand compared to the cost function approach of the LQR method or

the Lagrangian density method of the LDOC.

Resource Requirements: The RID control paradigm uses an algabraic control law that is easy to implement in a digital or analog environment. If an on-line model is needed for adaptation, the digital technology is more appropriate. It is clear that the RID computations do not require solving ordinary differential equations except for the on-line model. Thus, the real-time problem is not worse than using any other model-reference adaptive control (MRAC) method.

The simulation results show that the performance of the RID control paradigm is very close to that of the LDOC's. By analyzing the control signals generated by the two paradigms throughout the tests T1, T2, T3, and T4, it can be concluded that the RID control paradigm is as optimal as the LDOC paradigm within the accuracy of tuning parameters.

Chapter 4

Application to Nuclear Systems

4.1 Introduction

Advances in nuclear power plant technology depends upon improvements in its operating philosophy and related systems. The future generation of nuclear reactors will definitely require extended operational envelope using fault-tolerant strategies. In large-scale systems, automation frees operators from vigilance over routine and tedious tasks by emulating the human expertise in a faster and reliable fashion. Thus, the improvement in nuclear reactor operations hinges on an automatic control capability that functions efficiently under various operating conditions.

The existing operating philosophy in nuclear power plants is primarily dependent on plant operators because the conventional technology is not completely suitable for automatic control. In addition, the history of power plant operations indicates that the conventional control systems may fail when plant nonlinearities become significant. Typical examples in PWRs include the power oscillations due to nonlinear xenon behavior, and large swings in steam generator level during startup. When such problems arise, operators can maneuver to shutdown the plant if the emergency systems have not already intervened. The issues such as the trip avoidance and extended maneuverability, therefore, require new control technologies to be developed for improved plant availability and reliability.

The RID control paradigm can be incorporated within the automatic control

strategies because it provides robust nonlinear control for a wide range of operations. The high performance characteristics of the inverse dynamics concept were illustrated in Chapter 3, where a low order nuclear reactor model was used. The next step is taken to investigate the effectiveness of the RID control paradigm in applications to some of the typical control problems in nuclear reactors. These applications use detailed models that are validated against plant data.

The first application is the control of xenon induced axial power oscillations in PWRs. This problem often arises in conventional plants and it is primarily controlled by operators unless the oscillations exceed safety limits. Thus, an appropriate nonlinear controller would be useful for trip avoidance purposes. The main objective here is to investigate if the RID control paradigm is a potential candidate for this task.

The steam generator level in PWRs is known to swing during low power levels, particularly during startup. This problem often causes reactor trips. One of the most effective ways of improving steam generator control is to have rapid maneuvering capability of feedwater flow. The second application in this chapter includes a RID control design for the feedwater-train system.

Plant nonlinearities become very dominant during the startup phase of nuclear plants. It is not always possible to use linear controllers for the automation of startup. This constitutes another potential area where an appropriate nonlinear control technique may be very useful. The third application includes a RID control design for the Experimental Breeder Reactor-II (EBR-II) startup task. The simulation results include comparison with two other nonlinear control methods, namely, the fuzzy logic and neural network paradigms [29].

4.2 Xenon Oscillation Control in PWRs

The on-line control of core dynamics in large pressurized water reactors (PWRs) is known to degrade due to xenon induced power oscillations (XIPOs) during different modes of day-to-day reactor operations. Although the routine operational

decisions can avoid violating the safety requirements, the XIPO may cause unscheduled shutdowns or mandatory maneuvers which reduce the plant availability and trigger several other complications.

The xenon oscillation in large PWRs is a highly nonlinear phenomenon which is a function of several time-variant parameters such as the fuel cycle, boron level, rod position and power level. The physics involved in XIPO is particularly related to the fission product xenon-135 isotope which has high thermal neutron absorption cross section and relatively large fission yield. There is a small fraction of this isotope produced directly by fission, but the major portion is formed indirectly by the Te-Ba decay chain. Axially non uniform build-up and removal of the xenon-135 causes the power distribution in the core to oscillate between the top and the bottom with a period of 20 to 30 hours. The power distribution in the core is often indicated by the axial shape index (ASI). The steady-state reactor operation results in an equilibrium xenon concentration with significant absorption of neutrons (xenon poisoning). Thus, the reactors are designed to contain excessive amount of fuel or high fuel enrichment to compensate for possible xenon poisoning. In the dynamic phase, the use of control rods or boration for power maneuvers may disturb the equilibrium xenon concentration which causes a possible ASI oscillation. This situation is magnified in the case of a reactor trip, as it affects the timing and complexity of restarting the reactor.

The xenon distribution in a reactor core is detected through changes in the axial and radial power distribution, and core reactivity. The fact that there is no direct way of monitoring the xenon concentration often causes operators a great deal of difficulty in anticipating the amplitude, direction, and rate of change of the xenon imbalance. Once it is detected, the selection of the best strategy to recover from xenon oscillations also constitutes a complicated problem. The minimization of the detrimental transient thermal effects on the fuel rods often requires a slow change in the axial power shape which may interfere with the axial shape control. Optimal fuel utilization is best achieved by unrodded operation. The capability of borating or deborating the primary system coolant via the charging pumps may be limited. Even for high level soluble borons, the insertion of control rods, with

compensation by boron generates waste water causing high costs for the cleanup. Thus, a control action against XIPO requires the resolution of several conflicts and the use of optimized strategies.

4.2.1 Previous Accomplishments in Spatial Control

The most widely used form of effective XIPO control in PWRs employs the half-cycle damping strategy [30]. The operator inserts and withdraws control rods during the half cycle of the oscillation when the axial power shape is shifted toward the top of the core. With this strategy, the amplitude of the oscillation can be maintained within the limits determined by the technical specifications. However, the lack of direct measurements complicates the anticipation of the expected xenon behavior and the target axial offset (**TAO**). Thus the trajectory of the rod movement is often determined by analyzing the past behavior of the reactor.

There are several operating reactors using some form of automatic power distribution control system. Among them, gas-cooled reactors (**AGR**), presurrized heavy water reactors (**PHWR**) and boiling water reactors (**BWR**) employ computerized control schemes [31]. In these schemes, the core is axially divided into several imaginary control zones where each zone has a single-input single-output (**SISO**) proportional controller loop, and is equipped with its own detector and actuator. In one of the Swedish PWRs [32], three partially coupled set-point control loops are used for both axial and azimuthal oscillations. This system allows load following operation of the reactor with fast changes in power level. The latest applications in French PWRs [5] also include spatial control with an on-line micro computer where the tuning takes place.

The automatic spatial control systems already in use in plants often consist of SISO control loops where their interactions are adjusted by simply tuning the proportional gains provided the overall system performs well. The implementations in other fields (aerospace and chemical process) have shown that the closed-loop performance using systematic advanced control techniques can be several times

more efficient than that of simple proportional controllers. As Karpinnen [31] indicated in his collective study on proposed control methods for spatial reactor control, the practical implementation of most of the optimal control methods is not likely to take place due to major simplifications in problem formulation, core and controller modeling, and optimization methods. Particularly, most of the modern control theory methods require linear or linearized models which constitute a major handicap in representing the nonlinearities involved. The existing nonlinear optimal techniques also require simplifications as specific problems (like the two-point boundary value problem) are encountered.

4.2.2 Axial Xenon Oscillation Model

The control design and simulation studies include a previously developed xenon oscillation model [33]. The test results of Oconee Unit #2 (Duke Power Company,1974) were accurately estimated using the model including the limit cycle oscillations for spatial oscillations of the first harmonic. The validity of the model was also demonstrated for parameter identification and control purposes [34].

The two-point model employs the nonlinear xenon and iodine balance equations and one group, one-dimensional, neutron diffusion equation having nonlinear power reactivity feedback. A two-term spatial, harmonic-series solution was assumed for the flux, xenon and iodine distributions. The reactor model is made as nearly critical as possible using a variational estimate of the eigenvalue of the one-dimensional diffusion equation. The xenon and iodine equations are then directly solved. The cylindrical core of a pressurized water reactor is reduced to a slab geometry, which is further reduced to a two point representation by dividing the slab into two equal halves and integrating over each half to find the average values for the flux, xenon, and iodine spatial distributions. The total power of the reactor core is held constant even though the power density varies as a function of both time and position.

The spatial average of the normalized flux for the lower half of the core is

$$\overline{\psi_1}(t) = \frac{2}{\pi}[1 - A(t)]. \tag{4.1}$$

Similarly, the normalized xenon and iodine concentrations are

$$\overline{x_1} = \frac{2}{\pi}[1 - B(t)] \tag{4.2}$$

$$\overline{y_1} = \frac{2}{\pi}[1 - C(t)] \tag{4.3}$$

where $A(t)$, $B(t)$ and $C(t)$ are the amplitude functions of the flux, xenon, and iodine concentrations. The equations for the upper half of the core are

$$\overline{\psi_2} = \frac{2}{\pi}[1 + A(t)] \tag{4.4}$$

$$\overline{x_2} = \frac{2}{\pi}[1 + B(t)] \tag{4.5}$$

$$\overline{y_2} = \frac{2}{\pi}[1 + C(t)]. \tag{4.6}$$

The dynamics of the amplitude functions given in the literature [33] are

$$\frac{d}{dt}C(t) = \left(\gamma_I \Sigma_f \frac{\phi_0}{I_0}\right) A(t) - \lambda_I C(t) \tag{4.7}$$

$$\begin{aligned}\frac{d}{dt}B(t) &= \left(\gamma_x \Sigma_f \frac{\phi_0}{X_0}\right) A(t) + \left(\lambda_I \frac{I_0}{X_0}\right) C(t) - \lambda_x B(t) \\ &\quad - (\sigma_x \phi_0)\left(\frac{2}{3}(A(t) + B(t)) + \frac{\pi}{4}A(t)B(t)\right)\end{aligned} \tag{4.8}$$

and the xenon amplitude $A(t)$ satisfies a quadratic equation given by

$$-\beta_2 A^2 + 2(\beta_1 - \beta_3)A + \beta_2 = 0 \tag{4.9}$$

where

$$\beta_1 = \frac{1}{\Sigma_f}\left(4Db^2 + \frac{1}{2}(\Sigma_{a1} + \Sigma_{a2}) + \frac{32}{15\pi}(\sigma_x X_0 + 3\alpha_F \phi_0 \overline{\Sigma_a})\right) \tag{4.10}$$

$$\beta_2 = \frac{1}{\Sigma_f}\left(\frac{8}{3\pi}(-\Sigma_{a1} + \Sigma_{a2}) + \frac{64}{15\pi}\sigma_x X_0 B(t)\right) \tag{4.11}$$

$$\beta_3 = \frac{1}{\Sigma_f}\left(Db^2 + \frac{1}{2}(\Sigma_{a1} + \Sigma_{a2}) + \frac{8}{3\pi}(\sigma_x X_0 + \alpha_F \phi_0 \overline{\Sigma_a})\right) \tag{4.12}$$

The one group diffusion parameters of the dynamic equations stated above are listed in Table 4.1. Note that the parameters α_F, σ_x, and D are the optimized estimates obtained in a parameter identification study [34]. The $\overline{\Sigma_a}$ is the space averaged macroscopic absorption cross-section and is given by

$$\overline{\Sigma_a} = \frac{1}{H}\int_{-H/2}^{H/2} \Sigma_a(z)dz \tag{4.13}$$

The Σ_a (z) is expressed as the combination of absorption cross sections of the fuel, moderator, structure, and control poison. The control poison regulates each half of the core externally. In the model, this is represented as

$$\Sigma_a(z) = \left\{ \begin{array}{ll} \Sigma_{a1} & z \in \left(-\frac{H}{2}, 0\right) \\ \Sigma_{a2} & z \in \left(0, \frac{H}{2}\right) \end{array} \right\} \tag{4.14}$$

The peak steady-state values are calculated using the following equations.

$$I_0 = \frac{\gamma_I \Sigma_f \phi_0}{\lambda_I} \tag{4.15}$$

$$X_0 = \frac{(\gamma_I + \gamma_x)\Sigma_f \phi_0}{\lambda_x + \frac{\pi}{4}\sigma_x \phi_0} \tag{4.16}$$

The results of the model in comparison with the test results of Oconee Unit #2 (Duke Power Company, 1974) were found to be [33] very accurate inspite of the simplicity of the model. Figure 4.1 shows the normalized flux amplitude in the lower half of the core as a function of time for both the model and Oconee plant. The reactor had been at 75 % power level with steady-state xenon before the perturbation was applied. The perturbation was implemented using control rods and lasted 2.5 hrs. The simulation results included accurate estimations of the period (28.5 hrs) and average offset (3.0%).

Table 4.1: One group diffusion parameters of the axial xenon oscillation model.

Parameter	Unit	Value
ϕ_0	$cm^{-2}sec{-}1$	2.1×10^{13}
σ_x	cm^2	2.6×10^{-18}
α_F	cm^2sec	3.6×10^{-16}
γ_I	–	0.061
γ_x	–	0.003
λ_I	sec^{-1}	2.87×10^{-5}
λ_x	sec^{-1}	2.09×10^{-5}
D	cm	0.375
b	cm^{-2}	0.0085
H	cm	365.8
Σ_f	cm^{-1}	0.65
$\nu\Sigma_f$	cm^{-1}	1.56
$\overline{\Sigma_a}$	cm^{-1}	1.53
$\Delta\Sigma_a$	percent	0.18

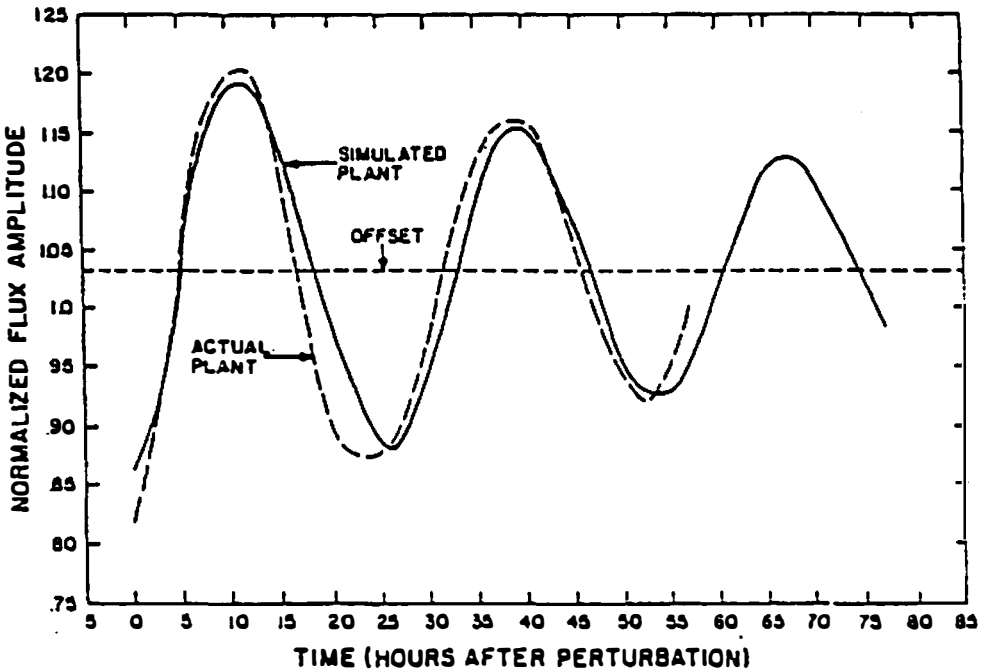

Figure 4.1: Limit cycle behavior due to xenon buildup in Oconee Unit #2 plant. The xenon oscillation estimated by the model is in agreement with the plant data.

4.2.3 RID Control Design

The primary task in this application is to design a RID controller to regulate the flux, xenon, and iodine oscillations in case of limit cycle behavior at 100 % power level. The generated control signal actuates partial-length rods. The reactor is assumed to be kept critical at all times using boron. The implementation of the control is made similar to the half-cyle damping strategy by activating the controller several hours after the initiation of the oscillations. This strategy was deliberately selected for two reasons. The first reason is to verify the control action regardless of how late the oscillations are detected. The second reason is to observe the rod motion in comparison with the bang-bang type strategies commonly studied in the literature.

The design phase starts with the formulation of the desired trajectories (demands) that must be achievable. Fortunately, the XIPO problem does not require any achievability calculations since the specific control task is a regulation problem around the initial states. Thus, the control task includes demands that are the valid initial conditions of the plant prior to the oscillation. The achievability is retained provided the controller is activated before the oscillations exceed the ASI band. The only other constraint within the definition of this problem is the limitation of the rod speed. A typical value of 30 inches per minute is adequate to satisfy the fuel integrity considerations [7]. However, the simulation results that are presented in the following, indicate that the rod speed using the RID design is far slower than the speed limit.

The control law is formulated using the inverse dynamics and state reconstruction principles explained earlier. Reconsidering the system of Eqs.(4.7-4.9), the demands are given

$$C_d(t) = C(t_0) \tag{4.17}$$

$$B_d(t) = B(t_0) \tag{4.18}$$

where t_0 is the initial time. The two demands above are the translations of a single demand (set-point axial offset). it can be easily seen that the RID control law will be of the indirect path type since the control (i.e. $\Delta\Sigma_a$) appears in β_2 and the

demands are assigned to the amplitude functions C(t) and B(t).

The control law derivation starts from the xenon amplitude equation (4.8). An auxiliary state variable C^* is defined which imitates the equilibrium behavior of the iodine amplitude C. The solution of C (call this as C^*_{eq}) from Eq. (4.8) is given by

$$C^*_{eq} = \left(\lambda_I \frac{I_0}{X_0}\right)^{-1} \left[(\sigma_x \phi_0)(\frac{2}{3}(A^* + B) + \frac{\pi}{4}A^* B) + \lambda_x B - \left(\gamma_x \Sigma_f \frac{\phi_0}{X_0}\right) A^*\right] \quad (4.19)$$

where

$$\frac{d}{dt}B(t) = 0$$

and where A^* is another auxiliary variable which imitates the equilibrium behavior of the amplitude function A. Before the treatment of A^*, we complete the definition of C^* by

$$C^* = C^*_{eq} - k_B(B - B_d). \quad (4.20)$$

Note that if the dynamics of the iodine amplitude C matches C^*, substituting C^* in Eq.(4.8) yields

$$\frac{d}{dt}B(t) = -k'_B(B - B_d) \quad (4.21)$$

where the xenon amplitude is forced to follow the demand B_d with a time-lag of k'_B which is adjustable. Similarly, the definition of A^* obtained from Eq.(4.7) is given

$$A^*_{eq} = \left(\frac{\lambda_I I_0}{\gamma_I \Sigma_f \phi_0}\right) C^* \quad (4.22)$$

where

$$\frac{d}{dt}C = 0 \quad (4.23)$$

The definition is completed by

$$A^* = A^*_{eq} - k_C(C - C_d) \quad (4.24)$$

Carrying out the substitutions in Eq. (4.24) and solving for A^* yields the following final algebraic equation.

$$A^* = \frac{\left(\frac{2}{3}\frac{X_0 \sigma_x}{\gamma_I \Sigma_f} + \frac{X_0 \lambda_x}{\gamma_I \Sigma_f \phi_0}\right) B - \frac{\lambda_I I_0}{\gamma_I \Sigma_f \phi_0}(k_B(B - B_d)) - k_C(C - C_d)}{1 - \frac{2}{3}\frac{\sigma_x X_0}{\gamma_I \Sigma_f} - \frac{\pi}{4}\frac{\sigma_x X_0}{\gamma_I \Sigma_f} B + \frac{\gamma_x}{\gamma_I}} \quad (4.25)$$

The above equation describes the desired dynamic behavior of the flux amplitude A(t). Returning to Eq. (4.9) and solving for β_2 yields

$$\beta_2 = \frac{1}{\Sigma_f}[0.848u + 1.358\sigma_x X_0 B] = \frac{-2(\beta_1 - \beta_3)A^*}{1 - A^{*2}} \tag{4.26}$$

where u is the control ($u = \Delta\Sigma_a$). The u is obtained from above to yield

$$u = \frac{-2.3585(\beta_1 - \beta_3)\Sigma_f A^*}{1 - A^{*2}} - 1.6014\sigma_x X_0 B \tag{4.27}$$

which is the final RID control law used in conjuction with Eq. (4.25).

The implementation of the control law given by Eqs. (4.25) and (4.27) requires the estimation of the amplitudes and diffusion parameters. In a computer environment, this is done by an on-line model and other estimation routines appended to the RID control routine. The model and the controller are continuously updated by using on-line power measurements in an adaptive routine. The controller output of $\Delta\Sigma_a$ is converted to the rod position units. Figure 4.2 shows the block diagram of the RID controller in application to the XIPO problem.

4.2.4 Closed-loop Simulation Results

The RID controller given by Eqs. (4.25) and (4.27) is appended to the axial xenon oscillation model. The control signal is the change in $\Delta\Sigma_a$ from its equilibrium value which is directly proportional to the change in partial-length rod position. The axial flux, xenon, and iodine oscillations first simulated without any control action. The normalized oscillations in the lower half of the core as shown in Fig. 4.3, are initiated by a step change in the absorber at t=0. The amount of step change in $\Delta\Sigma_a$ is 0.0076 cm^{-1} which approximately corresponds to 0.25 % change of absorber from its equilibrium position. Since the perturbation is a reactivity shift towards upper half of the core (rod withdrawal), the flux in the lower half first increases. The axial offset is shifted to approximately 1.05 due to the step reactivity insertion.

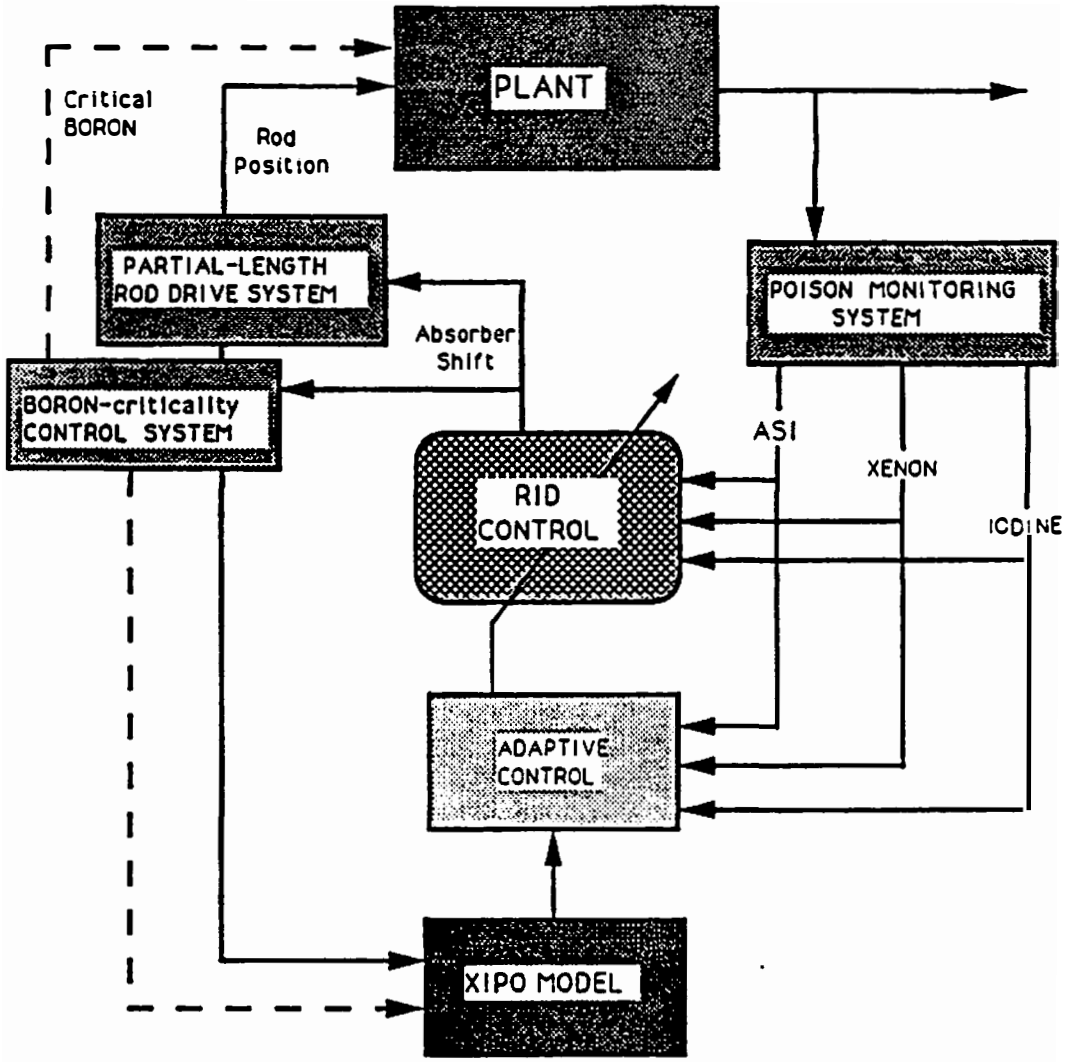

Figure 4.2: Block diagram of the RID controller in application to the xenon-oscillation control problem of PWRs.

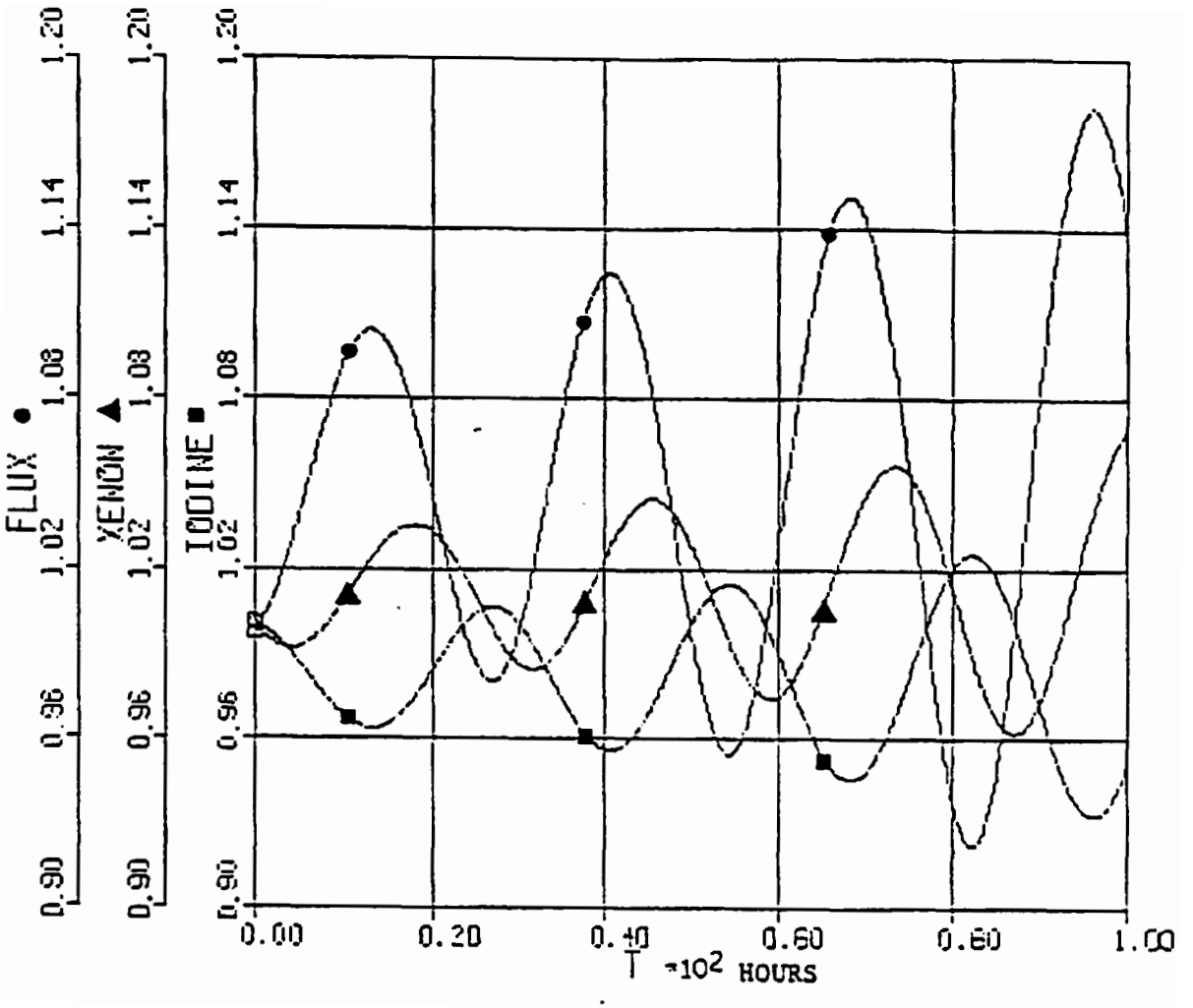

Figure 4.3: Normalized flux, xenon, and iodine oscillations in the lower half of the core. Oscillations are initiated by a step reactivity shift at t=0.

The RID controller is first activated 23 hours after the initiation of the oscillation which is close to the half-cycling time. The closed-loop responses in the lower half of the core as shown in Fig. 4.4 indicate that the oscillations are damped smoothly and the axial-offset is retained. Note that the new equilibrium is slightly different compared to the initial steady-state value due to the step reactivity at t=0.

The dynamic behavior of the control $\Delta\Sigma_a$ is shown in Fig. 4.5 The initial constant value of 0.0076 cm^{-1} corresponds to the perturbation applied to initiate the oscillations at $t = 0$. The control represents a dynamic equilibrium trajectory architectured by the inverse of the original dynamics. As it can be seen from the figure, the transition becomes very smooth compared to the bang-bang type strategies. The transition shown indicates that the absorber should be shifted towards the upper core region (i.e,Σ_{a2} increases and/or Σ_{a1} decreases) since the corresponding flux is going to increase during the second half-cycle period. Thus, the rod motion is similar to the half-cycle damping technique.

The peak observed in Fig. 4.5 is in fact a ramp change which is shown in Fig. 4.6 with a magnified time axis. The total ramp is a change from 0.250 % to 0.254 % in six minutes approximately corresponding to a 0.4 cent reactivity shift per minute which is far slower than the rod speed limit of 30 inches per minute at 100 % power level. The rest of the dynamics is even slower than the ramp as it can be seen from the Fig. 4.5. The reason for the slow response is because the control follows the inverse of the inherently slow original dynamics.

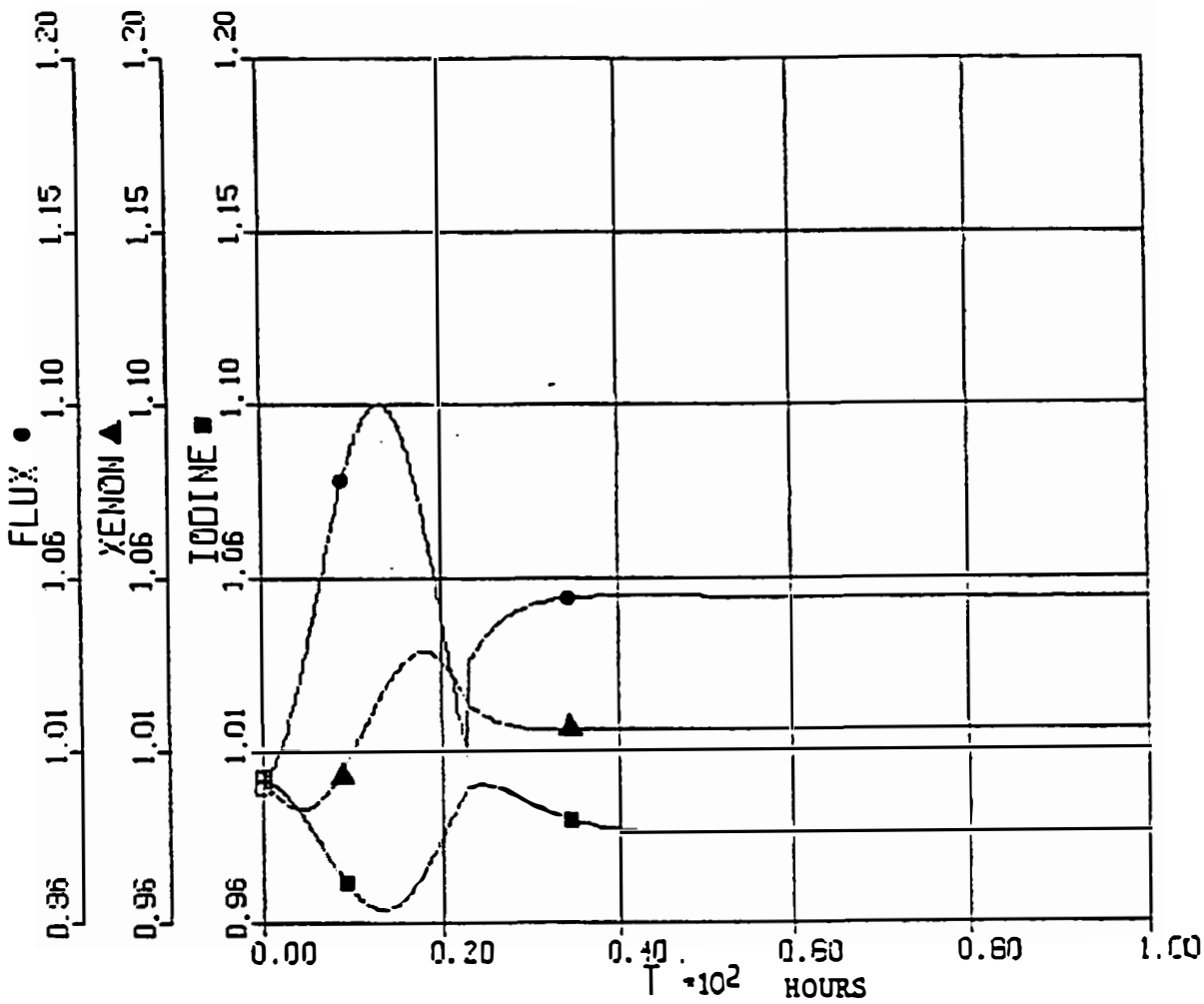

Figure 4.4: Normalized flux, xenon, and iodine oscillations in the lower half of the core. RID controller is activated at the 23rd hour.

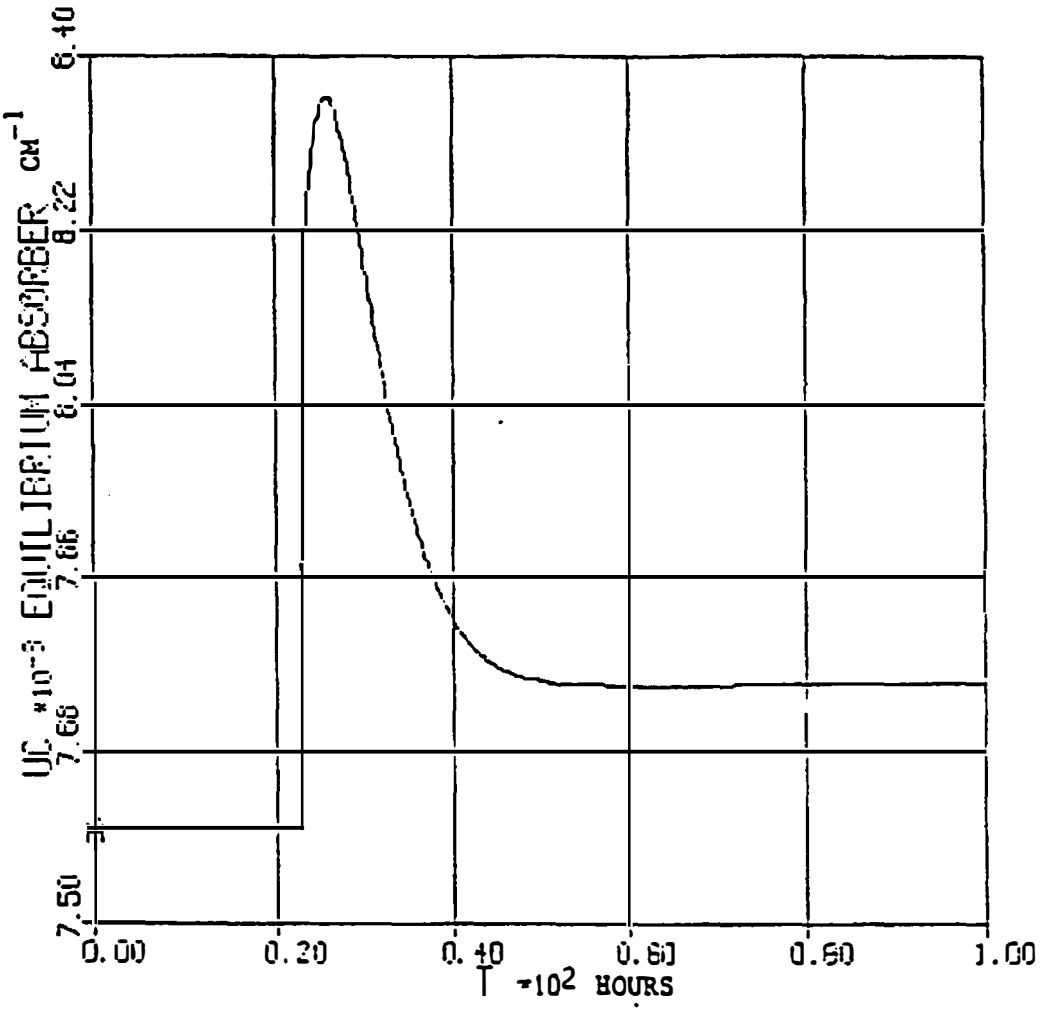

Figure 4.5: Control trajectory of the absorber shift towards the top of the core. RID controller is activated at the 23rd hour.

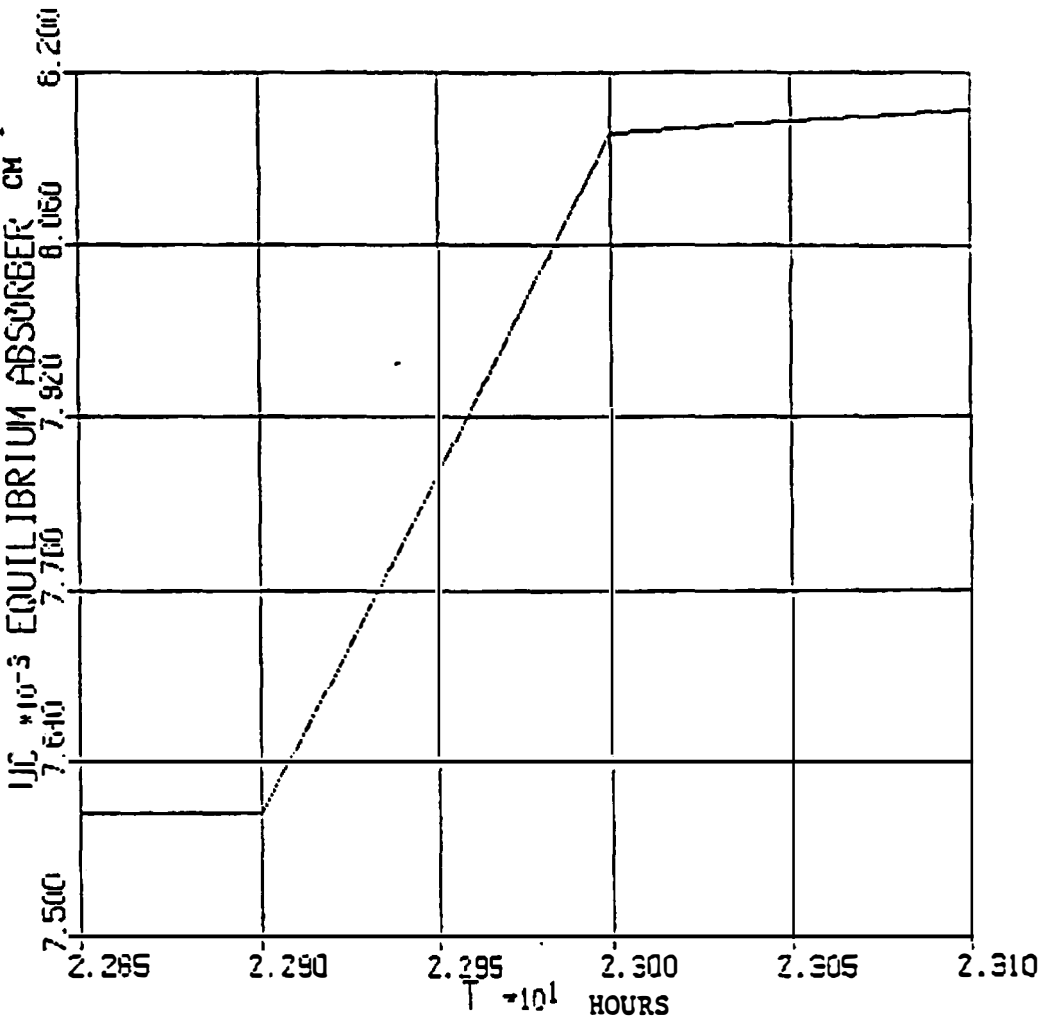

Figure 4.6: First 20 minutes of the control rod trajectory.

In the second application, the controller is activated 8 hours after the initiation of the oscillations. The normalized flux, xenon and iodine oscillations are shown in Fig.4.7. The oscillations are again damped very smoothly and the axial offset is retained. The control action is shown in Figs. 4.8 and 4.9, from the same two different perspectives.

Figures 4.10 and 4.11 show the xenon-iodine phase plane plots in two different cases where the controller was activated at the 8th and 23rd hours, respectively. Note that the final equilibrium points are different than the initial point due to the step reactivity change at t=0.

4.2.5 Conclusions

The analytical derivation of the reconstructive inverse dynamics (RID) control law and its application to the control of axial xenon oscillations are presented. The closed-loop simulation results using a previously validated model [33] show that the technique provides successful compensation with no residual oscillations until the desired axial offset is achieved. The control rod speed and the amount of insertion are far below the standard limits.

The RID performance is compared with the half-cycle damping method used in commercial plants. Figure 4.12 shows an example of the half-cycle damping strategy using full-length control rods [7]. Despite the fact that the oscillations in Fig. 4.12 and the oscillations produced in this study belong to different reactors under different operational conditions, the rod movements exhibit a major conceptual difference. In RID applications, control rods follow the inverse of the plant dynamics which yields a smooth overall transient behavior whereas the half-cycle method employing discrete rod movements suffers from residual oscillations. Note that the representations in Fig. 4.12 include the axial-shape-index and full-length rod withdrawal. The bang-bang strategy using optimal control methods [35] also exhibits some residual power oscillation.

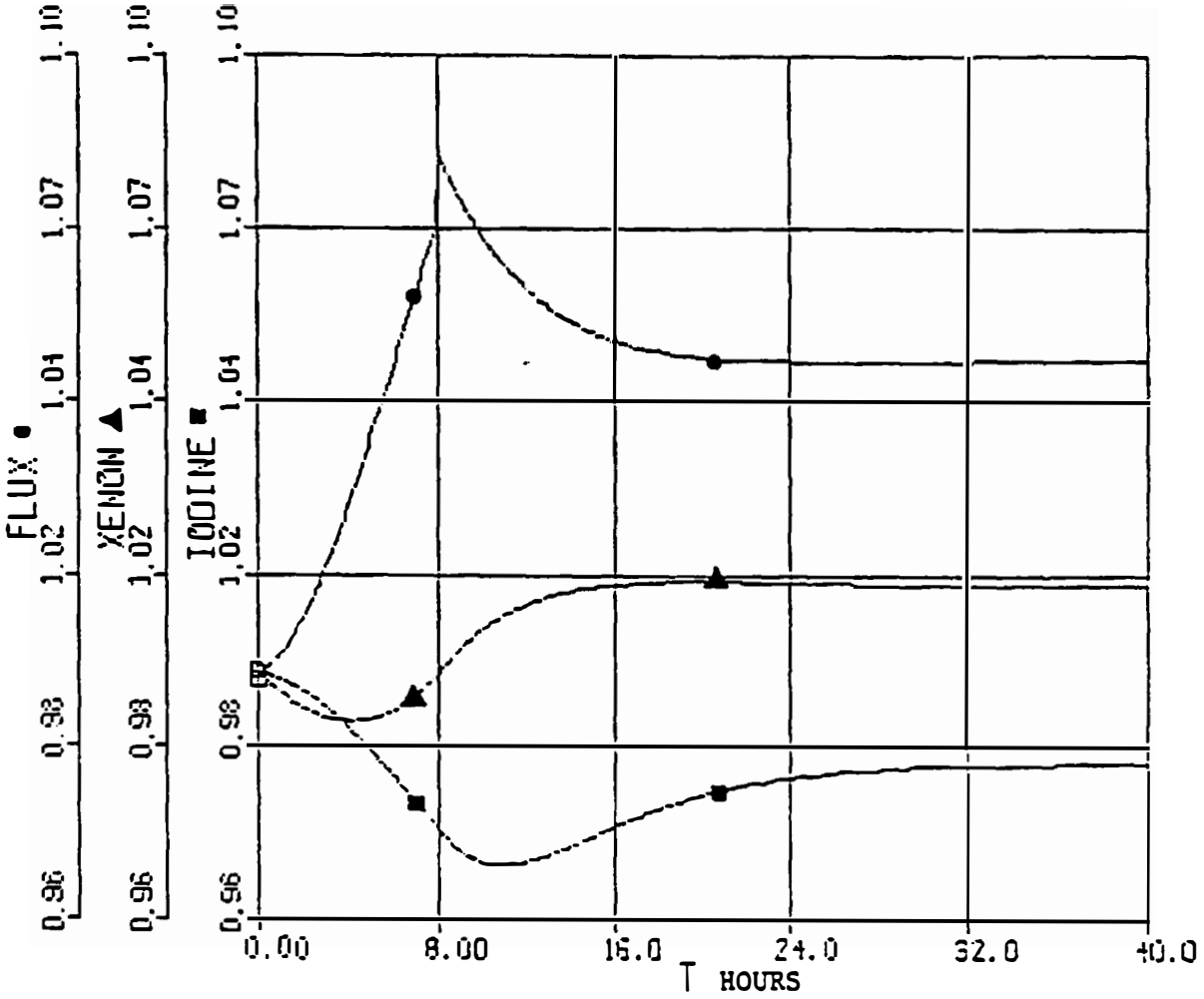

Figure 4.7: Normalized flux, xenon and iodine oscillations in the lower half of the core. RID controller is activated at the 8th hour.

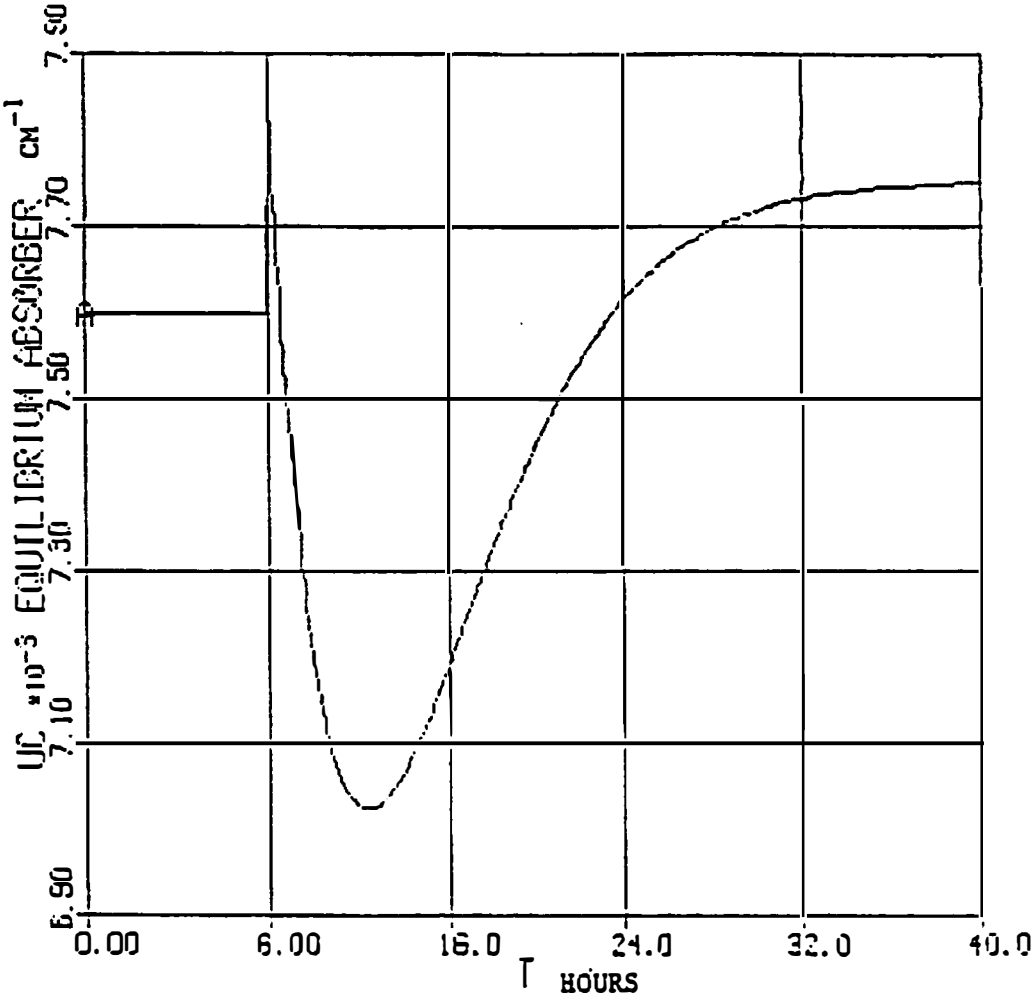

Figure 4.8: Control trajectory of the absorber shift. RID controller is activated at the 8th hour.

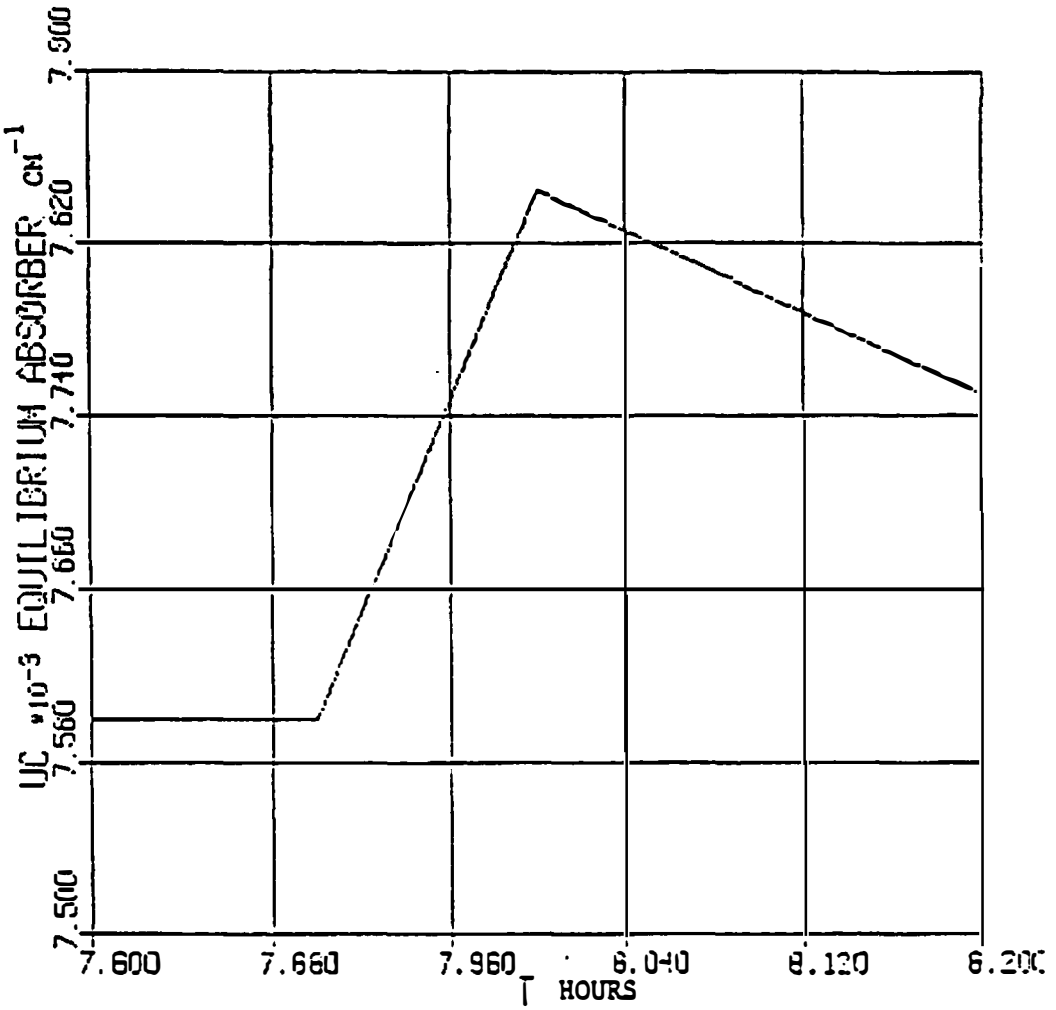

Figure 4.9: First 20 minutes of the control trajectory started at the 8th hour.

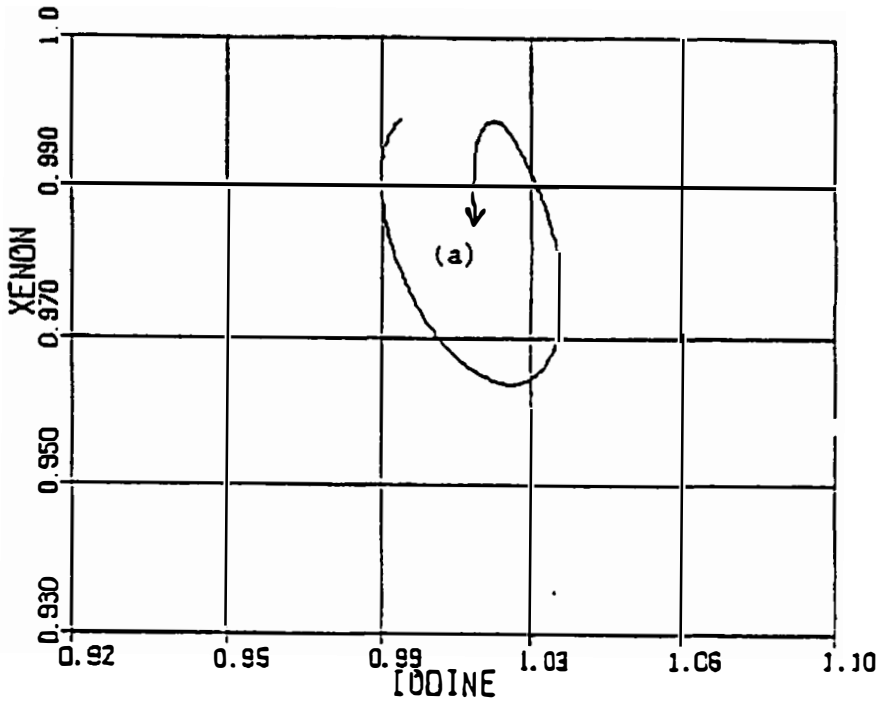

Figure 4.10: Normalized xenon-iodine phase plane plot. RID controller is activated at the 8th hour.

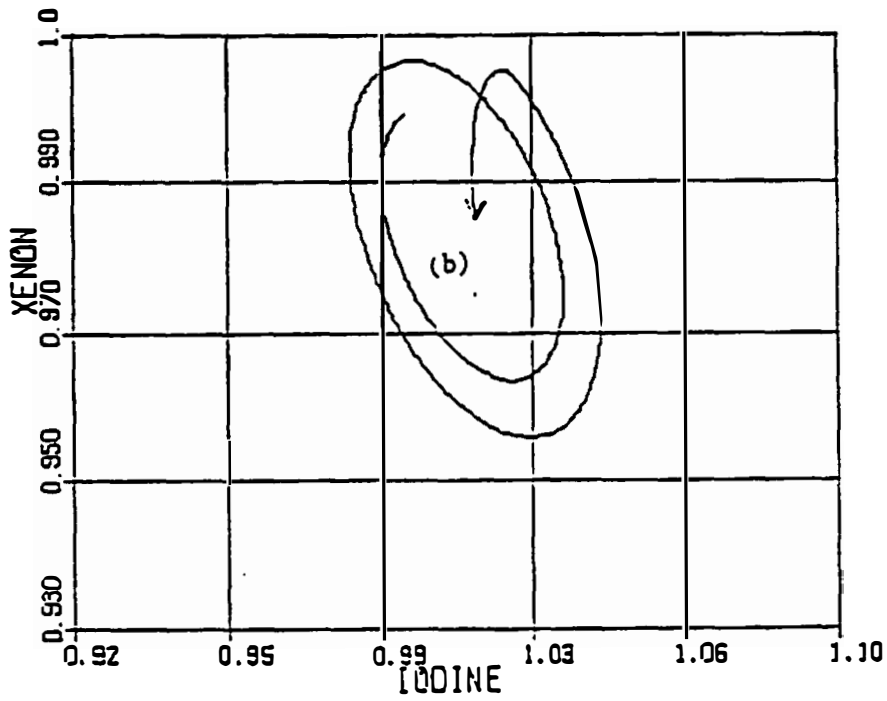

Figure 4.11: Normalized xenon-iodine phase plane plot. RID controller is activated at the 23rd hour.

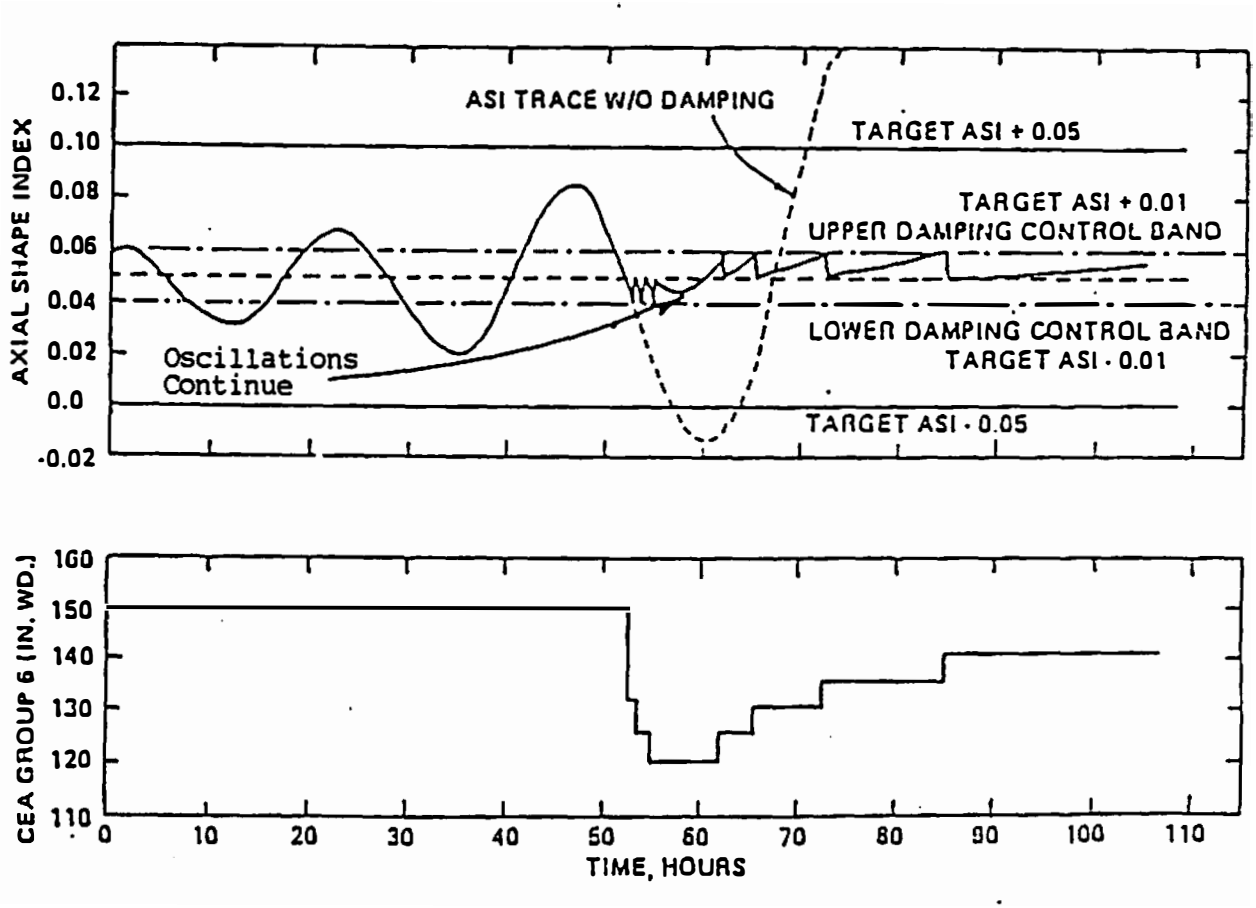

Figure 4.12: Axial xenon oscillation damping example: Half-Cycle Damping Strategy.

The results obtained in this study along with the performance of the RID design should be evaluated at the conceptual level since the application in this study is limited by the complexity of the model used. The scope of RID design can easily be extended using different codes and incorporating additional tasks. Provided all the demands are well defined (i.e, desired level of boron waste, rod positions), a multi-input multi-output RID design may accomplish more global control tasks. The inconsistencies between the plant and its model can be handled using the adaptive features of RID design. The RID design of this application is assumed to use flux measurements and the estimation of the xenon and iodine amplitudes using an on-line model. Because the oscillations occur in the time scale of hours, it is assumed that the model predictions can be easily corrected in the course of oscillations.

4.3 Feedwater-Train Control in PWRs

The primary function of the feedwater-train system is to provide the necessary feedwater flow into the four steam generators in a standard four-loop PWR. The system consists of a pump turbine, feedwater pump, feedwater piping, and valves for regulating steam and feedwater flow. This arrangement is shown in Fig.4.13.

A typical control problem in turbine driven feedwater pumps is to maintain the pressure difference (ΔP) variation across the feedwater valve constant. In routine operations, the feedwater valve is opened to satisfy feedwater demand. This results in a change in pressure difference across the valve. If the governer valve on feedwater driven turbine is not adjusted properly the ΔP across the valve may change unreasonably and damage the valve structure. It is also necessary to be able to satisfy rapid feedwater demands for quick maneuvers which is known to have vital importance in controlling the steam generator dynamics. The final design specification includes robustness against oscillatory steam generator pressure.

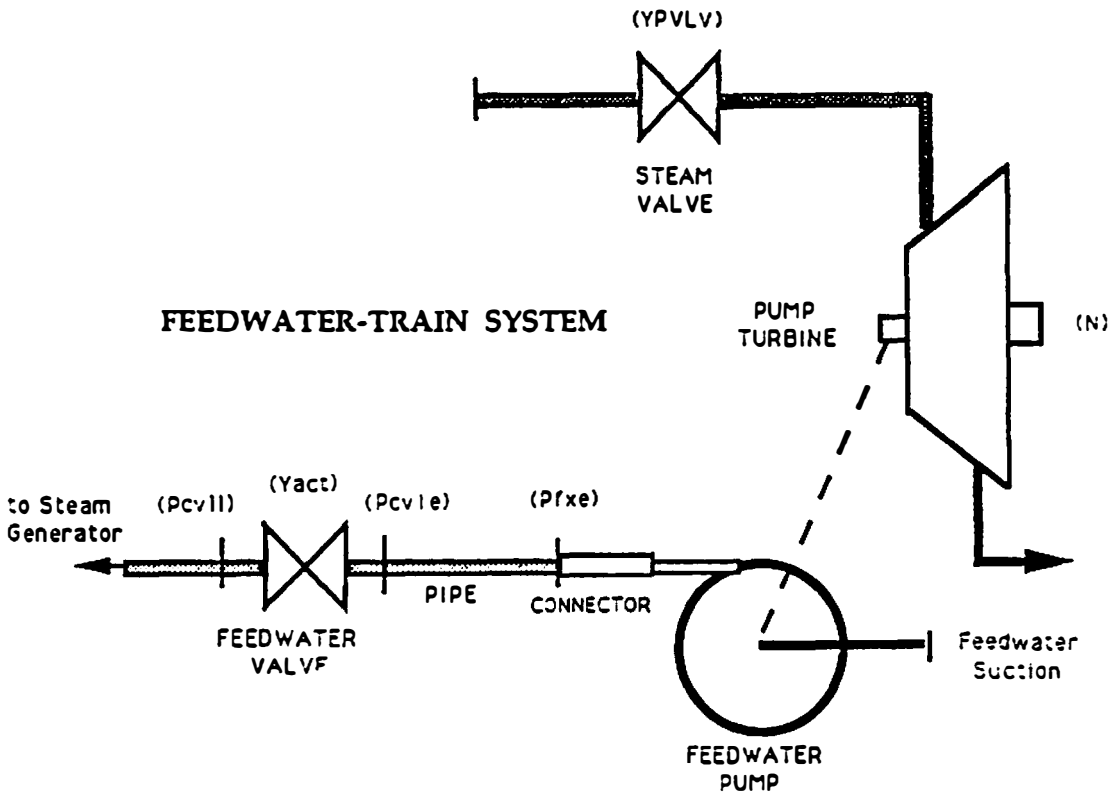

Figure 4.13: The schematic of the feedwater-train system and associated system variables.

4.3.1 Nonlinear Modeling of PWR Feedwater-Train

The model used in simulations consists of subroutines for the pump turbine, turbine valve, main pump, piping, feedwater valve, valve actuators and pipe connectors. The model includes a detailed, nonlinear representation of the physics involved in feedwater dynamics. Four state variables of the model are the turbine speed, feedwater valve inlet and outlet pressures, and the actuator dynamics. Equal percentage valve dynamics is used in the model. Two control signals are the turbine and feedwater valve positions. The simulations are performed using the MMS code written in ACSL environment.

The pump turbine model includes physical effects such as variable speed and steam turbine driver with single or dual pressure source whereas the windage losses are not included. The module does not allow negative speed and the operation depends on limited steam properties. The feedwater pump model includes variable speed pump head-flow characteristics as well as the pump power input to the system. Limitations of the pump model include cavitation, leakage, seal injection. seal cooling, windmilling and reverse flow. The feedwater pipe is a resistive-storage type that includes the following physical effects: pressure losses from friction and elevation, inertia, energy storage in fluid and pipe metal, fluid expansion, transport delay, and heat loss to ambient. It is assumed that the flow is one phase only, with no significant compressibility effects. Reverse flow is not allowed. The valve module used in the simulations includes frictional pressure losses for single phase water due to valve and associated piping and valve modulation with optional valve characteristics (linear). It is an adiabatic valve with quasi-steady state operation. Flashing, cavitation, packing effects and reverse flow are not included. The valve actuators employ first order lag type response with a limited rate.

The pump turbine speed is given as

$$\frac{dN}{dt} = 2936 \left\{ \frac{P_{in} - P_{out}}{I\,N} \right\} \tag{4.28}$$

where

$N \equiv$ Turbine speed (rpm)

$P_{in} \equiv$ Net power input from steam (ft-lbf/sec)

$P_{out} \equiv$ Net power output to load (ft-lbf/sec)

$I \equiv$ Load-turbine combined mass moment of inertia (lbm-ft^2/rad)

Net power input is calculated from the energy balance and given by

$$P_{in} = 0.21616\, W_{se}(h_{se} - h_{sl}) \tag{4.29}$$

$$W_{se} = Y_{LP} C_{LP}\, \rho_{selp} P_{selp} \tag{4.30}$$

where

$W_{se} \equiv$ Total steam flow rate (lbm/hr)

$h_{se} \equiv$ Bulk enthalpy of steam entering (Btu/lbm)

$h_{sl} \equiv$ Enthalpy of steam leaving (Btu/lbm)

$Y_{LP} \equiv$ Low pressure steam valve position (fraction open)

$C_{LP} \equiv$ Low pressure valve conductance

$\rho_{selp} \equiv$ Density of low pressure steam entering (lbm/ft^3)

$P_{selp} \equiv$ Pressure of low pressure steam (psi)

The pressure at the outlet of the pipe connecter is given by

$$\frac{dP_{fxe}}{dt} = \frac{1}{K_{dp}}(W_{mfpl} - W_{fxe}) \tag{4.31}$$

where

$P_{fxe} \equiv$ Feedwater pipe inlet pressure (psi)

$W_{mfpl} \equiv$ Main feedwater pump outlet flow (lbm/hour)

$W_{fxe} \equiv$ Feedwater pipe entrance flow (lbm/hour)

and the physical meaning of K_{dp} is

$$K_{dp} = V\left(\frac{\partial \rho}{\partial P}\right)\left(\frac{144}{778}\right)3600 \qquad (lbm/psi)(sec/hour)$$

The density deviation with respect to the operating pressure is evaluated at constant enthalpy. Similarly the outlet pressure of the feedwater pipe is expressed as

$$\frac{dP_{cvle}}{dt} = \frac{1}{k_{dv}}(W_{fxe} - W_{cvle}) \tag{4.32}$$

where

P_{cvle} ≡ Feedwater pipe exit pressure (psi)

W_{fxe} ≡ Feedwater pipe entrance flow (lbm/hour)

W_{cvle} ≡ Feedwater pipe exit flow (lbm/hour)

and k_{dv} is a tabulated physical constant same as k_{dp}. Feedwater pipe exit flow also represents the flow across the feedwater valve. The flow across the valve is given by

$$W_{cvle} = C_q\sqrt{\rho_{we}(P_{cvle} - P_{cvll})} \tag{4.33}$$

where ΔH across the valve is assumed zero and

C_q ≡ Valve conductance

ρ_{we} ≡ Water density (lbm/ft^3)

P_{cvll} ≡ Valve outlet pressure (psi).

Since the flow stream is incompressible, the valve conductance is combined with that of any pipe or valve with which it is associated. Combining the resistance of the pipe, C_p, and the valve, the resistance is

$$C_q = \frac{1}{\sqrt{\left(\frac{1}{C_{vmax}Y_{act}}\right)^2 + \left(\frac{1}{C_p}\right)^2}} \tag{4.34}$$

where

C_{vmax} ≡ Maximum valve conductance

C_p ≡ Resistance of the pipe

Y_{act} ≡ Actuator signal

Note that $C_{vmax}Y_{act}$ represents linear valve. The actuator dynamics is given by

$$\frac{dY_{act}}{dt} = \frac{1}{\tau_c}(Y_{bd} - Y_{act}) \tag{4.35}$$

where Y_{bd} and τ_c represent the bounded actuator signal and valve time-constant, respectively. The feedwater pipe inlet flow is derived from the pressure drop across the pipe and given by

$$W_{fxe} = C_f\sqrt{\rho_{av}(P_{fxe} - P_{cvle})} \tag{4.36}$$

where C_f and ρ_{av} are the pipe conductance and average density. The pump outlet flow can be related to the pump speed and pump-head flow characteristics as follows.

$$W_{mfpl} = 8.02\, N\, \rho_{we}(Q_p/N) \tag{4.37}$$

where the normalized head curve (Q_p/N) is related to the ratio of the pump volumetric flow rate Q_p, to the pump speed N, to the ratio of the developed head ΔH to the square of the pump speed $f(\Delta H/N^2)$.

4.3.2 RID Controller Design

The control requirement associated with the feedwater-train system includes maintaining ΔP across the feedwater valve reasonably small while following a feedwater flow demand. The control should yield large band-width since the rapid feedwater demand following capability is highly desired. In order to formulate the problem easily, the complete model given by Eqs.(4.28) through (4.37) is rewritten in a compact form with all the substitutions yielding four differential and one algebraic state equations.

$$\frac{dN}{dt} = 2936\left\{\frac{0.21616\, Y_{LP}C_{LP}\, \rho_{selp}P_{selp}(h_{se}-h_{sl}) - P_{out}}{I\, N}\right\} \tag{4.38}$$

$$\frac{dP_{fxe}}{dt} = \frac{1}{k_{dp}}\left\{8.02N\rho_{we}(Qp/N) - C_f\sqrt{P_{fxe}-P_{cvle})\rho_{av}}\right\} \tag{4.39}$$

$$\frac{dP_{cvle}}{dt} = \frac{1}{k_{dv}}\left\{C_f\sqrt{(P_{fxe}-P_{cvle})\rho_{av}} - \frac{\sqrt{\rho_{we}(P_{cvle}-P_{cvll})}}{\sqrt{\left(\frac{1}{C_{vmax}Y_{act}}\right)^2+\left(\frac{1}{C_p}\right)^2}}\right\} \tag{4.40}$$

$$\frac{dY_{act}}{dt} = \frac{1}{\tau_c}(Y_{bd}-Y_{act}) \tag{4.41}$$

$$W_{cvle} = \frac{\sqrt{\rho_{we}(P_{cvle}-P_{cvll})}}{\sqrt{\left(\frac{1}{C_{vmax}Y_{act}}\right)^2+\left(\frac{1}{C_p}\right)^2}} \tag{4.42}$$

The feedwater-train system given by Eqs.(4.38-4.42) is subject to boundary conditions (BCs). The variables representing the BCs are

$P_{out} \equiv$ Net power output to load (ft-lbf/sec)

$\rho_{selp} \equiv$ Density of low pressure steam entering (lbm/ft^3)

P_{selp} ≡ Pressure of low pressure steam (psi)

h_{se} ≡ Bulk enthalpy of steam entering (Btu/lbm)

h_{sl} ≡ Enthalpy of steam leaving (Btu/lbm)

P_{cvll} ≡ Steam generator pressure (psi)

The MMS routines provide parameters such as (Q_p/N), ρ_{we}, ρ_{av}, k_{dp}, k_{dv} and I from its library.

The control requirements can be translated into trajectories using the compact model stated above. The ΔP regulation task is formulated by assigning a pressure demand D_p to the valve inlet pressure that follows the steam generator pressure (boundary condition). If the demand following is efficient, the pressure drop will be small. From the model given above, the pressure demand can be assigned to any state equation containing P_{cvle} using an adequate auxiliary RID technique. The second trajectory is the feedwater flow demand that can be assigned to state equations (4.40) or (4.42). These two assignments has to be accomplished by designing controls Y_{LP} and Y_{act}.

The RID control design problem looks complex at first, but there are only two possibilities that include designing (1) Y_{LP} (turbine governer valve) to follow the flow demand and Y_{bd} (feedwater valve) to follow the pressure demand or (2) vice verse. Thus, this problem requires strategy evaluation that can be performed by the RID technique.

RID Control Design: Strategy-1

The formulation of the first strategy (governor valve adjustment to follow feedwater demand, and feedwater valve adjustment to follow pressure demand) using the RID control method requires the auxiliary states technique. The desired setting for the Y_{act} in the algebraic state equation (4.42) is defined to be the auxiliary state Y^*_{act}. This auxiliary state is designed to yield trajectory following of pressure demand D_p. Solving for $Y_{act}*$ in Eq.(4.42) yields

$$Y^*_{act} = \frac{1}{C_{vmax}\sqrt{\frac{(P_{cvle}-P_{cvll})\rho_{we}}{W^2_{cvle}} - \frac{1}{C_p^2}}} \tag{4.43}$$

The demand following assignment on the algebraic state equations do not require a FOTL dynamics. The solution above directly represents the desired state of Y_{act}. Thus the assignment $P_{cvle} = D_p$ is substituted above to give

$$Y^*_{act} = \frac{1}{C_{vmax}\sqrt{\frac{(D_p-P_{cvll})\rho_{we}}{W^2_{cvle}} - \frac{1}{C_p^2}}} \tag{4.44}$$

Note that the pressure demand D_p is selected such that it is always greater than the steam generator pressure P_{cvll} with a small fixed amount ϵ. This guarantees Y^*_{act} to be a real variable at the cost of creating some small ΔP across the feedwater valve. As long as the pressure measurement P_{cvll} is available and the pressure demand is $D_p = P_{cvll} + \epsilon$ with an appropriate selection of ϵ, the auxiliary state variable Y^*_{act} will never be a complex variable. It is also obvious that $\Delta P = 0$ is not desired to avoid the complex region. Thus, this small ΔP is vitally important and the control performance strictly depends on the resonable selection of ϵ. Refering to the state equation (4.41), the feedwater valve position Y_{bd} is solved such that the actuator dynamics $\dot{Y}_{act}$ follows the auxiliary state Y^*_{act}.

$$Y_{bd} = \tau_c \frac{dY_{act}}{dt} + Y_{act} \tag{4.45}$$

where

$$\frac{dY_{act}}{dt} = K_5(Y^*_{act} - Y_{act}) \tag{4.46}$$

The second assignment requires use of multiple auxiliary states in the RID control design. Among the state equations (4.38, 4.39, 4.40), the governer valve control Y_{LP} has to be related to the flow demand D_{wf}. It is clear that the last term in Eq. (4.40) gives W_{cvle} of Eq.(4.42). Thus, the derivation must start from Eq. (4.40) and continue up to Eq.(4.38). First, we select an auxiliary state P^*_{cvle} in Eq.(4.42) that results in $W_{cvle} = D_{wf}$.

$$P^*_{cvle} = \frac{D^2_{wf}}{\rho_{we}} \left\{ \left(\frac{1}{C_{vmax} Y_{act}} \right)^2 + \left(\frac{1}{C_p} \right)^2 \right\} + P_{cvll} \tag{4.47}$$

The auxiliary state P^*_{cvle} then represents a desired trajectory for the state variable P_{cvle}. Second, we select another auxiliary state variable P^*_{fxe} in Eq.(4.40) and solution yields

$$P^*_{fxe} = \frac{1}{\rho_{av} C_f^2} \left(k_{dv} \frac{dP_{cvle}}{dt} + W_{cvle} \right)^2 + P_{cvle} \tag{4.48}$$

where the trajectory following requires

$$\frac{dP_{cvle}}{dt} = K_1 (P^*_{cvle} - P_{cvle}) \tag{4.49}$$

K_1 is an adjustable parameter. The problem is converted into establishing the desired dynamics for P_{fxe} which will follow P^*_{fxe}. Then we select an auxilary state N^* in Eq.(4.39) such that

$$N^* = \frac{C_f \sqrt{\rho_{av}(P_{fxe} - P_{cvle})} + k_{dp} \frac{dP_{fxe}}{dt}}{8.02 \rho_{we} (Q_p / N)} \tag{4.50}$$

with the substitution

$$\frac{dP_{fxe}}{dt} = K_2 (P^*_{fxe} - P_{fxe}) \tag{4.51}$$

where K_2 is an adjustable parameter.

Finally, the control Y_{LP} is solved from Eq.(4.38) such that the state variable N follows the desired dynamics N^*.

$$Y_{LP} = \frac{P_{out} + \frac{IN}{2936} \frac{dN}{dt}}{0.21616 C_{LP}\, \rho_{selp} P_{selp} (h_{se} - h_{sl})} \tag{4.52}$$

where

$$\frac{dN}{dt} = K_3 (N^* - N) \tag{4.53}$$

and K_1 is an adjustable quantity. Note that the two controls Y_{LP} and Y_{bd} cross talk through the coupling in Eq.(4.47).

RID Control Design: Strategy-2

The second strategy can be designed in a similar fashion. In this case, the feedwater valve is used to satisfy the feedwater demand and governor valve is used to keep ΔP constant. Most of the control equations presented for the first strategy remain

unchanged except Eqs.(4.43, 4.47, 4.49). In Eq.(4.43) feedwater flow is replaced by the demand D_{wf} to give

$$Y^*_{act} = \frac{1}{C_{vmax}\sqrt{\frac{(P_{cvle}-P_{cvll})\rho_{we}}{D^2_{wf}} - \frac{1}{C_p^2}}} \tag{4.54}$$

The auxiliary state P^*_{cvle} is required to follow the pressure demand D_p in Eq.(4.47), thus this equation is no longer valid. Thus, the other auxiliary variable P^*_{fxe} is designed to accomplish this task. Equation (4.49) is rewritten as

$$\frac{dP_{cvle}}{dt} = K_1(D_p - P_{cvle}) \tag{4.55}$$

The second strategy is widely employed in conventional PWRs using linear controllers. However, the RID control derivation indicates that this strategy is vulnerable to severe changes in the steam generator pressure. This can be seen from Eq.(4.54) that a sudden pressure increase in the steam generator may result in Y^*_{act} to shift towards the complex region. Note that $P_{cvll} > P_{cvle}$ (reverse flow) is not necessarily required for Y^*_{act} to be complex. If the pressure drop gets small, the division by D^2_{wf} can make the first term become smaller than the second term inside the square root term. In the first strategy, the complex region is avioded by designing the pressure demand, appropriately (always greater than the steam generator pressure signal with a fixed amount). It is not possible to modify the feedwater demand D_{wf} in the second strategy to avoid the complex region because of two reasons. First, it is not clear what kind of modification is necessary to the feedwater demand as a function of steam generator pressure for this particular case. Second, any modification to the feedwater demand violates the basic control requirement (prescribed trajectory) since the effect of such a modification may cause a significant departure from the desired trajectory. The problem of complex variables is not a concern in the first strategy using the auxiliary state P^*_{fxe} of Eq.(4.48) because the direct measurement of feedwater flow W_{cvle} is used.

4.3.3 Implementation

Implementation of the RID design presented above requires digital technology including an on-line computer where various system parameters are updated with respect to the nature of the operation. Figure 4.14 shows the RID controller and its interaction with the plant and on-line model. The control uses three measurements from the plant and one state estimation from the model. Other important parameters are either measured or calculated.

The RID control design presented above makes use of a very detailed system model. In general, this may not be necessary since the adaptive control yields high performance even with significant modeling errors. It may be possible to design an adaptive RID controller to implement the second strategy presented above by using a reduced order model. In such an application, the uncertainty terms can be selected to avoid complex variables.

4.3.4 Simulation Results

The simulations are performed using the ACSL package on the ICENET VAX mainframe located at the I&C Division, ORNL. The feedwater-train model is constructed by appending the MMS modules for each component.

A typical feedwater demand in a four-loop PWR is around 5 % per minute ramp change. The control task consists of maintaining a small ΔP across the feedwater, that is not more than 80 psi. However, rapid feedwater maneuvers are needed to improve the control capability of steam generators. Thus, the simulations presented here include a feedwater demand that is 10 times faster than the standard operation. The feedwater demand has three distinct features: (1) 50 % per minute ramp increase, (2) steady-state, and (3) 50 % per minute ramp decrease. These features are deliberately employed to investigate the closed-loop performance during various maneuvers. The simulations also include a disturbance in the form of an exponential and oscillatory pressure drop in the steam generator pressure (boundary condition) that causes 200 psi pressure drop across the feedwater valve without any control action.

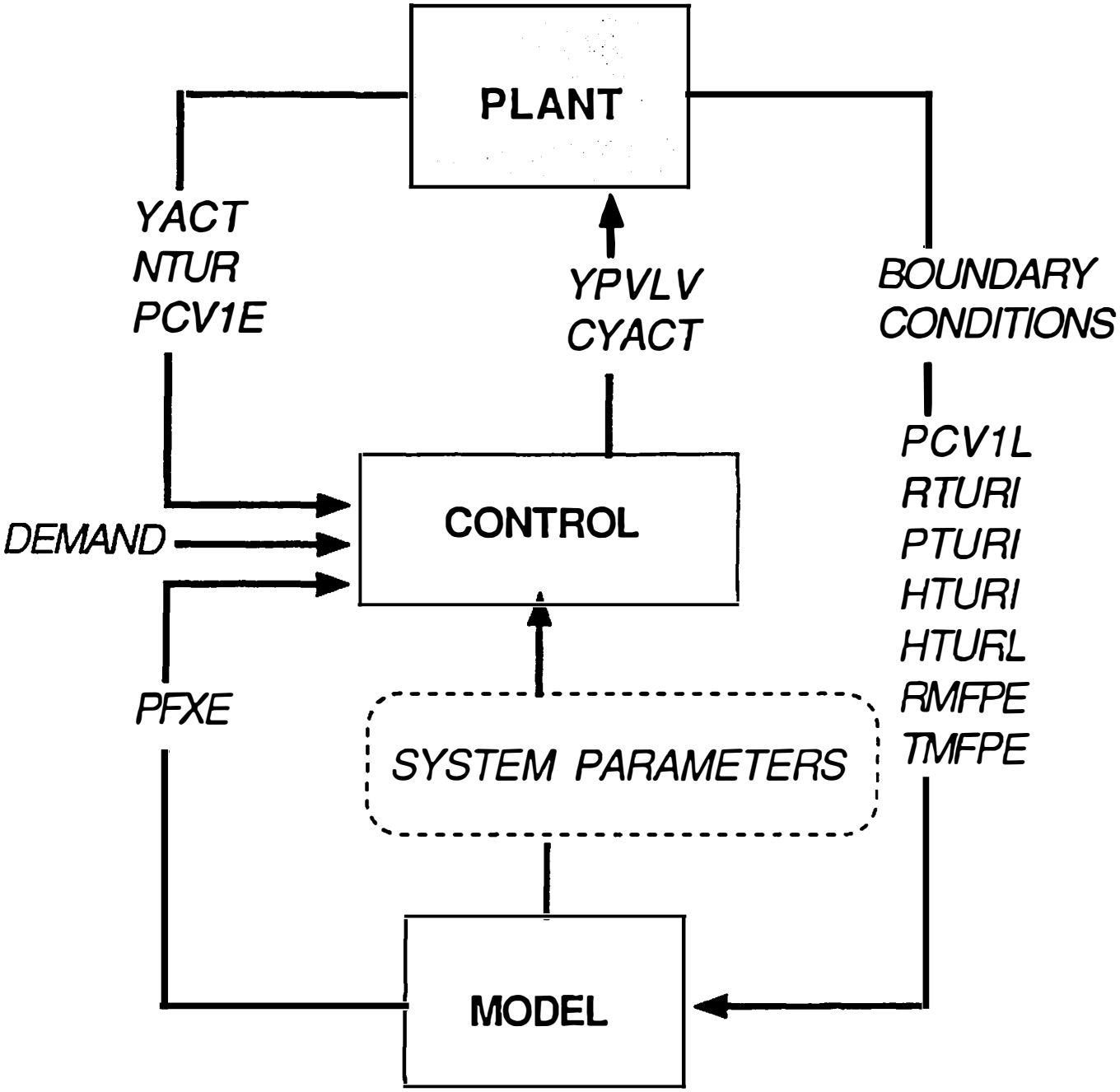

Figure 4.14: RID controller and its interaction with the plant (feedwater-train system) and on-line model. Model estimates one of the four state variables where the rest are obtained from the plant as direct measurements.

The feedwater flow response in comparison with the demand is shown in Fig 4.15. The demand is followed with a negligible error that is not visible in the figure. The external disturbance is shown in Fig 4.16 where the steam generator pressure is lowered almost 25 %. Figure 4.17 compares the two control inputs that are the percent openings of the governor valve and the feedwater valve. The feedwater valve opening illustrates the compensation for the disturbance in ΔP whereas the governer valve primarily satisfies the flow demand. The change in ΔP is shown in Fig 4.18. The amount of change in ΔP (about 5 psi) clearly indicates the power of the RID control paradigm. The simulations are repeated with higher oscillations in the external disturbance. Higher frequency oscillations are observed to cause no deterioration on the closed-loop performace although the actuator dynamics is constrained. Figure 4.19 shows the external disturbance (steam generator pressure change) with reasonably high frequency oscillations. The feedwater response in comparison with the demand is shown in Fig 4.20. The demand is followed with a negligible error that is again not visible. Feedwater valve and governer valve positions are compared in Fig 4.21. The comparison shows more clearly that the feedwater valve control primarily compensates for the external disturbance to achieve a reasonable ΔP. Although a cross talk exists between the two control inputs, the governor valve position is almost entirely dedicated to follow the feedwater demand. Figure 4.22 shows ΔP response that is again within 5 psi range.

The effect of inaccurate state estimation on the closed-loop performance is investigated by introducing a local error to the feedwater pipe inlet pressure P_{fxe}. Although the RID controller does not include any adaptive features in this particular design, a desirable robustness is observed. Figure 4.23 shows the feedwater response in comparison with the demand in case of 10 % error in the estimation of P_{fxe}. Note that other state variables are available as measurements. Figure 4.24 compares the feedwater flow response with the demand in case of 25 % state estimation error. These results indicate that the RID control paradigm is inherently robust against tolerable estimation errors.

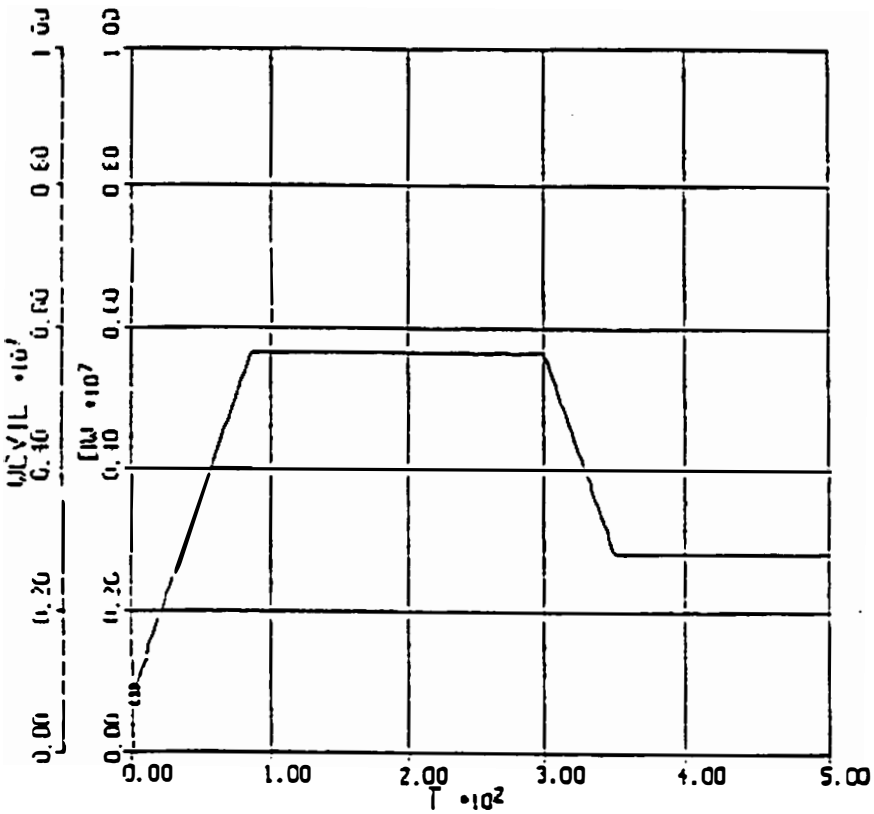

Figure 4.15: Feedwater flow response in comparison with the demand. The demand is followed with a negligible error that is not visible in the figure. As an external disturbance, the steam generator pressure (boundary condition) is lowered 25 % with oscillation.

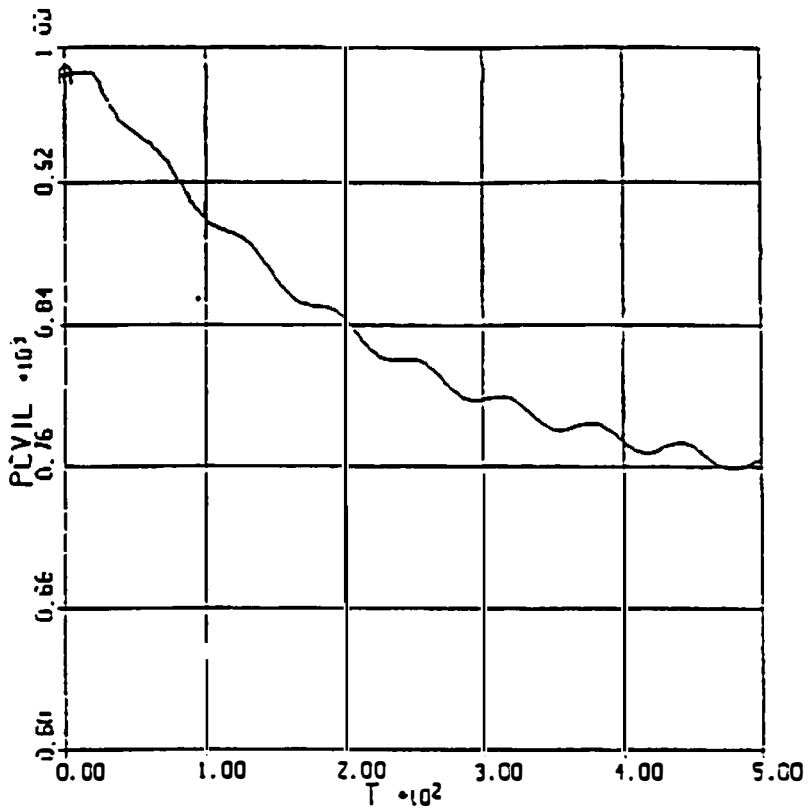

Figure 4.16: External disturbance during the demand following control. Steam generator pressure (boundary condition) is lowered 25 % with oscillation.

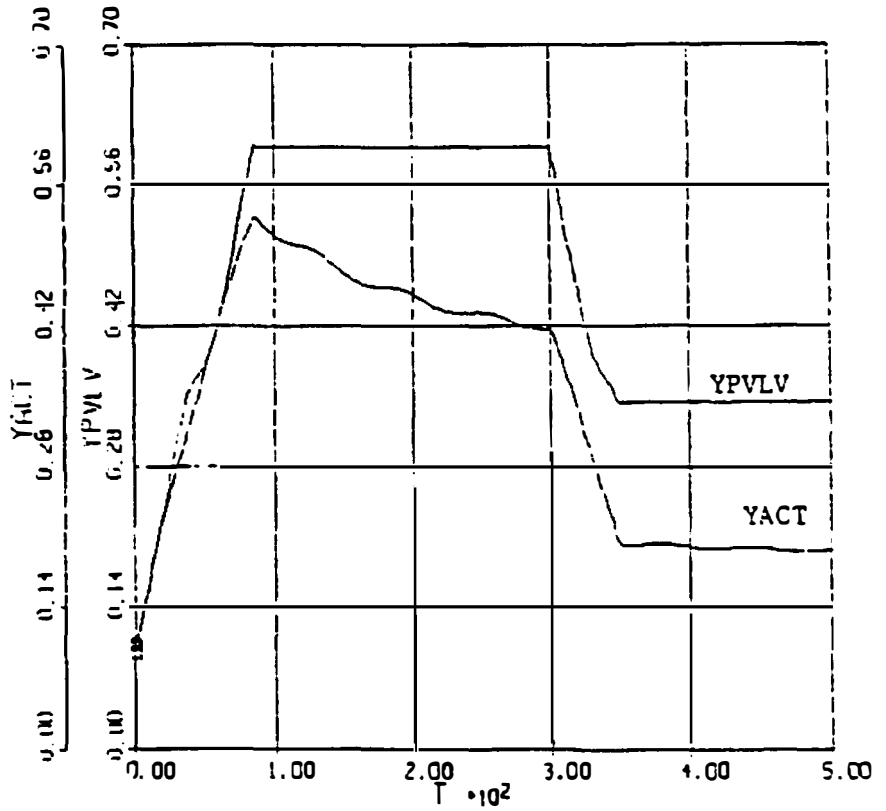

Figure 4.17: Turbine (YPVLV) and feedwater valve (YACT) positions (control inputs) during the demand following control. As an external disturbance, the steam generator pressure (boundary condition) is lowered 25 % with oscillation.

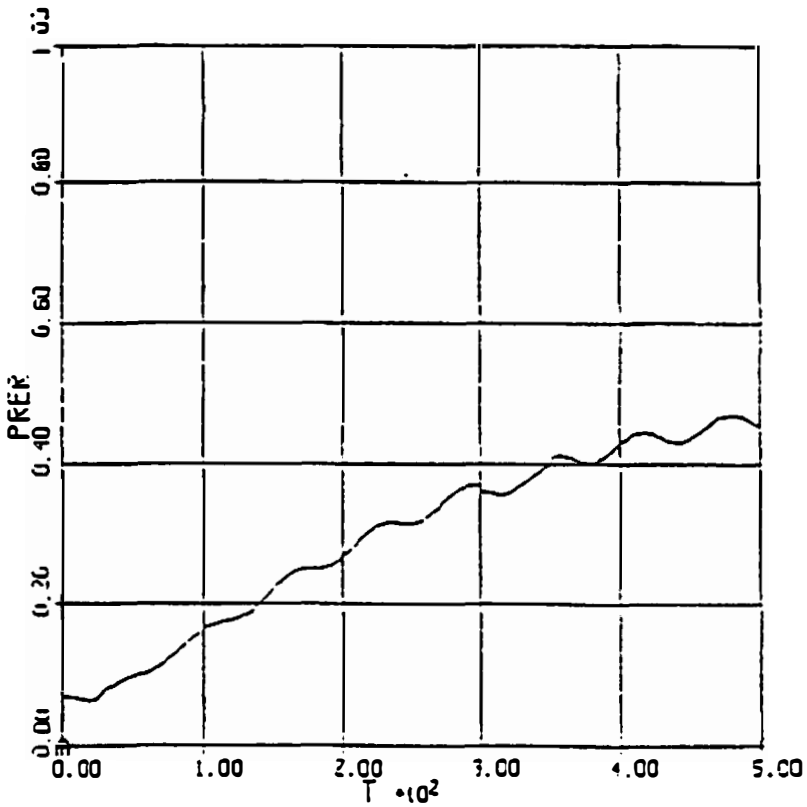

Figure 4.18: Pressure drop across the feedwater valve. As an external disturbance, the steam generator pressure (boundary condition) is lowered 25 % with oscillation.

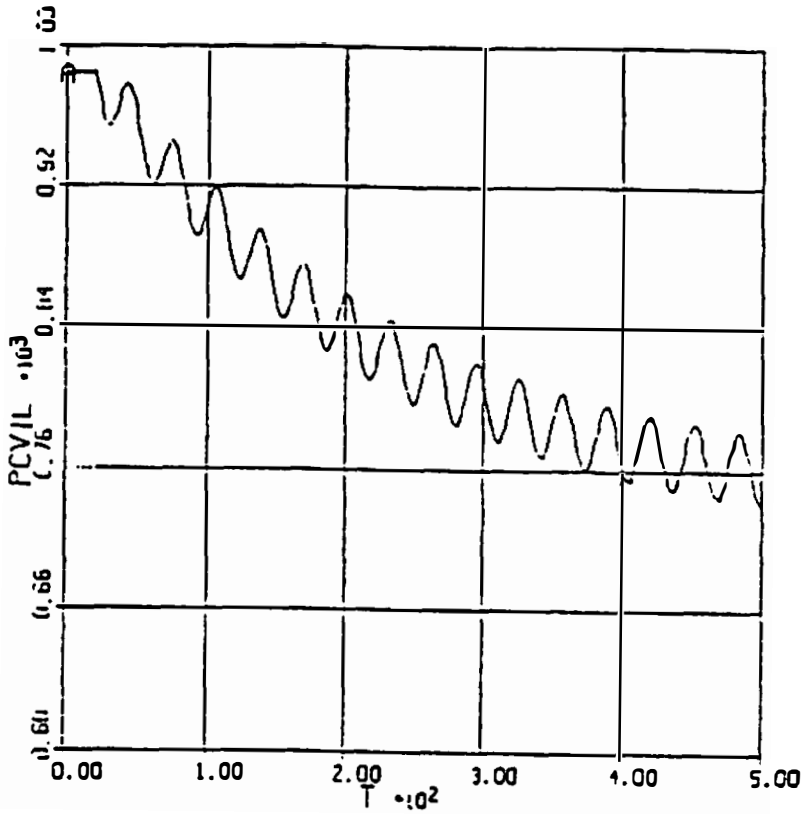

Figure 4.19: External disturbance during the demand following control. Steam generator pressure (boundary condition) is lowered 25 % with high frequency oscillation.

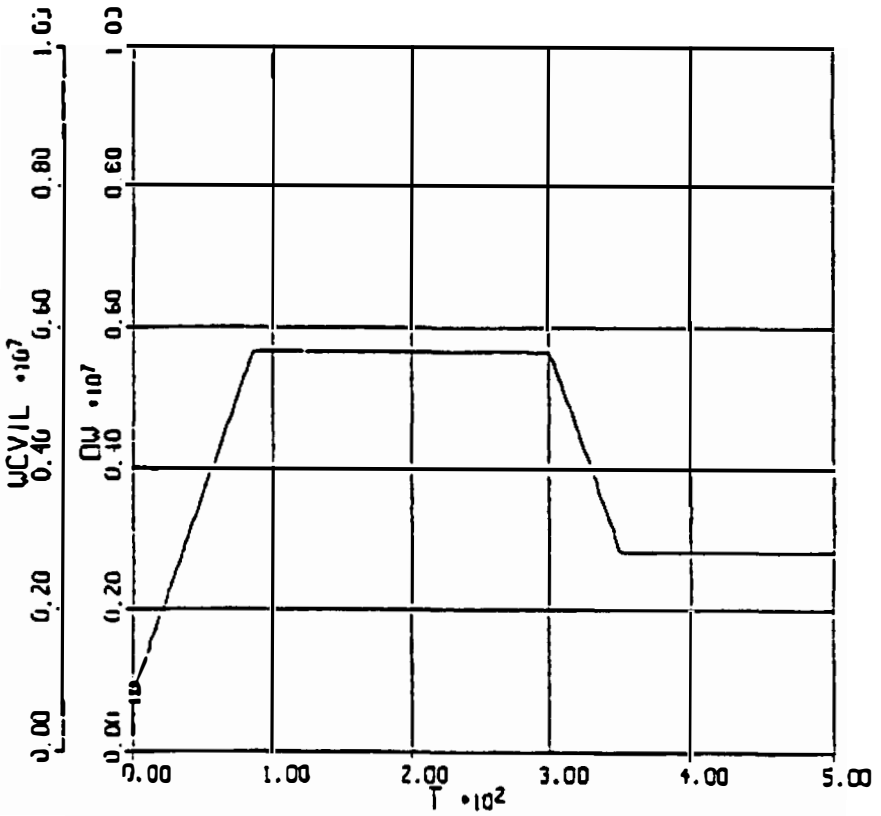

Figure 4.20: Feedwater flow response in comparison with the demand. The demand is followed with a negligible error that is not visible in the figure. As an external disturbance, the steam generator pressure (boundary condition) is lowered 25 % with high frequency oscillation.

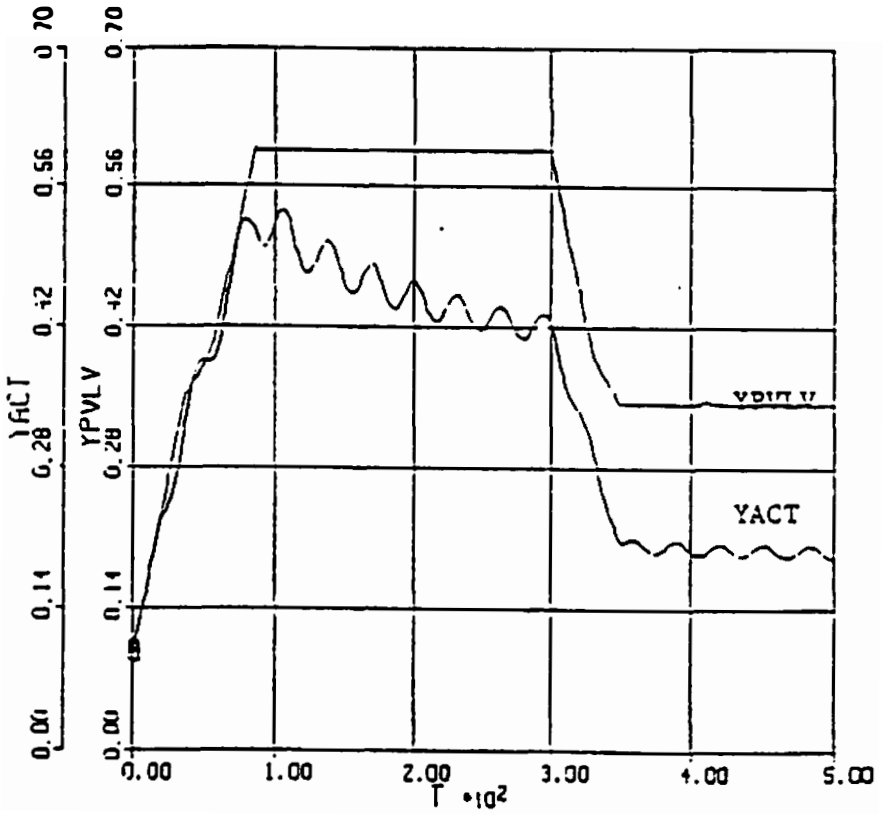

Figure 4.21: Turbine (YPVLV) and feedwater valve (YACT) positions (control inputs) during the demand following control. As an external disturbance, the steam generator pressure (boundary condition) is lowered 25 % with high frequency oscillation.

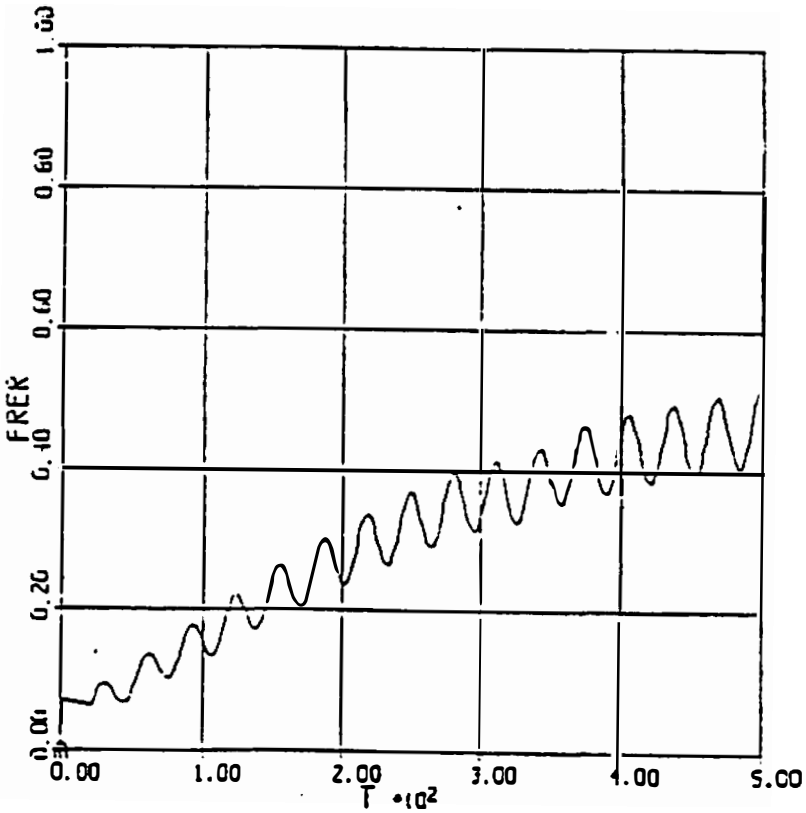

Figure 4.22: Pressure drop across the feedwater valve. As an external disturbance, the steam generator pressure (boundary condition) is lowered 25 % with high frequency oscillation.

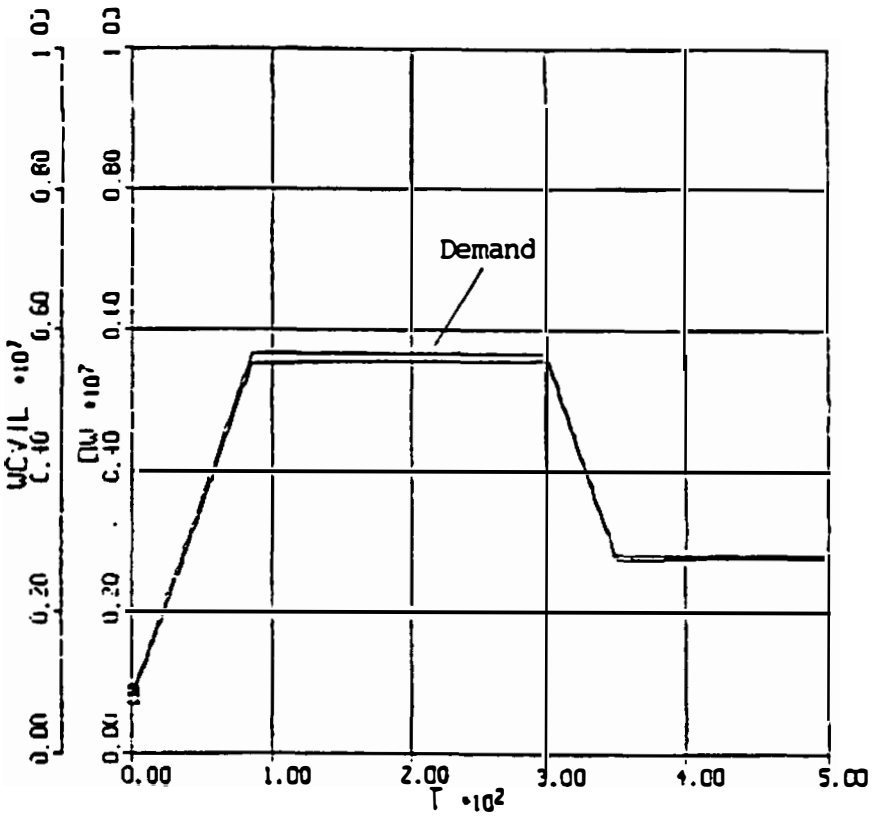

Figure 4.23: Feedwater flow response in comparison with the demand. A 10 % error is introduced to the model based state estimation. Responses verify the robustness against estimation errors.

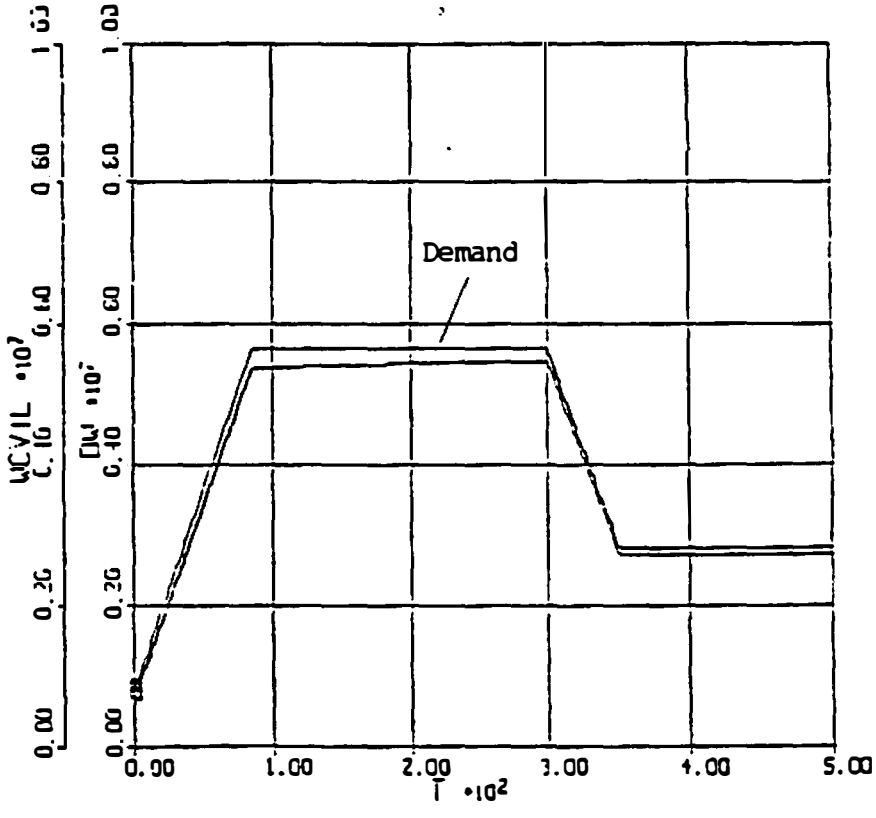

Figure 4.24: Feedwater flow response in comparison with the demand. A 25 % error is introduced to the model based state estimation. Responses verify the robustness against estimation errors.

4.3.5 Conclusions

The given control problem is of a multi-input multi-output (MIMO) form in which the RID design requires state reconstruction among four state variables. The formulation yielded a strategy where the turbine valve provides the feedwater demand and the feedwater valve controls the ΔP. This strategy is a reverse choice compared to the standard designs. The RID requires the estimation of the feedwater valve inlet pressure using an on-line model. Other three state variables are normally available as measurements from the plant.

Simulation results showed an outstanding performance for demands up to 40 percent per minute, which is eight times faster than the allowable maneuvering rate. The demand is followed with less than one percent error and the ΔP variation is maintained within 5 psi at the maximum. Note that a ΔP variation up to 80 psi is considered reasonable in current designs where the target demand is a flowrate of 5 percent per minute. The simulations included an external disturbance in the form of a 30 psi oscillatory change in the steam generator pressure. It is observed that the RID controller, without any adaptive features, is inherently robust against state estimation errors that can reach upto 25 %.

4.4 EBR-II Startup Control

The startup of EBR-II includes a complicated procedure for calibration, status verification, and configuration validation. The automation of the EBR-II startup, therefore, requires a computer based information system as an operator aid. A recent study [36] presents a startup procedure-prompting system developed in an expert system environment. Once the procedure is appropriately followed, the control of the EBR-II startup is a straight forward task. However, the plant nonlinearities over the startup range and the multitude of control variables indicate that advanced, nonlinear multivariate control techniques may perform more efficiently than the conventional, linear methods. Furthermore, a supervisory, intelligent system is required to maneuver around abnormal process conditions or provide safe routes to shutdown.

4.4.1 Plant Description

Experimental Breeder Reactor-II is a liquid metal fast breeder reactor located at the National Reactor Testing Station in Idaho. The original purpose of this facility was to demonstrate the feasibility of fast reactors for central station power plant applications. The purpose was later redirected to provide irradiation services for the development of fuels and structural materials. Changes were made in operating philosophy from that of an engineering test facility to that of a high-priority neutron producer.

The plant consists of a heterogoneous, unmoderated, sodium-cooled reactor (62.5 MWth); an intermediate sodium coolant loop; a steam plant which produces 20 MW of electrical power through a conventional turbine generator; and a fuel processing system consisting of systems for disassembly, decontamination, fabrication, and assembly of fuel elements and subassemblies. Both the reactor and the associated fuel recycle facilities were designed with the philosophy of providing a highly flexible installation that would permit the investigation and evaluation of various core configurations, types of fuel, fuel element design, and processing techniques. The reactor, primary cooling system, and the fuel-handling system components are submerged in a large primary sodium tank. This concept is also sometimes refered to as the pool-type design (such as the Phoenix and Super-Phoenix liquid metal reactors in France).

4.4.2 Existing Control Capabilities

The EBR-II control systems are distributed over the subsystems and are mostly coordinated from the central control room by plant operators. These controllers are designed to function locally and the global control decisions are made by the operators. The following describes the local controllers usedin the EBR-II plant.

EBR-II reactivity control is maintained using 12 control rod and two safety rod subassemblies. A computer controlled rod drive system is capable of controling reactor power during steady-state and power change. An error signal from the reactor power reading is the input to the digital computer. The on-line com-

puter implements a proportional control action to minimize the error reading. The permanent automatic control rod drive system (ACRDS) provides a fast speed automatic mode plus two slow-speed modes, manual and automatic.

The primary sodium flow (loop between core and IHX) is controlled by the primary pumps where the pumping rate is variable from 0 to 100 % in a continuous stepless manner. There are no valves or other control devices in the main sodium loop. Secondary sodium loop is controlled by an electro-magnetic (EM) pump. Flow is adjustable from 0 to 100 % of full flow capacity by varying the voltage applied to the pump windings. The actuation signal is adjusted manually from the sodium recirculating pump panel. The control task of this actuator includes controlling reactor inlet temperature by means of controlling the bulk temperature in the sodium tank. Since the secondary sodium loop constitutes the coupling between the primary and secondary systems, the flow adjustment also directly affects the steam pressure and other system variables in the secondary side.

The feedwater temperature is controlled by bypassing some feedwater around the last heater, mixing a portion of 480 F feedwater with the 568 F water to maintain 550 F input. The bypass valve is manually controlled from the steam panel in the control room.

Turbine generator is controlled by two circuits. The primary circuit controls the speed and load of the turbine whereas the secondary circuit controls the turbine stop valve to trip the turbine when an abnormal condition occurs.

The main control of the steam generator is performed by means of the drum level control. The control system is capable of single-element, four-element, or manual control. The controller accepts four analog signals: steam drum level, feedwater flow, steam flow, and blowdown flow. The actuator is the feedwater valve. A schematic of the EBR-II plant is shown in Fig. 4.25.

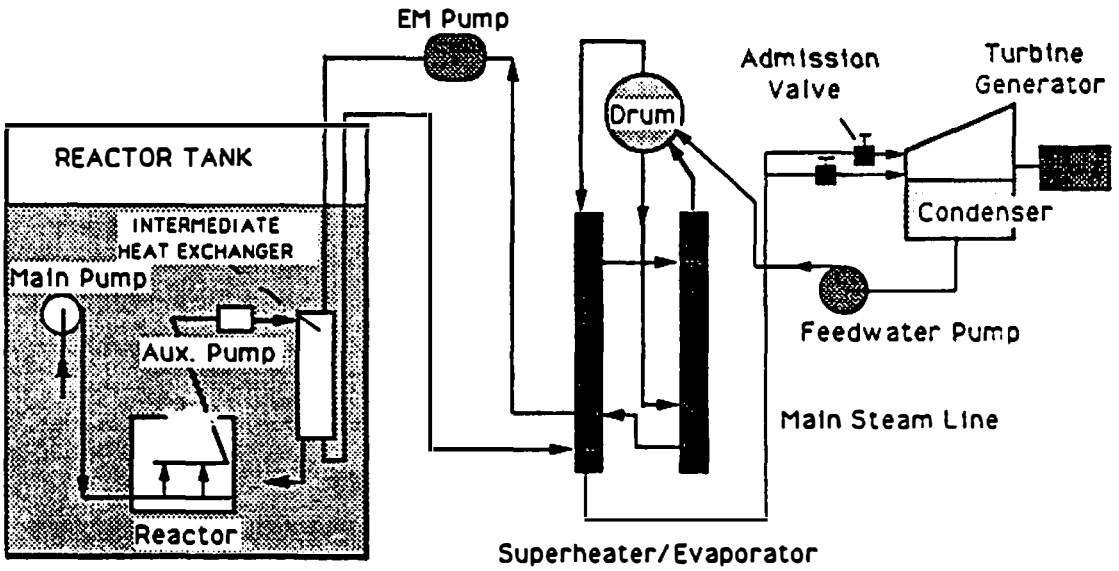

Figure 4.25: EBR-II Plant Schematic

4.4.3 EBR-II Operations

There are eleven identified modes of operation at the EBR-II, classified as normal or non-routine operations. The normal operations include plant startup, plant standby, reactor restart, steady power, changing power, plant shutdown, and fuel handling. The non-routine operations include reactor scram, anticipatory reactor shutdown, plant cooldown, and plant heatup. The startup of the EBR-II is performed in two modes (plant startup, reactor restart) which distinguish the conditions prior to startup. The terminology "reactor restart" emphasizes that the last shutdown was within the 24 hours and no reactor loading change has been made. In plant standby situation, all of the auxiliary systems meet the pre-startup requirements. Unless the plant standby conditions exist, no startup is allowed.

The startup procedures [37] include raising the safety rods into the core and moving control rods in the order specified in the Reactor Run Plan and Authorization. The control rods in the EBR-II contain fuel at the bottom and poison at the top. The core is subcritical when the fuel section of the rods are removed from the core. Therefore, the criticality is achieved by withdrawing the rods which removes the poison section out from the top of the core and replaces the fuel from the bottom. After the control rods are calibrated at about 50 KW, power is incremented until the desired power level is reached. The primary pumps operate at full power throughout the startup. The secondary pump flow is adjusted to maintain a normal steam pressure in the drum. The steam header is pressurized when the primary sodium reaches 620 F. Increase of reactor power is regulated to maintain a 10 F per hour rise in bulk sodium temperature. The secondary sodium flow adjustments also aim at maintaining the primary bulk sodium at 700 F. When the reactor power is stable at 30 MW, and adequate steam is available, the steam system is operated and the turbine-generator is started. A brief summary of the startup procedure including validity checks is shown in Fig.4.26.

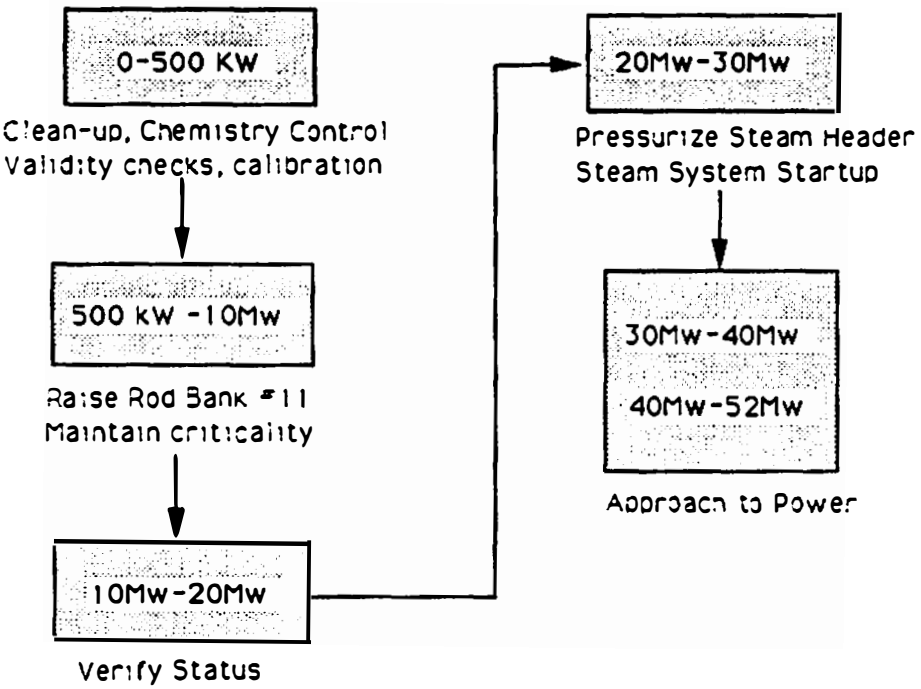

Figure 4.26: EBR-II Startup Procedure.

4.4.4 Startup Control Strategy

EBR-II startup is primarily controlled by two actuators. These are the control rod bank and EM pump (sodium-loop between the secondary side of IHX and sodium side of the steam generator). There are several discrete-event control actions on the steam-side of the reactor, most of which consist of one-time actions. These actuators are not remotely controlled and the control action is taken manually by a plant technician who in some cases walks to the physical location of the actuator. Therefore, the steam side of the EBR-II is not suitably equipped for automation by any means. System upgrading for remote control on the steam-side is considered unnecessarily costly since EBR-II is a small-scale test reactor and the existing operations are considered to be efficient. This reduces the automation control task to a somewhat limited scale and consists of controling the two actuators as stated above [29].

When the automation task is constrained to one part of the system, the control task may become quite complicated or sometimes impossible according to the nature of subsystem couplings. Fortunately, the coupling between EBR-II subsystems does not impose any difficulty for the startup task. The automation strategy consists of imitating a previous startup that is considered as the reference. The imitation simply means that the state variables of the EBR-II primary-side should follow the trajectories of the reference startup (desired behavior). In addition, the output from the primary-side to the steam-side should agree with the demand (the reference trajectory) This agreement must hold in case of time-varying boundary conditions that represent the down-stream effects on the primary system.

The corresponding coupling in the EBR-II reactor takes place in the piping between the IHX and steam generator. The IHX secondary outlet piping carries liquid-sodium to the steam generator. Accordingly, the requirement includes the demand following that represents the energy output of the primary system. Energy is characterized by temperature and mass-flow rate. Thus, demand is stated in terms of the secondary sodium temperature and flow rate. Other important state variables include the reactor power, core-exit temperature, bulk sodium temperature, IHX primary outlet temperature and primary flow. According to the control

technique, some of these variables are selected for trajectory following. However, the controllers are expected to perform such that all of the state variables are within the desired boundaries.

4.4.5 RID Control Design

The EBR-II startup control task consists of a MIMO design with control rod position and secondary sodium flow as the actuating signals. The RID controller design uses two trajectories to be followed: reactor power and the IHX secondary sodium outlet temperature. These trajectories are obtained from the available startup data [38].

A previously developed linear model [39] is modified by including nonlinearities using an adaptive modeling technique described in Chapter-2. The nonlinear model is used for the derivation of the RID control law. This model was previously validated against the EBR-II startup data [40].

The EBR-II model includes seven state variables representing the reactor core and eleven state variables representing the IHX and primary sodium tank. Reactor power is modeled using point reactor kinetics formulation with a precursor concentration averaged over six delayed-neutron groups. The core heat transfer is represented by the Mann's model [39]. Active core region dynamics is given by

$$\frac{dP}{dt} = -\frac{\beta_t}{\Lambda}P + \bar{\lambda}P + \sum_i \frac{\alpha_i}{\Lambda}T_i + \frac{\rho_{ext} + G_\rho}{\Lambda} \tag{4.56}$$

$$\frac{dC}{dt} = \frac{\beta_t}{\Lambda}P - \bar{\lambda}C \tag{4.57}$$

$$\frac{dT_f}{dt} = \frac{E_f}{(MC_p)_f}P - \frac{T_f - T_b)}{R_1(MC_p)_f} \tag{4.58}$$

$$\frac{dT_b}{dt} = \frac{(T_f - T_b)}{R_1(MC_p)_b} - \frac{T_b - T_c)}{R_2(MC_p)_b} \tag{4.59}$$

$$\frac{dT_c}{dt} = \frac{(T_b - T_c)}{R_2(MC_p)_b} - \frac{(T_c - T_1}{R_3(MC_p)_c} \tag{4.60}$$

$$\frac{dT_1}{dt} = \frac{(T_c - T_1)}{R_3(MC_p)_c} + \frac{2}{\tau}(T_{in} - T_1) \tag{4.61}$$

$$\frac{dT_2}{dt} = \frac{(T_c - T_1)}{R_3(MC_p)_c} + \frac{2}{\tau}(T_1 - T_2) + G_{T_2} \tag{4.62}$$

where the seven state variables are fractional power P, precursor concentartion C, fuel temperature T_f, blanket temperature T_b, cladding temperature T_c, coolant inlet-node temperature T_1, and coolant outlet-node temperature T_2. The reactivity feedback terms α_i and T_i in Eq. (4.56) correspond to the contributions from fuel and coolant temperatures given above. There are two adaptive terms G_ρ and G_{T_2} that are corrections for the uncertainties in reactivity and core heat transfer at the outlet, respectively. Reactor power is controlled by external reactivity ρ_{ext}. The adaptive RID control design includes derivations for ρ_{ext}, G_ρ and G_{T_2} for the demand following reactor.

The IHX model includes Mann's heat-transfer model using 10 state variables. The primary and secondary sides of the IHX are divided up to 4 lumps whereas the tube material is represented by 2 axial nodes. The state variables of the model correspond to average temperatures in these 10 axial nodes. The secondary outlet node temperature T_{out} is given by

$$\frac{dT_{out}}{dt} = \frac{W_s}{M_s}(T_{in} - T_{out}) + \frac{(Q_{ms} + G_Q)}{(MC_p)_s} \tag{4.63}$$

where T_{in} is the inlet temperature to the node. The heat transfer from the tube wall to the secondary sodium Q_{ms} is corrected by the adaptive term G_Q. The control input is the secondary sodium flow W_s.

The derivation of RID control laws for reactivity ρ_{ext} and secondary sodium flow W_s is carried out using Eqs.(4.56) and (4.63). The reactivity control is given by

$$\rho_{ext} = \Lambda\frac{dP}{dt} + \beta P - \bar{\lambda}\Lambda C - \sum_i \alpha_i T_i - G_\rho \tag{4.64}$$

where

$$\frac{dP}{dt} = K_1(D_p - P) \tag{4.65}$$

K_1 is an adjustable constant and D_p is the startup tajectory of reactor power. Note that reator power P, and coolant outlet and inlet temperatures T_{out}, T_{in} are available as direct measurements. The remaining state variables are estimated by

an on-line model. In order to clearify the usage of measurements and model based estimations, the control law is rewritten with a new notation where the subscript m denotes the estimations.

$$\rho_{ext} = \Lambda\frac{dP}{dt} + \beta P - \bar{\lambda}\Lambda C_m - \sum_j \alpha_j T_{jm} - \sum_k \alpha_k T_k - G_\rho \tag{4.66}$$

where

$$\frac{dP}{dt} = K_1(D_p - P) \tag{4.67}$$

Then the uncertainty term G_ρ is designed to match the plant and model dynamics.

$$G_\rho = \Lambda\frac{dP_m}{dt} + \beta P_m - \bar{\lambda}\Lambda C_m - \sum_i \alpha_i T_{im} - \rho ext \tag{4.68}$$

where

$$\frac{dP_m}{dt} = KG_1(P - P_m) \tag{4.69}$$

KG_1 is an adjustable constant.

The uncertainty in the outlet coolant node is designed in a similar way. From Eq.(4.62)

$$G_{T_2} = \frac{(T_{cm} - T_{1m})}{R_3(MC_p)_c} + \frac{2}{\tau}(T_{1m} - T_{2m}) + \frac{dT_{2m}}{dt} \tag{4.70}$$

where

$$\frac{dT_{2m}}{dt} = KG_2(T_2 - T_{2m}) \tag{4.71}$$

with an adjustable constant KG_2.

The secondary sodium flow control is designed using Eq.(4.63).

$$W_s = \frac{(Q_p + G_Q)}{(C_p)_s(T_{in} - T_{out})} + K_2\frac{(D_T - T_{out})M_s}{(T_{in} - T_{out})} \tag{4.72}$$

where K_2 is an adjustable constant and D_T is the startup trajectory for the secondary sodium outlet temperature. The flow control law uses only one measurement from the plant that is the outlet temperature of the secondary sodium T_{out}. The remaining state variable T_{in} is estimated by an on-line model. Similar to the

reactivity control, the control law is rewritten to clarify the model based estimations using subscript m.

$$W_s = \frac{(Q_{pm} + G_Q)}{(C_p)_s(T_{inm} - T_{out})} + K_2 \frac{(D_T - T_{out})M_s}{(T_{inm} - T_{out})} \tag{4.73}$$

The uncertainty term D_Q is designed such that the model and plant behavior match.

$$G_Q = (MC_p)_s \frac{dT_{outm}}{dt} - \frac{W_s}{(C)_s}(T_{inm} - T_{outm}) - Q_{pm} \tag{4.74}$$

where

$$\frac{dT_{outm}}{dt} = KG_3(T_{out} - T_{outm}) \tag{4.75}$$

KG_3 is an adjustable constant. The RID control system for the EBR-II startup task is shown in Fig 4.27.

4.4.6 Simulation Results

The EBR-II startup simulations are performed using MATRIXx/SYSTEM-BUILD software on a VAX 3100 Work Station [41]. The plant is driven by three different control paradigms (RID, Fuzzy Logic, and Neural Network [42]) in three separate simulations. The results of these three simulations are compared with plant data.

Figure 4.28 shows the power response controlled by three different controllers and the operator during startup. The plant follows the power trajectory (plant data) very efficiently. The following figures include core-exit temperature (Fig.4.29), bulk tank temperature (Fig.4.30), IHX secondary sodium outlet temperature (Fig. 4.31, in-core sodium temperature (Fig.4.32), control rod position (Fig.4.33), and secondary sodium flow rate (Fig.4.34). The plant responses indicate that the three controllers accomplish the startup task with desirable performance, the RID strategy being closest to the actual plant control.

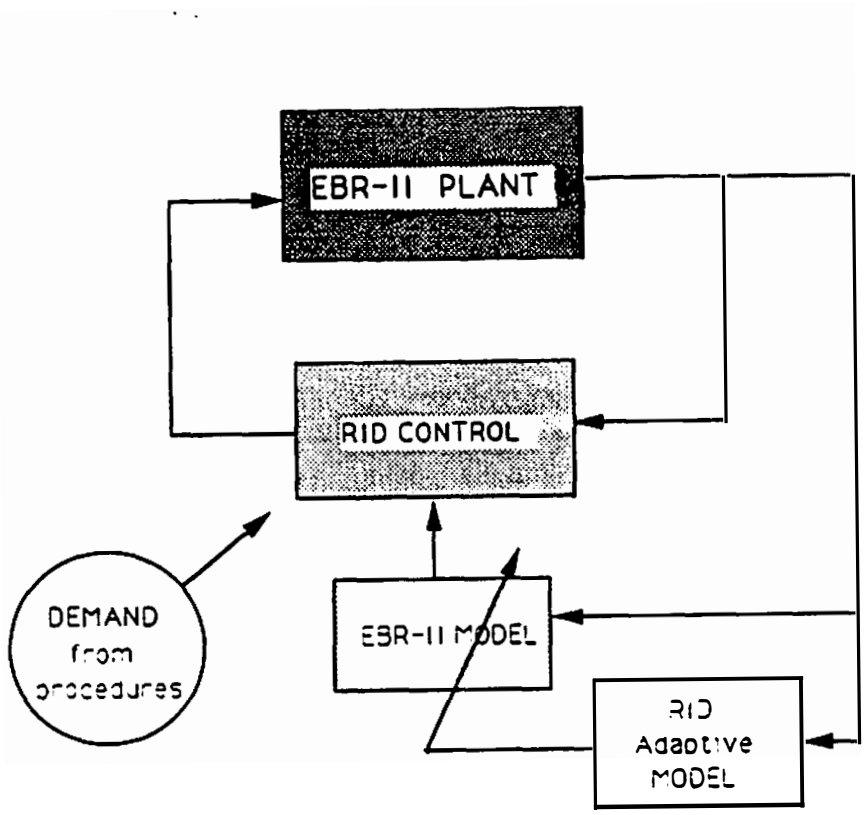

Figure 4.27: RID controller in application to the EBR-II startup task.

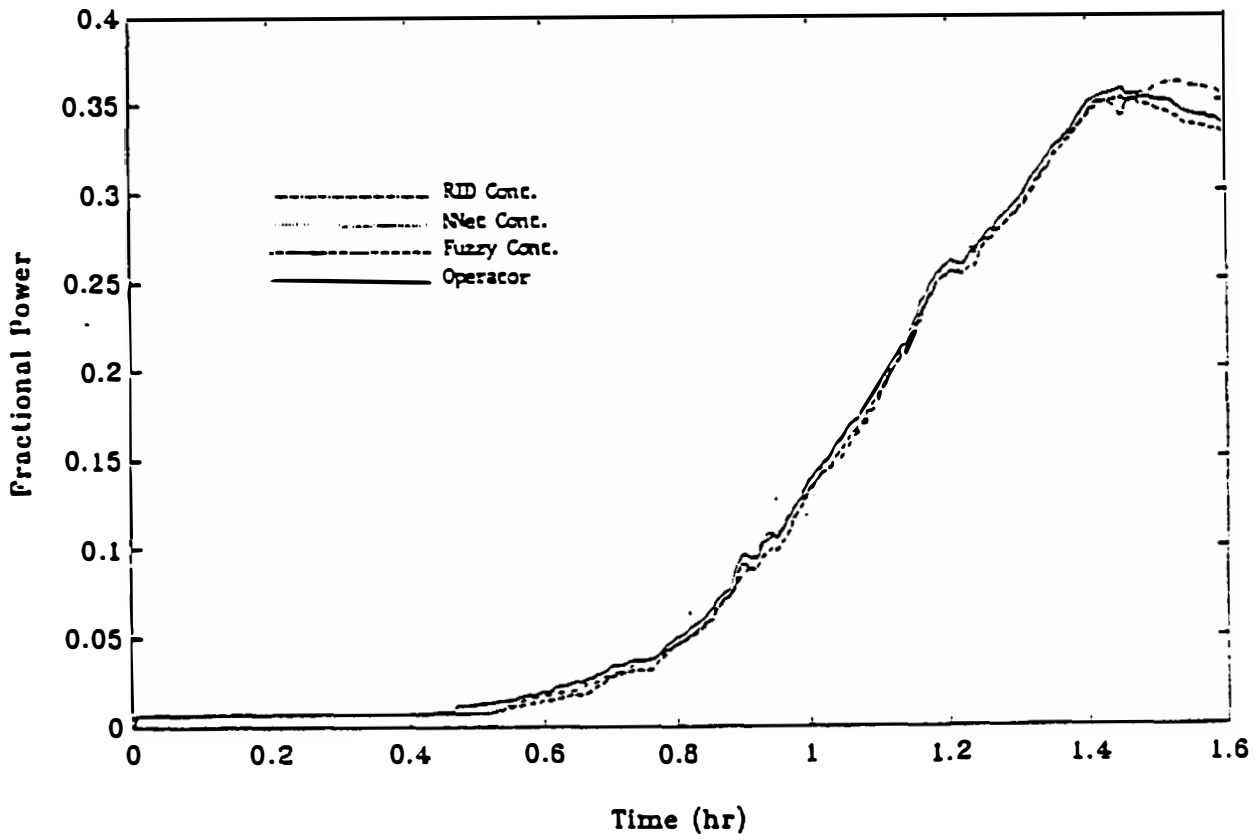

Figure 4.28: Reactor power responses during startup at EBR-II. Reactor controlled by RID, Fuzzy, and NNET controllers. Simulation results compared with plant data.

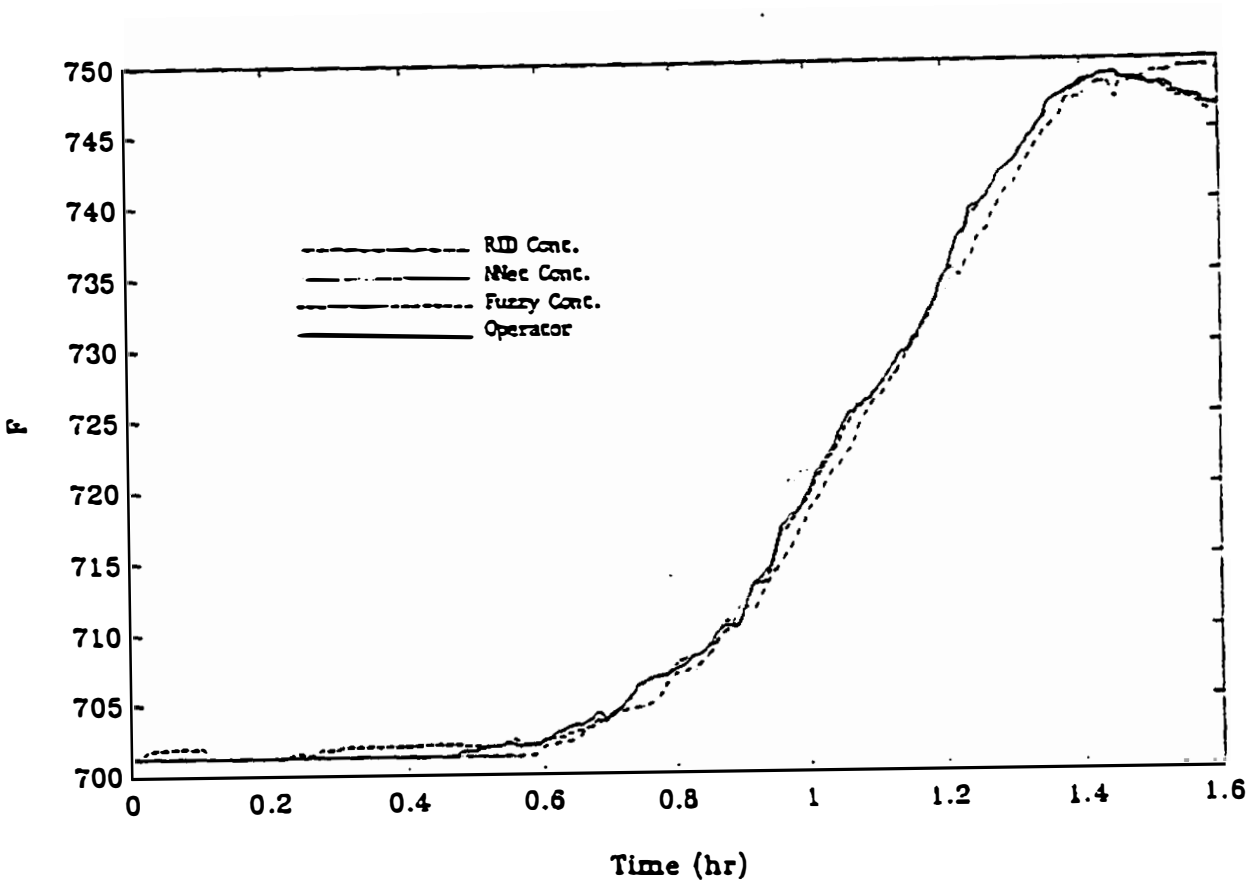

Figure 4.29: Core exit temperature responses during startup at EBR-II. Reactor controlled by RID, Fuzzy, and NNET controllers. Simulation results compared with plant data.

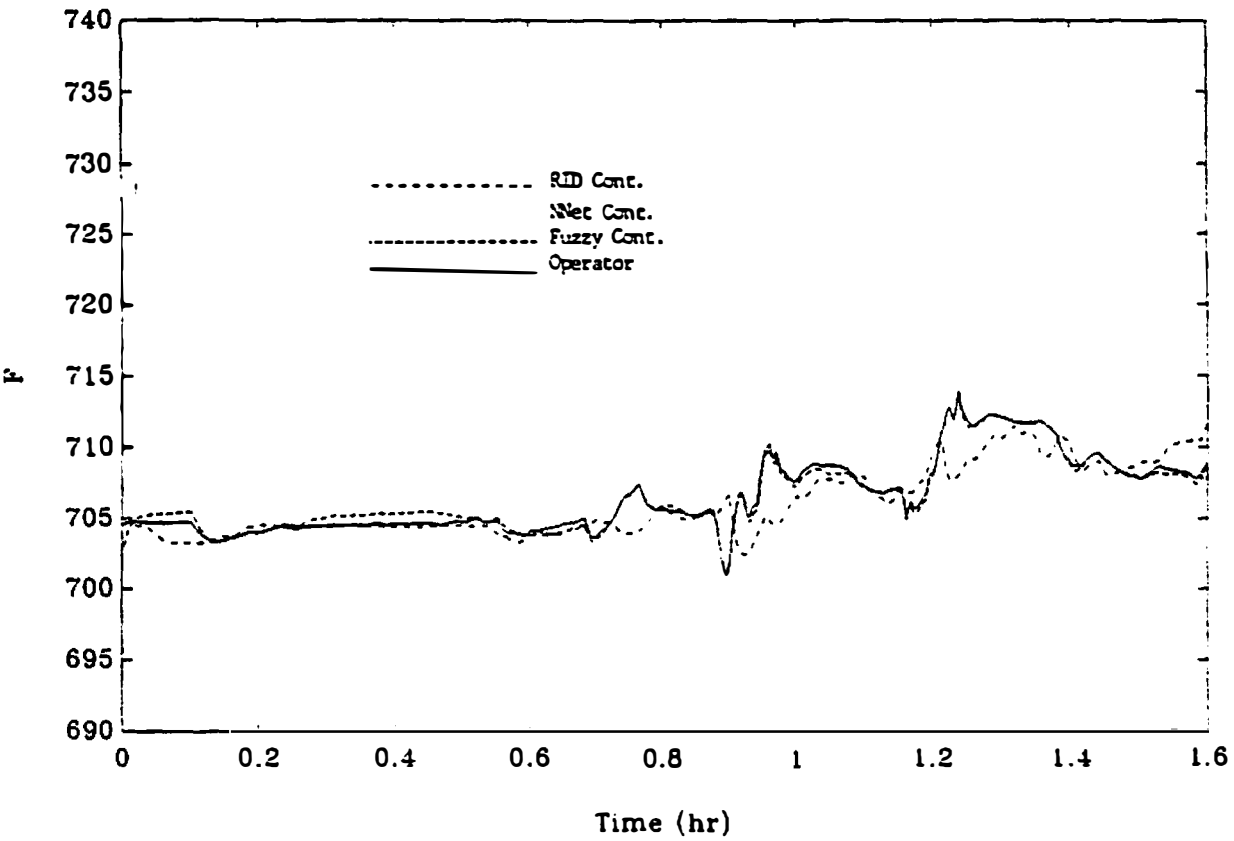

Figure 4.30: Bulk tank temperature responses during startup at EBR-II. Reactor controlled by RID, Fuzzy, and NNET controllers. During the startup mode, sodium bulk temperature is desired to remain constant. Simulation results compared with plant data.

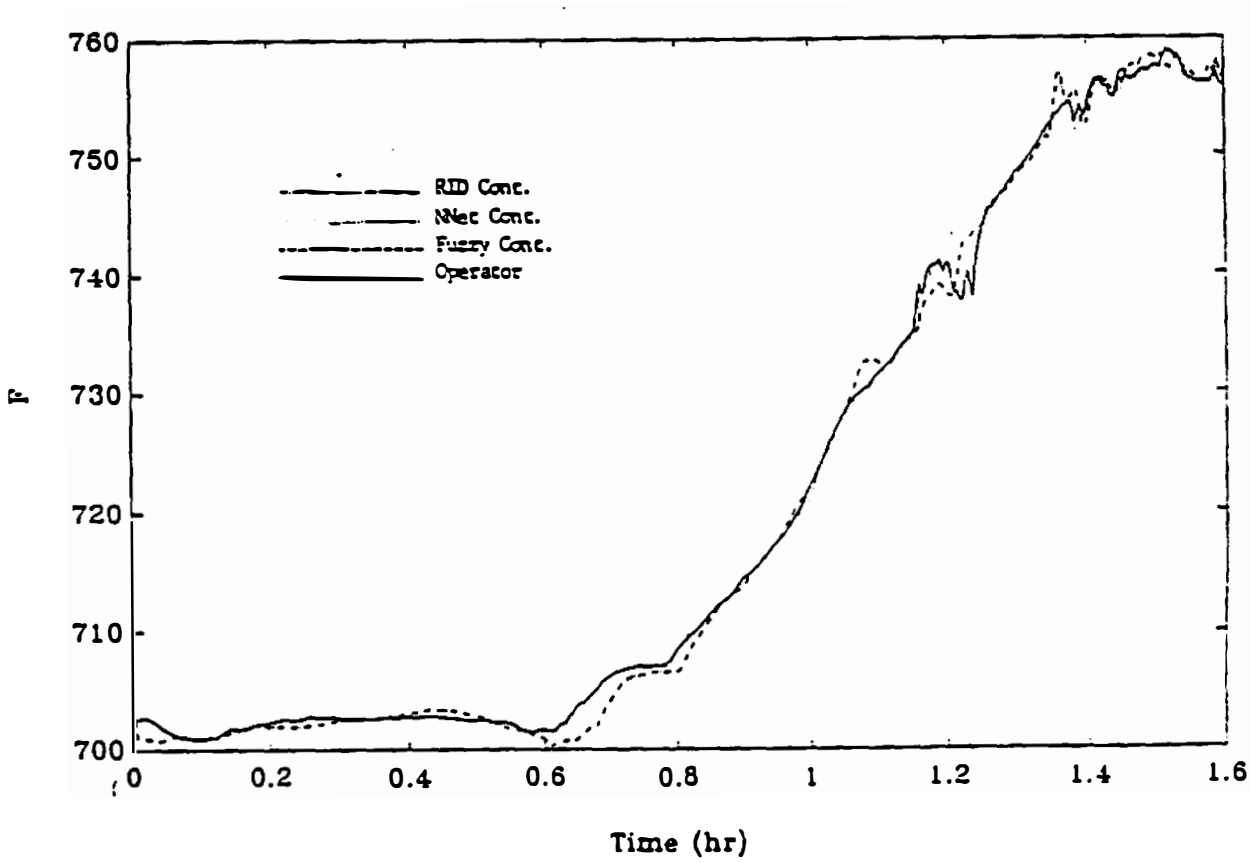

Figure 4.31: IHX secondary-outlet temperature responses during startup at EBR-II. Reactor controlled by RID, Fuzzy, and NNET controllers. Simulation results compared with plant data.

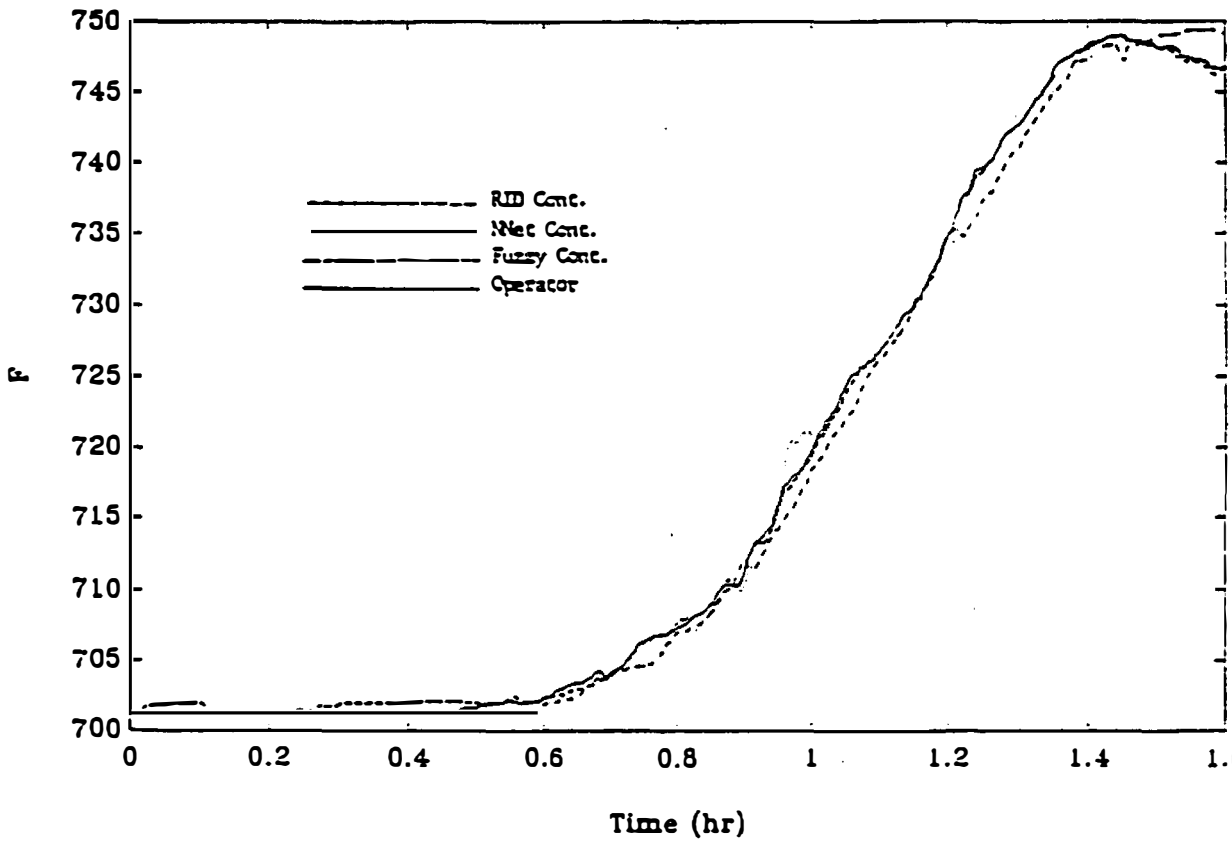

Figure 4.32: In-core sodium temperature responses during startup at EBR-II. Reactor controlled by RID, Fuzzy, and NNET controllers. Simulation results compared with plant data.

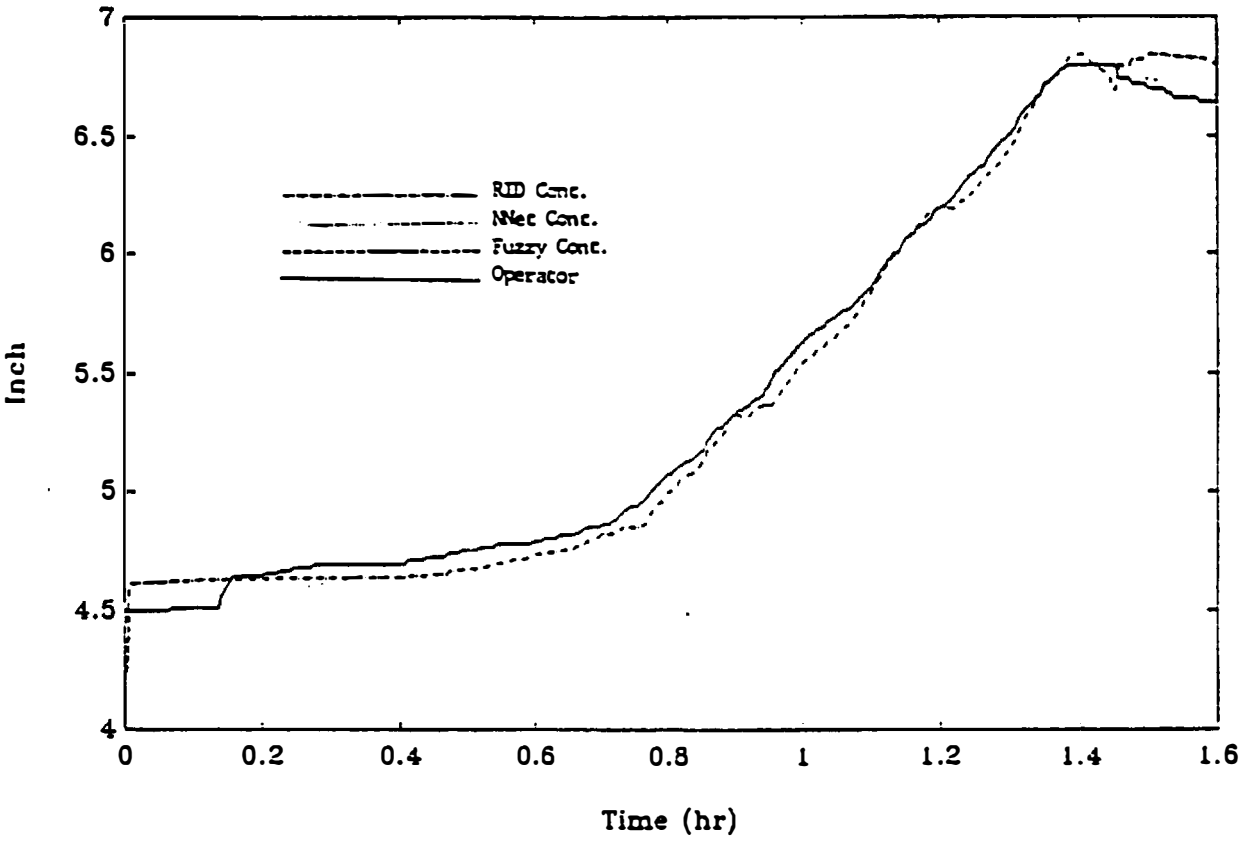

Figure 4.33: Control rod position (control input-1) during startup at EBR-II. Reactor controlled by RID, Fuzzy, and NNET controllers. Simulation results compared with plant data.

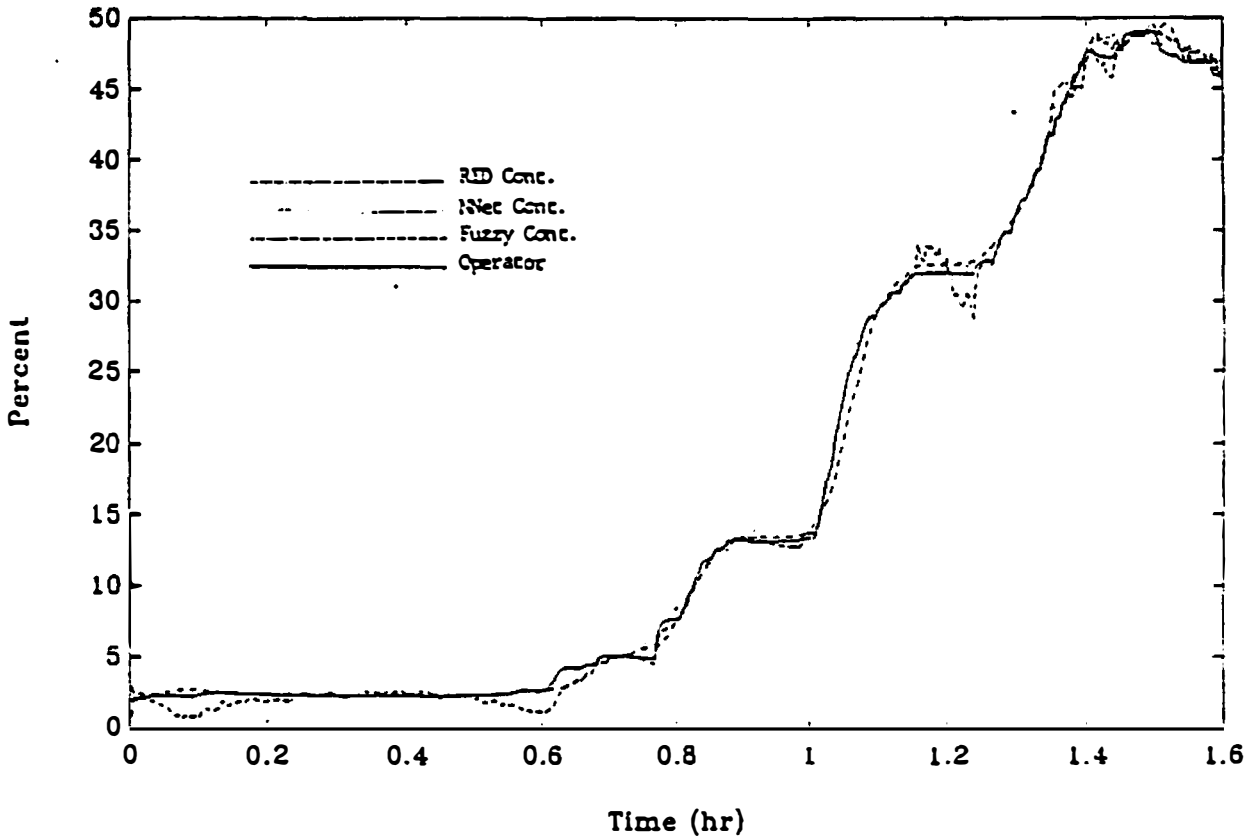

Figure 4.34: Secondary sodium flow (control input-2) response during startup at EBR-II. Reactor controlled by RID, Fuzzy, and NNET controllers. Simulation results compared with plant data.

The control rod motion generated by the RID control paradigm is very close to the operator's actions. However, the secondary sodium flow is controlled more abruptly. The difference in flow control between the operator and RID controller is reflected in the power response as a small delay. This is caused by the deviation in reactor inlet temperature and tank temperature. It is important to note that the RID controller is tuned extra tightly to accomplish efficient trajectory following.

The fuzzy control results show a strong agreement with the RID and operator actions. The system responses are also very consistent with the startup data. The trajectory of the IHX secondary outlet temperature is followed with more error compared with the RID performance. However, this error is negligible for all practical purposes. The fuzzy controller is not dependent on a model and it is very simple to implement. Thus, the trade-off between the RID and fuzzy controllers represents a bargain between the performance and complexity.

The neural network controller yields the least preferable strategy due to deviations in system responses with respect to the desired behavior. However, the neural network design was restricted to a very simple structure due to the difficulty in implementing control design in this particular simulation environment. Although the performance is the poorest among the others, the commands generated by this controller lie in the valid region and the overall performance is reasonable.

Chapter 5

Integration of Artificial Intelligence Tools

This chapter is dedicated to the analysis of the inverse dynamics (ID) concept in relation to Artificial Intelligence (AI), and development of tools for strategy design and adaptive modeling.

5.1 Significance of the "Inverse" Approach

In order to incorporate AI methods such as expert systems and neural networks with the RID paradigm, it is important to review the inverse dynamics concept. The concept is best understood by considering the *mirror* image dynamics of a mass-spring system shown in Fig 5.1. Assume a hypothetical mirror placed perpendicular to the plane of motion. The dynamics of the mass is described by its coordinates in a fixed frame and by their evolution in time. The coordinates represent the physical world. The mirror-coordinate frame represents the imaginary world. Apparently, the force vector acting upon the mass in the "mirror" space is in the opposite direction and is equal to that of the real system. Thus, it represents the equilizer effect in a dynamic fashion. Since it is not possible to couple the physical world with the imaginary world, the control objective is to emulate the force acting upon the mass in the imaginary world. The origin of the coordinate frame can be shifted to a desired position for cases where there is a demand for the final equilibrium point. The RID control paradigm is developed with this approach.

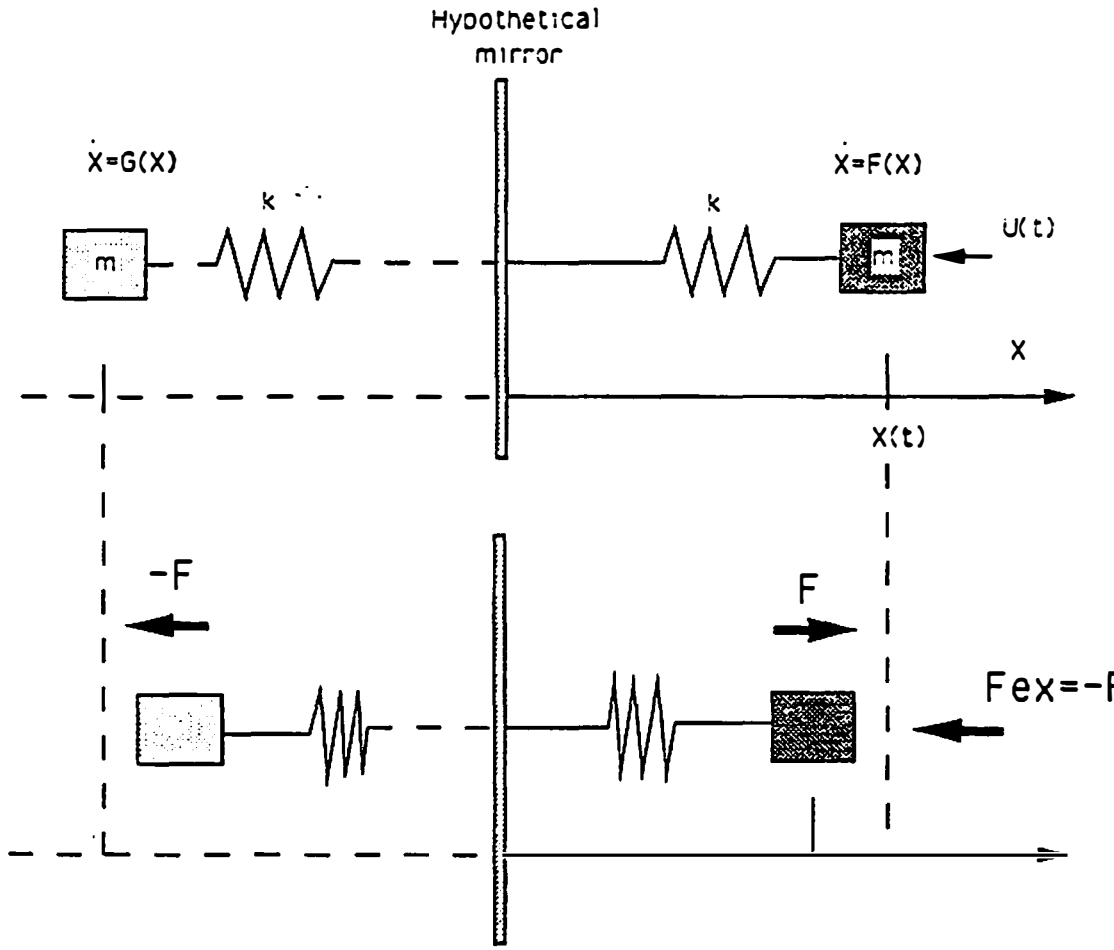

Figure 5.1: A hypothetical mirror placed perpendicular to the plane of motion yields inverse dynamics of the mass-spring system. If unknown control u employs the inverse dynamics, system remains at equilibrium.

The inverse dynamics concept, therefore, yields a very simple principle for control. The goal is to convert the description of the mass motion from the real coordinate frame into the imaginary one. Once the state space representation in real frame is available, the inverse solution of control in the real frame yields the dynamics in the imaginary frame. This was illustrated in Chapter 2. Thus, the only required knowledge to create an inverse is the state space representation of the system under consideration. The following corollary summarizes this distinct fact.

The knowledge of open-loop system dynamics automatically represents the knowledge of control when the inverse property is used.

Comparing with some of the criteria used in standard control theory (cost function, output error minimization, desired pole-zero locations, desired gain/phase margins, Hamiltonian, Lyapunov function, Lagrangian mechanics, fuzzy-rules), the RID control paradigm may be viewed as a straight forward approach.

5.2 Strategy Design

Although the conventional control systems are general purpose devices, their implementation requires a strategy development. The strategy development involves selecting important signals, determining control system arrangement (feedback, feedforward, cascade arrangements) and set-points, choosing actuators, tuning, and other modifications according to system specifications. Thus, a complete control design scenario involves considerable amount of knowledge about the system. In standard control theory, the development of control law is limited to shaping the transient behavior of actuator signals to implement a pre-selected strategy. Therefore, if the strategy is inappropriate, control will fail.

A control law which can explicitly identify the reasonable strategies is of great value. This can be achieved if the control law reflects an important part of the system dynamics. The inverse dynamics can be used for this purpose. Forward and inverse operators $\mathcal{F}$ and $\mathcal{G}$ are appropriate representations to develop a new, high

level control language in which the strategy problem is formulated. This allows using an expert systems to solve the strategy problem. Note that a need for such an approach would emerge for systems with high degrees of freedom (large number of assignments and control variables).

5.2.1 Representation of the Control Problem

The operators $\mathcal{G}$ and $\mathcal{F}$ are based on the standard state-space representation of dynamic systems. Consider the following n*th* order system.

$$\dot{x_1} = f_1(x_1, x_2, \cdots, x_n, u_1)$$

$$\dot{x_2} = f_2(x_1, x_2, \cdots, x_n, u_2)$$

$$\vdots$$

$$\dot{x_n} = f_n(x_1, x_2, \cdots, x_n, u_n)$$

where x_i and u_i $(i = 1, \cdots, n)$ are state and control variables, respectively. Suppose that there is a set of control tasks $\mathcal{R}$ that are described by set points or trajectories $r_j, (j = 1, \cdots, m)$ where $m \leq n$. The control problem representation is made with reference to the set $\mathcal{R}$. Thus, the problem can not be represented if $\mathcal{R}$ is empty (no assignments, m=0). This system can be redefined by n forward operators $\mathcal{F}_1, \mathcal{F}_2, \cdots, \mathcal{F}_n$.

$$\dot{x_1} = \mathcal{F}_1$$

$$\dot{x_2} = \mathcal{F}_2$$

$$\vdots$$

$$\dot{x_n} = \mathcal{F}_n$$

Refering to the control entries, we can define inverse operators $\mathcal{G}_1, \mathcal{G}_2, \cdots, \mathcal{G}_n$. Note that the existence of each inverse control yet to be determined. The inverse operator by a direct control entry is denoted by $\exists$.

$$\mathcal{F}_1 \exists \mathcal{G}_1$$

$$\mathcal{F}_2 \exists \mathcal{G}_2$$

$$\vdots$$

$$\mathcal{F}_n \exists \mathcal{G}_n$$

The control problem representation starts from the assignment r_j to the forward dynamics $\mathcal{F}_j$ and denoted as follows:

$$r_j \rightarrow \mathcal{F}_j$$

Then a possible solution is

$$r_j \rightarrow \mathcal{F}_j \exists \mathcal{G}_j \tag{5.1}$$

The statement (5.1) is the control problem solution for the j*th* task.

Refering to the auxiliary states technique described in Chapter 2, the problem definition can be expanded to yield more than one solution. This requires the selection of an auxiliary state to accomplish the given control task. For the j*th* task, it is possible to use control variables other than u_j. Then, the inverse operator $\mathcal{G}_j$ will be indirectly coupled to other forward operators. The indirect entry is denoted by $\ni$.

$$r_j \rightarrow \mathcal{F}_j \ni \mathcal{G}_j$$

The problem is to provide all possible couplings which will satisfy $\mathcal{G}_j$. A coupling between each forward operator is denoted by a membership $\mu_{i,j}$. One directional coupling, that is the state equation j has an entry of the i*th* state variable but vice verse is not true, is denoted by $\bar{\mu}_{ij}$. Suppose the k*th* forward operator has a direct control entry u_k. Then the j, k strategy will require:

$$\mathcal{F}_j \mu_{jk} \mathcal{F}_k$$

Similarly, another strategy for the k+1 *th* control entry will require:

$$\mathcal{F}_j \; \mu_{j,k+1} \; \mathcal{F}_{k+1}$$

Finally, the two strategies for the j*th* task are given by

$$r_j \rightarrow \mathcal{F}_j \ni \mathcal{G}_j = \left\{ \begin{array}{lll} (\mathcal{F}_j & \mu_{jk} & \mathcal{F}_k) \\ (\mathcal{F}_j & \mu_{j,k+1} & \mathcal{F}_{k+1}) \end{array} \right\} \begin{array}{lll} \mathcal{F}_k & \exists & \mathcal{G}_k \\ \mathcal{F}_{k+1} & \exists & \mathcal{G}_{k+1} \end{array} \tag{5.2}$$

The representation above is called the stable-inverse map (SIM). The number of lines on the right hand side indicate the number of possible strategies. Big curly

bracket identifies couplings between the subsystems. The solution above suggests that there are two couplings of $\mathcal{F}_j$ yielding two distinct strategies using either $\mathcal{G}_k$ or $\mathcal{G}_{k+1}$.

The symbols used in a SIM analysis are summarized below.

$\exists \equiv$ direct entry of control
$\ni \equiv$ indirect entry of control
$\mu \equiv$ membership (strength and nature of coupling)
$\rightarrow \equiv$ decision (assignment of demand)

5.2.2 Potential Advantage of the SIM Analysis

In large-scale systems (or systems with high degrees of freedom), the abundance of possible strategies may complicate the control design, unless a systematic approach is taken to evaluate all the possibilities exhaustively. Such an attempt may be considered unreasonable using control techniques such as the PID. Because the error based techniques do not include process-related dynamics within the control law, the criteria for evaluation is not control law dependent. The RID control paradigm is suitable for such analysis due to unique solutions.

The primary goal of the stable inverse maps is to provide a foundation for symbolic computations which may be performed in an expert system environment. It is apparent that the membership μ_{ij} between forward operators $\mathcal{F}_i$, $\mathcal{F}_j$ represents a rule in the form "IF subsystems i-j are coupled". Similarly, the operators $\ni$ and $\exists$ translate into "IF subsystem j is controllable" and "IF subsystem j has a direct control entry", respectively. The assignment denoted by $\rightarrow$ gives the predicate "THEN task r is achievable".

When the IF-THEN querries yield possible solutions, the problem must be resolved considering low-level problems. For example, the controllability statements correspond to the auxiliary-states method of control law derivation whereas the membership statements deal with the existence of inverses. Solving these problems clearly indicates the necessary signals, required parameter estimations, desired ac-

tuator characteristics and other requirements. Refering to the availability of such requirements, the cost of control can be determined. Once the costs are determined, the best strategy is found.

The SIM procedure offers a systematic way to distinguish between the high and low level problems. **The solution of high level problem yields possible strategies, whereas the solution of low level problems determines the best.** The overall solution yields a global control capability. The assignment set $\mathcal{R}$ can be made a matrix, each column containing reference trajectories of a prescribed mode of operation. This approach is analogous to the hierarchical and supervisory control methods. Figure 5.2 illustrates the topological representation of SISO, MISO, and MIMO control strategies.

5.2.3 SIM Analysis for Previous Applications

Although the applications presented in Chapters 3 and 4 do not include a large combination of control possibilities, the topology of solutions are given below as examples. Refering back to the feedwater-train system, the SIM can be developed as follows. The system described by Eqs.(4.38- 4.42) is rewritten in terms of SIM operators where the subscripts 1, 2, 3, 4, 5 indicate the state equations in the order they are presented previously. The problem definition is given with reference to two tasks (demands) denoted by D_3 and D_5.

$$
\begin{array}{lll}
\mathcal{F}_2\bar{\mu}_{21}\mathcal{F}_1 & \mathcal{F}_1 \exists \mathcal{G}_1 & D_3 \rightarrow \mathcal{F}_3 \\
\mathcal{F}_3\mu_{32}\mathcal{F}_2 & \mathcal{F}_4 \exists \mathcal{G}_4 & D_5 \rightarrow \mathcal{F}_5 \\
\mathcal{F}_4\mu_{45}\mathcal{F}_5 & & \\
\mathcal{F}_5\mu_{53}\mathcal{F}_3 & &
\end{array}
$$

where $\bar{\mu}_{21}$ indicates one directional coupling that is $\mathcal{F}_2$ has an input from $\mathcal{F}_1$ whereas vice verse is not true. If the coupling is mutual, the order of the terms is not important. The SIM solutions are given by

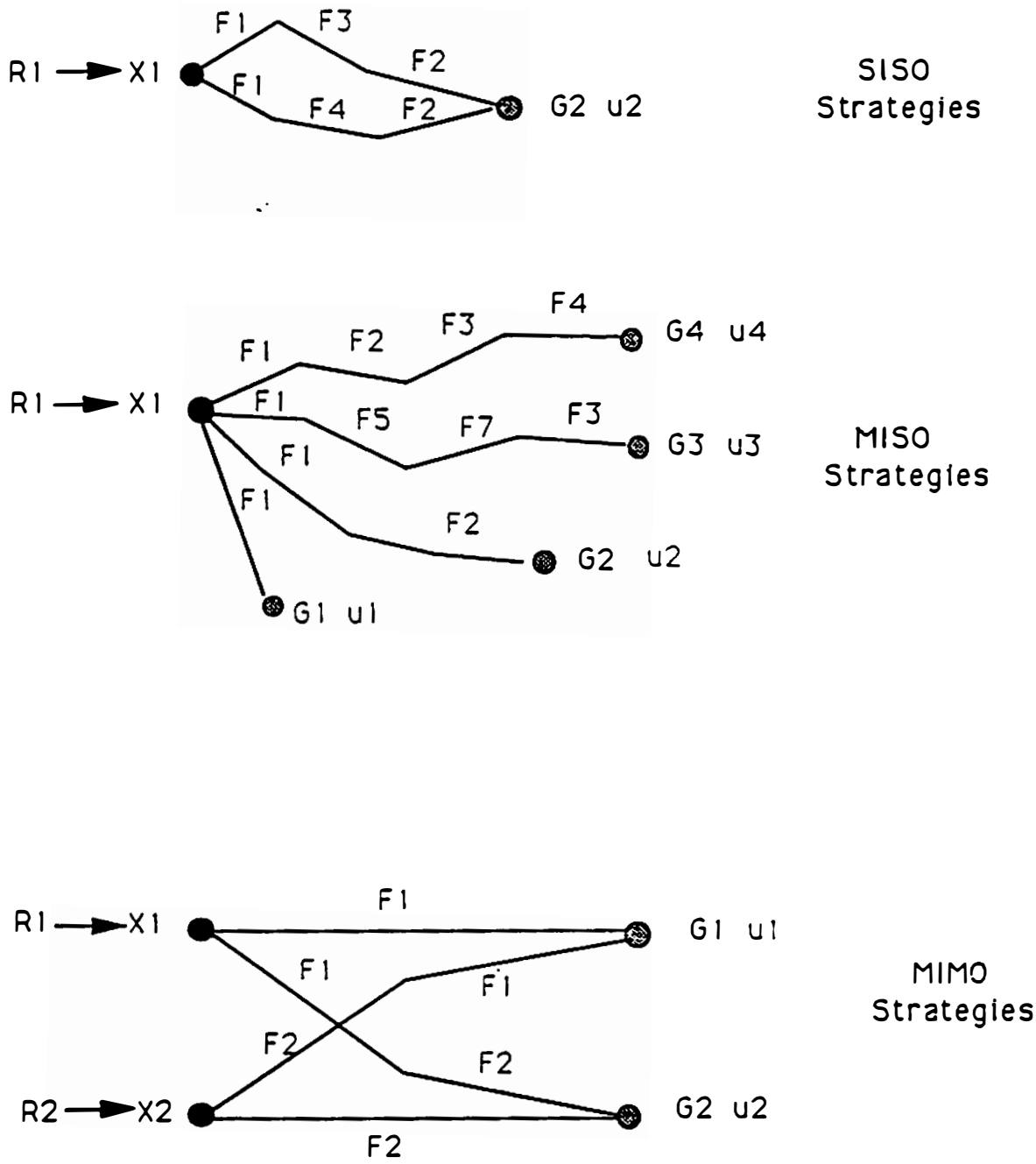

Figure 5.2: Topological representation of SISO, MISO, and MIMO control strategies (high level problems). These solutions may be obtained using symbolic computations for systems with large degrees of freedom.

$$D_3 \rightarrow \mathcal{F}_3 \ni \mathcal{G}_3 = \left\{ \begin{array}{ll} (\mathcal{F}_3\mu_{32}\mathcal{F}_2) & (\mathcal{F}_2\mu_{21}\mathcal{F}_1) \\ (\mathcal{F}_3\mu_{35}\mathcal{F}_5) & (\mathcal{F}_5\mu_{54}\mathcal{F}_4) \end{array} \right\} \begin{array}{lll} \mathcal{F}_1 & \exists & \mathcal{G}_1 \\ \mathcal{F}_4 & \exists & \mathcal{G}_4 \end{array} \tag{5.3}$$

$$D_5 \rightarrow \mathcal{F}_5 \ni \mathcal{G}_5 = \left\{ \begin{array}{lll} (\mathcal{F}_5\mu_{53}\mathcal{F}_3) & (\mathcal{F}_3\mu_{32}\mathcal{F}_2) & (\mathcal{F}_2\mu_{21}\mathcal{F}_1) \\ (\mathcal{F}_5\mu_{54}\mathcal{F}_4) & & \end{array} \right\} \begin{array}{lll} \mathcal{F}_1 & \exists & \mathcal{G}_1 \\ \mathcal{F}_4 & \exists & \mathcal{G}_4 \end{array} \tag{5.4}$$

The strategy selected for feedwater-train control is given by

$$D_5 \rightarrow \mathcal{F}_5 \ni \mathcal{G}_5 = \{(\mathcal{F}_5\mu_{53}\mathcal{F}_3)\,(\mathcal{F}_3\mu_{32}\mathcal{F}_2)\,(\mathcal{F}_2\mu_{21}\mathcal{F}_1)\}\mathcal{F}_1 \exists \mathcal{G}_1 \tag{5.5}$$

$$D_3 \rightarrow \mathcal{F}_3 \ni \mathcal{G}_3 = \{(\mathcal{F}_3\,\mu_{35}\,\mathcal{F}_5)\,(\mathcal{F}_5\,\mu_{54}\,\mathcal{F}_4)\}\,\mathcal{F}_4 \exists \mathcal{G}_4 \tag{5.6}$$

The benchmark problem presented in Chapter 3 is considered next. Problem definition uses subscript letters 1, 2, 3, 4 corresponding to the order of the state equations.

$\mathcal{F}_1\,\mu_{12}\,\mathcal{F}_2$	$\mathcal{F}_1 \exists \mathcal{G}_1$	$D_1 \rightarrow \mathcal{F}_1$
$\mathcal{F}_1\,\mu_{13}\,\mathcal{F}_3$	$\mathcal{F}_4 \exists \mathcal{G}_4$	$D_4 \rightarrow \mathcal{F}_4$
$\mathcal{F}_1\,\mu_{14}\,\mathcal{F}_4$		
$\mathcal{F}_3\,\mu_{34}\,\mathcal{F}_4$		

The SIM solution for the first demand yields

$$D_1 \rightarrow \mathcal{F}_1 \exists \mathcal{G}_1 \tag{5.7}$$

$$D_1 \rightarrow \mathcal{F}_1 \ni \mathcal{G}_1 = \{(\mathcal{F}_1\,\mu_{14}\,\mathcal{F}_4)\}\,\mathcal{F}_4 \exists \mathcal{G}_4 \tag{5.8}$$

Similarly, the second demand is satisfied by

$$D_4 \rightarrow \mathcal{F}_4 \exists \mathcal{G}_4 \tag{5.9}$$

$$D_4 \rightarrow \mathcal{F}_4 \ni \mathcal{G}_4 = \{(\mathcal{F}_4\,\mu_{14}\,\mathcal{F}_1)\}\,\mathcal{F}_1 \exists \mathcal{G}_1 \tag{5.10}$$

Between the two strategies, the following was selected:

$$D_1 \rightarrow \mathcal{F}_1 \exists \mathcal{G}_1 \tag{5.11}$$

$$D_4 \rightarrow \mathcal{F}_4 \exists \mathcal{G}_4 \tag{5.12}$$

The xenon oscillation problem is defined through SIM operators where subscripts 1, 2, 3 correspond to Eqs. (4.7, 4.8, 4.9).

$$\mathcal{F}_1\,\mu_{13}\,\mathcal{F}_3 \qquad \mathcal{F}_3\,\exists\,\mathcal{G}_3 \qquad D_1 \rightarrow \mathcal{F}_1$$
$$\mathcal{F}_2\,\bar{\mu}_{21}\,\mathcal{F}_1 \qquad\qquad\qquad D_2 \rightarrow \mathcal{F}_2$$
$$\mathcal{F}_2\,\mu_{23}\,\mathcal{F}_3$$

Since the xenon oscillation control is a regulator problem rather than a trajectory following problem, the demands D_1, D_2 represent initial conditions. This allows a cascade solution given by

$$D_2 \rightarrow \mathcal{F}_2 \ni \mathcal{G}_2 = \{\underbrace{(\mathcal{F}_2\,\bar{\mu}_{21}\,\mathcal{F}_1) \ni \mathcal{G}_1}_{D_1 \rightarrow \mathcal{F}_1 \ni \mathcal{G}_1}\,(\mathcal{F}_1\,\mu_{13}\,\mathcal{F}_3)\}\mathcal{F}_3\,\exists\,\mathcal{G}_3 \tag{5.13}$$

Obviously, the startup problem of the EBR-II and the benchmark problem given above have similar SIM solutions provided the subscripts are appropriately selected.

5.3 Fuzzy Control and Inverse Dynamics

It is important to investigate the relationship between the model-reference and rule-based control strategies. One of the similarities between these approaches is the use of process related knowledge within the control law, whereas in conventional analog control systems (which are based on the classical control theory), control law is a function of errors determined by set points. In this section, the merit of inverse dynamics concept is investigated in relation to fuzzy control paradigm. The main objective is to provide a systematic approach for the rule-based (fuzzy control) strategy using the inverse dynamics concept which is a model-reference strategy.

The concept of fuzzy logic is best characterized by a linguistic variable [18] whose values are words or sentences in a synthetic language. A linguistic variable includes an adjective-like term (and its antonym), a modifier, and a connective. The modifier is a measure of intensity which is associated with a possibility distribution. This is often refered to as the *membership function* in the literature.

The fuzzy control policy is represented as a finite collection of rules of the form if $(X_1$ is $A_1^i)$ and $\cdots$ $(X_n$ is $A_n^i)$ then

$$Y^i = a_0^i + a_1^i X_1 + \cdots + a_n^i X_n \tag{5.14}$$

where A_j^i is a linguistic value of X_j in the ith rule, Y_i is the control variable, and a_n^i are adjustable parameters. The truth value of the antecedent is given as

$$W^i = A_1^i(X_1) \wedge \cdots \wedge A_n^i(X_n) \tag{5.15}$$

where A_j^i is the grade of membership of X_j^i in A_j^i. The aggregated value of control Y may be a normalized linear combination given by

$$Y = \frac{W_1 Y^1 + \cdots + W_n Y^n}{W_1 + \cdots W_n} \tag{5.16}$$

There are two distinct places in the design stated above where a heuristic approach is required. The first heuristic task is to determine the set $(X_1, \cdots X_n)$ for control Y^i in Eq. (5.14). This task determines: **which state variables should contribute to the decision of** Y^i. The second heuristic task is to determine the boundaries and the shape of membership functions given in Eq. (5.15). Depending upon the specific application, these tasks may be quite difficult for complex, nonlinear processes.

Considering the benchmark problem presented in Chapter 3, the reactivity and flow control given by Eqs. (3.18, 3.21) were found using the following inverse functions.

$$V_1 = \mathcal{G}_\infty(P_1, P_2, P_3, P_4, D_1, \lambda_j, \alpha_j) \tag{5.17}$$

$$V_4 = \mathcal{G}_\Delta(P_3, P_4, D_4, \lambda_j) \tag{5.18}$$

There are three different applications of the inverse dynamics concept to provide a systematic tool for fuzzy control design.

(1) As shown in the benchmark problem, the inverses $\mathcal{G}_\infty$ and $\mathcal{G}_\Delta$ clearly indicate the important state variables and parameters. Thus, the set

of fuzzy variables can be systematically determined. An important conclusion is that the requirement of an operational experience can be minimized for this purpose.

(2) The explicit forms of the inverses provide a preliminary foundation to create fuzzy rules. For example, it is clear from Eq. (3.17) that the reactivity V_1 should be increased if the coolant temperature P_4 gets higher than its equilibrium value. Another rule can be composed to increase the reactivity V_1 if the error between the reactor power P_1 and demand D_1 increases. The inverses above also indicate the dependence of the controls on plant parameters λ_j, α_j. This information allows plant diagnostics to be incorporated within the fuzzy control paradigm. Again, these inferences can be drawn without an operational experience.

(3) The third application includes the determination of membership boundaries and shapes. The explicit form of the inverse dynamics can be used within a parametric study. Since the inverse dynamics has an algebraic solution, it is possible to assign values to state variables and determine the control boundaries. For example, a low-level operation can be characterized by intervals (0-0.1 % for the reactor power, 600-700 degrees F for the coolant temperature, etc.) The corresponding reactivity values can be calculated from the inverse dynamics. Similarly, the behavior of control can be determined by changing the state variables in an iterative algorithm. This would yield a preliminary idea about the shape of the membership function (as a function of state variables) for each interval or universe defined by a linguistic statement.

The use of inverse dynamics in three forms stated above does not necessarily mean that the fuzzy control would imitate an RID controller. This is due to the flexibility of fuzzy rules which can include more variables, exclude unnecessary ones, and incorporate unique logic. However, the inverse dynamics can be a useful systematic tool to provide a foundation.

5.4 Artificial Motor-Learning

One of the objectives in the AI area is to study biological information systems and explore the principles such that these principles can be emulated in the engineering field to improve system operations. Artificial Neural Networks (ANNs) is such an approach [42]. The objective of this analysis is to discuss the possibility of incorporating the inverse dynamics and ANNs to create a model for motor-control/motor-learning capability of biological systems.

Although there is no direct evidence that the biological intelligence systems make use of $\mathcal{G}$, the inverse dynamics concept may constitute a basis to model the motor-control capability. Among the many different definitions of control in biology, "motor-control" is used to identify the control mechanism of moving body parts in mammals that do not strongly rely on decision making [43]. Motor-control is analogous to hard-wired control systems where the reaction time is a function of signal transmission path rather than a decision process.

One of the examples of motor control includes controlling the eye movement with respect to the position of the head. The basic anatomic circuitry for eye-head coordination in humans involves only a three-neuron arc from the inner ear to the extraocular muscles [43]. If the head is moved during the observation of a fixed object, motor control provides "locked-on-target" eye movement for a stable image on the retina. Because head movement with respect to the eye is the mirror image dynamics of eye movement with respect to the head, we can suggest that the corresponding motor control can be modeled by the inverse dynamics approach. Then a legitimate question may arise "how do we create the inverse dynamics of a complex biological system?".

It is well known that motor control skills are developed through training. Cerebellum is known to have a role in motor learning as well as in the sensory guidance of movement. Most of the recent explanations of the motor control of eye-head coordination are based on motor learning phenomena. The three-neuron arc between the inner ear and extraocular muscles is a vestibuloocular reflex (VOR) circuitry

where motor learning is believed to take place [44].

To complete the model, we can suggest that the inverse dynamics can be learned using ANNs analogous to motor-learning in biological systems. Such a model includes two cascaded neural networks. The first neural network is dedicated for mapping (learning) between the forcing function f and state vector x whereas the other is dedicated for inverse mapping, that is between x and f. The equilibrium is achieved by $-f$ within the domain of the training set. When an input vector x is applied to a fully trained network, the corresponding forcing f is known, so is the equilibrium control $-f$. Figure 5.3 shows a functionally symmetric, coupled neural networks as a model for motor-control. Similar studies were performed in the area of robotics [45] where neural networks are trained to learn the inverse kinematics property for control purposes.

The merit of modeling motor-learning in application to engineering systems is yet to be investigated. However, a few comments may be made at this stage. This approach offers the capability of self-control through on-line learning without the need for an off-line control design procedure. It may be considered as an extended version of adaptive control where the system derives its own control law at different situations rather than adapting time-varying parameters. Obviously, the implementation of artificial motor-learning in engineering systems heavily depends on the speed and convergence characteristics of learning algorithms.

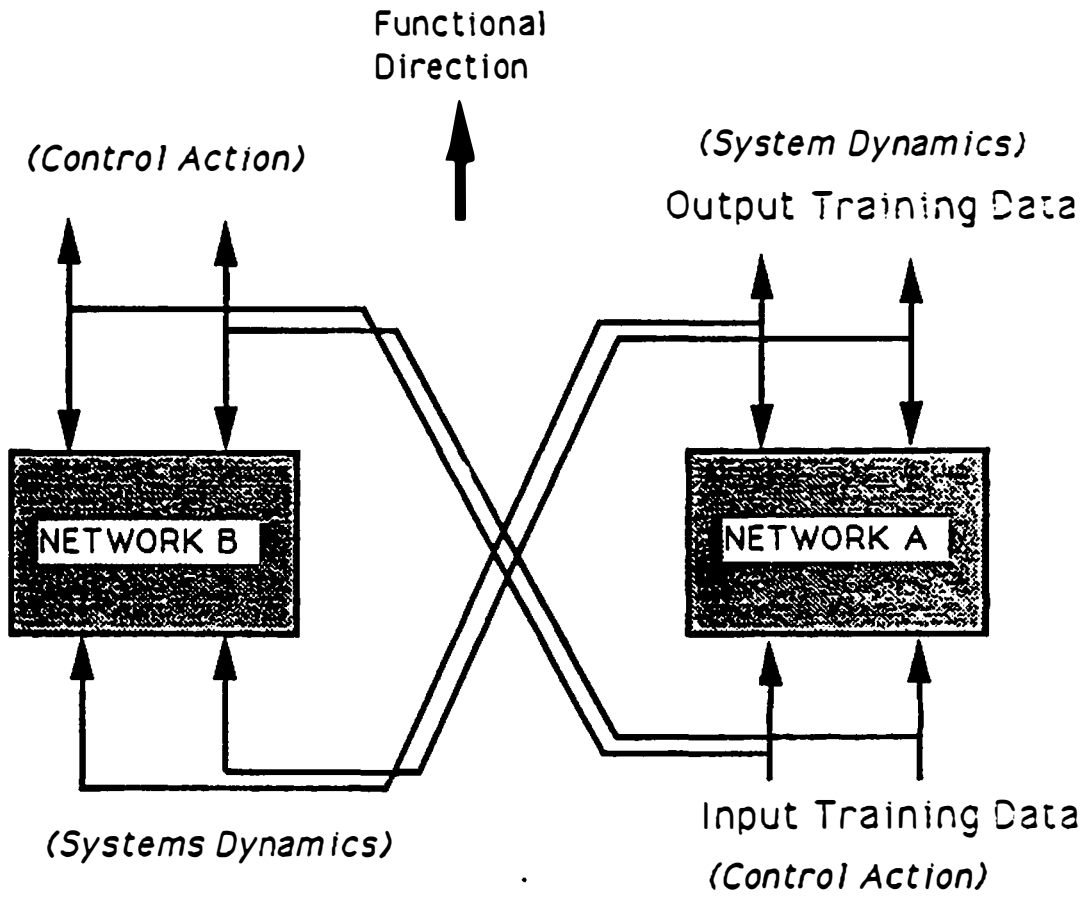

Figure 5.3: Functionally symmetric neural networks for modeling motor-control phenomena of biological systems. Model is based on the inverse dynamics approach. Network (A) learns the dynamics of the body through routine movements whereas network (B) learns the inverse dynamics for the purpose of control

Chapter 6

Concluding Remarks

The emergence of microprocessor technology has offered new possibilities in the area of control. Traditional analog systems are being replaced by their digital counterparts in many recent industrial applications. Because on-line computations are possible with the new technology, a number of advanced control algorithms has found feasible grounds for implementation. In addition, the recent computer simulation capabilities have improved our understanding of the gap between theory and practice. As a result, there is a considerable amount of effort to renovate previous theoretical accomplishments and derive new theories such that they can be digitally applied to actual systems within a reasonable CPU requirement. The main objective of this work was to use the oppurtunity offered by digital technology, to develop a robust nonlinear control method without relying on number crunching algorithms. This section includes a list of accomplishments in theory and application, most of which may be considered as the direct evidence for improvement in complex systems operations. Nevertheless, the specific designs presented here require further testing before application to actual systems. This is because computer simulations yield a limited capability to anticipate what type of problems may arise during actual implementation.

6.1 Accomplishments

Theoretical derivations and applications are summarized in this section.

1. The reconstruction problem defined in the mathematics literature was adopted to create an inverse dynamics paradigm for the purpose of trajectory following control.

2. The closed-form nonlinear control law was stated. Formulation was extended to include adaptive control features. The auxilary states method was outlined that makes the multi-input control option possible. A set of design procedures was presented.

3. The existence of inverse solutions and robustness against inexact inverses were investigated. Existence is guaranteed within a limited dynamic range and is based on the implicit function theorem. The stability characteristics in case of inexact inverses were illustrated by considering an N*th* order linear system.

4. The RID control was compared with the LQR method. It was shown that the LQR design for the first-order systems yields a similar analytical solution to that of the RID paradigm. It was verified that optimal control in the form of LQR utilizes an inverse dynamics component which is independent of the cost adjustments.

5. An exhaustive robustness testing was performed in a simulated environment using a benchmark problem. The definition of the benchmark control problem included a nonlinear model of a compact nuclear reactor core with two control variables: rod reactivity and coolant flow. The tests consisted of modeling errors, unknown dynamics, time-delay, and actuator constraints. Robustness tests showed that the RID controller yields stable performance even for extreme cases such as 200 % modeling errors and uncertainties. Same tests were applied to the Lagrangian derivation of optimal control (LDOC). The simulation results indicate that the RID and LDOC methods produce almost identical results.

6. The RID control was applied to specific nuclear reactor problems: Xenon oscillation in PWRs, feedwater control in PWRs, and automatic startup at EBR-II. The simulation results showed that the RID control significantly improves reactor operations and has a potential to increase plant availability.

7. The possibility of incorporating Artificial Intelligence methods was investigated. A systematic strategy design procedure was developed for the RID control. Stable-inverse-maps (SIM) technique allows a topological representation of all possible strategies for a given system. An expert system environment is appropriate to produce SIM given the state-space representation, and select the best strategy. A model for self-learning control system is proposed. The model is developed using artificial neural networks, analogous to the motor-learning in biological systems.

6.2 Comparison with Similar Methods

Fuzzy control and the RID control paradigms have some similarities because they both depend on process related information. This similarity also holds between other rule-based and model-reference techniques. The RID Control method requires the state-space representation of dynamics systems, whereas fuzzy control is more flexible, and does not require any specific format. Regardless of the simplicity of the system under consideration, a unique inverse solution may not exist. Since the fuzzy control does not rely on such existence, the correponding fuzzy rules may be available through pure heuristic approach. On the other hand, the development of membership functions in fuzzy control is not based on a systematic method. For example, the xenon oscillation in PWRs shows a complicated nonlinear behavior. Even the most experienced plant operator may fail to control XIPO. Thus, representing operator's expertise in the form of fuzzy rules will not resolve this control problem. The inverse dynamics concept serves a great deal of purpose in such cases by explicitly providing the necessary dynamic information which is ambiguos to human judgement.

The inverse dynamics component of the RID control paradigm functions in a similar way to that of the Lyapunov function. One of the conclusions of the Lyapunov's stability theorem states that if control tends to yield a negative gradient of the Lyapunov function then the closed-loop system is asymptotically stable. The problem with this approach is to find an appropriate Lyapunov function for a given process. Theoretically, the Lyapunov function defines the minimum energy states of a given system. On the other hand, the inverse dynamics is a function which continuously defines the dynamic equilibrium of the closed-loop system. Because the stable equilibrium points represent a minimum energy path, the inverse dynamics can be viewed as a special form of the Lyapunov function.

Comparing the RID control with the inverse modeling adaptive technique of Widrow [17], several important differences are noticed. Instead of the open-loop cancellation by inverse modeling, the RID control synthesis with a feedback arrangement yields robust and stable performance. One important consequence is that the delay time between the trajectory and plant improves the stability when it is decreased. This is contrary to Widrow's method. The RID paradigm yields a nonlinear algebraic control law, thus the inverse cancellation is not based on an inverse model. This eliminates the stability problems in case of non-minimum systems.

6.3 Advantages

The following are some of the advantages of the RID control technique in application to large-scale complex systems. The advantages are distinguished as compared to traditional methods.

1. Through the simulation studies presented in Chapters 3 and 4, it is found that the RID control paradigm offers a high degree of flexibility in tuning. With other standard methods, the tuning problem has a greater level of difficulty. The optimal control allows adjustment of costs by tuning. However, the tuning task may become difficult in

application to complex systems when costs are ambiguous.

2. The RID control performance is found to be impressively robust against uncertainties of the plant. Modeling errors (inexact inverses), unknown (unmodeled) dynamics, measurement time-delay, and actuator constraints do not deteriorate the closed-loop performance unless these effects are unreasonably large.

3. The RID control law development requires only the state-space representation of a given system. Therefore, the control law is relatively user-friendly. Some standard criteria used in other control techniques (cost function, Hamiltonian, Lagrangian density, desired pole locations, minimum distance, phase/gain margins) are not required but can be incorporated.

4. Using a set of available transient data, the inverse dynamics component of the RID control law can be validated off-line during the design stage. Similar to validating dynamic models for signal validation, this capability is a distinct advantage for safety purposes.

5. The RID control has a solid feedback structure. There are no other possibilities such as cascade, feedforward or open-loop arrangements which simplifies the design procedure. If all the state variables used in the RID control law are available as measurements, analog technology is applicable.

6. The RID control law is an algebraic equation. Thus, the control is not generated by a complex iterative algorithm. This significantly eliminates the real time problems. In case of incorporating an on-line model for state estimations, real-time problems may arise. However, because the RID control is highly robust against modeling errors, on-line models can be simplified and reduced.

6.4 Limitations

Although computer simulations indicate the high performance characteristics of the RID control method, a number of limitations have been addressed.

1. Inverse solutions may be ambiguous or may not exist for certain types of systems. Although the implicit function theorem yields linear solutions, a nonlinear RID controller may not be feasible for every system. This is a distinct limitation of this approach, since none of the nonlinear methods of the literature imposes such a restriction. However, nonexistence of inverses in actual systems is very rare.

2. The RID control law is strongly dedicated to the system it is designed for. An RID controller may not be implemented in two similar systems without major differences. A similar limitation holds for fuzzy control and MRAC methods.

3. The design of a RID controller requires extensive knowledge of the open-loop system. Since the RID control receives a considerable amount of heuristic input, its performance depends upon the experience of the designer. Between the two designers, the same control problem may be formulated differently. Although this seems like a freedom rather than a limitation, the lack of consistent modeling principles may be viewed as a negative factor. Except the conventional analog control systems, this limitation holds for most of the advanced control methods.

4. Controling large-scale complex systems is an economical problem as well as a technical one. The cost requirement of the RID control algorithm strictly depends on the system specifics and task requirement. In some cases, the RID control law may require an excessive number of system parameters (many auxiliary states) to be known or estimated. Thus, the application of the RID control will make sense only if the required complexity and cost results in a higher return. The cost-benefit

issue of the RID paradigm is a limitation compared with the simple conventional control techniques. Note that the same limitation holds for the MRAC and optimal control methods.

5. Some RID applications may require an on-line model for state estimations. Similar to the MRAC methods of the literature, the implementation of the RID control will suffer from long sampling intervals of the measurements. When a process undergoes a fast transient, long sampling interval may cause a large phase difference between the plant and model which may result in stability problems in the on-line model.

6. All the set-point change requirements of a given problem must be represented by continuous trajectories. Large step changes in the reference signal may deteriorate the closed-loop performance.

6.5 Recommendations for Future Research

This dissertation has introduced a new approach which is open to further analysis in theory and practice. The potential areas for future research are outlined.

1. The significance of the inverse dynamics is yet to be analyzed in a broader sense. It is shown here that the optimal control for the first-order systems (LQR solution) has a distinct inverse dynamics component in the control law. It will be an interesting task to investigate if other control methods contain an inverse dynamics component. This will help clarify whether the inverse dynamics is a universal criterion or a particular approach.

2. The difference between the optimal control and RID control paradigms is not fully established in this work because of the extreme similarities in the simulation results. It is important to illustrate analytically as to what extent the RID control yields optimal solutions.

3. Although the robustness test against measurement time delays have resulted satisfactory performance, a discrete-domain analysis would be useful. Because the RID control law is algebraic, numerical solutions will not be affected by large sampling intervals. However, the on-line model estimations if used, can be deteriorated.

4. During any transient, the inverse dynamics component of the RID control law always points out the equilibrium point. This may be closely related to the properties of the Lyapunov function. A systematic analysis may yield interesting and useful results.

5. Extending applications to different nuclear reactor systems would certainly improve our understanding of the inverse dynamics approach and its feasibility. Future research must focus on more global control tasks such as satisfying grid-power demand in multi-modular reactors.

6. The systematic solution of the strategy problem presented here represents a challenging topic for scientists in the AI area. The strategy solutions using the SIM method is a typical expert systems problem and is worth applying to complex systems with high degrees of freedom.

7. The development of tools for a systematic fuzzy control design may be possible using the inverse dynamics concept. The general form of the RID control, presented in Chapter 2, can be used for this purpose. Such a study should focus on determining the most important set of fuzzy variables, fuzzy rule production, and the characteristics of membership functions.

BIBLIOGRAPHY

Bibliography

[1] V. V. Chalam, *Adaptive Control Systems.* New York: Dekker, 1987.

[2] J. J. Downs and J. E. Doss, "Present Status and Future Needs- A View from North American Industry,," *4th International Conference on Chemical Process Control*, South Padre Island, Texas, February, 17-22 1984.

[3] H. Nakakura and A. Ishiguro, "Automatic Load Follow Control System for PWR Plants,," *Nuclear Safety*, vol. 29, pp. 451–462, October 1988.

[4] R. J. Carter and R. E. Uhrig, *Human Factors Issues with Advanced Instrumentation and Controls Technologies in Nuclear Plants,*. ORNL/TM-11319: NUREG/CR-5439, June 1990.

[5] J. L. Tyran, D. Colin, and G. Zwingelstein, "An Automatic Boration-Dilution System with Optimal Control Strategy,," *Proc. 6th Power Plant Dynamics, Control, and Testing Symposium, Knoxville, Tennessee*, vol. 2, pp. 53.01–53.09, April 1986.

[6] A. R. Foster and R. L. Wright, *Basic Nuclear Engineering.* Massachussets: Allyn and Bacon, 1983.

[7] W. C. Jordan *et al.*, "Preliminary Design Concept for Axial Xenon Oscillation Modeling and Control,," *Report written for ANS Student Design Competition, Graduate Entry*, July 1986.

[8] R. C. Berkan, B. R. Upadhyaya, and R. A. Kisner, "Reconstructive Inverse Dynamics in Feedwater Control,," *Trans., International ANS Mtng.*, vol. 61, pp. 920–925, July 1990.

[9] J. H. Rust, *Nuclear Power Plant Engineering.* Buchanan, GA: Haralson Publishing Company, 1979.

[10] R. A. Kisner and G. V. S. Raju, *Automating Large-Scale Power Plant Systems: A Perspective and Philosophy,.* Oak Ridge National Laboratory: ORNL/TM-9500, 1984.

[11] B. Hoffman, *Regularization for Applied Inverse and Ill-posed Problems,.* Teubner-Verlag, 1986.

[12] J. Baumeister, *Stable Solutions of Inverse Problems.* Braunschweig: Friedr. Vieweg & Sohn Verlagsgesellschaft mbH, 1987.

[13] C. W. Wampler, "Inverse Kinematic Functions for Redundant Spherical Wrists,," *Trans. Robotics and Automation IEEE*, vol. 5. pp. 106–111, February 1989.

[14] P. D. Krutko, N. A. Lakota, and E. P. Popov, "The Concept of Inverse Problems in Dynamics and Synthesis of Algorithms to Control the Motion of Manipulator Robots,," *Proc. IFAC 9th Triennial World Congress.* vol. 1. pp. 457–462, June 1984.

[15] B. C. Kuo, *Automatic Control Systems.* Englewood Cliffs, N.J.: Prentice-Hall, 1982.

[16] B. Friedland, *Control System Design.* New York: McGraw-Hill Book Company, 1986.

[17] B. Widrow and J. M. McCool, "Adaptive Control by Inverse Modeling," *Proc. ASILOMAR Conf.*, vol. 2, May 1978.

[18] L. A. Zadeh, "Fuzzy Algorithms," *Information and Control*, vol. 12, pp. 94–102, May 1968.

[19] J. C. Hsu and A. U. Meyer, *Modern Control Principles and Applications.* New York: McGraw-Hill Book Company, 1968.

[20] R. B. Perez, *Lagrangian Derivation of Optimum Control.* American Nuclear Society Transactions: to appear.

[21] W. H. Fleming, *Functions of Several Variables.* Massachusetts: Addison-Wesley Publishing Company, 1965.

[22] R. S. Varga, *Matrix Iterative Analysis.* New Jersey: Prentice-Hall, 1971.

[23] R. E. Kalman, "On the General Theory of Control Systems," *Proc. First International Congress, IFAC*, vol. 1, pp. 481–492, 1960.

[24] C. March-Leuba and R. B. Perez, "Optimal Control Theory of Load-Following and Parameter Tracking of Nonlinear Systems: An Application of Pontryagin's Maximum Principle to Reactor Dynamics,," *ORNL/TM*, vol. 10662, May 1987.

[25] R. E. Kalman, "When Is a Linear Control System Optimal," *Trans. ASME*, vol. 86D, pp. 51–60, 1964.

[26] H. Kwakernaak and R. Sivan, *Linear Optimal Control Systems.* New York: Wiley-Interscience, 1972.

[27] R. A. Kisner, R. C. Berkan, and B. R. Upadhyaya, "Performance Characteristics For Advanced Control Systems,," *Proc. 7th Power Plant Dynamics, Control and Testing Symposium, Knoxville, Tennessee*, vol. 1, pp. 4.01–4.13, May 1989.

[28] M. Abu-Shehadeh, *A Dynamic Model for the Advanced Neutron Source (ANS) Reactor* . University of Tennessee: Ph.D. Dissertation, 1989.

[29] R. C. Berkan, B. R. Upadhyaya, and R. L. Bywater, *Advanced Automation Concepts Applied to EBR-II Startup,*. Febuary: ORNL/TM-11716, 1991.

[30] P. J. Sipush, "Load Follow Demonstrations Employing Constant Axial Offset Power Distribution Control Procedures,," *Nuclear Technology*, vol. 31, pp. 35–48, October 1976.

[31] J. Karpinnen, "Spatial Reactor Control Methods,," *Nuclear Science and Engineering*, vol. 64, pp. 657–672, May 1977.

[32] W. Aleite, "The Power Distribution Controls of Biblis A Nuclear Power Station and Future Developments with Process Computers,," *Proc. IAEA NPPCI Specialists Mtg. Spatial Control Problems, Studsvik, Sweden*, vol. 75, p. 3125, October 1975.

[33] R. J. Onega and R. A. Kisner, "An Axial Xenon Oscillation Model," *Annals of Nuclear Energy*, vol. 5, pp. 13–19, Pergamon Press 1978.

[34] R. J. Onega and R. A. Kisner, "Parameter Identification For Spatial Xenon Transient Analysis and Control," *Annals of Nuclear Energy*, vol. 6, pp. 369–374, Pergamon Press 1979.

[35] A. M. Christie and C. G. Poncelet, "On the Control of Spatial Xenon Oscillations,," *Nuclear Science and Engineering*, vol. 51, p. 21, May 1973.

[36] R. P. Corcuera, C. E. Ford, S. J. Ball, and R. B. Perez, *Designing an AI-Environment Prototype for the Automatic Startup of EBR-II.* January: ORNL/TM-11296, 1990.

[37] *EBR-II System Description Manual.* ANL-East, Chicago, IL, 1985.

[38] E. E. Feldman, "Personal Communication, ANL-West," 1989.

[39] R. C. Berkan, B. R. Upadhyaya, and R. A. Kisner, "Low-Order Dynamic Modeling of the Experimental Breeder Reactor-II,," *ORNL/TM*, vol. 11161, July 1990.

[40] R. C. Berkan, B. R. Upadhyaya, and R. L. Bywater, "Advanced Automation Concepts Applied to EBR-II Startup Operation,," *UTNE/MMES/BRU90*, vol. 1, December 1990.

[41] MATRIXx, *User Guide Vax Work Station Version 3.1.* California: Integrated Systems, Inc., 1989.

[42] E. Eryurek, *Development and Application of Multi-layer Neural Networks for Estimation of Power Plant Variables.* Master's thesis, The University of Tennessee, 1991.

[43] R. F. Mark and R. W. Sperry, "Bimanual Coordination in Monkeys," *Exp. Neurol.*, vol. 21, pp. 92–104, 1968.

[44] R. W. Sperry, "Neural Basis of the Spontaneous Optokinetic Responses Produced by Visual Inversion," *J. Comp. Physiol.*, vol. 43. pp. 482–9, 1950.

[45] A. Guez and Z. Ahmad, "Solution to the Inverse Kinematics Problem in Robotics by Neural Networks," *ICNN 88*, vol. 27, pp. 221–229, March 1988.

APPENDIXES

Appendix A

ACSL Code of the Benchmark Problem

The following pages include the computer code of the benchmark problem presented in Chap 3. It is written using the Advanced Computer Simulation Language (ACSL). The code contains a compact nuclear core model, and two controllers (RID, LDOC) described in Chap 3. Parameters *FLAGxx* control the simulation (1 for discrepancy, 0 for perfect match) corresponding to the 8 parameters of the model. There are different codes for each test shown in Table 3.2. More information is provided within the command lines in each program.

*** PROGRAM LISTING ***

```
PROGRAM  PWR Model Using 4 state variables.
' LAGRANGIAN DERIVATION OF OPTIMAL CONTROL '
' AND ADAPTIVE RID CONTROL COMPARED '

          INITIAL

'++++++++++++++++++++++++++++++++++++++++'
'PARAMETERS '
'-----------'
     CONSTANT LSP0=0.1218,LDP0=0.0686,LRP0=115.87965
     CONSTANT BETA=0.00721,ALFF=1.E-5
     CONSTANT AH=2.7559E5,CC=4.1845,MC=2.4163E4
     CONSTANT TH=.0002,P0=2.8E8,CP=.565,MP=0.6785E4
     CONSTANT TIN=49.,ALFC=1.1E-4,WDOT=1.4E6

'RUN CONTROL'
'-----------'
     CONSTANT TMAX=200.

     CONSTANT FLAG1=1,FLAG11=1,FLAG2=1,FLAG22=1
     CONSTANT FLAG3=1,FLAG33=1,FLAG4=1,FLAG44=1
     CONSTANT FLAG5=1,FLAG55=1,FLAG6=1,FLAG66=1
     CONSTANT FLAG7=1,FLAG77=1,FLAG8=1,FLAG88=1

     CONSTANT FLAGD=1.

'PLANT DEVIATIONS'
'----------------'
     CONSTANT GOTIME=10,DVRAMP=0.01,FREQ=5.0,DVMAX=1
     CONSTANT BR1=10,BR2=30,BR3=50,BR4=70

'DEMANDS'
'-------'
     CONSTANT T1=100.,DECAY1=0.08,DECAY2=0.05

'(PERD1= percentage increase in demand 1)'
'(PERD12=AMOUNT of decrease in demand 1 after t=TAU)'
'(PERD4=percentage incerase in demand 4)'

     CONSTANT PERD1=0.25,PERD12=0.2,PERD4=0.2

'++++++++++++++++++++++++++++++++++++++++++++++++++++++++++
```

```
++'
'PARAMETERS OF LAGRANGIAN DYNAMICS '

     Z1B0=0.
     Z4B0=0.
     Z1A0=0.
     Z4A0=0.
     PC10=0.
     PC40=0.

'LDOP TUNING PARAMETERS'
'----------------------'

     CONSTANT K1I=-0.5
     CONSTANT K4I=-4.2
     CONSTANT K1P=0.5
     CONSTANT K4P=0.1
     CONSTANT R1P=4.0
     CONSTANT R4P=0.1
     CONSTANT P1I=-0.5
     CONSTANT P4I=-0.04

'RID TUNING PARAMETERS'
'----------------------'

     CONSTANT  K1=1000.
     CONSTANT  K4=1000.
     CONSTANT KG1=1000.
     CONSTANT KG3=1000.
     CONSTANT KG4=1000.

'++++++++++++++++++++++++++++++++++++'

     CINTERVAL CINT=1.
     IALG=2

     HP=1./(.0649+44.44*TH)
     D40=1.97542
     D10=1.
     DMAX1=D10*(1+PERD1)
     DMAX4=D40*(1+PERD4)
```

```
'+++++++++++++++++++++++++++++++++++++++++'
' STATE VARIABLES INITIAL VALUES'

     N10=1.
     N20=1.
     N30=3.50539
     N40=1.97542
     P10=1.
     P20=1.
     P30=3.50539
     P40=1.97542
     M10=1.
     M40=1.97542
     H10=1.
     H20=1.
     H30=3.50539
     H40=1.97542

' ------------------'
     LSM=LSP0
     LDM=LDP0
     LPP0=P0/(CP*MP*TIN)
     LPM=LPP0

     LFP0=AH*HP/(CP*MP)
     LFM=LFP0

     AFP0=ALFF*TIN/(BETA*LSP)
     AFM=AFP0

     LCP0=AH*HP/(CC*MC)
     LCM=LCP0

     LRM=LRP0

     ACP0=ALFC*TIN/(BETA*LSP)
     ACM=ACP0

     CONSTANT Y10=0.0
     CONSTANT Y40=0.5

     U10=Y10
```

```
      U40=Y40

      G10=-(U10-1)*M10/LSP0
      G40=U40*LRP0*(M40-1)

      F10=M10/LSP0
      F40=LRP0*(M40-1)


      END

'++++++++++++++++++++++++++++++++++++++++'

      DYNAMIC
      DERIVATIVES

'++++++++++++++++++++++++++++++++++++++++'
'TRAJECTORIES'
'------------'

      PROCEDURAL(TAU,GOD=T,T1)
      TAU=0
      GOD=0
      IF(T.GE.T1) TAU=T-T1
      IF(T.GE.T1) GOD=1
      END


'MISMATCH BETWEEN PLANT AND MODEL'
'--------------------------------'

PROCEDURAL(GO,OS1,OS2,OS3,DVA,DVE=T,GOTIME,DVMAX,DVRAMP
,FREQ)
      DVA=0
      DVE=0
      OS1=0
      OS2=0
      OS3=0
      GO=0
      IF(T.GE.GOTIME) GO=1
      DVA=DVA+DVRAMP*T
      DVE=DVE-DVRAMP*2*T
```

```
      OS1=OS1+SIN(FREQ*T)
      OS2=OS2+COS(FREQ*0.2*T)
      OS3=OS3+COS(FREQ*3.7*T)
      END

'LOGIC CONTROL PARAMETERS'
'------------------------'
      LSP=LSP0+(FLAG1*DVA+FLAG11*OS1)*LSP0/10*GO
      ACP=ACP0+(FLAG2*DVE+FLAG22*OS2)*ACP0/10*GO
      AFP=AFP0+(FLAG3*DVE+FLAG33*OS3)*AFP0/10*GO
      LDP=LDP0+(FLAG4*DVA+FLAG44*OS1)*LDP0/10*GO
      LPP=LPP0+(FLAG5*DVA+FLAG55*OS2)*LPP0/10*GO
      LCP=LCP0+(FLAG6*DVE+FLAG66*OS3)*LCP0/10*GO
      LFP=LFP0+(FLAG7*DVA+FLAG77*OS2)*LFP0/10*GO
      LRP=LRP0+(FLAG8*DVA+FLAG88*OS3)*LRP0/10*GO
'++++++++++++++++++++++++++++++++++++++++'
' PLANT DRIVEN BY LDOP CONTROL'


DP1=(Y1-1.)*P1/LSP+P2/LSP-(ACP*(P4-P40)+AFP*(P3-P30))*P1
      DP2=LDP*(P1-P2)
      DP3=LPP*P1-LFP*(P3-P4)+FLAGD*DISTP
      DP4=LCP*(P3-P4)-Y4*LRP*(P4-1.)

'++++++++++++++++++++++++++++++++++++++++'
'PLANT DRIVEN BY RID CONTROL'


DH1=(V1-1.)*H1/LSP+H2/LSP-(ACP*(H4-H40)+AFP*(H3-H30))*H1
      DH2=LDP*(H1-H2)
      DH3=LPP*H1-LFP*(H3-H4)+FLAGD*DISTH
      DH4=LCP*(H3-H4)-V4*LRP*(H4-1.)

'UNKNOWN DYNAMICS '
'-----------------'
      DISTP=GO*COS(P4-P3)*SIN(P1)*OS2
      DISTH=GO*COS(H4-H3)*SIN(H1)*OS2

'++++++++++++++++++++++++++++++++++++++++'
' MODEL FOR RID CONTROL '
```

```
DN1=(V1-1.)*N1/LSM+N2/LSM-(ACM*(N4-N40)+AFM*(N3-N30))*N
1+RG1
      DN2=LDM*(N1-N2)
      DN3=LPM*N1-LFM*(N3-N4)+RG3
      DN4=LCM*(N3-N4)-V4*LRM*(N4-1.)

'++++++++++++++++++++++++++++++++++++++'
' MODEL FOR LAGRANGIAN CONTROL '

      DM1=C1*F1+G1
      DM4=C4*F4+G4

      C1=U1-1
      C4=-U4

      F1=M1/LSM
      F4=LRM*(M4-1)

'++++++++++++++++++++++++++++++++'
' DEMAND '

      D1=DMAX1+(D10-DMAX1)*EXP(-DECAY1*T)-EK
      EK=GOD*(PERD12-PERD12*EXP(-DECAY2*TAU))
      D4=DMAX4+(D40-DMAX4)*EXP(-DECAY1*T)

'++++++++++++++++++++++++++++++'
'RID CONTROL'

      V1=1+LSM*K1*(D1-H1)/H1-N2/H1+EK1
      EK1=LSM*(ACM*(H4-H40)+AFM*(N3-N30))


V4=LCM*(N3-H4)/((H4-1.)*LRM)-K4*(D4-H4)/((H4-1.)*LRM)

      RG1=KG1*(H1-N1)-(V1-1.)*N1/LSM-N2/LSM+EKG1
      EKG1=(ACM*(N4-N40)+AFM*(N3-N30))*N1

      N3S=LRM*V4*(N4-1.)/LCM+KG4*(H4-N4)/LCM+N4
      RG3=KG3*(N3S-N3)-LPM*N1+LFM*(N3-N4)

'++++++++++++++++++++++++++++++++++++++++'
```

```
'LAGRANGIAN CONTROL '

     Y1=U1
     Y4=U4

     U1=R1A*U10+R1B-R1C*C1T
     U4=R4A*U40+R4C*C4T

     R1A=(1+ALOG(F10))/(1+ALOG(F1))
     R1B=ALOG(F1/F10)/(1+ALOG(F1))
     R1C=F1/(1+ALOG(F1))
     R4A=(1+ALOG(F40))/(1+ALOG(F4))
     R4C=F4/(1+ALOG(F4))

     C1T=PC10-P1I*Z1B+R1P*(P1-D1)
     C4T=PC40-P4I*Z4B+R4P*(P4-D4)
     DZ1B=P1-D1
     DZ4B=P4-D4

'++++++++++++++++++++++++++++++++'
'UNKNOWN DYNAMICS'

     G1=G10+F10-F1-B1T
     G4=G40+F40-F4-B4T

     B1T=-K1I*Z1A+K1P*(M1-P1)
     B4T=-K4I*Z4A+K4I*(M4-P4)

     DZ1A=M1-P1
     DZ4A=M4-P4

'++++++++++++++++++++++++++++++++++++++++'
     P1=INTVC(DP1,P10)
     P2=INTVC(DP2,P20)
     P3=INTVC(DP3,P30)
     P4=INTVC(DP4,P40)
     N1=INTVC(DN1,N10)
     N2=INTVC(DN2,N20)
     N3=INTVC(DN3,N30)
     N4=INTVC(DN4,N40)
     H1=INTVC(DH1,H10)
     H2=INTVC(DH2,H20)
```

```
      H3=INTVC(DH3,H30)
      H4=INTVC(DH4,H40)

      Z1B=INTVC(DZ1B,Z1B0)
      Z4B=INTVC(DZ4B,Z4B0)
      Z1A=INTVC(DZ1A,Z1A0)
      Z4A=INTVC(DZ4A,Z4A0)
      M1=INTVC(DM1,M10)
      M4=INTVC(DM4,M40)

'+++++++++++++++++++++++++++++++++++++++'

      END
      TERMT(T.GE.TMAX)
      END
END
```

```
PROGRAM  PWR Model Using 4 state variables.
' LAGRANGIAN DERIVATION OF OPTIMAL CONTROL '
' AND ADAPTIVE RID CONTROL COMPARED '


'++++++++++++++++++++++++++++++++++++++++'
'++++++++++++++++++++++++++++++++++++++++'
' CASE: Disturbance rejection using      '
'       Limited Actuators                '
'++++++++++++++++++++++++++++++++++++++++'
'++++++++++++++++++++++++++++++++++++++++'

     INITIAL

'++++++++++++++++++++++++++++++++++++++++'
'PARAMETERS '
'-----------'
CONSTANT LSP0=0.1218,LDP0=0.0686,LRP0=115.87965
CONSTANT BETA=0.00721,ALFF=1.E-5
CONSTANT AH=2.7559E5,CC=4.1845,MC=2.4163E4
CONSTANT TH=.0002,P0=2.8E8,CP=.565,MP=0.6785E4
CONSTANT TIN=49.,ALFC=1.1E-4,WDOT=1.4E6

'RUN CONTROL'
'-----------'
CONSTANT TMAX=60.

CONSTANT FLAG1=0,FLAG11=0,FLAG2=0,FLAG22=0
CONSTANT FLAG3=0,FLAG33=0,FLAG4=0,FLAG44=0
CONSTANT FLAG5=0,FLAG55=0,FLAG6=0,FLAG66=0
CONSTANT FLAG7=0,FLAG77=0,FLAG8=0,FLAG88=0
CONSTANT DISCON=1.

'PLANT DEVIATIONS'
'----------------'
CONSTANT GOTIME=10,DVRAMP=0.01,FREQ=5.0,DVMAX=1
CONSTANT BR1=10,BR2=30,BR3=50,BR4=70

'DEMANDS'
'-------'
```

```
      CONSTANT T1=100.,DECAY1=0.08,DECAY2=0.05

      '(PERD1= percentage increase in demand 1)'
      '(PERD12=AMOUNT of decrease in demand 1 after t=TAU)'
      '(PERD4=percentage incerase in demand 4)'

      CONSTANT PERD1=0.25,PERD12=0.2,PERD4=0.2


'++++++++++++++++++++++++++++++++++++++++++++++++++++++++++++++++'
      'PARAMETERS OF LAGRANGIAN DYNAMICS '

      Z1B0=0.
      Z4B0=0.
      Z1A0=0.
      Z4A0=0.
      PC10=0.
      PC40=0.

      'LDOP TUNING PARAMETERS'
      '----------------------'

      CONSTANT K1I=-0.5
      CONSTANT K4I=-4.2
      CONSTANT K1P=0.5
      CONSTANT K4P=0.1
      CONSTANT R1P=4.0
      CONSTANT R4P=0.1
      CONSTANT P1I=-0.5
      CONSTANT P4I=-0.04

      'RID TUNING PARAMETERS'
      '---------------------'

      CONSTANT  K1=1000.
      CONSTANT  K4=1000.
      CONSTANT KG1=1000.
      CONSTANT KG3=1000.
      CONSTANT KG4=1000.

      '++++++++++++++++++++++++++++++++++++'
```

```
CINTERVAL CINT=1.
IALG=2

HP=1./(.0649+44.44*TH)
D40=1.97542
D10=1.
DMAX1=D10*(1+PERD1)
DMAX4=D40*(1+PERD4)

'++++++++++++++++++++++++++++++++++++++++'
' STATE VARIABLES INITIAL VALUES'

N10=1.
N20=1.
N30=3.50539
N40=1.97542
P10=1.
P20=1.
P30=3.50539
P40=1.97542
M10=1.
M40=1.97542
H10=1.
H20=1.
H30=3.50539
H40=1.97542

'------------------'
LSM=LSP0
LDM=LDP0
LPP0=P0/(CP*MP*TIN)
LPM=LPP0

LFP0=AH*HP/(CP*MP)
LFM=LFP0

AFP0=ALFF*TIN/(BETA*LSP)
AFM=AFP0

LCP0=AH*HP/(CC*MC)
LCM=LCP0
```

```
LRM=LRP0

ACP0=ALFC*TIN/(BETA*LSP)
ACM=ACP0

CONSTANT Y10=0.0
CONSTANT Y40=0.5

U10=Y10
U40=Y40

YY10=Y10
YY40=Y40
VV10=Y10
VV40=Y40

G10=-(U10-1)*M10/LSP0
G40=U40*LRP0*(M40-1)

F10=M10/LSP0
F40=LRP0*(M40-1)


END

'++++++++++++++++++++++++++++++++++++++++++'

DYNAMIC
DERIVATIVES

'++++++++++++++++++++++++++++++++++++++++++'
'TRAJECTORIES'
'------------'

PROCEDURAL(TAU,GOD=T,T1)
TAU=0
GOD=0
IF(T.GE.T1) TAU=T-T1
IF(T.GE.T1) GOD=1
END
```

```
      'MISMATCH BETWEEN PLANT AND MODEL'
      '--------------------------------'

PROCEDURAL(FLAGD,OS1,OS2,OS3,DVA,DVE=T,GOTIME,DVMAX,DVRAMP,F
REQ)
      DVA=0
      DVE=0
      OS1=0
      OS2=0
      OS3=0
      GO=0
      FLAGD=0
      IF(T.GE.GOTIME) FLAGD=1
      DVA=DVA+DVRAMP*T
      DVE=DVE-DVRAMP*2*T
      OS1=OS1+SIN(FREQ*T)
      OS2=OS2+COS(FREQ*0.2*T)
      OS3=OS3+COS(FREQ*3.7*T)
      END


      'LOGIC   NTROL PARAMETERS'
      '------------------------'
      LSP=LSP0+(FLAG1*DVA+FLAG11*OS1)*LSP0/10*GO
      ACP=ACP0+(FLAG2*DVE+FLAG22*OS2)*ACP0/10*GO
      AFP=AFP0+(FLAG3*DVE+FLAG33*OS3)*AFP0/10*GO
      LDP=LDP0+(FLAG4*DVA+FLAG44*OS1)*LDP0/10*GO
      LPP=LPP0+(FLAG5*DVA+FLAG55*OS2)*LPP0/10*GO
      LCP=LCP0+(FLAG6*DVE+FLAG66*OS3)*LCP0/10*GO
      LFP=LFP0+(FLAG7*DVA+FLAG77*OS2)*LFP0/10*GO
      LRP=LRP0+(FLAG8*DVA+FLAG88*OS3)*LRP0/10*GO
      '++++++++++++++++++++++++++++++++++++++'
      ' PLANT DRIVEN BY LDOP CONTROL'


DP1=(YY1-1.)*P1/LSP+P2/LSP-(ACP*(P4-P40)+AFP*(P3-P30))*P1+di
stp
      DP2=LDP*(P1-P2)
      DP3=LPP*P1-LFP*(P3-P4)
      DP4=LCP*(P3-P4)-YY4*LRP*(P4-1.)

      '++++++++++++++++++++++++++++++++++++++'
```

```
      'PLANT DRIVEN BY RID CONTROL'

DH1=(VV1-1.)*H1/LSP+H2/LSP-(ACP*(H4-H40)+AFP*(H3-H30))*H1+di
sth
      DH2=LDP*(H1-H2)
      DH3=LPP*H1-LFP*(H3-H4)
      DH4=LCP*(H3-H4)-VV4*LRP*(H4-1.)

      'UNKNOWN DYNAMICS '
      '-----------------'
      DISTH=DISCON*FLAGD
      DISTP=DISTH
      '++++++++++++++++++++++++++++++++++++++++'
      ' MODEL FOR RID CONTROL '


DN1=(VV1-1.)*N1/LSM+N2/LSM-(ACM*(N4-N40)+AFM*(N3-N30))*N1+RG1
      DN2=LDM*(N1-N2)
      DN3=LPM*N1-LFM*(N3-N4)+RG3
      DN4=LCM*(N3-N4)-VV4*LRM*(N4-1.)

      '++++++++++++++++++++++++++++++++++++++'
      ' MODEL FOR LAGRANGIAN CONTROL '

      DM1=C1*F1+G1
      DM4=C4*F4+G4

      C1=U1-1
      C4=-U4

      F1=M1/LSM
      F4=LRM*(M4-1)

      '++++++++++++++++++++++++++++++++'
      ' DEMAND '

      D1=DMAX1+(D10-DMAX1)*EXP(-DECAY1*T)-EK
      EK=GOD*(PERD12-PERD12*EXP(-DECAY2*TAU))
      D4=DMAX4+(D40-DMAX4)*EXP(-DECAY1*T)

      '++++++++++++++++++++++++++++++'
```

```
      'RID CONTROL'

      V1=1+LSM*K1*(D1-H1)/H1-N2/H1+EK1
      EK1=LSM*(ACM*(H4-H40)+AFM*(N3-N30))

      V4=LCM*(N3-H4)/((H4-1.)*LRM)-K4*(D4-H4)/((H4-1.)*LRM)

      RG1=KG1*(H1-N1)-(V1-1.)*N1/LSM-N2/LSM+EKG1
      EKG1=(ACM*(N4-N40)+AFM*(N3-N30))*N1

      N3S=LRM*V4*(N4-1.)/LCM+KG4*(H4-N4)/LCM+N4
      RG3=KG3*(N3S-N3)-LPM*N1+LFM*(N3-N4)

'CONSTRAINED CONTROL RID'
'-----------------------'

     C       O       N       S       T       A       N       T
BB1=-0.1,TB1=0.1,BB4=-0.005,TB4=0.005,KV1=100,KV4=100

      DVV1=CONR1
      CONR1=BOUND(BB1,TB1,CONS1V)
      CONS1V=KV1*(V1-VV1)

      DVV4=CONR4
      CONR4=BOUND(BB4,TB4,CONS4V)
      CONS4V=KV4*(V4-VV4)

'CONSTRAINED CONTROL LDOC'
'------------------------'


      CONSTANT KY1=100,KY4=100

      DYY1=CONY1
      CONY1=BOUND(BB1,TB1,CONS1Y)
      CONS1Y=KY1*(Y1-YY1)

      DYY4=CONY4
      CONY4=BOUND(BB4,TB4,CONS4Y)
      CONS4Y=KY4*(Y4-YY4)
```

```
'++++++++++++++++++++++++++++++++++++'
'LAGRANGIAN CONTROL '

Y1=U1
Y4=U4

U1=R1A*U10+R1B-R1C*C1T
U4=R4A*U40+R4C*C4T

R1A=(1+ALOG(F10))/(1+ALOG(F1))
R1B=ALOG(F1/F10)/(1+ALOG(F1))
R1C=F1/(1+ALOG(F1))
R4A=(1+ALOG(F40))/(1+ALOG(F4))
R4C=F4/(1+ALOG(F4))

C1T=PC10-P1I*Z1B+R1P*(P1-D1)
C4T=PC40-P4I*Z4B+R4P*(P4-D4)
DZ1B=P1-D1
DZ4B=P4-D4

'++++++++++++++++++++++++++++++++'
'UNKNOWN DYNAMICS'

G1=G10+F10-F1-B1T
G4=G40+F40-F4-B4T

B1T=-K1I*Z1A+K1P*(M1-P1)
B4T=-K4I*Z4A+K4I*(M4-P4)

DZ1A=M1-P1
DZ4A=M4-P4

'++++++++++++++++++++++++++++++++++++++++'
P1=INTVC(DP1,P10)
P2=INTVC(DP2,P20)
P3=INTVC(DP3,P30)
P4=INTVC(DP4,P40)
N1=INTVC(DN1,N10)
N2=INTVC(DN2,N20)
N3=INTVC(DN3,N30)
N4=INTVC(DN4,N40)
H1=INTVC(DH1,H10)
```

```
      H2=INTVC(DH2,H20)
      H3=INTVC(DH3,H30)
      H4=INTVC(DH4,H40)

      Z1B=INTVC(DZ1B,Z1B0)
      Z4B=INTVC(DZ4B,Z4B0)
      Z1A=INTVC(DZ1A,Z1A0)
      Z4A=INTVC(DZ4A,Z4A0)
      M1=INTVC(DM1,M10)
      M4=INTVC(DM4,M40)

      VV1=INTVC(DVV1,VV10)
      VV4=INTVC(DVV4,VV40)
      YY1=INTVC(DYY1,YY10)
      YY4=INTVC(DYY4,YY40)


      '++++++++++++++++++++++++++++++++++++++++'

      END
      TERMT(T.GE.TMAX)
      END
END
```

```
PROGRAM  PWR Model Using 4 state variables.
' LAGRANGIAN DERIVATION OF OPTIMAL CONTROL '
' AND ADAPTIVE RID CONTROL COMPARED '

'++++++++++++++++++++++++++++++++++++++++'
'++++++++++++++++++++++++++++++++++++++++'
'CASE:   Time-delay in measurements      '
'++++++++++++++++++++++++++++++++++++++++'
'++++++++++++++++++++++++++++++++++++++++'

          INITIAL

'++++++++++++++++++++++++++++++++++++++++'
'PARAMETERS '
'-----------'
     CONSTANT LSP0=0.1218,LDP0=0.0686,LRP0=115.87965
     CONSTANT BETA=0.00721,ALFF=1.E-5
     CONSTANT AH=2.7559E5,CC=4.1845,MC=2.4163E4
     CONSTANT TH=.0002,P0=2.8E8,CP=.565,MP=0.6785E4
     CONSTANT TIN=49.,ALFC=1.1E-4,WDOT=1.4E6

'RUN CONTROL'
'-----------'
     CONSTANT TMAX=200.

     CONSTANT FLAG1=0,FLAG11=0,FLAG2=0,FLAG22=0
     CONSTANT FLAG3=0,FLAG33=0,FLAG4=0,FLAG44=0
     CONSTANT FLAG5=0,FLAG55=0,FLAG6=0,FLAG66=0
     CONSTANT FLAG7=0,FLAG77=0,FLAG8=0,FLAG88=0

     CONSTANT FLAGD=0.

'PLANT DEVIATIONS'
'----------------'
     CONSTANT GOTIME=10,DVRAMP=0.01,FREQ=5.0,DVMAX=1
     CONSTANT BR1=10,BR2=30,BR3=50,BR4=70

'DEMANDS'
'-------'
     CONSTANT T1=100.,DECAY1=0.08,DECAY2=0.05

'(PERD1= percentage increase in demand 1)'
```

```
'(PERD12=AMOUNT of decrease in demand 1 after t=TAU)'
'(PERD4=percentage incerase in demand 4)'

     CONSTANT PERD1=0.25,PERD12=0.2,PERD4=0.2

'++++++++++++++++++++++++++++++++++++++++++++++++++++++++++++++'
'PARAMETERS OF LAGRANGIAN DYNAMICS '

     Z1B0=0.
     Z4B0=0.
     Z1A0=0.
     Z4A0=0.
     PC10=0.
     PC40=0.

'LDOP TUNING PARAMETERS'
'----------------------'

     CONSTANT K1I=-0.5
     CONSTANT K4I=-4.2
     CONSTANT K1P=0.5
     CONSTANT K4P=0.1
     CONSTANT R1P=4.0
     CONSTANT R4P=0.1
     CONSTANT P1I=-0.5
     CONSTANT P4I=-0.04

'RID TUNING PARAMETERS'
'---------------------'

     CONSTANT  K1=1000.
     CONSTANT  K4=1000.
     CONSTANT KG1=1000.
     CONSTANT KG3=1000.
     CONSTANT KG4=1000.

'++++++++++++++++++++++++++++++++++++++'

     CINTERVAL CINT=1.
     IALG=2

     HP=1./(.0649+44.44*TH)
```

```
      D40=1.97542
      D10=1.
      DMAX1=D10*(1+PERD1)
      DMAX4=D40*(1+PERD4)

'+++++++++++++++++++++++++++++++++++++++++'
' STATE VARIABLES INITIAL VALUES'

      N10=1.
      N20=1.
      N30=3.50539
      N40=1.97542
      P10=1.
      P20=1.
      P30=3.50539
      P40=1.97542
      M10=1.
      M40=1.97542
      H10=1.
      H20=1.
      H30=3.50539
      H40=1.97542
      P1S0=1.
      P4S0=1.97542
      H1S0=1.
      H4S0=1.97542
' -----------------'
      LSM=LSP0
      LDM=LDP0
      LPP0=P0/(CP*MP*TIN)
      LPM=LPP0

      LFP0=AH*HP/(CP*MP)
      LFM=LFP0

      AFP0=ALFF*TIN/(BETA*LSP)
      AFM=AFP0

      LCP0=AH*HP/(CC*MC)
      LCM=LCP0

      LRM=LRP0
```

```
      ACP0=ALFC*TIN/(BETA*LSP)
      ACM=ACP0

      CONSTANT Y10=0.0
      CONSTANT Y40=0.5

      U10=Y10
      U40=Y40

      G10=-(U10-1)*M10/LSP0
      G40=U40*LRP0*(M40-1)

      F10=M10/LSP0
      F40=LRP0*(M40-1)


      END

'++++++++++++++++++++++++++++++++++++++++++'

      DYNAMIC
      DERIVATIVES

'++++++++++++++++++++++++++++++++++++++++++'
'TRAJECTORIES'
'------------'

      PROCEDURAL(TAU,GOD=T,T1)
      TAU=0
      GOD=0
      IF(T.GE.T1) TAU=T-T1
      IF(T.GE.T1) GOD=1
      END


'MISMATCH BETWEEN PLANT AND MODEL'
'-------------------------------'

PROCEDURAL(GO,OS1,OS2,OS3,DVA,DVE=T,GOTIME,DVMAX,DVRAMP,FREQ)
      DVA=0
      DVE=0
      OS1=0
```

```
      OS2=0
      OS3=0
      GO=0
      IF(T.GE.GOTIME) GO=1
      DVA=DVA+DVRAMP*T
      DVE=DVE-DVRAMP*2*T
      OS1=OS1+SIN(FREQ*T)
      OS2=OS2+COS(FREQ*0.2*T)
      OS3=OS3+COS(FREQ*3.7*T)
      END


'LOGIC CONTROL PARAMETERS'
'------------------------'
      LSP=LSP0+(FLAG1*DVA+FLAG11*OS1)*LSP0/10*GO
      ACP=ACP0+(FLAG2*DVE+FLAG22*OS2)*ACP0/10*GO
      AFP=AFP0+(FLAG3*DVE+FLAG33*OS3)*AFP0/10*GO
      LDP=LDP0+(FLAG4*DVA+FLAG44*OS1)*LDP0/10*GO
      LPP=LPP0+(FLAG5*DVA+FLAG55*OS2)*LPP0/10*GO
      LCP=LCP0+(FLAG6*DVE+FLAG66*OS3)*LCP0/10*GO
      LFP=LFP0+(FLAG7*DVA+FLAG77*OS2)*LFP0/10*GO
      LRP=LRP0+(FLAG8*DVA+FLAG88*OS3)*LRP0/10*GO
'++++++++++++++++++++++++++++++++++++++++'
' PLANT DRIVEN BY LDOP CONTROL'

      DP1=(Y1-1.)*P1/LSP+P2/LSP-(ACP*(P4-P40)+AFP*(P3-P30))*P1
      DP2=LDP*(P1-P2)
      DP3=LPP*P1-LFP*(P3-P4)+FLAGD*DISTP
      DP4=LCP*(P3-P4)-Y4*LRP*(P4-1.)

'++++++++++++++++++++++++++++++++++++++++'
' Measurement System'

'Delay problem'
'-------------'

      CONSTANT TP1=0.1,TP4=0.1
      DP1S=TP1*(P1-P1S)
      DP4S=TP4*(P4-P4S)

      CONSTANT TH1=0.1,TH4=0.1
      DH1S=TH1*(H1-H1S)
```

```
      DH4S=TH4*(H4-H4S)

'+++++++++++++++++++++++++++++++++++++++'
'PLANT DRIVEN BY RID CONTROL'

      DH1=(V1-1.)*H1/LSP+H2/LSP-(ACP*(H4-H40)+AFP*(H3-H30))*H1
      DH2=LDP*(H1-H2)
      DH3=LPP*H1-LFP*(H3-H4)+FLAGD*DISTH
      DH4=LCP*(H3-H4)-V4*LRP*(H4-1.)

'UNKNOWN DYNAMICS '
'-----------------'
      DISTP=GO*COS(P4-P3)*SIN(P1)*OS2
      DISTH=GO*COS(H4-H3)*SIN(H1)*OS2

'+++++++++++++++++++++++++++++++++++++++'
' MODEL FOR RID CONTROL '


DN1=(V1-1.)*N1/LSM+N2/LSM-(ACM*(N4-N40)+AFM*(N3-N30))*N1+RG1
      DN2=LDM*(N1-N2)
      DN3=LPM*N1-LFM*(N3-N4)+RG3
      DN4=LCM*(N3-N4)-V4*LRM*(N4-1.)

'+++++++++++++++++++++++++++++++++++++++'
' MODEL FOR LAGRANGIAN CONTROL '

      DM1=C1*F1+G1
      DM4=C4*F4+G4

      C1=U1-1
      C4=-U4

      F1=M1/LSM
      F4=LRM*(M4-1)

'+++++++++++++++++++++++++++++++'
' DEMAND '

      D1=DMAX1+(D10-DMAX1)*EXP(-DECAY1*T)-EK
      EK=GOD*(PERD12-PERD12*EXP(-DECAY2*TAU))
      D4=DMAX4+(D40-DMAX4)*EXP(-DECAY1*T)
```

```
      B4T=-K4I*Z4A+K4I*(M4-P4S)

      DZ1A=M1-P1S
      DZ4A=M4-P4S

'+++++++++++++++++++++++++++++++++++++++++++'

      P1S=INTVC(DP1S,P1S0)
      P4S=INTVC(DP4S,P4S0)
      H1S=INTVC(DH1S,H1S0)
      H4S=INTVC(DH4S,H4S0)
      P1=INTVC(DP1,P10)
      P2=INTVC(DP2,P20)
      P3=INTVC(DP3,P30)
      P4=INTVC(DP4,P40)
      N1=INTVC(DN1,N10)
      N2=INTVC(DN2,N20)
      N3=INTVC(DN3,N30)
      N4=INTVC(DN4,N40)
      H1=INTVC(DH1,H10)
      H2=INTVC(DH2,H20)
      H3=INTVC(DH3,H30)
      H4=INTVC(DH4,H40)

      Z1B=INTVC(DZ1B,Z1B0)
      Z4B=INTVC(DZ4B,Z4B0)
      Z1A=INTVC(DZ1A,Z1A0)
      Z4A=INTVC(DZ4A,Z4A0)
      M1=INTVC(DM1,M10)
      M4=INTVC(DM4,M40)

'+++++++++++++++++++++++++++++++++++++++++++'

      END
      TERMT(T.GE.TMAX)
      END
END
```

Appendix B

ACSL Code of the Xenon Oscillation Problem

The following pages include the computer code of the xenon oscillation problem presented in Chap 4. It is written using the Advanced Computer Simulation Language (ACSL). The code contains the xenon model of PWR, and the RID controller described in Chap 4.

```
PROGRAM  XENON OSCILLATION RID CONTROL USING ONEGA MODEL
"  CONTROL MOUNTED  , MODELING ERROR INTRODUCED  "
"  ADAPTIVE CONTROL MOUNTED   "

      INITIAL
      CONSTANT GAMMAX=0.003,SIGF=0.65,CROSSX=2.72E-18
      CONSTANT GAMMAI=0.061
      CONSTANT P=2500,D=0.395,H=365.8
      CONSTANT V=3.079E+7,SIGA=1.53
      CONSTANT U0=0.0076
      CONSTANT FLAG=-1
      CONSTANT KICK=0
      CONSTANT K1=1,K2=1

"-----------------------------------"
"  CONVERTABLE PARAMETERS           "
"-----------------------------------"
      CONSTANT LAMIC=2.87E-5,LAMXC=2.09E-5
      CONSTANT ALFAFC=3.64E-16,GC=8.456E-21,FI0C=2.1E+13
      CONSTANT T1C=36000,TMAXC=360000
      CONSTANT ALFMFC=3.6E-16,DM=0.375,CROSMX=2.6E-18

"-------------------------------------"
"   CONVERSIONS  1 MEANS SECOND SCALE "
"                60 MEANS MIN SCALE   "
"              3600 MEANS HR SCALE    "
"-------------------------------------"
      CONSTANT CONV=3600
      LAMI=LAMIC*CONV
      LAMX=LAMXC*CONV
      ALFAF=ALFAFC/CONV
      ALFMF=ALFMFC/CONV
      G=GC/CONV
      FI0=FI0C*CONV
      T1=T1C/CONV
      T2=T2C/CONV
      TMAX=TMAXC/CONV

      CINTERVAL CINT=0.1
      IALG=2

      I0=GAMMAI*SIGF*FI0/LAMI
```

```
      X0=(GAMMAI+GAMMAX)*SIGF*FI0/(LAMX+0.785*CROSSX*FI0)
      X0M=(GAMMAI+GAMMAX)*SIGF*FI0/(LAMX+0.785*CROSMX*FI0)
      BK=3.1415/H

      EK1=1.358*CROSSX*X0

      CONSTANT A0=-0.139555,B0=-0.100589
      C0=A0*GAMMAI*SIGF*FI0/(LAMI*I0)

      CONSTANT BM0=-0.10058900
      CONSTANT CM0=-0.139555
      CONSTANT AFLAG=0

      END

      DYNAMIC
      DERIVATIVES

      PROCEDURAL
      U=U0
      CFLAG=1
      IF(T.GE.T1) CFLAG=0
      END
"----------------------------"
"     MODEL                  "
"----------------------------"
      DC=A*GAMMAI*SIGF*FI0/I0-LAMI*C
      DCM=AM*GAMMAI*SIGF*FI0/I0-LAMI*CM

      DB=A*GAMMAX*SIGF*FI0/X0+C*LAMI*I0/X0+EK
      DBM=AM*GAMMAX*SIGF*FI0/X0M+CM*LAMI*I0/X0M+EKM

      EK=-LAMX*B-(CROSSX*FI0)*(0.6667*(A+B)+0.785*A*B)
      EKM=-LAMX*BM-(CROSMX*FI0)*(0.6667*(AM+BM)+0.785*AM*BM)

      A=BETA13/BETA2+FLAG*(SQRT(1+(BETA13/BETA2)**2))
      AM=BETAM3/BETM2+FLAG*(SQRT(1+(BETAM3/BETM2)**2))


BETA13=(3*D*KB**2-0.169*CROSSX*X0+1.188*ALFAF*FI0*SIGA)/SIGF

BETAM3=(3*DM*KB**2-0.169*CROSMX*X0M+1.188*ALFMF*FI0*SIGA)/SIGF
```

```
      BETA2=(0.848*UC+1.358*CROSSX*X0*B)/SIGF
      BETM2=(0.848*UC+1.358*CROSMX*X0M*BM)/SIGF

      KB=3.1415/H
      UC=CFLAG*U+(1-CFLAG)*U1

      PL=0.636*(1-A)
      PLM=0.636*(1-AM)

      XL=(1-B)*0.636
      XLM=(1-BM)*0.636

      IL=(1-C)*0.636
      ILM=(1-CM)*0.636


      FLUX=PL/0.699684
      FLUXP=PLM/0.699684

      XENON=XL/0.699975
      XENONP=XLM/0.699975

      IODINE=IL/0.724757
      IODINP=ILM/0.724757

"  CONTROLS "
"--------------------------"

      BD=B0
      CD=C0
      AST=AS+AFLAG*F*K5
      CONSTANT K5=100
      F=1.5707*(PLMS-PLS)
      DPLMS=K3*(PLM-PLMS)
      DPLS=K4*(PL-PLS)
      AS=UST/ALT
      UST=UST1+UST2+UST3
      UST1=X0*B*(0.667*CROSSX+LAMX/FI0)/(GAMMAI*SIGF)
      UST2=-K1*LAMI*I0*(B-BD)/(GAMMAI*SIGF*FI0)
      UST3=-K2*(C-CD)
      ALT=1+ALT1+ALT2+ALT3
      ALT1=-0.667*CROSSX*X0/(GAMMAI*SIGF)
```

```
      ALT2=-0.785*CROSSX*X0*B/(GAMMAI*SIGF)
      ALT3=GAMMAX/GAMMAI

      U1=BIR+IKI
      BIR=-2.3585*BETA13*SIGF*AST/(1-AST**2)
      IKI=-1.6014*CROSSX*X0*B

"ONLY FOR OBSERVATION  THE PARTIAL CONTROL BEHAVIOR "
      EQLBRM=(UST1-LAMI*I0/(GAMMAI*SIGF*FI0))/ALT
      RECNS1=K1*(BD-B)
      RECNS2=K2*(CD-C)

      CONSTANT PLMS0=0.699684,PLS0=0.696335,K3=100,K4=100

      PLS=INTVC(DPLS,PLS0)
      PLMS=INTVC(DPLMS,PLMS0)
      B=INTVC(DB,B0)
      BM=INTVC(DBM,BM0)
      C=INTVC(DC,C0)
      CM=INTVC(DCM,CM0)

      END
      TERMT (T.GE.TMAX)
      END
END
```

VITA

Riza C. Berkan was born in 1961, in Istanbul, Turkey. He graduated from Moda Primary School and Private Moda High School in 1972 and 1978, respectively. Between 1970 and 1983, he was heavily involved in sports at the Galatasaray Swimming Club as a water-polo player and as a swimmer. Mr. Berkan graduated from the Hacettepe University in Ankara, Turkey, in 1984, with a B.S. degree in Physics. He attended the Nuclear Engineering Institute at Istanbul Technical University between 1984 and 1985 to pursue a Master's degree. However, he came to the U.S. in 1985 and continued his graduate study at the University of Tennessee, Knoxville. He held a graduate research assistant position starting from 1986 under the contract sponsored by Oak Ridge National Laboratory, Instrumentation and Controls Division. Mr. Berkan obtained a Master's degree in Nuclear Engineering in 1988. His Master's thesis and research interests included dynamic modeling of the Experimental Breeder Reactor-II for control purposes. Then, he continued his graduate study to pursue a doctorate degree in the same area. His research interests included modern control theory, nonlinear systems, inverse dynamics, fuzzy logic, neural networks, signal and command validation, nuclear reactor operations and human factors. During the different phases of the research sponsored by Oak Ridge National Laboratory, Mr. Berkan has published more than 30 articles in conference proceedings and technical journals. His dissertation was accepted by the committee in July 1991. Mr. Berkan intends to pursue an academic career as a faculty and to continue research and development in the area of large-scale system operations and artificial intelligence.